

The background of the cover is an aerial photograph of a river delta, likely the Rhine-Meuse delta, showing a complex network of channels and distributaries. The entire image is overlaid with a semi-transparent blue color.

GEOLOGICA ULTRAIECTINA

mededelingen van de
Faculteit Aardwetenschappen
Universiteit Utrecht

No. 154

**Late Quaternary variability of the
Arabian Sea monsoon and oxygen
minimum zone**

Gert-Jan Reichart

GEOLOGICA ULTRAIECTINA

mededelingen van de
Faculteit Aardwetenschappen
Universiteit Utrecht

No. 154

**Late Quaternary variability of the
Arabian Sea monsoon and oxygen
minimum zone**

Gert-Jan Reichart

ISBN 90-5744-012-1

Late Quaternary variability of the Arabian Sea monsoon and oxygen minimum zone

Laat Kwartaire variabiliteit van de moesson en de zuurstof minimum zone in de Arabische Zee

(met een samenvatting in het Nederlands)

Proefschrift

ter verkrijging van de graad van doctor
aan de Universiteit Utrecht
op gezag van de Rector Magnificus Prof. Dr. H. O. Voorma
ingevolge het besluit van het College van Decanen
in het openbaar te verdedigen
op woensdag 3 december 1997 des morgens te 10.30 uur

door
Gerardus Jan Reichart
geboren op 30 oktober 1966 te Amsterdam

PROMOTOR: PROF. DR. C.H. VAN DER WEIJDEN

CO-PROMOTOR: DR. W.J. ZACHARIASSE



The Research reported in this thesis was carried out at the institute of Earth sciences, Department of Geochemistry, Budapestlaan 4, 3508TA Utrecht, The Netherlands. This study was supported by the Netherlands Organization for Scientific Research (NWO).

Contents

Overzicht	Inleiding en samenvatting van het onderzoek in het Nederlands	9
Chapter 1	Introduction	15
Chapter 2	A 225 kyr record of dust supply, paleoproductivity and the oxygen minimum zone from the Murray Ridge (northern Arabian Sea) Reprint from: Reichart et. al., <i>Palaeogeogr. Palaeoclim. Palaeoecol.</i> (in press)	23
Chapter 3	Enhanced preservation of organic matter in sediments underlying the oxygen minimum zone in the northeastern Arabian Sea Preprint from: Van der Weijden et al., <i>Deep Sea Res.</i> (accepted)	53
Chapter 4	Orbital- and suborbital-controlled variability in the Oxygen Minimum Zone (OMZ) of the northern Arabian Sea during the last 225,000 yr Preprint from: Reichart et al., <i>Paleoceanography</i> (submitted)	79
Chapter 5	Organic carbon preservation and Oxygen Minimum Zone (OMZ) variability in the northern Arabian Sea	121
Chapter 6	Low latitude forcing of glacial cycles	153
Acknowledgements		171
Curriculum Vitae		173

Overzicht

De Moesson

Alexander de Grote was een van de eerste Europeanen die de moesson meemaakten, tijdens zijn veldtocht naar de monding van de Indus (325 v.Chr.). De oudst bekende geschriften die melding maken van het moesson klimaat, echter dateren van ongeveer 2500 v. Chr.. Scheepvaartdocumenten van die tijd beschrijven al hoe koopvaardij schepen op de Arabische Zee de per seizoen wisselende winden gebruikten. De Moesson heeft altijd een belangrijke rol gespeeld in het leven van de bewoners rond de Arabische Zee, omdat zij voor hun handel afhankelijk waren van de seizoensgebonden verandering van de wind richting. Het Arabische woord voor seizoen, 'mausim', is dan ook de oorsprong van ons woord 'moesson'.

De moesson-cyclus is het gevolg van de jaarlijkse beweging van de Inter Tropische Convergence Zone (ITCZ), tussen de kreefts- en steenbokkeerkring, als deze de zone van maximale opwarming door de zon volgt. De ITCZ is het gevolg van het opstijgen van warme, vochtige lucht, waarbij deze afkoelt en zware regenval veroorzaakt in de tropen. De latente warmte die vrijkomt als gevolg van wolkenvorming en neerslag vormt een extra warmtebron voor de ITCZ. De resulterende luchtstroming langs het aard oppervlak naar de ITCZ wordt afgebogen door de Corioliskracht en veroorzaakt zo het karakteristieke Passaatwindpatroon. De

jaarlijkse beweging van de zon veroorzaakt relatief grote temperatuursveranderingen boven de continenten, maar slechts geringe veranderingen boven oceanen. Deze verschillen in opwarming ontstaan doordat de warmtecapaciteit van de zee veel groter is dan die van het land. Dit heeft tot gevolg dat in de zomer de subtropische hogedrukcel boven het continent eenvoudig wordt vervangen door een lagedrukcel. Tijdens de winter herstelt de subtropische hogedrukcel zich en veroorzaakt het draaien van de overheersende windrichting. Hierdoor ervaren de continenten en de daaraan grenzende oceanen een halfjaarlijkse wisseling van de windrichting, de moesson. De kracht en richting van de moessonwinden worden beïnvloed door de ligging en de grootte van de continenten. De zomer-moesson van India is met name zo sterk door de hoogte en de ligging van de Himalaya en het Tibetaanse Plateau en door de aanvoer van latente warmte vanaf de Indische Oceaan.

De landbouw in India en China, de twee landen met de grootste bevolking, is sterk afhankelijk van de regenval tijdens de zomer-moesson. Gedurende de zomer op het noordelijk halfrond vallen er zware moesson regens in India, Zuidoost-Azië en Zuid China. Plaatselijk worden deze regens door de bergen versterkt, waardoor in delen van Assam gedurende de drie maanden van de zomer-moesson gemiddeld meer dan

1200cm neerslag valt. Veranderingen in de sterkte van moessonregens hebben geresulteerd in zowel extreme droogte, met het verloren gaan van de oogst, als extreme regenval, resulterend in catastrofale overstromingen. Omstreeks 1500 v. Chr., bijvoorbeeld, was het uitblijven van regelmatige moessonregens (als gevolg van klimaatveranderingen veroorzaakt door cyclische variaties in de stand van de aardas) waarschijnlijk de oorzaak van de ondergang van de bloeiende Harrapan-cultuur in de Indus-vallei. In wat nu de Thar-woestijn is, werd tot dan tarwe, gerst, meloenen en mogelijk katoen verbouwd.

Hydrografie van de Arabische Zee en het klimaat

De geringe zonneinstraling en een verhoogd albedo, als gevolg van sneeuwbedekking, veroorzaken een atmosferisch hogedrukgebied boven Centraal-Azië tijdens de winter. De resulterende luchtdruk gradiënt tussen Centraal Azië en de ITCZ, op ongeveer 10°S, zorgt voor de koude en droge noordoostenwind die kenmerkend is voor de wintermoesson. In het voorjaar smelten de sneeuw en het ijs onder invloed van de toename in zonneinstraling. Een lager albedo en de toegenomen zonneinstraling zorgen ervoor dat de atmosfeer opwarmt en lucht begint te stijgen. De vochtige lucht die wordt aangezogen van de Indische Oceaan om de stijgende lucht te vervangen, brengt een grote hoeveelheid latente warmte mee, die vrijkomt als de lucht de zuidelijke hellingen van de

Himalaya opstroomt. Deze extra-energie zorgt voor een versterking van de zomer-moessoncirculatie. De resulterende drukgradiënt tussen Centraal-Azië en het winter-hogedrukgebied boven de zuidelijke Indische Oceaan is de drijvende kracht achter de zuidwestelijke winden. De Oost-Afrikaanse bergen bundelen deze winden tot de lage straalstroom over de Arabische Zee die bekend staat als de Findlater Jet. De afname van de zonneinstraling tijdens de hersfst verzwakt het lagedrukgebied boven het Tibetaanse Plateau en betekent het einde van de zomer-moesson.

De sterke veranderingen per seizoen die het gevolg zijn van het moesson-klimaat veroorzaken grote verschillen in oceaanstromingen en in omvang en samenstelling van de deeltjes regen vanaf het zeeoppervlak. De zuidwestenwinden tijdens de zomer moesson veroorzaken het opwellen van dieper water voor de kust van Jemen en Oman en open-oceanopwelling ten noordoosten van de 'Findlater Jet'. De nutriënten die vanuit diepere water-massa's worden aangevoerd door het opwellen, zorgen voor een verhoogde productiviteit aan het zeeoppervlak, waarbij de productiviteit oploopt tot 400 gC/m²yr. Tijdens de wintermoesson is de productiviteit over het algemeen laag, behalve in enkele gebieden voor de kust van Pakistan en India. Sedimentvallen laten zien dat 70% van het biologisch geproduceerde sediment in de noordwestelijke Arabische Zee wordt afgezet tijdens de zomer-moesson.

Veranderingen in de produktiviteit aan het zeeoppervlak, zoals vastgelegd in de sedimenten van de Pakistaanse continent-rand en de Murray-rug zijn synchroon

met de productiviteits-veranderingen in het opwellingsgebied van Oman [Hoofdstuk 2 en 4]. Dit betekent dat de veranderingen in de intensiteit van de zomer-moesson de belangrijkste factor hebben gevormd voor de productiviteits-variaties aan het zeeoppervlak in de Arabische Zee.

De zuurstof minimumzone (ZMZ) in de Arabische Zee is een van de meest extreme zuurstof arme milieus van de huidige open oceaan. De hoge productiviteit aan het zeeoppervlak en een matige verversingssnelheid van de thermocline waters veroorzaken een sterk ontwikkeld zuurstofminimum tussen waterdieptes van 150 en 1250 m. In de ZMZ bereikt de zuurstof-concentratie waarden van <0.05 ml/l, resulterend in de reductie van nitraat in de waterkolom. De Arabische Zee kent geen subtropische convergentie aan de noordzijde, aangezien deze zijde begrensd wordt door land. Hierdoor moet het intermediaire water verversd worden vanuit het Zuiden. De belangrijkste bron voor het ventileren van het thermocline water is het zuurstof-arme Centraal Indische Oceaan Water, met kleine bijdragen van het relatief zuurstofrijke Rode Zee Water en Perzische Golf Water. Convectieve menging door afkoeling van het zeeoppervlak tijdens de winter bereikt maximaal een diepte van 100m, te ondiep om de ZMZ van vers water te voorzien. De ZMZ heeft door de tijd heen aanzienlijk gevarieerd [Hoofdstuk 2, 4 en 5]. Veranderingen in de intensiteit van de ZMZ in het verleden waren gekoppeld aan zowel de productiviteit aan het zeeoppervlak [Hoofdstuk 2 en 4] als aan geïntensiveerd convectief mengen in de waterkolom

tijdens de winter [Hoofdstuk 4].

Variaties van de moesson cyclus op een Milankovitch en een sub-Milankovitch tijdschaal

Variaties in de verdeling van de instralingsenergie van de zon over de seizoenen veroorzaakt door veranderingen in de baan van de aarde hebben een sterk effect op de intensiteit van de moesson-circulatie. Een toename van de zonneinstraling tijdens de zomer boven Centraal-Azië, gekoppeld aan de precessiecomponent van de baanparameters van de aarde, resulteert in sterkere zomer-moessonwinden. Maxima in de intensiteit van de zomer-moesson vertonen echter een grote vertraging ten opzichte van de maximale instraling. Het toepassen van een nieuw leeftijdsmodel [Hoofdstuk 4] heeft echter laten zien dat deze vertraging tussen instraling tijdens de zomer op het noordelijk halfrond en zomer-moesson-indicators tot nog toe overschat was. De maximale intensiteit van de zomer-moesson lijkt bovendien vooraf te gaan aan de maximale zomer-moesson-productiviteit, waarbij de laatste voornamelijk bepaald wordt door de duur van het opwellingsseizoen, in plaats van door de intensiteit [Hoofdstuk 4].

Tijdens de ijstijden zorgde een langer aanhoudende sneeuwbedekking in Centraal-Azië voor een zwakkere zomer-moesson en intensiverde tegelijkertijd de winter-moesson. Naast de glaciaal-interglaciaal-afwisselingen in de intensiteit van de winter-moesson kunnen ook sub-Milankovitch variaties worden herkend [Hoofdstuk 4]. Zowel de paleoproductiviteit als het diepe

convectief mengen van de waterkolom in het noorden van de Arabische Zee zijn beïnvloed door deze sub-Milankovitch variaties in de wintermoesson. Deze hoogfrequente veranderingen kunnen gecorreleerd worden met temperatuursveranderingen boven de Noord-Atlantische Oceaan, zoals die zijn gereconstrueerd met behulp van de Groenlandse ijskernen.

Organisch materiaal preservatie

De rol die zuurstof speelt bij de afbraak van organische koolstofverbindingen in mariene sedimenten is momenteel het onderwerp van verhit wetenschappelijk debat. Binnen dit debat speelt de Arabische Zee een belangrijke rol vanwege de lokaal sterk ontwikkelde ZMZ. Op de plaatsen waar de ZMZ de continentrand raakt en daar waar submariene ruggen tot in de ZMZ reiken, vindt sedimentatie plaats onder suboxische omstandigheden. De grote verschillen in zuurstofconcentratie van het bodemwater, waarbij de andere factoren grotendeels constant blijven, bieden de ideale omstandigheden om de invloed van ernstige zuurstofdepletie op de vroeg-diagenetische afbraak van organisch materiaal te bepalen. De continent rand van Oman is echter tamelijk stijl en de sedimentatie wordt beïnvloed door hydrodynamische sorteringprocessen en massatransport. Sedimentologische processen zijn hierdoor in dit gebied de bepalende factor voor de preservatie van organisch materiaal in de smalle intersectie van de continentrand met de ZMZ. Deze grote sedimentologische invloed, samen met

de iets hogere zuurstofconcentraties gedurende in ieder geval een deel van het jaar, maken de continentrand van Oman minder geschikt voor het bestuderen van het effect van lage zuurstofconcentraties in het bodemwater op de preservatie van organisch materiaal. De bredere continentrand van Pakistan, die minder wordt beïnvloed door deze processen, biedt een betere mogelijkheid voor het bestuderen van de invloed van de ZMZ op de preservatie van organisch materiaal. Een duidelijk positief effect van zuurstofdepletie op de preservatie van organisch materiaal kon worden bewezen met behulp van 'boxcores' van de Pakistaanse continentrand en de Murray-rug [*Hoofdstuk 3*].

De gebrekkige tijdscontrole in 'oude' sedimenten maakt het over het algemeen onmogelijk om met voldoende precisie de sedimentatiesnelheden te berekenen. Om uitsluitsel te krijgen over de rol van zuurstof op preservatie is het het beste te kijken naar vergelijkbare oxische en anoxische settings met een lage sedimentatiesnelheid. Dit zijn relatief zeldzame omstandigheden. Tijdseries van de gereconstrueerde productiviteit aan het zeeoppervlak en van de intensiteit van de ZMZ in twee sedimentkernen, van verschillende diepte van de Murray-rug [*Hoofdstuk 5*] laten zien dat de variaties in de ZMZ een uitgesproken effect hebben gehad op de afbraaksnelheid van organisch materiaal door de tijd in de Arabische Zee.

Interacties tussen de moesson en het klimaat op aarde

Recentelijk is er meer aandacht

gekomen voor een mogelijk verband tussen veranderingen in het (moesson) klimaat op lage breedtegraden en veranderingen van het mondiale klimaat. Omdat waterdamp het belangrijkste broeikasgas op aarde is, wordt het beschouwd als het meest waarschijnlijke medium waarmee klimaatsveranderingen op aarde doorgegeven worden. Veranderingen in de intensiteit van de moesson van de zomer op het noordelijk halfrond zouden verantwoordelijk kunnen zijn voor de glaciaal-interglaciaal-afwisselingen op aarde. Een geïntensiveerde moessoncirculatie brengt grote hoeveelheden 'extra' waterdamp in de atmosfeer via de ITCZ en kan daardoor, mogelijk via positieve terugkoppelingsprocessen, zorgen voor een algemene temperatuurstijging op aarde en het smelten van ijskappen.

Variaties van de Afrikaanse en Indische moesson zijn met elkaar in fase en worden primair bepaald door veranderingen in de instralingsgradiënt tussen de kreefts- en steenbokskeerkring gedurende de zomer [*Hoofdstuk 6*]. Het patroon van de veranderingen van deze instralingsgradiënt door de tijd is identiek aan dat van de instralingscurve op 65°N, die tegenwoordig op grote schaal wordt toegepast bij het modelleren van veranderingen in ijsvolume. De gelijkenis tussen de twee curves suggereert dat veranderingen in de waterdamp op aarde, gekoppeld aan het moessonklimaat op lage breedtegraad, mogelijk de primaire forcering hebben geleverd voor het aangroeien en weer afsmelten van de ijskappen gedurende het Pleistoceen [*Hoofdstuk 6*].

Introduction

The Monsoon

Among the first Europeans observing the Asiatic monsoon was Alexander the Great during his campaign to the mouth of the Indus (325 B.C.). The oldest known records of the Arabian Sea monsoonal climate, however, are shipping documents, dated about 2300 B.C., which refer to the use of the seasonal changing winds by traders [Warren, 1987]. The monsoon has always played an important role in the lives of the sailors inhabiting the coasts of the Arabian Sea, because they depended for their trade on the seasonal change in wind direction. The Arabic word 'mausim', which means season, is also the origin of the term monsoon.

The monsoon cycle is caused by the annual shifting position of the Inter Tropical Convergence Zone (ITCZ) which oscillates between approximately the tropics of Capricorn and Cancer, following the region of maximum solar heating. The ITCZ results from the rise of warm humid air, which cools with increasing height causing heavy rainfall in the tropics. The latent heat released during cloud formation and rainfall provides an additional heat source for the ITCZ. The resulting surface air flow towards the ITCZ is deflected by the Coriolis force, causing the characteristic trade wind pattern. The yearly course of the sun causes large temperature differences on the continents, whereas

differences in the ocean are relatively small. This differential heating originates from the difference in heat capacity being smaller for land than for sea, and results in the breakdown of the subtropical high pressure cell and the formation of a low pressure cell over the continent during summer. During winter the subtropical high pressure cell restores causing a reversal in wind direction. Thus, continents in the tropical region and adjacent ocean experience a semi-annual reversal in wind direction, which is termed monsoon. Strength and direction of the monsoon is influenced by the position and size of the continents. The Indian monsoon is particularly strong due to height and position of Himalayas and Tibetan Plateau, and the supply of latent heat from the Indian Ocean.

The agriculture in India and China, the two countries in the world with the largest population, depends heavily on the rainfall during the summer monsoon. During the boreal summer heavy monsoonal rains fall in India, southeast Asia and southern China. Locally they are orographically amplified, so that, for example in parts of Assam, in the three monsoon months of June, July and August, precipitation averages more than 1200 cm. Variability in the intensity of the monsoonal rains has resulted in extreme drought, with failing crops, or extreme rainfall, resulting in catastrophic floods. For example,

the failure in the late Holocene of regular monsoonal rains about 3,500 yr. BP. - related to astronomical forced climate change- is thought to have caused the collapse of the flourishing Harrapan culture in the Indus valley [Bryson and Swain, 1981]. Until this decrease in monsoonal rainfall wheat, barley, melons, and perhaps cotton were grown in what is now the Thar desert of Radjasthan [Lamb, 1995].

The Arabian Sea climatic and oceanographic setting

Low solar insolation and an increased albedo, due to the seasonal snow cover, cause high atmospheric pressures over Central Asia during winter. The resulting pressure gradient between Central Asia and the ITCZ, at about 10°S forces the dry and cold northeasterly winds of the winter monsoon. Increased solar insolation in spring causes the snow and ice to melt. Due to the reduced albedo and increased solar insolation, the overlying air heats up and rises. Moist air, attracted from the Indian Ocean to replace the ascending air, releases large amounts of latent heat, when rising over the southern slopes of the Himalayas, thus strengthening the summer monsoonal circulation. The resulting strong pressure gradient between Central Asia and the winter high over the southern Indian Ocean drives the south westerlies. The east African mountains channel these southwesterlies into a low level jet stream over the Arabian Sea, known as the Findlater Jet [Findlater, 1971]. Decreased solar insolation during the autumn weakens the low-pressure

cell above the Tibetan Plateau, marking the end of the summer monsoon.

The strong seasonal variability, due to the monsoonal climate, invokes large changes in oceanography and particle fluxes. Southwesterly winds during the summer monsoon cause coastal upwelling offshore Oman and Yemen, and open ocean upwelling to the northeast of the Findlater Jet axis. Nutrients brought to the surface by upwelling cause high sea surface productivity, up to 400 gC/m²yr [Kabanova, 1968; Codispoti, 1991]. During the winter monsoon productivity is generally low, except in some areas offshore Pakistan and India [Wyrki, 1971; Mathupratap et al., 1996]. Sediment trap studies indicate that 70% of the biological sediment in the northwestern Arabian Sea is deposited during the summer monsoon [Nair et al., 1989].

Variations in surface water productivity recorded in sediments from the Pakistan Margin and the Murray Ridge are synchronous with changes in productivity in the Oman upwelling area [Chapters 2 and 4]. This implies that, across the Arabian Sea, past variations in summer monsoon intensity have been the primary cause for changes in sea surface productivity.

The Arabian Sea oxygen minimum zone (OMZ) is one of the most pronounced low oxygen environments in the open ocean today. High productivity and moderate ventilation of the thermocline [Swallow 1984, You and Tomczak, 1993] leads to an intense OMZ at water depths between 150 and 1250 m [Wyrki et al., 1971; 1973; Deuser et al., 1979; Olson et al., 1993]. In the OMZ oxygen concentrations reach values

<0.05ml/l [Van Bennekom and Hiehle, 1994], resulting in the reduction of nitrate in the water column [Deuser *et al.*, 1979; Naqvi, 1987]. Because the Arabian Sea is land-locked at the northern boundary there is no subtropical convergence in the north, and intermediate waters have to be ventilated from the south [Swallow, 1984]. The main source for thermocline ventilation is the oxygen poor (~1 ml/l [Olson *et al.*, 1993]) Indian Ocean Central water, with minor contributions from oxygen rich Red Sea Water (~3.5 ml/l [Wyrki, 1971]) and Persian Gulf Water (~2.6 ml/l [You and Tomczak, 1993]). Convective turnover through winter cooling of the sea surface extends to depths of about 100 m [Banse, 1984; Madhupratap *et al.*, 1996], which is too shallow to introduce significant amounts of oxygen into the OMZ. It has been shown that the OMZ has varied considerably in the past [Hermelin, 1991; Ten Kate *et al.*, 1991; Altabet *et al.*, 1995; Chapters 2, 4 and 5]. Past variations in the intensity of the OMZ are linked to both sea surface productivity [Altabet *et al.*, 1995; Chapters 2 and 4] and intensified winter turnover [Chapter 4].

Orbital and sub-orbital variations in the monsoonal cycle

Variations of the seasonal distribution of solar radiation due to changes in the Earth's orbit have a pronounced effect on the intensity of the monsoon circulation [Rossignoll-Strick, 1983; Kutzbach and Guetter, 1986; Clemens *et al.*, 1991]. Increased summer radiation over Central Asia, related to the precessional

component of orbital forcing, results in stronger southwest monsoon winds. Maximum southwest monsoon intensity, however, has been shown to significantly lag maximum insolation [Shimmiel *et al.*, 1990; Clemens *et al.*, 1991; Murray and Prell, 1992; Chapter 2]. Application of a new age model [Chapter 4] shows that the timelag between northern hemisphere summer insolation and summer monsoon indicators has previously been overestimated. Maximum monsoon intensity, furthermore, appears to lead maximum summer monsoon productivity, the latter being controlled by the duration rather than by the intensity of the upwelling season [Chapter 4].

During glacial periods, a prolonged snow and ice cover in Central Asia weakened the summer monsoon, and at the same time strengthened the winter monsoon [Van Campo, 1982; Rostek *et al.*, 1993; Emeis *et al.*, 1995]. Superimposed on the glacial-interglacial variations in the intensity of the winter monsoon, sub-Milankovitch variations can be recognised [Chapter 4]. These sub-Milankovitch variations in winter monsoon intensity have influenced paleoproductivity and deep convective turnover in the northern most Arabian Sea. This high frequency variability can be correlated to temperature changes recorded in Greenland ice cores [Chapter 4].

Organic matter preservation

The role of oxygen in the preservation of organic carbon in marine sediments has been a subject of considerable debate [Demaison and Moore, 1980; Calvert,

1987]. Because of its very intense OMZ the Arabian Sea has been a key area in this debate [Pedersen *et al.*, 1992; Paropkari *et al.*, 1992; 1993; Calvert *et al.*, 1995]. Where the intense OMZ impinges on the continental slope or when sub-marine elevations reach into the OMZ, sedimentation takes place under suboxic conditions. The large differences in oxygen concentration of the bottom water, all other factors remaining approximately constant, offer an ideal situation to study the influence of severe oxygen depletion on organic matter diagenesis. The Oman Margin, however, is rather steep, and affected by winnowing and other downslope processes. In that area C_{org} accumulation in the narrow intersection with the OMZ is largely controlled by sedimentological processes. Their large influence together with the somewhat higher oxygen contents in the OMZ, during at least part of the year, makes the Oman Margin less suited to unravel the role of bottom water oxygen content on the preservation of C_{org} . The broad Pakistan Margin, which is less influenced by these effects, offers a better opportunity to investigate the role of the OMZ on the preservation of organic matter. Based on a study of boxcores from the Pakistan Margin and the Murray Ridge it was found that severe oxygen depletion does have a profound effect on the preservation of organic matter [Chapter 3].

The poor age control in ancient sediments generally makes it impossible to calculate fluxes with appropriate precision. The critical test for the evaluation of C_{org} preservation is in the comparison of equivalent anoxic and oxic sites where sediment accumulation

rates are low, a relatively rare condition [Tyson, 1995]. Timeseries of tracers for sea surface productivity and OMZ intensity in two cores from the Murray Ridge [Chapter 5] show that OMZ variability has had a pronounced effect on the burial efficiency of organic matter through time in the Arabian Sea.

Interactions between the monsoonal and global climate

Recently, attention has been growing for a possible link between low latitude (monsoonal) climate and global climatic changes. Water vapor, being by far the most important global greenhouse gas, might have been the medium through which climatic changes have propagated on earth [Broecker, 1994]. Changes in the intensity of the northern hemisphere summer monsoon could have been responsible for the observed glacial-interglacial variations. An intensified monsoon introduces significant amounts of moisture to the higher atmosphere through the ITCZ, thereby stimulating, possibly via feedback processes, general global warming and the melting of ice sheets. Variability in the African and Indian monsoon climate are in phase, and controlled primarily by changes in the summer insolation gradient between the Tropics of Cancer and Capricorn [Chapter 6]. The pattern reflected in this insolation gradient is identical to the summer insolation pattern at 65°N, which is presently widely used as a target curve for modelling changes in ice volume. The similarity between both patterns suggests a low latitude origin, via atmospheric water vapor content, of

the observed growth and decay of the ice sheets during the Pleistocene [Chapter 6].

References:

- Altabet, M.A., Francois, R., Murray, D.W., and W.L. Prell, Climate-related variations in denitrification in the Arabian Sea from sediment $^{15}\text{N}/^{14}\text{N}$ ratios, *Nature*, 373, 506-509, 1995.
- Banse, K., Overview of the hydrography and associated biological phenomena in the Arabian Sea, off Pakistan. In: B.U. Haq and J.D. Milliman (eds.), *Marine geology and oceanography of Arabian Sea and coastal Pakistan*, Van Nostrand Reinhold, New York: 271-303, 1984.
- Broecker, W.S., Massive iceberg discharge as triggers for global climate change, *Nature*, 372, 421-424, 1994.
- Bryson, R.A. and A.M. Swain, Holocene variations of monsoon rainfall in Rajasthan. *Quat. Res.*, 16, 135-145, 1981.
- Calvert, S.E., Oceanographic controls on the accumulation of organic matter in marine sediments. In: *Marine petroleum source rocks* (eds. J.P. Riley and R. Chester), *Geological Society Special Publication*, 26, 137-151, 1987.
- Calvert, S.E., Pedersen, T.F., Naidu, P.D. and U. von Stackelberg, On the organic carbon maximum on the continental slope of the eastern Arabian Sea. *J. Mar. Res.*, 53, 269-296, 1995.
- Clemens, S., Prell, W., Murray, D., Shimmield, G. and G. Weedon, Forcing mechanisms of the Indian Ocean monsoon. *Nature*, 353, 720-725, 1991.
- Codispoti, L.A. Primary productivity and carbon and nitrogen cycling in the Arabian Sea. In *U.S. JGOFS: Arabian Sea Process Study* (Eds. S.L. Smith, K. Banse, J. K. Cochran, L.A. Codispoti, H.W. Ducklow, M.E. Luther, D.B. Olson, W.T. Peterson, W.L. Prell, N. Surgi, J.C. Swallow & K. Wishner), U.S. JGOFS Planning Report No. 13, 1991.
- Demaison, G.J. and G.T. Moore, Anoxic environments and oil source bed genesis. *Org. Geochem.*, 2, 9-31, 1980.
- Deuser, W.G., Ross, E.H. and Z.J. Mlodzinska, Evidence for and rate of denitrification in the Arabian Sea. *Deep-Sea Res.*, 25, 431-445, 1978.
- Emeis, K.C., Anderson, D.M., Doose, H., Kroon, D. and D. Schulz-Bull, Sea-surface temperatures and the history of monsoon upwelling in the northwest Arabian Sea during the last 500,000 years, *Quat. Res.*, 43, 355-361, 1995.
- Findlater, J. Mean monthly airflow at low levels over the western Indian Ocean. *Geophys. Mem.*, 115, 53 pp., 1971.
- Kabanova, Y.G., Primary production in the northern part of the Indian Ocean. *Oceanology*, 8, 214-225, 1968.
- Kutzbach, J.E. and P.J. Guetter, The influence of changing orbital parameters and surface boundary conditions on climate simulations for the past 18,000 years, *J. Atmos. Sci.*, 43, 1726-1759, 1986.
- Lamb, H.H., *Climate history and the modern world*, second edition, 433 pp., Routledge, London, 1995.
- Madhupratap, M., Kumar, S.P., Bhattathiri, P.M.A., Kumar, M.D., Raghukumar, S., Nair, K.K.C. and N. Ramaiah, Mechanism

- of the biological response to winter cooling in the northeastern Arabian Sea. *Nature*, 384, 549-552, 1996.
- Murray, D.W. and W.L. Prell, Late Pleistocene climatic oscillations and monsoon upwelling recorded in sediments from the Owen Ridge, northwestern Arabian Sea. In: *Upwelling Systems: Evolution since the Early Miocene*. (Eds. C.P. Summerhayes, W.L. Prell & K.C. Emeis) Geological Society Special Publication No. 64, 301-321, 1992.
- Nair, R.R., Ittekkot, V., Manginni, S.J., Ramaswamy, V., Haake, B., Degens, E.T., Desai, B.N. and S. Honjo, Increased particle flux to the deep ocean related to monsoons. *Nature*, 338, 749-751, 1989.
- Naqvi, S.W.A. Some aspects of the oxygen-deficient conditions and denitrification in the Arabian Sea. *Journal of Marine Research*, 45, 1049-1072, 1987.
- Olson, D.B., Hitchcock, G.L., Fine, R.A. and B.A. Warren, Maintenance of the low-oxygen layer in the central Arabian Sea. *Deep-Sea Res. II.*, 40, 673-685, 1993.
- Paropkari, A.L., Babu, C.P. and A. Mascarenhas, A critical evaluation of depositional parameters controlling the variability of organic carbon in Arabian Sea sediments. *Mar. Geol.*, 107, 213-226, 1992.
- Paropkari, A.L., Babu, C.P. and A. Mascarenhas, New evidence for enhanced preservation of organic carbon in contact with oxygen minimum zone on the western continental slope of India. *Mar. Geol.*, 111, 7-13, 1993.
- Pedersen, T.F., Shimmield, G.B. and N.B. Price, Lack of enhanced preservation of organic matter in sediments under the oxygen minimum on the Oman Margin. *Geochim. Cosmochim. Acta*, 56, 545-551, 1992.
- Rostek, F., Ruhland, G., Bassinot, F.C., Müller, P.J., Labeyrie, L.D., Lancelot, Y. and E. Bard, Reconstructing sea surface temperature and salinity using $\delta^{18}\text{O}$ and alkenone records. *Nature*, 364, 319-321, 1993.
- Rosignol-Strick, M., African monsoons, an immediate climatic response to orbital insolation, *Nature*, 303, 46-49, 1983.
- Shimmield, G.B., Mowbray, S.R. and G.P. Weedon, A 350 ka history of the Indian Southwest Monsoon--evidence from deep-sea cores, northwest Arabian Sea. *Trans. R. Soc. Edinburgh Earth Sci.*, 81, 289-299, 1990.
- Swallow, J.C., Some aspects of the physical oceanography of the Indian Ocean. *Deep-Sea Res.*, 31, 639-650, 1984.
- Ten Kate, W.G.H.Z., Sprenger, A., Steens, T.N.F. and C.J. Beets, Late Quaternary monsoonal variations in the western Arabian Sea based on cross-spectral analyses of geochemical and micropalaeontological data (ODP Leg 117, core 728A). *Spec. Publ. Int. Ass. Sediment.*, 19, 127-143, 1994.
- Tyson, R.V., Sedimentary organic matter, organic facies and palynofacies. Chapman and Hall, London, 1995.
- Van Bennekom, A.J. and M.A. Hiehle, CTD operations and calibrations during legs D1, D2 and D3 of the Netherlands Indian Ocean Programme. In: *Geological study of the Arabian Sea*. (Eds. W.J.M. van der Linden & C.H. van der Weijden) Netherlands Geosciences Foundation, The Hague, 37-66, 1994.
- Van Campo, E., Duplessy, J.C. and M.

Rosignol-Strick, Climatic conditions deduced from a 150-kyr oxygen isotope-pollen record from the Arabian Sea, *Nature*, 296, 56-59, 1982.

Warren, B.C., Ancient and medieval records of the monsoon winds and currents of the Indian Ocean. In: *Monsoons* (Eds.J.S. Fein and P.L. Stephen), Wiley, New York, pp. 632, 1987.

Wyrki, K., *Oceanographic atlas of the*

international Indian Ocean expedition, 531pp, 1971.

Wyrki, K., Physical Oceanography of the Indian Ocean. in: *The Biology of the Indian Ocean*.(ed. B. Zeitschel), 18-36, Springer, Berlin, 1973.

You, Y. and M. Tomczak, Thermocline circulation and ventilation in the Indian Ocean derived from water mass analysis. *Deep-Sea Res. I*, 40, 13-56, 1993.

A 225 kyr record of dust supply, paleo-productivity and the oxygen minimum zone from the Murray Ridge (northern Arabian Sea)

Gert Jan Reichart, Maryke den Dulk, Hendrik Jan Visser, Cornelis H. van der Weijden and Willem J. Zachariasse

Institute for Paleoenvironment and Paleoclimate Utrecht (IPPU), Utrecht University, Budapestlaan 4, P.O. Box 80.021, Utrecht, The Netherlands.

Abstract

Analysis of a (15 m long) sediment core recovered from the Murray Ridge (northern Arabian Sea) reveals a 225,000 year record of climate-induced variations in surface water productivity, mid-water ventilation, and dust-input in the northern Arabian Sea. Productivity and dust-input records closely resemble those from the Owen Ridge and Oman Margin. Also the phase lag of ~10 kyr between maximum productivity and precession minimum is in phase with the summer monsoon upwelling record from the Owen Ridge and the Oman Margin. This implies that the productivity variations in the northern Arabian Sea during the last 225 kyrs are primarily controlled by changes in the Indian Ocean summer monsoon. The winter monsoon obviously played a minor role in the productivity history of the northern Arabian Sea.

Another result from this study is that the Mg/Al record from the Murray Ridge nicely documents the post-glacial flooding of the Persian Gulf, which is the main glacial source for dolomite-dust in this region.

Finally, it is concluded that the intensity of the OMZ covaries with surface water productivity, being weak during periods of reduced summer monsoon, especially at glacial time.

Introduction

Sediments in the Arabian Sea represent an important archive for unravelling the history of the Indian Ocean monsoonal circulation. This

archive has been intensively studied in the western Arabian Sea and the analyses of proxy records for surface water productivity and dust input have revealed that past variations in northern hemisphere summer insolation and

changes in climatic boundary conditions associated with glacial cycles have caused variations in monsoon intensity [e.g. *Prell, 1984; Shimmield et al., 1990; Clemens and Prell, 1991; Prell et al., 1991; Clemens et al., 1996*]. The archive in the northern Arabian Sea on the other hand has been sparsely studied [*Von Stackelberg, 1972; Sirocko and Ittekkot, 1992*]. Sediments from the northern edge of the Arabian Sea, collected during the Netherlands Indian Ocean Programme in 1992, fill this gap. Sediments from the Murray Ridge are particularly interesting because they have been deposited in the open ocean, beyond the reach of turbidity currents. In this paper we report on a sediment core recovered from the southern flank of the Murray Ridge in 1470 m of water (Fig. 1). As will be shown this 15 m long core comprises a climatic record of 225 kyr, covering more than two complete glacial cycles.

Present climatic and hydrographic setting

The climate in the Arabian Sea region is characterized by strong monsoonal

winds invoking large seasonal changes in hydrography and particle fluxes. During the northern winter, when the snow cover increases the albedo, atmospheric pressures are high over Central Asia. This sets up a pressure gradient between Central Asia and the Inter Tropical Convergence Zone (ITCZ) at about 10°S, forcing the dry and cold northeasterly winds of the winter monsoon.

Snow and ice melt at the end of the winter diminishes the albedo over Central Asia, boosting the overlying air to heat up and rise. The resultant pressure gradient between Tibet and the winter high over the southern ocean drives southeasterly winds which change to southwesterlies when crossing the equator. When these winds rise over the southern slopes of the Himalayas they release large amounts of latent heat, thus, strengthening the summer monsoonal circulation. The east African mountains channel the southwesterlies into a low-level jet stream, which is commonly known as the Findlater Jet [*Findlater, 1971*]. Decreased solar radiation during the fall weakens the low pressure cell above the Tibetan Plateau, marking the end of the summer monsoon.

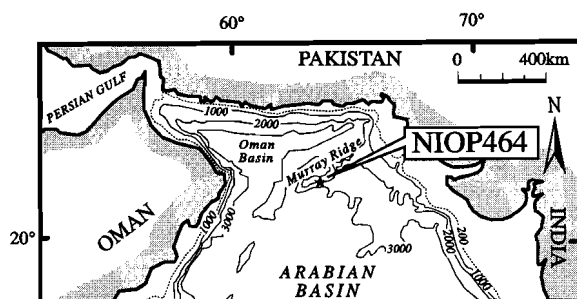


Fig. 1. Location of NIOP464 (22.15°N, 63.35°E); waterdepth 1470 m.

Biological production in the Arabian Sea is generally low during winter, except in some areas off the Pakistan coast [Wyrki, 1973; Banse, 1987]. In summer, however, coastal upwelling off Oman and open ocean upwelling, induced by Ekman pumping, drive the productivity to values that are among the highest known for the open ocean. The area of Ekman pumping is sharply defined by the position of the Findlater Jet [Brock *et al.*, 1992]. Northwest of the jet axis, extreme values of positive (cyclonic) wind stress cause divergent Ekman transport which promotes an intense phytoplankton bloom over a large part of the basin. Annual productivity rates in this upwelling region are between 200 and 400 g C/m²yr [Qasim, 1982; Codispoti, 1991].

The combination of high productivity and moderate ventilation of the thermocline [You and Tomczak, 1993] leads to an intense Oxygen Minimum Zone (OMZ) at water depths between 150 and 1250 metres [Wyrki, 1971; 1973; Deuser *et al.*, 1978; Olson *et al.*, 1993]. Since there is no subtropical convergence in the north, thermocline water in the Arabian Sea has to be ventilated from the south [Swallow, 1984]. You and Tomczak [1993] used a mixing model in which Indian Ocean Central Water (IOCW) is identified as the main source for thermocline ventilation with a small contribution from the Red Sea and Persian Gulf. Inflowing IOCW (~6Sv) is relatively poor in oxygen (~1 ml/l), which, together with high productivity, maintains OMZ oxygen concentrations at their present low values of <2μM [Van Bennekom and Hiehle, 1994].

The Arabian Sea is bounded in the

west and north by deserts, which are known to supply a sizeable fraction of the sediments that accumulate in the Arabian Basin [e.g. DeMenocal *et al.*, 1991; Sirocko *et al.*, 1991]. The dry northwesterly Shamal winds, that blow from the Arabian Peninsula, transport large amounts of dust into the basin during the summer. These dust-laden, dry and hot northwesterlies override the cooler and more humid southwesterly winds at the ITCZ, causing a strong temperature inversion. Northwesterly winds also transport dust from the Iran-Makran area which is the major dust source for the Oman Basin [Kolla *et al.*, 1981]. Changes in continental aridity, wind strength and the position of the ITCZ all contribute to dust input in the northwestern Arabian Basin [Prell and Van Campo, 1986; Shimmiel and Mowbray, 1991; Sirocko, 1991]. In the north, the Indus river has been the major fluvial sediment source for the Arabian Basin [Kolla *et al.*, 1981]. Although the core site is beyond the reach of turbidites some of the suspended load from the Indus river might reach the Murray Ridge.

Material and methods

Visual observation and X-ray radiographs show that NIOP 464 essentially consists of a succession of alternating dark-greenish (7.5y4/2) to light-greenish/grey (7.5y7/2) hemipelagic muds (Fig.2). Over the length of the core a total of 210 samples were taken for subsequent sedimentological, micro-paleontological and chemical analyses.

The water content of the sediment was

determined by the weight loss of fixed volume samples after freeze-drying. Thereafter dry and wet bulk density values were calculated. Part of the sample was dried at 60°C for 4 days and thoroughly ground in an agate mortar prior to an HClO₄, HNO₃, HF acid digestion. The final residue was taken up in 1 M HCl, after which the elements Al, Ba, Be, Ca, Fe, K, Mg, Mn, P, S, Sr, Ti, Y, Zn and Zr were measured using an Inductively Coupled Plasma Emission Spectrometer (ARL 34.000). After calibration, the analytical precision and accuracy were checked by replicate analyses of samples, an international, and in-house standards. Both were found to be better than 3% for all elements. The carbonate content was calculated from the total Ca concentration, using a correction for clay-derived Ca; $CaCO_3 = 2.5(Ca_{tot} - (Ca/Al_{clay} *_{tot} Al))$, where Ca/Al_{clay} is 0.345 [Turekian and Wedepohl, 1961]. This method works well with CaCO₃-rich sediments [Shimmield and Mowbray, 1991]. X-ray diffraction was used on some selected samples to check for the presence of dolomite with a Guinier de Wolff camera using CuK α radiation.

The magnetic susceptibility was measured with a Bartington Instruments' MS2 pass-through loop sensor, at 2 cm intervals. Magnetic susceptibility is a measure of the concentration of magnetic material in the sediment.

Determination of C_{org} and $\delta^{13}C_{org}$ of carbonate rich samples requires that, prior to the analyses, all carbonate should be removed. The carbonate was extracted by mechanical shaking with 1 M HCl for 12 hours followed by a 4 hour extraction with 1 M HCl on the residue at room

temperature. Hydrochloric acid, rather than acetate acid or phosphoric acid must be used to assure complete removal of carbonate phases including dolomite. To avoid overpressure, the centrifuge tubes were carefully degassed during the first hour of the procedure. After extraction of the carbonate the samples were rinsed with demineralised water to remove CaCl₂. Subsequently the samples were dried and organic carbon was determined volumetrically following dry oxidation with CuO at 900°C in a closed circulation system at 0.2×10⁵ Pa O₂. The released CO₂ was cryogenically separated from the other gases. The $\delta^{13}C_{org}$ was measured with a VG SIRA 24 mass spectrometer with a precision better than 0.1‰.

The $\delta^{18}O$ curve is based on the analyses of about 100 handpicked specimens of *Neogloboquadrina duterrei* per sample, which were subsequently roasted for 30 minutes at 470°C under a helium flow to remove organic remains. Samples were then transferred into glass reaction tubes that were evacuated for 14 hours, followed by 6 hours reaction with 100% phosphoric acid at 25.0°C under high vacuum. Again the released CO₂ was cryogenically separated from the other gases and the isotopic composition measured on a VG SIRA 24 mass spectrometer. Replicate analyses and repetitive analyses of the laboratory standard showed a standard deviation of 0.1 ‰ for $\delta^{18}O$ and 0.05 ‰ for $\delta^{13}C$.

Planktonic foraminiferal counts were made on splits (using an Otto microsplitter) from the 150-595 μ m fraction. 200-400 specimens per sample were picked, mounted on Chapman

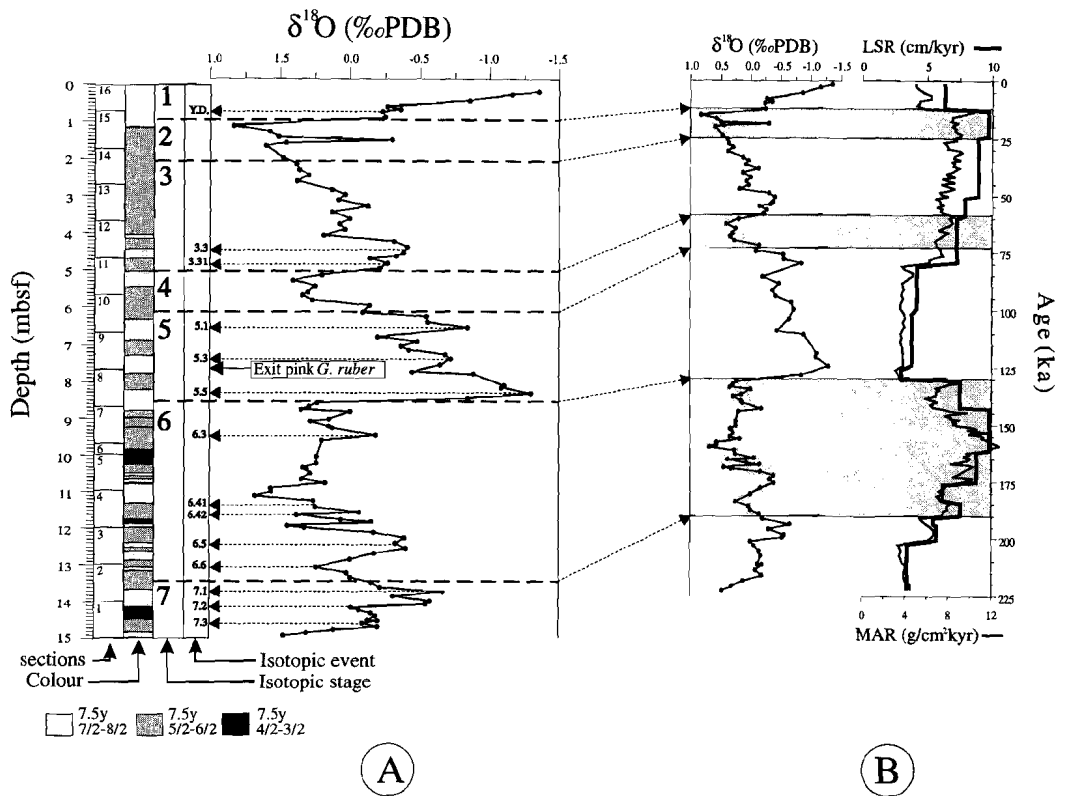


Fig. 2

A) $\delta^{18}\text{O}$ of *Neogloboquadrina dutertrei* (‰ relative to PDB). Grey tones for sediment colour are from visual core description. Exit of pink-pigmented *Globigerinoides ruber* (7.65 metres below sea floor) is positioned between SPECMAP isotopic events 5.5 and 5.3. The small plateau in the $\delta^{18}\text{O}$ curve during the last deglaciation might indicate the Younger Dryas (Y.D.). B) Chronology of $\delta^{18}\text{O}$ record and calculated linear sedimentation rates (LSR's) and mass accumulation rates (MAR's). Glacial isotopic stages are shaded.

slides, identified, and counted. Pteropod preservation is defined by an index which ranges from 0 to 3 (0 = no pteropods; 1 = some small fragments; 2 = many medium-sized fragments; 3 = abundant large-sized fragments).

The chronology of NIOP464 (Fig. 2) is primarily based on comparing the oxygen isotope record with the SPECMAP $\delta^{18}\text{O}$ chronology [Imbrie *et al.*, 1984; Martinson *et al.*, 1987]. Ages of samples (Appendix) are based on

linear interpolation between identified SPECMAP $\delta^{18}\text{O}$ events. Mass accumulation rates (MAR's) were calculated by multiplying the linear sedimentation rates (LSR's) with the dry bulk densities (Fig. 2). The oldest identified $\delta^{18}\text{O}$ event is 7.3, implying that NIOP464 contains two full glacial cycles. The position of SPECMAP events 5.5 and 5.3 is confirmed by the last occurrence of pink-pigmented *Globigerinoides ruber*, which level in the

Table 1
AMS-¹⁴C dates for boxcore at site NIOP464.

Boxcore 464		,1511mbsf.					
sample	UtC-nr.	material	delta ¹³ C (‰,PDB)	depth (cmbsf)	age (yr bp)	error (yr)	sed.rate (cm/kyr)
464b/0	3064	OM	-21.5	0	1210	60	6.35
464b/0	3065	forams	1.18	0	2590	50	
464b/20	3063	forams	1.15	20	5050	100	

Indo-Pacific has been reported to occur between events 5.5 and 5.3 [Thomson *et al.*, 1979].

AMS ¹⁴C dates for two surface samples from a boxcore at site NIOP464 (Table 1) (based on *Globorotalia menardii* and organic matter) differ by about 1400 years. This discrepancy most likely resulted from the upward mixing (via bioturbation) of different quantities of subsurface organic matter and foraminiferal calcite. The sedimentation rate for the uppermost 20 cm at site NIOP464 was calculated by using the average age for the boxcore top and the one at 20 cm depth.

Geochemistry

The geochemical data are given in the Appendix, correlation coefficients in Table 2. Principal component analysis [Davis, 1986] resulted in three factors, which together describe almost 90% of the variation in the data set (Table 3). A K-means cluster analysis [Davis, 1986] of the element factor loadings on the three principal component axes distinguished four clusters (Fig.3).

- I Al, Be, Fe, K, Mg, Mn, Ti and Zr
- II Ca and Sr
- III Ba, P, Y and Zn
- IV S

The first and second cluster occupy opposite positions on the first principal component axis and describe together almost 60% of the variance. Cluster III shows a positive loading on the second principal component axis, while cluster IV shows a negative loading on the third principal components axis.

The elements of cluster I are characteristic for aluminosilicate detritus, whereas those of cluster II belong to biogenic carbonates. Aluminium is typically present in clay minerals which in this region are of continental origin [Shimmield *et al.*, 1990]. Illite, chlorite, smectite with minor amounts of palygorskite are the dominant clay minerals in the Arabian Basin [Kolla *et al.*, 1981; Sirocko and Lange, 1991].

The factor 1 scores are controlled by the relative contribution of the elements of clusters I and II, and portray the relative input of dust, mostly aluminosilicates, and of biogenic carbonate (Fig. 4). Variations in dust input in the Arabian Basin are also revealed in the changes in magnetic susceptibility of the sediment [Kent, 1982; DeMenocal *et al.*, 1991; Reichert *et al.*, 1994]. Ongoing oxidation of organic matter in the sediment, however, affects the redox stability of the iron-bearing minerals causing an overall down-core decrease in magnetic susceptibility [Karlin and Levi, 1985].

Table 2
Inter-element correlation coefficients.

Zn	0.50																			
Y	0.63	0.83																		
Ti	0.91	0.61	0.73																	
Sr	-0.60	-0.45	-0.50	-0.73																
S	-0.13	0.29	0.01	0.00	-0.16															
P	-0.16	0.47	0.35	-0.09	0.14	0.39														
Mn	0.81	0.30	0.46	0.87	-0.60	-0.12	-0.34													
Mg	0.71	0.23	0.24	0.73	-0.64	0.08	-0.24	0.79												
K	0.91	0.55	0.70	0.97	-0.70	-0.12	-0.15	0.88	0.75											
Fe	0.60	0.79	0.73	0.77	-0.64	0.47	0.21	0.57	0.54	0.72										
Ca	-0.74	-0.42	-0.43	-0.34	0.86	0.12	0.18	-0.77	-0.81	-0.83	-0.69									
Be	0.79	0.68	0.79	0.93	-0.75	0.06	0.04	0.79	0.65	0.92	0.84	-0.81								
Ba	-0.06	0.61	0.54	-0.02	0.04	0.13	0.58	-0.25	-0.38	-0.03	0.29	0.20	0.13							
Al	0.89	0.62	0.77	0.98	-0.70	-0.09	-0.07	0.85	0.69	0.99	0.76	-0.82	0.95	0.05						
	Zr	Zn	Y	Ti	Sr	S	P	Mn	Mg	K	Fe	Ca	Be	Ba						

Table 3
Results of principal component analysis of the element abundances.

Factor analyses: factor matrix			
	Factor 1	Factor 2	Factor 3
Al	0.98	-0.03	0.17
Ba	0.05	0.87	0.29
Be	0.96	0.10	0.04
Ca	-0.88	0.23	0.26
Fe	0.83	0.37	-0.28
K	0.97	-0.13	0.15
Mg	0.76	-0.40	-0.29
Mn	0.85	-0.38	0.06
P	-0.04	0.83	-0.11
S	0.06	0.43	-0.86
Sr	-0.79	0.08	0.25
Ti	0.98	-0.06	0.07
Y	0.75	0.51	0.33
Zn	0.67	0.67	0.04
Zr	0.89	-0.17	0.19
Factor	Eigenvalue	Variance %	Cumulative %
1	8.96	59.7	59.7
2	2.90	19.3	79.1
3	1.32	8.8	87.9

However, the NIOP464 record (Fig. 4) shows that the primary signal, although attenuated, is still present. Figure 4 also shows that glacial stages are characterised by increased dust input (as represented by high magnetic susceptibilities), positive factor 1 scores, high Al and low CaCO₃ content. The correlation between MAR, ice volume and the terrigenous sediment fraction (factor 1 and magnetic susceptibility) indicates increased dust accumulation during more arid, glacial periods (cf. Fig. 2 and 4).

The inter-element correlation (Table 2) shows a strong positive correlation of Fe, K, Mg, Mn, Ti, Zr, Be, Zn and Y with Al because concentrations of these elements are primarily controlled by the relative contribution of detrital and biogenic components. To distinguish changes that are not caused by dilution of CaCO₃, elements are plotted as Al ratios.

The elements of cluster III (Ba, P, Y and Zn) are often associated with biological productivity. CaCO₃ also results from biogenic productivity but is in this setting not significantly correlated with cluster III.

The record of S is influenced by porewater sulphate, organic sulphur compounds and pyrite. Changes in S are, therefore, controlled by MAR, the flux of organic matter and possibly also by bottom water oxygen concentration. The sulphur content in NIOP464 shows a strong correlation with the Fe-Al ratio (Fig. 5). This might indicate that pyrite is an important sulphur phase. The higher glacial S content in NIOP464 (Appendix) is most probably related to a higher glacial MAR since higher sedimentation rates are believed to result in higher rates of sulphate reduction [Berner, 1978; Canfield, 1989].

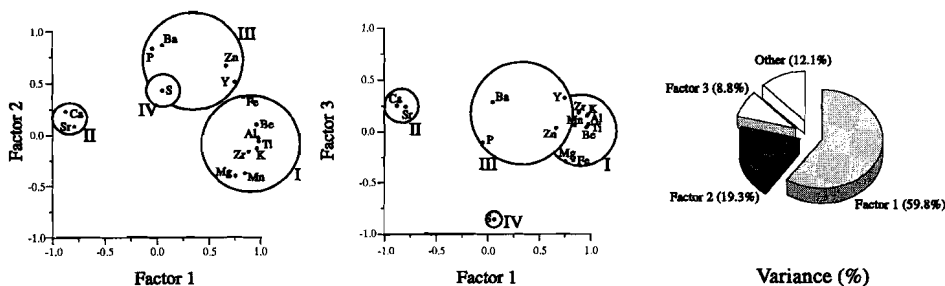


Fig. 3. Results of a principal component analysis on the element distribution. The three factors describe together 87.9% of the variation in the data set. Shaded circles enclose the four distinct element clusters.

Paleoproductivity

Factor 2 scores, the abundance of cluster III elements (Ba, Zn, P and Y) and C_{org} reflect past variations in surface water productivity.

Barium

Ba and surface water productivity, are linked through barite precipitation in decaying particulate organic matter while it settles through the water column [e.g. *Dehairs et al.*, 1980; *Bishop*, 1988; *Dymond et al.*, 1992]. However, Ba could be remobilised in organic-rich sediments that have shallow sulphate reduction zones [*Van Os et al.*, 1991; *Von Breymann et al.*, 1992]. This would have resulted in the formation of barite precipitation fronts above and below organic-rich layers [*Van Os et al.*, 1991]. Since no such fronts have been observed in the Ba record (cf. Fig. 6) it is unlikely that the Ba signal in NIOP464 is affected by remobilisation.

Zinc

The record of the Zn-Al ratio closely resembles that of Ba/Al (Fig. 6). The distribution of Zn in the ocean shows an almost perfect covariance with H_4SiO_4

[*Broecker and Peng*, 1982]. This suggests that Zn is associated with the production of opal. Alternatively, Zn may be easily scavenged by particulate organic matter.

Phosphorus and Yttrium

Sediments under high productivity areas are known to contain elevated concentrations of biogenic and diagenetic phosphate [*Burnett*, 1977; *Froelich et al.* 1988]. Phosphates are known to concentrate the rare earth elements, such as Yttrium. Elevated P/Al and Y/Al ratios are therefore interpreted to reflect high surface water productivity conditions (Fig. 6).

Organic Carbon

The organic carbon content of sediments in areas of hemipelagic sedimentation should not be significantly influenced by continental organic matter. The input of terrigenous organic matter by the river Indus, and erosion of shelf sediments, however, could interfere with the marine organic carbon signal. Assuming a $\delta^{13}C_{org}$ value of -26‰ for terrigenous and of -20‰ for marine organic matter [*Fontugne and Duplessy*, 1986], then, we can calculate that 80% of

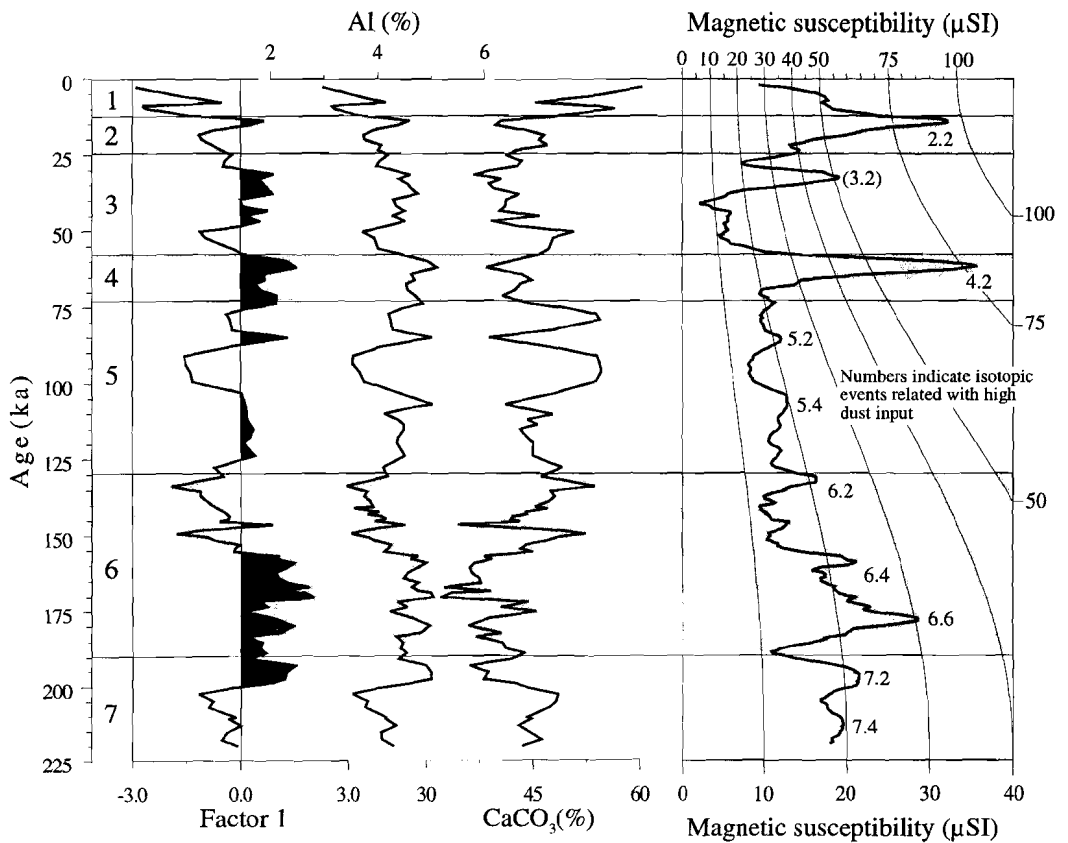


Fig. 4. Score plot of Factor 1 (dust input), Al(%), CaCO₃(%), and magnetic susceptibility (no dimension and plotted on a continuously changing scale). Periods of increased dust input are associated with glacials; highest dust input during maximum glacial conditions. Note perfect negative correlation between CaCO₃(%) and Al(%).

the organic carbon has a marine origin. Fig. 7 shows that the organic carbon in samples with maximum C_{org} is almost for 100% of marine origin. The $\delta^{13}\text{C}_{\text{org}}$ values, thus, indicate a negligible contribution of terrigenous organic matter. The absence of a 100 kyr frequency signal in the power spectrum of organic matter (see also Fig. 9B) indicates that the input of organic carbon from the shelf during glacio-eustatic sea level lowstands is negligible as well.

Fluctuations in C_{org} content are,

therefore, controlled by variations in marine-produced organic matter invoked either by increased surface water productivity or by enhanced preservation of the labile marine component. Fig. 8 shows that the C_{org} fluctuations reflect variations in surface water productivity since the C_{org} record correlates very well with the score plot for factor 2. Also the abundance pattern of *Globigerinoides bulloides*, being an indicator species for upwelling conditions in the Arabian Sea [e.g. *Prell et al.*, 1980; *Cullen and Prell*,

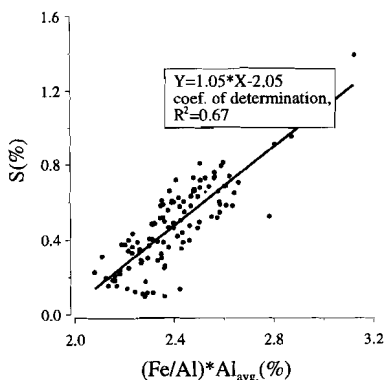


Fig. 5. Relationship between the sulphur- and iron content, normalized to aluminium (to correct for clay-derived iron). The S/Fe weight ratio of pyrite is 1.15, close to the slope of the correlation line ($R^2=0.67$).

1984; *Prell, 1984; Prell, 1993*], show strong covariance with the record of organic carbon (Fig. 8).

Percentages of *G. bulloides* and scores of factor 2 show highest values during interglacials indicating that average interglacial boundary conditions were more favourable for surface water productivity than glacial ones. C_{org} values, however, are not systematically higher in interglacials, possibly due to the opposite effect of higher glacial MAR's which are known to enhance the preservation of C_{org} [e.g. *Müller and Suess, 1979*]. C_{org} records from the northwestern Arabian Sea, for example, seem to be largely shaped by variations in dust input [*Murray and Prell, 1992; Shimmield, 1992; Prell et al., 1992*].

Shimmield [1992] suggested that co-varying values of planktonic foraminiferal $\delta^{18}O$ and Ba/Al in sediments from the northwestern Arabian Sea reflect the influence of global ice volume

on the nutrient supply. *Weedon and Shimmield* [1991] explained this by suggesting a link between continental aridity (dust record) and surface water productivity (Ba/Al record) via increased runoff and nutrient supply during wetter, interglacial periods. Runoff, however, cannot be used as an explanation for the co-varying pattern of surface water $\delta^{18}O$, Ba/Al, and $CaCO_3$ in NIOP464, because of the open ocean setting of the Murray Ridge region. We assert that the higher interglacial Ba/Al values and percentages of *G. bulloides* reflect increased upwelling.

The prominent C_{org} maximum at 140 ka is accompanied by a modest *G. bulloides* maximum and a minor peak in Ba/Al (cf. Figs. 6 and 8). The high C_{org} values (compared to modest numbers of *G. bulloides*) suggests an additional effect of enhanced C_{org} preservation, due to high MAR's at this time. Since the Ba content is a function of surface water productivity and water chemistry [*Dymond et al., 1992; Hermelin and Shimmield, 1995*] we hypothesize that the relatively low Ba/Al values at 140 ka reflect lower initial Ba/ C_{org} values due to reduced Ba-scavenging.

Dust input

Titanium is known to be concentrated in the coarser sediment fraction, particularly in the heavy mineral assemblage which often contains ilmenite, rutile, titanomagnetite and augite [*Schmitz, 1987*]. Since the Murray Ridge is a submarine ridge and thus beyond the reach of turbidity currents, variations in Ti/Al ratios result from

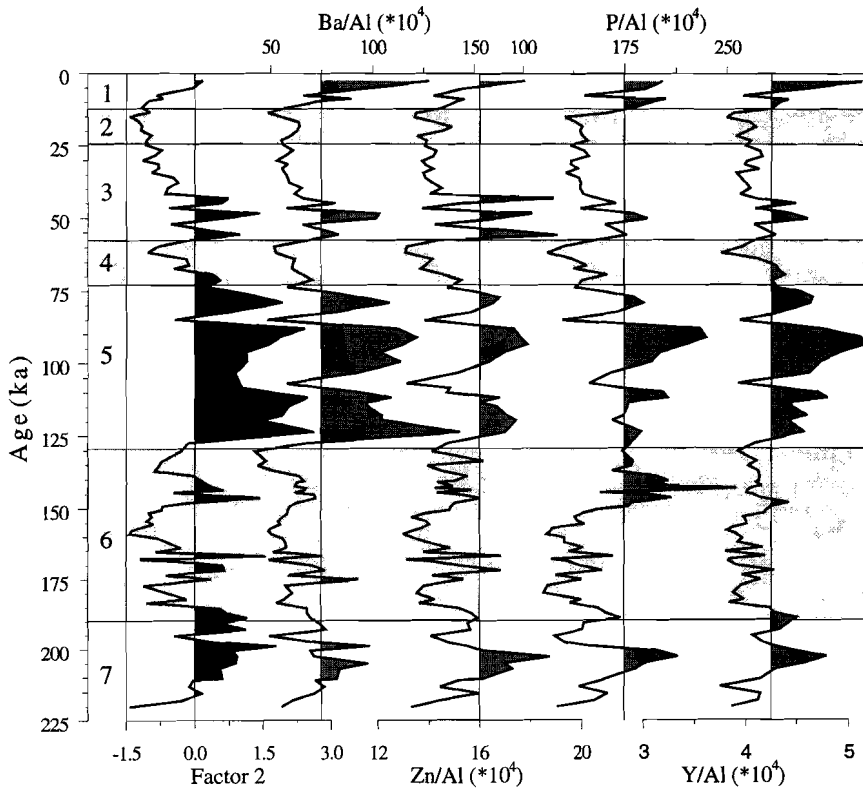


Fig. 6. Score plot of Factor 2 (paleoproductivity), Ba/Al, Zn/Al, P/Al and Y/Al.

changes in wind speed since that affects the grain-size and density distribution of (heavy) minerals [Weedon and Shimmiel, 1991]. The downcore record of Ti/Al (Fig.9A) shows a positive correlation with global ice volume, suggesting increased wind speed over the Murray Ridge region during glacials. Apart from wind speed, other factors, such as the availability of dust and the wind trajectory, are also of importance [Shimmiel and Mowbray, 1991]. A spectral analysis of the Ti/Al record of NIOP464 shows a strong forcing at the 100 and the 23 kyr frequency band (Fig.

9B), reflecting changes in glacial conditions (100 kyr) and precession (23 kyr). Interglacial Ti/Al values show a good correlation ($R^2=0.53$) with the C_{org} content of the sediment (Fig. 9C), and thus with productivity. Maxima in C_{org} content at ~50, ~75, ~90, ~115, and ~205 ka are all accompanied by higher Ti/Al values (Fig. 9A). These precession-related maxima in C_{org} (Fig. 9B) show no timelag with maxima in Ti/Al, suggesting that high interglacial Ti/Al values are related to maximum summer monsoonal wind strength, which also caused high surface water productivity.

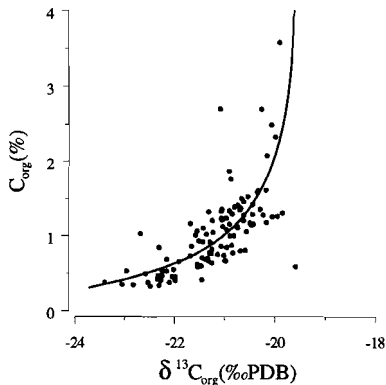


Fig. 7. Relationship between $\delta^{13}\text{C}_{\text{org}}$ and C_{org} content. Curve indicates general trend. With increasing organic carbon content the $\delta^{13}\text{C}_{\text{org}}$ (± 20 ‰ PDB) approaches marine values, while low organic carbon samples have values of ± 22 – 24 ‰, approaching those of continental organic matter [Deines, 1980].

The absence of a clear co-variance between glacial C_{org} and Ti/Al values (Fig. 9C) is attributed to an overall higher glacial wind speed over the Murray Ridge, which may have resulted from a different position of the ITCZ and increased winter monsoonal winds. The position of the ITCZ (= the region where the dust-laden Shamal winds override the south westerlies) affects the transport of dust to the Murray Ridge region. A migration of the ITCZ towards the southeast during the glacial summer monsoon may have increased the speed of the Shamal winds over the Murray Ridge, thus, contributing to increased dust input and to elevated Ti/Al values in this region. An increased winter monsoon, supplying dust from the Pakistan and Indian deserts might furthermore have contributed to the higher glacial Ti/Al values. The good correlation between

summer monsoon proxies and Ti/Al excludes a significant contribution from northern dust sources during interglacials (Fig. 9B and C).

An important dust component in the northern Arabian Basin is dolomite [Sirocko *et al.*, 1991]. Variations in the amount of dolomite rather than changes in the composition of the aluminosilicates are held responsible for changes in the Mg/Al ratio. The most striking feature in the Mg/Al record of NIO-P464 is the significant drop at the end of glacial stage 6 and to a lesser extent also at the end of stage 2 (Fig. 9A). This may very well reflect the effect that sea level has on the exposure of the Persian Gulf, which is an area of dolomite formation through the reaction of highly saline waters with calcite at the tidal salt flats (sabkhas) [Illings *et al.*, 1965]. A basinward migration of the sabkhas during falling sea level increases the area of dolomite deposition, which then can be transported by the Shamal winds from the desiccated Persian Gulf into the Arabian Basin. The abrupt change in the Mg/Al ratio at the end of stages 6 and 2 might reflect the reflooding of the Persian Gulf during deglaciation, cutting off the main source of airborne dolomite. The suggested relationship between glacio-eustatic sea level change and the Mg/Al ratio is reflected in the spectrum by a strong 100 kyr component (Fig. 9B).

The Zr/Al and K/Al records show an overall good correlation with the Mg/Al record (Fig. 9A). Zr/Al and K/Al values, however, are anomalously low compared to the Mg/Al values in the early part of stage 5. Since Zr/Al values are high ($\sim 30 \times 10^{-4}$; Shimmiel and Mowbray [1991]) in sediments off Oman,

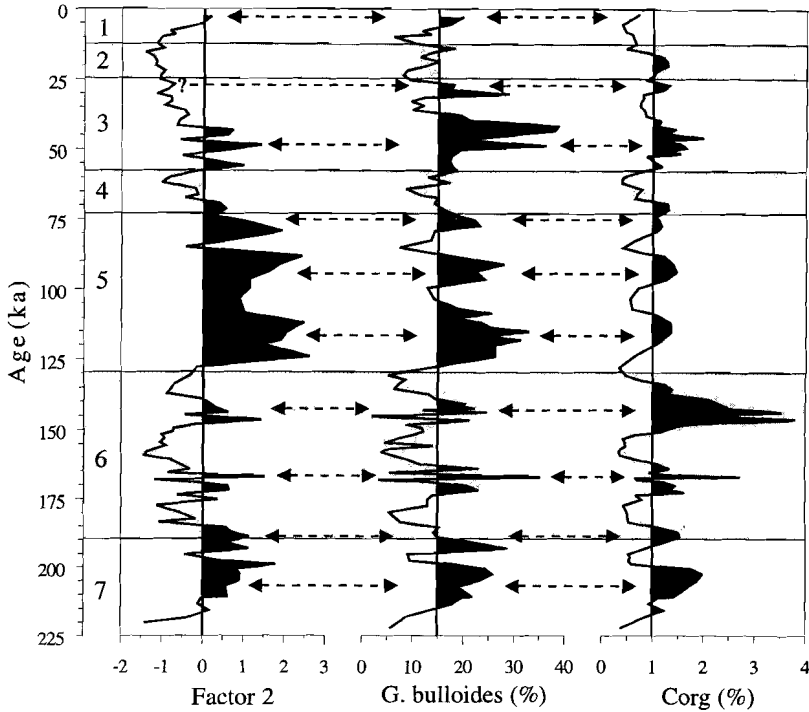


Fig. 8. Score plot of Factor 2, abundance pattern of *Globigerina bulloides*, and C_{org} content.

increased dust input by stronger northwestern winds (as indicated by increased Ti/Al values, Fig. 9A) cannot explain the early stage 5 anomaly in Zr/Al values of NIOP464. NIOP cores from the Pakistan Margin show high Zr/Al values ($\sim 15 \times 10^4$) in hemipelagic sediments and low ones ($\sim 2 \times 10^4$) in turbidites. The early stage 5 anomaly in the Zr/Al values of NIOP464 coincides with an interval of major turbidite sedimentation at the Pakistan Margin, probably caused by high Indus River runoff at that time. Part of the suspended load may have reached the Murray Ridge, thus, diluting the sediments with a

Zr/Al depleted component.

Shimmield et al. [1990] used the phase relationship between the Ti/Al ratio and $CaCO_3$ content in northwestern Arabian Sea sediments to unravel the relationship between continental aridity and heavy mineral transport. They suggested that continental aridity and wind strength together control dust transport in the region. The Mg/Al record of NIOP464, however, suggests that dust input in the Murray Ridge area is also controlled by sea level since the Persian Gulf would be a major source for Mg during low stands of sea level.

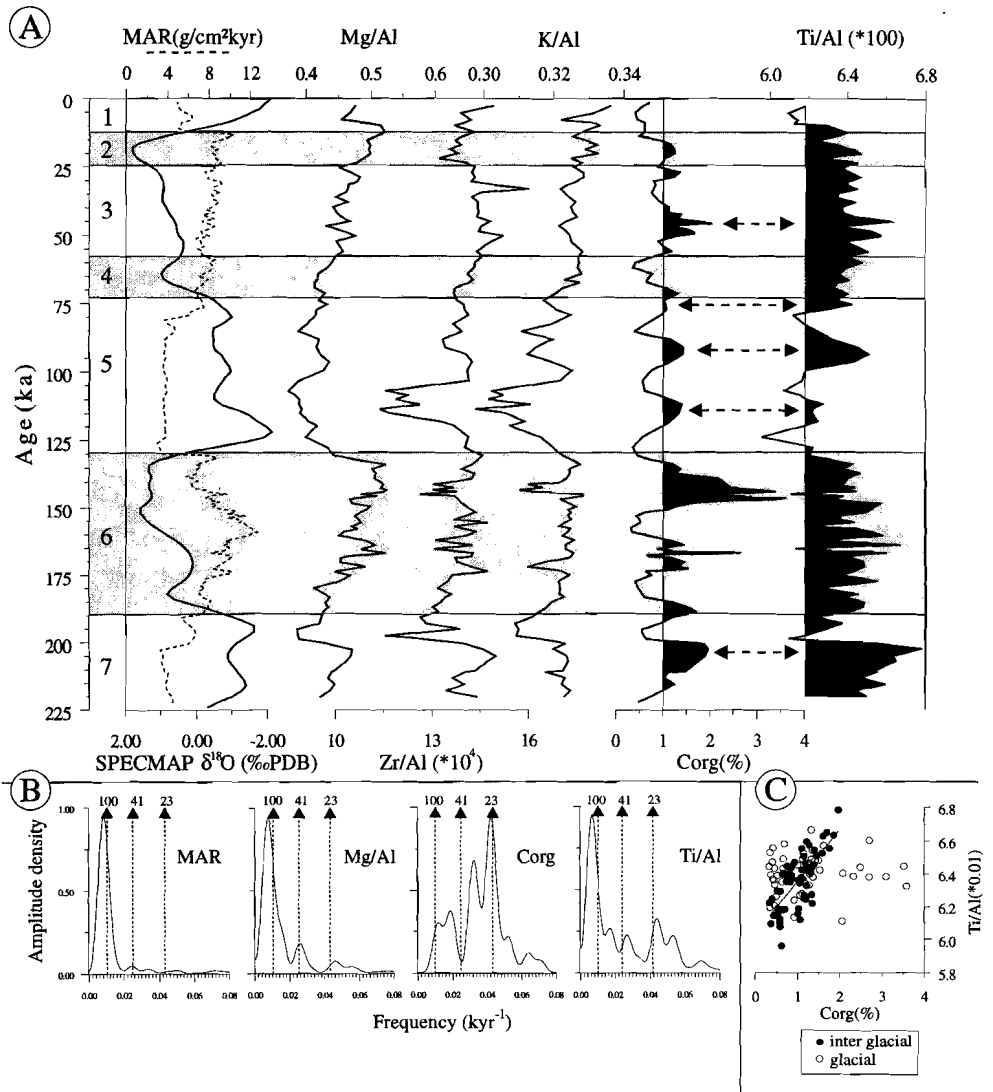


Fig. 9. A) Ti/Al, Mg/Al, Zr/Al, K/Al and MAR. The SPECMAP $\delta^{18}\text{O}$ record is plotted to indicate glacial boundary conditions. B) Spectra of the MAR and Mg/Al are dominated by 100 kyr (ice volume) periodicity, C_{org} spectrum is dominated by the 23 kyr (low latitude insolation) periodicity, while Ti/Al spectrum shows 100 kyr and 23 kyr periodicities. C) Relationship between C_{org} and the Ti/Al ratio. Correlation coefficient (R^2) is 0.53 for glacial samples (●) and 0.01 for interglacial samples (○). Line indicates interglacial trend.

CaCO₃ dissolution and the intensity of the OMZ

CaCO₃ values are on the average higher during interglacials and during periods of high surface water productivity when dust supply is reduced because of wetter conditions in the dust source regions. Correlation between CaCO₃ and surface water productivity, however, is not perfect as shown by the absence of a CaCO₃ maximum during surface water productivity peaks at 120, 140, and 170 ka (Fig. 10).

The absence of a CaCO₃ maximum during these three periods of increased productivity might be the result of increased CaCO₃ dissolution. Although NIOP464 (1470 m) is located well above the presentday lysocline (3000 m), dissolution of CaCO₃ can occur even as the overlying water is supersaturated with respect to calcite. Release of CO₂ during oxic decomposition of organic matter below the sediment-water interface can result in supralysocline CaCO₃ dissolution [Morse and Mackenzie, 1990] as long as bioturbation prevents the build-up of HCO₃⁻. For instance, the CaCO₃ content in the interval that centres at 120 ka appears to be at least 15% lower than expected, 45% instead of 60% based on the overall pattern (Fig. 10). This implies that, assuming a constant terrestrial input, 27.3 g [(1-0.40/0.55)×100g] of 60 g CaCO₃ must have dissolved. To dissolve this amount of CaCO₃ about 12/100 (molecular weights C_{org}/CaCO₃) × 27.3 = 3.27 wt% C_{org} has to be decomposed directly below the sediment water interface. The drop in the ratio planktonic/ benthic foraminifers

(=P/P+B) (Fig.10) indeed suggests a significant loss of CaCO₃ at ~120 ka since planktonic foraminifers are more prone to dissolution than benthic foraminifers. Planktonic foraminiferal densities also indicate a relative loss at ~120 ka since values are higher above and below (Fig. 10). If CaCO₃ dissolution would be responsible for this drop in planktonic foraminiferal densities, then ~95% of the planktonic foraminiferal tests must have been dissolved. This is not very likely in view of the presence of dissolution-prone planktonic foraminiferal species and glossy benthic foraminifers, while foraminiferal fragments are not significantly increased.

Alternatively one may argue that the pelagic carbonate production, including the planktonic foraminifers, decreased. It is known from off Oregon and off southwest Africa [Ortiz and Mix, 1992; Hays and Brock, 1992], and suggested for Mediterranean sapropels [Van Os *et al.*, 1994], that increased surface water productivity favours the flourishing of organic-walled and siliceous organisms. Sediments underlying such high-productivity areas are characterized by a high silica and organic carbon content [e.g. Broecker and Peng, 1982]. The missing carbonate peak at ~ 120 ka, therefore, seems the result of decreased pelagic carbonate production and increased supralysocline dissolution during a period of high surface water production. A more or less similar explanation may hold for the inverse correlation between C_{org} and CaCO₃ at 140 and 170 ka (Fig. 10).

Since aragonite is more soluble than calcite, pteropod shells (made up of

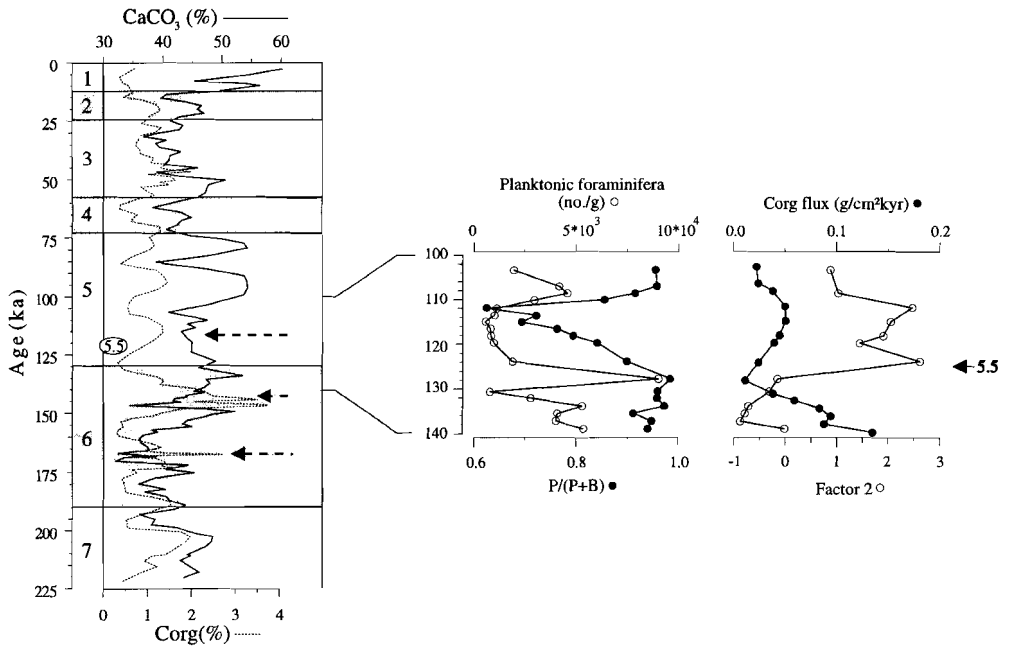


Fig. 10. $\text{CaCO}_3(\%)$ in NIOP464 compared with the $\delta_{13}\text{C}_{\text{org}}$ record. Planktonic foraminifers per gram, $\text{P}/(\text{P}+\text{B})$, C_{org} flux, and scores of factor 2 during the high productivity period at ~ 120 ka.

aragonite) dissolve rapidly when sinking through the CO_2 -rich water of OMZ. The regional aragonite compensation depth (ACD), therefore, lies in the middle of the OMZ at about 500 m [Berger, 1977] preventing pteropod deposition at site NIOP464. Preservation of pteropod shells at this site thus requires a substantial lowering of the ACD. We believe that variations in the number of pteropod shells in NIOP464 should be attributed to changes in the CO_2 -content of the OMZ. Figure 11 shows that variations in the pteropod preservation index are nicely reflected in the Sr/Ca record due to the fact that aragonite has higher Sr values compared to calcite [Sutherland *et al.*, 1984]. Diagenetic overprinting is very unlikely to have

affected the Sr/Ca-ratio because of the shallow depth of the core. Significant is that high Sr/Ca and pteropod preservation index values are associated with low C_{org} values in glacial intervals (Fig. 11). This suggests that glacial periods of low surface water production were characterized by a substantially deeper ACD and, thus, by a weakened OMZ.

If high Sr/Ca and pteropod preservation values reflect periods of a weakened OMZ, then, this should be recorded by the redox sensitive elements as well. Manganese is such a redox sensitive element because under suboxic conditions Mn(IV) is reduced to the soluble Mn(II) state. The Mn/Al ratio, thus, can be used for tracing variations in

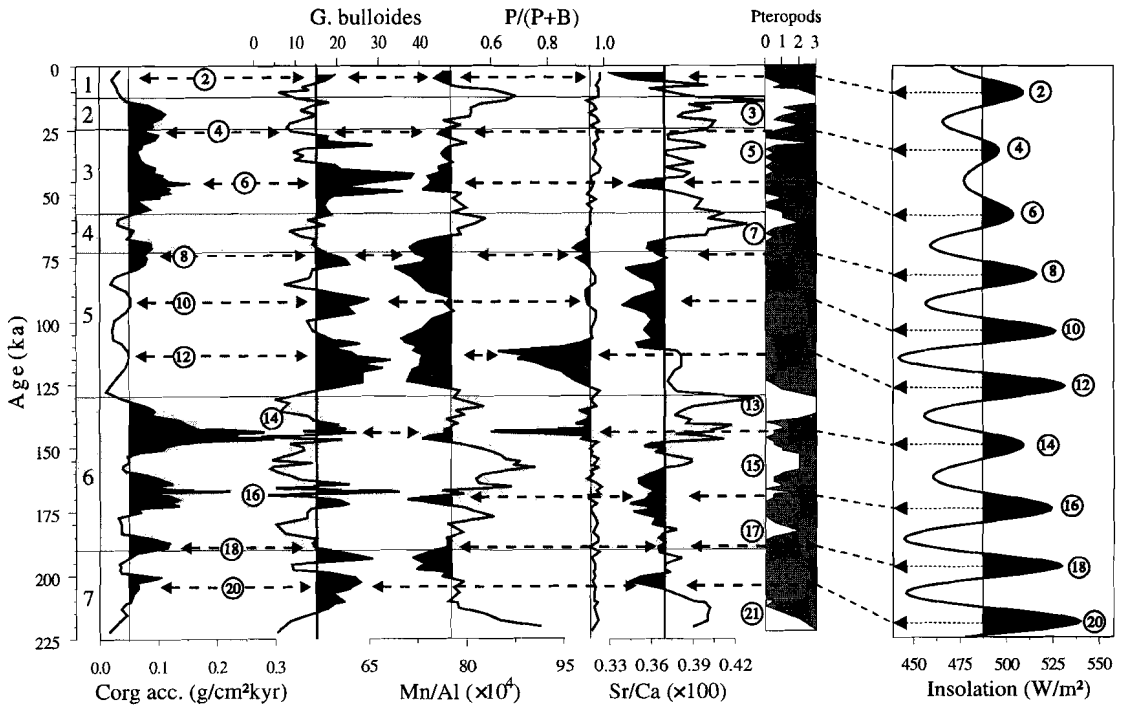


Fig. 11. C_{org} accumulation, percentages of *Globigerina bulloides*, Mn/Al ratio, P/(P+B) ratio, Sr/Ca ratio and pteropod preservation index in NIOP464 compared with summer insolation at 35°N [Laskar *et al.*, 1993]. High productivity periods are indicated in black and show a one to one correlation with maximum northern summer (June) insolation, although with a time lag of ~10 kyrs (coherency between insolation and C_{org} at the precession frequency is 0.97 with a phase lag of $160.3 \pm 44.7^\circ (=10.2 \pm 2.9$ kyrs). Precession minima (=northern summer (June) insolation maxima) correspond with high productivity periods, which are numbered (from the Recent) after the correlative precession minimum. Odd numbers indicate periods with low productivity, better pteropod preservation, higher Mn/Al values, and a weakened OMZ.

bottom-water oxygen, being low in sediments deposited under low oxygen conditions. Figure 11 shows that average Mn/Al values are distinctly lower during interglacials, which fits the overall poor pteropod preservation during these periods. Mn/Al values are also low during periods of increased productivity (even numbers in Fig. 11). This suggests a more intense OMZ and a shallow ACD during periods of high surface water production, especially under interglacial conditions. This conclusion is in line

with the overall higher interglacial foraminiferal fragmentation in the northwestern Arabian Sea [Steens *et al.*, 1991; Bassinot *et al.*, 1994; Ten Kate *et al.*, 1994].

High glacial Sr/Ca and pteropod preservation values on the other hand are associated with low C_{org} and high Mn/Al values and would reflect periods with a weakened OMZ and a deep ACD. This agrees well with depleted Cd/Ca values at intermediate depths during the last glacial maximum [Boyle *et al.*, 1995].

The connection between low (high) surface production and weak (strong) OMZ indicates that variations in the intensity of the OMZ are controlled by mid-water oxygen consumption rates, although changes in mid-water oxygen advection cannot be completely disregarded.

Discussion

The various surface water productivity records show a strong variability on the precession frequency band (Fig. 9B) with maximum productivity occurring ~10 kyrs after maximum summer (June) insolation at 35°N (being the average latitude of the central Asian low pressure cell during the northern summer) (Fig. 11). A similar large phase lag of ~9 kyrs between productivity and maximum northern summer (June) insolation is shown for the northwestern Arabian Sea [Shimmield *et al.*, 1990; Clemens and Prell, 1991; Murray and Prell, 1992]. The productivity record from the Murray Ridge is, therefore, in phase with that from the northwestern Arabian Sea. Evidence for an inverse relation between summer and winter monsoonal activity has been provided by a.o. Emeis *et al.*, 1995. This implies that surface water productivity in the Murray Ridge region is primarily controlled by nutrients supplied from the northwestern Arabian Sea upwelling area, being high during periods of an intensified summer monsoon.

Clemens and Prell [1991] explained the large phase lag of ~9 kyrs between maximum productivity (inferred from maximum percentages of *G. bulloides*)

and maximum northern summer (June) insolation by assuming that maximum cross-equatorial latent heat transport (maximizing summer monsoon strength) occurred ~9 kyrs after the precession minimum. Maximum cross-equatorial latent heat transport has been connected to lower sea surface temperatures (SST's) and stronger winds in the southern hemisphere during minimum (June) insolation [Clemens *et al.*, 1990; 1996].

Supporting evidence for the proposed link between cross-equatorial latent heat transport and summer monsoon intensity may be found in the prominent mid-stage 3 productivity peak in the northwestern Arabian Sea [Prell, 1984; Murray and Prell, 1992; Hermelin and Shimmield, 1995; Emeis *et al.*, 1995] and concomitant low SST in the southeast Arabian Sea near the equator [Rostek *et al.*, 1993]. These low SST's must reflect surface water cooling, which may have affected temperatures south of the equator as well, thus, providing the conditions required for increased cross-equatorial latent heat transport and summer monsoonal winds during mid-stage 3.

Increased cross-equatorial latent heat transport and an intensified summer monsoon during southern summer minimum insolation [Clemens *et al.*, 1996], however, would result in increased rainfall over Tibet and northwestern India due to latent heat release. The youngest southern summer insolation minimum at 1 ka [Laskar *et al.*, 1993], however, is not characterised by increased rainfall. Reconstructions of precipitation from lake records in Tibet and northwest India consistently show

that maximum precipitation occurred between 10 and 6 ka [Bryson and Swain, 1981; Swain *et al.*, 1983; Gasse *et al.*, 1991; Gasse and Van Campo, 1994]. This wet period was followed by a drier conditions from ~4 ka to Recent. This discrepancy between model and geological evidence indicates that the large phase lag between northern summer (June) insolation and surface water productivity in the Arabian Sea is still poorly understood. This problem is presently the subject of a study on the phase-relationships between various proxy records in a number of cores collected during the Netherlands Indian Ocean Programme across the northern Arabian Sea from east to west.

Conclusions

1) The organic carbon record from the Murray Ridge is primarily controlled by surface water productivity. The input of organic matter from the shelf and adjacent continent is negligible.

2) The surface water productivity record from the Murray Ridge is in phase with that from the upwelling regions in the northwestern Arabian Sea, which indicates that productivity in the Murray Ridge region is primarily driven by the summer monsoon. The large phase lag of ~10 kyrs between maximum surface water productivity and northern summer (June) insolation is still poorly understood.

3) Aragonite preservation seems controlled by the intensity of the OMZ, thus, providing a proxy for portraying the history of the OMZ. It has been shown that the intensity of the OMZ varied

significantly over the past 225 kyrs being extremely weak during glacial periods of reduced summer monsoon.

4) Supply of dolomite dust to the Murray Ridge region is controlled by sealevel, being low during glacio-eustatic high stands when the areal extent of tidal salt flats (sabkhas) in the Persian Gulf is small. These sabkhas are presently sites of dolomite formation and thus a potential source for dolomite dust.

Acknowledgements

This research was carried out during the execution of a joint Dutch-Pakistan marine geosciences programme as part of the Netherlands Indian Ocean Programme 1992-1993. The Government of the Republic of Pakistan granted permission to carry out research in the Pakistan EEZ. We thank the director and our colleagues G.M. Memon, A.R. Tabrez and A.A. Khan of the National Institute of Oceanography, Karachi, for their cooperation. Chief scientist of our cruise was W.J.M. van der Linden. The collection of the material would not have been possible without the professional help of crew and technicians of the R.V. Tyro. Thanks are also due to G. Ypenburg and F. Slangen for analytical support, and to G. Nobbe, A. van Dijk, P. Anten, G.J. van het Veld and G. Ittman for laboratory support. The constructive reviews by G. Shimmiel and F. Sirocko significantly improved the manuscript. This research was partly funded by the Netherlands Organization for Scientific research (NWO) and SHELL (contract no.11107072-epr).

References

- Banse, K., Seasonality of phytoplankton chlorophyll in the central and northern Arabian Sea. *Deep-Sea Res.*, 34, 713-723, 1987.
- Bassinot, F.C., Beaufort, L., Vincent, E., Labeyrie, L.D., Rostek, F., Muller, P.J., Quidelleur, X. and Y. Lancelot, Coarse fraction fluctuations in pelagic carbonate sediments from the tropical Indian Ocean: A 1500-kyr record of carbonate dissolution. *Paleoceanography*, 9, 579-600, 1994.
- Berger, W.H., Deep-sea carbonate: pteropod distribution and the aragonite compensation depth. *Deep Sea Res.*, 25, 447-452, 1977.
- Berner, R.A., Sulphate reduction and the rate of deposition of marine sediments. *Earth and Planet. Sci. Lett.*, 37, 492-498, 1978.
- Bishop, J.K.B., The barite-opal-organic carbon association in oceanic particulate matter. *Nature*, 331, 341-343, 1988.
- Boyle, E.A., Labeyrie, L. and J. Duplessy, Calcitic foraminiferal data confirmed by cadmium in aragonitic *Hoeglundina* : Application to the last glacial maximum in the northern Indian Ocean. *Paleoceanography*, 10, 881-900, 1995.
- Brock, J.C., McClain, C.R., Anderson, D.M., Prell, W.L. and W.W. Hay, Southwest monsoon circulation and environments of recent planktonic foraminifera in the Arabian Sea. *Paleoceanography*, 7, 799-813, 1992.
- Broecker, W.S. and T.H. Peng, *Tracers in the sea.*, Eldigio, New York, 690 pp, 1982.
- Burnett, W.C., Geochemistry and origin of phosphorite deposits off Peru and Chile. *Geol. Soc. Am. Bull.*, 88, 813-823, 1977.
- Bryson, R.A. and A.M. Swain, Holocene variations of monsoon rainfall in Rajasthan. *Quat. Res.*, 16, 135-145, 1981.
- Canfield, D.E., Sulfate reduction and oxic respiration in marine sediments: implications for organic carbon preservation in euxinic environments. *Deep-Sea Res.*, 36, 121-138, 1989.
- Clemens, S.C. and W.L. Prell, Late Pleistocene variability of Arabian Sea summer monsoon winds and continental aridity: eolian records from the lithogenic component of deep-sea sediments. *Paleoceanography*, 5, 109-145, 1990.
- Clemens, S.C. and W.L. Prell, One million year record of summer monsoon winds and continental aridity from the Owen Ridge (site 722), Northwest Arabian Sea. in *Proc. Ocean Drill. Program, Sci. Results.*, Vol. 117, (Eds. W.L. Prell and N. Niitsuma), 365-388. Ocean Drilling Program, College Station Tex., 1991.
- Clemens, S.C., Prell, W., Murray, D., Shimmield, G.B. and G. Weedon, Forcing mechanisms of the Indian Ocean monsoon. *Nature*, 353, 720-725, 1991.
- Clemens, S.C., Murray, D.W. and W.L. Prell, Nonstationary phase of the Plio-Pleistocene Asian Monsoon. *Science*, 274, 943-948, 1996.
- Codispoti, L.A., Primary productivity and carbon and nitrogen cycling in the Arabian Sea. In *U.S. JGOFS: Arabian Sea Process Study* (Eds. S.L. Smith, K. Banse, J. K. Cochran, L.A. Codispoti, H.W. Ducklow, M.E. Luther, D.B. Olson, W.T. Peterson, W.L. Prell, N. Surgi, J.C. Swallow & K. Wishner), U.S. JGOFS Planning Report No. 13., 1991.

- Cullen, J.L. and W.L. Prell, Planktonic foraminifera of the northern Indian Ocean: distribution and preservation in surface sediments. *Mar. Micropaleontol.*, 9, 1-52, 1984.
- Davis, J.C., *Statistics and data analysis in geology, second edition.*, John Wiley & Sons, New York., 646 pp, 1986.
- Dehairs, F., Chesselet, R. and J. Jedwab, Discrete suspended particles of barite and the barium cycle in the open ocean. *Earth Planet. Sci. Lett.*, 49, 528-550, 1980.
- Deines, P., The isotopic composition of reduced organic carbon. In : *Handbook of environmental isotope geochemistry. Vol. 1* (Eds. P. Fritz and J. Fontes) Elsevier, Amsterdam, 329-406, 1980.
- Demenocal, P., Bloemendaal, J. and J. King, A rock-magnetic record of monsoonal dust deposition to the arabian Sea: Evidence for a shift in the mode of deposition at 2.4 Ma. in *Proc.Ocean Drill. Program, Sci. Results.*, Vol. 117, (Eds. W.L.Prell and N.Niitsuma), 389-401.Ocean Drilling Programm, College Station Tex., 1991.
- Deuser, W.D., Ross, E.H. and Z.J. Mlodzinska, Evidence for and rate of denitrification in the Arabian Sea. *Deep-Sea Res.*, 25, 431-445, 1979.
- Dymond, J. Suess, E. and M. Lyle, Barium in deep-sea sediment: a geochemical proxy for paleoproductivity. *Paleoceanography*, 7, 163-181, 1992.
- Emeis, K.C., Anderson, D.M., Doose, H., Kroon, D. and D. Schutz-Bull, Sea-surface temperatures and the history of monsoon upwelling in the northwest Arabian Sea during the last 500,000 years. *Quat. Res.*, 43, 355-361, 1995.
- Findlater, J., Mean monthly airflow at low levels over the western Indian Ocean. *Geophys. Mem.*, 115, 53 pp, 1971.
- Froelich, P.N., Arthur, M.A., Burnett, W.C., Deakin, M., Hensley, V., Jahnke, R., Kaul, L., Kim, K.H., Roe, K., Soutar, A. and C. Vathakonon, Early diagenesis of organic matter in Peru continental margin sediments: Phosphorite precipitation. *Mar. Geol.*, 80, 309-343, 1988.
- Fontugne, M.R. and J.C. Duplessy, Variations of the monsoon regime during the upper Quaternary: evidence from carbon isotopic record of organic matter in north Indian Ocean sediment cores. *Palaeogeogr. Palaeoclim. Palaeoecol.*, 56, 69-88, 1986.
- Gasse, F., Arnold, M., Fontes, J.C., Fort, M., Gibert, E., Huc, A., Bingyan, L., Yuanfang, L., Qing, L., Melieres, F., Van Campo, E., Fubao, W. and Z. Qingsong, 13,000-year climate record from western Tibet, *Nature*, 353, 742-745, 1991.
- Gasse, F. and E. Van Campo, Abrupt post-glacial climate events in West Asia and North Africa monsoon domains, *Earth and Planet. Sci. Lett.*, 126, 435-456, 1994.
- Hays, W.W. and J.C. Brock, Temporal variation in intensity of upwelling off southwest Africa. In: *Upwelling Systems: Evolution Since the Early Miocene.* (Eds.C.P. Summerhayes, W.L. Prell & K.C. Emeis) Geological Society Special Publication No. 64, 463-497, 1992.
- Hermelin, J.O.R. and G.B. Shimmield, Impact of productivity events on the benthic foraminiferal fauna in the Arabian Sea over the last 150,000 years. *Paleoceanography*, 10, 85-116, 1995.
- Illings, L.V., Wells, A.J. and J.C. Taylor,

- Penecontemporary dolomite formation in the Persian Gulf. In: *Dolomitization and limestone diagenesis*, (eds. L.C. Pray & R.C. Murray), Society of economic paleontologists and mineralogists, Special Publication, No. 13, 89-111, 1965.
- Imbrie, J., Hays, J.D., Martinson, D.G., McIntyre, A., Mix, A.C., Morley, J.J., Pisias, N.G., Prell, W.L. and N.J. Shackleton, The orbital theory of Pleistocene climate: support from a revised chronology of the marine $\delta^{18}\text{O}$ record. In: *Milankovitch and Climate, Part I*, (Eds. A.L. Berger, J. Imbrie, J. Hays, G. Kukla, B. Saltzman), 269-305, Reidel Dordrecht, 1984.
- Karlin, R. and S. Levi, Geochemical and sedimentological control of the magnetic properties of hemipelagic sediments. *J. Geophys. Res.*, 90, 10,373-10,392, 1985.
- Kent, D.V., Apparent correlation of palaeomagnetic intensity and climatic records in deep-sea sediments. *Nature*, 299, 538-539, 1982.
- Kolla, V., Kostecky, J.A., Robinson, F., Biscaye, P.E. and P.K. Ray, Distributions and origins of clay minerals and quartz in surface sediments of the Arabian Sea. *J. Sediment. Petrol.*, 51, 563-569, 1981.
- Laskar, J., Joutel, F. and F. Boudin, Orbital, precessional, and insolation quantities for the Earth from -20Myr to +10Myr, *Astron. Astrophys.*, 270, 522-533, 1993.
- Martinson, D.G., Pisias, N.G., Hays, J.D., Imbrie, J., Moore Jr, T.C. and N.J. Shackleton, Age dating and the orbital theory of the ice ages: development of a high-resolution 0-300,000-year chronostratigraphy. *Quat. Res.*, 27, 1-29, 1987.
- Morse, J.W. and F.T. Mackenzie, Geochemistry of sedimentary carbonates, *Developments in Sedimentology*, 48, pp 707, Elsevier, New York, 1990.
- Muller, P.J. and E. Suess, Productivity, sedimentation rate, and sedimentary organic matter in the oceans-I. Organic carbon preservation. *Deep-Sea Res.*, 26A, 1347-1362, 1979.
- Murray, D.W. and W.L. Prell, Pliocene to pleistocene variations in calcium carbonate, organic carbon, and opal on the Owen Ridge, northern, Arabian Sea. In: *Proc. Ocean Drill. Program, Sci. Results.*, Vol. 117, (Eds. W.L. Prell and N. Niitsuma), 343-363. Ocean Drilling Program, College Station Tex., 1991.
- Murray, D.W. and W.L. Prell, Late Pleistocene climatic oscillations and monsoon upwelling recorded in sediments from the Owen Ridge, northwestern Arabian Sea. In: *Upwelling Systems: Evolution Since the Early Miocene*. (Eds. C.P. Summerhayes, W.L. Prell & K.C. Emeis) Geological Society Special Publication No. 64, 301-321, 1992.
- Olson, D.B., Hitchcock, G.L., Fine, R.A. and B.A. Warren, Maintenance of the low-oxygen layer in the central Arabian Sea. *Deep-Sea Res. II.*, 40, 673-685, 1993.
- Ortiz, J.D. and A.C. Mix, The spatial distribution and seasonal succession of planktonic foraminifera in the California Current off Oregon, September 1987-September 1988. In: *Upwelling Systems: Evolution Since the Early Miocene*. (Eds. C.P. Summerhayes, W.L. Prell & K.C. Emeis) Geological Society Special Publication No. 64, 197-213, 1992.
- Prell, W.L., Hutson, W.H., Williams, D.F., Be, A.W.H., Geitzenauer, K. and B. Molfino, Surface circulation of the Indian ocean during the Last Glacial Maximum,

- approximately 18,000 yr B.P.. *Quat. Res.*, 14, 309-336, 1980.
- Prell, W.L., Monsoonal climate of the Arabian Sea during the late Quaternary: a response to changing solar radiation. *Milankovitch and Climate*, (Eds. A. Berger, J. Imbrie, J. Hays, G. Kukla & B. Saltzman) Part I, 349-366. Reidel, Dordrecht, 1984.
- Prell, W.L. and E. Van Campo, Coherent response of Arabian Sea upwelling and pollen transport to late Quaternary monsoonal winds. *Nature*, 323, 526-528, 1986.
- Prell, W.L., Niitsuma, N., et al. *Proc. ODP, Sci. Results*, 117: College Station, TX (Ocean Drilling Program), 1990.
- Prell, W.L., Murray, D.W. and S.C. Clemens, Evolution and variability of the Indian Ocean summer monsoon: Evidence from the Western Arabian Sea Drilling Program. In: *Synthesis of results from scientific drilling in the Indian Ocean. Geophysical Monograph*, 70 (Eds. R.A. Duncan, D.K. Rea, R.B. Kidd, U. von Rad & J.K. Weissel) American Geophysical Union, Washington, 447-469, 1992.
- Prell, W.L., Variation of monsoonal upwelling: a response to changing solar radiation. *Climatic processes and climate sensitivity*, Vol. 29 (Eds. J.E. Hansen and T. Takahasi) American Geophysical Union. Geophys. Monogr. Ser., 48-57, Washington, D.C., 1993.
- Qasim, S.Z., Oceanography of the northern Arabian Sea. *Deep-Sea Res.*, 29, 1041-1068, 1982.
- Reichart, G.J., Prins, M.A. and H.J. Visser, Magnetic susceptibility, gamma ray transmissivity and XRF core-scanning. In: *Geological study of the Arabian Sea*. (Eds. W.J.M. van der Linden & C.H. van der Weijden) Netherlands Geosciences Foundation, The Hague, 97-115, 1994.
- Rostek, F., Ruhland, G., Bassinot, F.C., Müller, P.J., Labeyrie, L.D., Lancelot, Y. and E. Bard, Reconstructing sea surface temperature and salinity using $\delta^{18}\text{O}$ and alkenone records. *Nature*, 364, 319-321, 1993.
- Schmitz, B., The $\text{Ti}_2/\text{Al}_2\text{O}_3$ ratio in the Cenozoic Bengal abyssal fan sediments and its use as a paleostream energy indicator. *Mar. Geol.*, 76, 195-206, 1987.
- Shimmield, G.B., Mowbray, S.R. and G.P. Weedon, A 350 ka history of the Indian Southwest Monsoon--evidence from deep-sea cores, northwest Arabian Sea. *Trans. R. Soc. Edinburgh Earth Sci.*, 81, 289-299, 1990.
- Shimmield, G.B. and S.R. Mowbray, The inorganic geochemical record of the northwest Arabian Sea: A history of productivity variation over the last 400 k.y. from sites 722 and 724. in *Proc. Ocean Drill. Program, Sci. Results.*, Vol. 117, (Eds. W.L. Prell and N. Niitsuma), pp 409-429. Ocean Drilling Program, College Station Tex., 1991.
- Shimmield, G.B., Can sediment geochemistry record changes in coastal upwelling paleoproductivity? Evidence from northwest Africa and the Arabian Sea.-In: *Upwellings Systems: Evolution Since the Early Miocene* (Eds. C.P. Summerhayes, W.L. Prell & K.C. Emeis), Geol. Soc. Spec. Publ. Vol. 64, 29-46, 1992.
- Sirocko, F., Deep-Sea sediments of the Arabian Sea: a paleoclimatic record of the Southwest-Asian summer monsoon. *Geologische Rundschau*, 80/3, 557-566, 1991.

- Sirocko, F. and H. Lange, Clay mineral accumulation rates in the Arabian Sea during the late Quaternary. *Mar. Geol.*, 97, 105-119, 1991.
- Sirocko, F., Sarnthein, M., Lange, H. and H. Erlenkreuser, Atmospheric Summer Circulation and Coastal Upwelling in the Arabian Sea during the Holocene and the Last Glaciation. *Quat. Res.*, 36, 72-93, 1991.
- Sirocko, F. and V. Ittekkot, Organic carbon accumulation rates in the holocene and glacial Arabian Sea: implications for O₂-consumption in the deep-sea and atmospheric CO₂ variations. *Climate Dynamics*, 7, 167-172, 1992.
- Steens, T.N.F., Kroon, D., Ten Kate, W.G. and A. Sprenger, Late Pleistocene periodicities of oxygen isotope ratios, calcium carbonate contents, and magnetic susceptibilities of western Arabian Sea Margin hole 728A. In: *Proc.Ocean Drill. Program, Sci. Results.*, Vol. 117, (Eds. W.L.Prell and N.Niitsuma), 309-320. Ocean Drilling Programm, College Station Tex., 1991.
- Sutherland, H.E., Calvert, S.E. and R.J. Morris, Geochemical studies of the recent sapropel and associated sediment from the Hellenic outer ridge, eastern Mediterranean Sea. I: Mineralogy and chemical composition. *Mar. Geol.*, 56, 79-92, 1984.
- Swain, A.M., Kutzbach, J.E. and S. Hastenrath, Estimates of Holocene precipitation for Rajasthan, India, based on pollen and lake-level data. *Quat. Res.*, 19, 1-17, 1983.
- Swallow, J.C., Some aspects of the physical oceanography of the Indian Ocean. *Deep-Sea Res.*, 31, 639-650, 1984.
- Ten Kate, W.G.H.Z., Sprenger, A., Steens, T.N.F. and C.J. Beets, Late Quaternary monsoonal variations in the western Arabian Sea based on cross-spectral analyses of geochemical and micropalaeontological data (ODP Leg 117, core 728A). *Spec. Publs Int. Ass. Sediment.*, 19, 127-143, 1994.
- Thomson, P.R., Be, A.W.H., Duplessy, J.C., N.J. Shackleton, Disappearance of pink-pigmented Globigerinoides ruber at 120,000 yr BP in the Indian and Pacific Oceans. *Nature*, 280, 554-558, 1979.
- Turekian, K.K. and K.H. Wedepohl, Distribution of the elements in some major units of the earth's crust. *Geol. Soc. Am. Bull.* 72, 175-192, 1961.
- Van Bennekom, A.J. and M.A. Hiehle, CTD operations and calibrations during legs D1, D2 and D3 of the Netherlands Indian Ocean Programme. In: *Geological study of the Arabian Sea*. (Eds. W.J.M. van der Linden & C.H. van der Weijden) Netherlands Geosciences Foundation, The Hague, 37-66, 1994.
- Van Os, B.J.H., Middelburg, J.J. and G.J. De Lange, Possible diagenetic mobilization of barium in sapropelic sediments from the eastern Mediterranean. *Mar. Geol.*, 100, 125-136, 1991.
- Van Os, B.J., Lourens, L.J., Hilgen, F.J. and De Lange, Pliocene sapropel formation in the eastern Mediterranean: Dilution, dissolution and productivity. *Paleoceanography*, 9, 601-617, 1994.
- Von Breymann, M. T., Emeis, K. C. and E. Suess, Waterdepth and diagenetic constraints on the use of barium as a paleoproductivity indicator. In: *Upwellings Systems: Evolution Since the Early Miocene* (Eds. C.P. Summerhayes, W.L. Prell and K.C. Emeis), Geol. Soc. Spec. Publ. Vol. 64, 273-284, 1992.

Von Stackelberg, U., Faziesverteilung in Sedimenten des indisch pakistanischen Kontinentalrandes. *"Meteor" Forschungs Ergebnisse*, C9, 1-73, 1972.

Weedon, G.P. and G.B. Shimmiel, Late Pleistocene upwelling and productivity variations in the Northwest Indian Ocean deduced from spectral analyses of geochemical data from sites 722 and 724. In: *Proc.Ocean Drill. Program, Sci. Results.*, Vol. 117, (Eds. W.L.Prell and N.Niitsuma), 431-443.Ocean Drilling Programm, College Station Tex., 1991.

Wyrcki, K., Oceanographic atlas of the international Indian Ocean expedition, 531pp, 1971

Wyrcki, K., Physical Oceanography of the Indian Ocean. in: *The Biology of the Indian Ocean.*(ed. B. Zeitschel), 18-36, Springer-Verlag, NewYork, Heidelberg, Berlin, 1973.

You, Y. and M. Tomczak, Thermocline circulation and ventilation in the Indian Ocean derived from water mass analysis. *Deep-Sea Res. I*, 40, 13-56, 1993.

Sample	Depth (cmbsf.)	age kyr B.P.	sed. rate cm/kyr	MAR g/cm kyr	water (%)	WBD (g/cm ³)	Al (wt %)	Ba (ppm)	Be (ppm)	Ca (wt %)	Fe (wt %)	K (wt %)	Mg (wt %)	Mn (ppm)	P (ppm)	S (wt %)	Sr (ppm)	Ti (ppm)	Y (ppm)	Zn (ppm)	Zr (ppm)	
1	1494	222	3.51	4.50	30.22	1.84																
2	1487	220	3.51	4.51	30.65	1.85	4.30	239	1.27	18.89	2.13	1.39	1.82	394	539	0.309	737	0.280	16.6	57.2	62.1	
3	1479	218	3.51	3.98	33.05	1.76	4.08	249	1.23	19.85	2.40	1.33	1.78	348	624	0.716	795	0.263	16.8	58.6	54.9	
4	1470.5	216	3.51	3.84	35.15	1.73	4.07	291	1.23	19.24	2.39	1.31	1.81	337	661	0.677	771	0.268	16.8	64.9	56.9	
5	1462	213	3.51	3.99	34.51	1.74	4.34	333	1.29	18.69	2.52	1.40	1.89	342	613	0.630	752	0.281	16.3	62.7	59.3	
6	1454.5	211	3.51	4.08	33.98	1.69	4.16	300	1.27	19.32	2.30	1.32	1.83	327	660	0.497	771	0.272	16.9	63.0	58.4	
7	1453	211	3.51	3.75	36.59	1.68	4.16	343	1.27	19.12	2.53	1.34	1.84	321	666	0.793	748	0.272	17.2	67.0	59.6	
8	1440.5	207	3.51	3.43	37.81	1.61	3.77	318	1.18	20.22	2.32	1.22	1.74	298	689	0.738	760	0.251	16.2	65.1	55.5	
9	1433.5	205	3.51	3.59	38.74	1.67	3.82	373	1.18	20.59	2.27	1.24	1.79	298	725	0.682	753	0.253	17.4	64.7	57.2	
10	1425	203	3.51	3.30	38.69	1.50	3.53	253	1.12	20.58	2.32	1.13	1.66	281	754	0.910	708	0.239	16.9	66.1	51.8	
11	1418	201	5.73	6.01	37.71	1.63	4.02	280	1.27	19.11	2.38	1.30	1.74	307	798	0.727	673	0.263	18.0	64.9	56.2	
12	1408	199	5.73	6.47	34.57	1.69	4.64	458	1.48	18.57	3.13	1.47	1.81	356	682	0.952	695	0.283	19.7	72.0	59.3	
13	1401	198	5.73	6.65	33.29	1.66	5.00	364	1.51	16.96	2.60	1.55	1.94	362	656	1.139	626	0.310	20.9	74.0	57.7	
15	1387.5	195	5.73	6.53	33.12	1.71	5.00	248	1.47	17.20	2.50	1.55	1.94	368	618	1.152	637	0.315	20.3	70.4	69.3	
17	1375	193	5.49	5.89	35.69	1.75	4.90	378	1.49	16.15	2.96	1.52	2.06	352	705	0.517	617	0.312	21.2	76.5	62.8	
19	1362.5	191	5.49	5.36	39.43	1.61	4.39	325	1.35	18.30	2.66	1.38	1.86	326	636	0.600	670	0.274	19.4	68.1	55.5	
21	1349.5	189	7.61	7.55	40.11	1.59	4.53	317	1.43	19.13	2.75	1.43	1.93	349	719	0.586	698	0.291	20.4	72.1	59.8	
23	1336.5	187	7.61	7.97	38.65	1.63	4.43	301	1.39	17.99	2.77	1.41	1.93	342	774	0.704	665	0.287	19.0	69.3	57.7	
25	1323.5	185	7.61	7.93	39.10	1.68	4.47	304	1.40	17.79	2.69	1.43	1.92	344	695	0.728	650	0.290	18.9	68.0	59.4	
27	1308	183	6.24	7.22	33.07	1.95	4.35	230	1.32	16.29	2.35	1.40	1.90	345	585	0.404	601	0.270	16.7	59.2	58.3	
28	1301	182	6.24	7.15	34.79	1.82	4.80	272	1.51	17.84	2.54	1.55	2.06	379	685	0.386	675	0.318	19.1	68.3	65.3	
30	1286.5	180	6.24	7.58	30.90	1.71	4.97	301	1.53	16.09	2.58	1.60	2.05	383	573	0.338	581	0.311	19.3	67.2	65.5	
32	1270.5	177	6.24	7.67	31.40	1.84	4.66	268	1.42	17.11	2.39	1.50	2.10	392	550	0.236	622	0.305	18.4	64.2	62.8	
34	1256.5	175	8.83	8.91	37.96	1.66	4.24	393	1.33	19.62	2.58	1.37	1.98	344	607	0.682	680	0.270	17.5	65.0	57.8	
36	1243.5	174	8.83	10.18	33.36	1.73	4.55	269	1.36	17.75	2.61	1.47	2.02	363	565	0.549	646	0.293	18.0	64.3	67.0	
37	1235	173	8.83	8.41	39.80	1.64																
38	1228.5	172	8.83	8.77	40.17	1.60	4.37	335	1.42	19.22	2.56	1.37	2.15	327	691	0.629	662	0.283	18.7	73.4	62.2	
40	1214	170	8.83	9.48	36.77	1.69	5.04	356	1.55	14.52	2.93	1.60	2.28	357	713	0.668	517	0.326	19.7	76.2	69.4	
42	1200.5	169	8.83	10.05	34.56	1.73	4.99	265	1.51	15.14	2.75	1.62	2.27	383	661	0.514	543	0.321	19.1	70.7	68.5	
43	1195.5	168	8.83	10.22	33.43	1.79	4.77	235	1.42	17.25	2.46	1.55	2.20	379	578	0.371	618	0.305	18.3	62.5	67.8	
44	1190.5	168	8.83	9.86	33.06	1.67																
45	1185	167	8.83	8.22	40.66	1.49	4.65	350	1.49	14.58	3.41	1.51	2.43	354	771	1.392	529	0.307	19.4	78.0	66.3	
46	1179	166	8.83	9.13	37.26	1.59																
47	1172	165	8.83	9.78	33.90	1.74	4.76	244	1.52	16.70	2.65	1.54	2.31	413	638	0.466	596	0.292	18.1	65.6	62.2	
48	1165.5	165	8.83	9.95	33.56	1.70																
49	1159.5	164	8.83	9.41	36.13	1.68	4.48	259	1.41	16.51	2.70	1.45	2.27	367	646	0.732	580	0.299	18.6	66.4	63.8	
51	1144	162	8.83	9.60	35.54	1.62	4.56	263	1.39	16.13	2.75	1.49	2.25	372	597	0.757	566	0.287	17.9	64.1	59.8	
53	1128	161	9.81	11.87	32.15	1.79	4.77	268	1.44	16.09	2.50	1.54	2.15	394	622	0.432	575	0.314	18.9	64.0	67.1	
55	1113.5	159	9.81	12.70	29.93	1.78	4.90	248	1.42	16.40	2.39	1.59	2.25	423	576	0.225	598	0.320	19.1	63.6	70.4	
57	1101.5	158	9.81	12.14	30.92	1.82	4.62	227	1.40	17.24	2.51	1.50	2.21	419	557	0.479	638	0.298	17.6	61.7	64.4	
58	1093	157	9.81	11.70	31.01	1.70	4.75	237	1.41	16.88	2.44	1.53	2.23	414	577	0.374	645	0.294	18.3	64.9	65.0	
60	1078.5	156	9.81	10.95	35.41	1.75	4.13	226	1.27	19.36	2.36	1.33	2.00	364	599	0.601	753	0.265	16.5	57.7	60.7	
62	1068.5	155	9.81	10.98	34.82	1.69	4.19	225	1.27	18.75	2.28	1.36	2.01	360	587	0.486	729	0.266	16.8	58.1	57.3	
64	1054	153	9.81	11.52	33.85	1.70	4.24	237	1.29	19.09	2.39	1.38	2.02	362	586	0.599	714	0.270	16.9	56.5	59.7	
66	1040.5	152	9.81	10.61	37.47	1.65	3.95	230	1.19	20.05	2.18	1.28	1.91	331	570	0.519	728	0.256	16.5	54.7	56.7	
67	1035.5	151	9.81	10.46	38.27	1.56																
68	1029.5	151	9.81	9.47	41.09	1.59	3.83	224	1.20	20.64	2.22	1.24	1.89	316	589	0.578	765	0.250	16.1	56.7	54.3	
69	1024	150	9.81	8.76	42.60	1.54																
70	1018	149	9.81	8.41	43.42	1.55	3.50	210	1.06	22.11	1.99	1.14	1.75	281	621	0.575	785	0.229	14.9	52.1	49.3	
72	1006	148	9.81	8.32	43.41	1.54	3.81	239	1.15	20.30	2.14	1.24	1.79	297	688	0.605	731	0.250	16.8	57.2	53.0	
73	1000	148	9.81	9.04	43.77	1.53																
74	995	147	9.81	8.09	47.34	1.48																
75	990	147	9.81	8.29	45.89	1.44	4.51	325	1.38	15.30	2.75	1.45	2.11	330	942	0.811	631	0.285	18.7	72.3	62.2	
76	984.5	146	9.81	7.70	48.20	1.42																
77	977.5	145	9.81	8.15	46.46	1.47	3.95	282	1.23	18.59	2.32	1.30	2.01	294	761	0.805	740	0.252	16.1	60.3	54.1	
78	971	145	9.81	9.74	40.63	1.58	4.15	258	1.26	18.13	2.28	1.36	2.01	317	651	0.581	685	0.253	16.6	59.5	52.4	
79	962	144	9.81	7.99	48.12	1.51	4.07	272	1.29	18.20	2.30	1.28	2.12	312	909	0.717	738	0.262	16.3	63.7	56.1	
80	955.5	143	9.81	7.67	48.53	1.43	3.81	257	1.22	18.94	2.20	1.18	2.00	292	977		763	0.243	15.4	54.3	49.7	
81	948.5	142	7.56	6.60	42.89	1.53	4.02	250	1.30	18.95	2.34	1.27	2.07	312	836	0.730	778	0.259	16.7	60.1	54.9	
82	939	141	7.56	6.30	45.84	1.54	3.57	225	1.15	20.01	2.06	1.12	1.85	278	704		836	0.226	14.6	51.2	46.5	
83	935.5	141	7.56	6.40	46.16	1.48	3.92	261	1.23	19.44	2.19	1.26	2.03	309	811	0.659	749	0.250	16.2	58.8	52.8	
84	929.5	140	7.56	6.92	45.01	1.54																
85	923	139	7.56	6.47	46.75	1.49	3.86	248	1.19	20.14	2.13	1.25	1.95	297	760	0.609	782	0.247	16.0	59.9	55.0	
87	910	137	7.56	6.79	43.33	1.54	3.76	196	1.20	20.47	2.10	1.22	1.91	300	623	0.557	772	0.243	15.5	54.6	5	

Sample	Depth (cmbsf.)	age kyr B.P.	sed. rate cm/kyr	MAR g/cm kyr	water (%)	WBD (g/cm ²)	Al (wt %)	Ba (ppm)	Be (ppm)	Ca (wt %)	Fe (wt %)	K (wt %)	Mg (wt %)	Mn (ppm)	P (ppm)	S (wt %)	Sr (ppm)	Ti (wt %)	Y (ppm)	Zn (ppm)	Zr (ppm)
102	814	118	3.85	3.80	41.47	1.62	4.37	457	1.33	19.18	2.70	1.36	1.77	318	760	0.578	732	0.273	20.1	74.5	58.0
103	808	117	3.85	3.74	41.10	1.59															
104	802	115	3.85	3.70	41.40	1.58	4.49	440	1.42	18.81	2.78	1.38	1.76	328	794	0.647	718	0.279	20.0	74.7	52.3
105	796.5	114	3.85	3.58	41.07	1.63	4.48	433	1.51	19.75	2.68	1.33	1.77	329	795		754	0.279	19.8	71.5	51.0
106	790	112	3.85	3.72	40.98	1.59	4.37	477	1.37	19.16	2.57	1.37	1.70	314	903	0.492	726	0.274	20.9	73.3	55.2
107	783	110	3.85	3.60	42.43	1.60	4.11	388	1.31	20.46	2.28	1.24	1.61	298	835		718	0.254	19.3	60.5	48.9
108	777	108	3.85	3.75	41.47	1.61	4.49	330	1.41	19.17	2.53	1.37	1.72	317	772	0.488	670	0.276	19.4	66.5	55.1
109	771	107	3.85	3.99	38.43	1.59	5.01	292	1.59	18.11	2.72	1.52	1.87	351	747		655	0.304	19.7	65.9	57.9
111	757	103	3.85	3.99	38.13	1.65	4.41	408	1.34	20.67	2.25	1.42	1.72	323	726	0.153	734	0.272	20.4	66.6	62.4
113	742	99	4.22	3.56	45.95	1.48	3.75	426	1.15	22.78	2.17	1.22	1.60	281	730	0.396	822	0.232	17.7	61.4	52.9
115	729	96	4.22	3.63	44.43	1.68	3.66	379	1.11	23.03	2.19	1.17	1.60	286	734	0.523	818	0.235	18.0	62.0	52.2
117	717.5	94	4.22	3.66	45.05	1.49	3.53	405	1.14	22.94	2.16	1.10	1.49	271	778	0.581	780	0.230	18.2	63.0	49.6
119	707	91	4.22	3.86	43.34	1.61	3.56	432	1.14	22.77	2.16	1.12	1.48	276	834	0.546	791	0.230	18.2	62.5	47.7
121	694.5	88	4.22	3.74	42.93	1.56	4.06	455	1.33	20.32	2.46	1.30	1.71	300	934	0.657	740	0.257	19.2	70.4	54.1
122	689	87	4.22	4.18	47.21	1.58															
123	682	85	4.22	4.69	35.22	1.68	5.00	242	1.53	17.24	2.50	1.56	1.94	363	647	0.195	624	0.312	19.7	69.1	69.6
125	671	83	4.22	4.05	43.09	1.50	4.27	344	1.29	20.51	2.36	1.37	1.72	305	723	0.323	722	0.264	18.5	66.8	58.4
127	657	79	7.30	6.19	45.25	1.52	4.24	460	1.31	23.18	2.48	1.38	1.76	292	799	0.461	792	0.259	19.6	70.0	59.9
129	643	77	7.30	6.68	42.66	1.55	4.20	395	1.26	22.94	2.40	1.35	1.75	308	764	0.438	831	0.263	19.5	70.4	58.9
131	628.5	75	7.30	7.33	41.45	1.58	4.46	343	1.33	21.38	2.53	1.42	1.93	330	717	0.618	793	0.286	20.2	70.4	62.3
132	618	74	7.26	7.30	39.56	1.59	4.84	282	1.39	19.47	2.61	1.53	2.03	349	671	0.368	711	0.307	20.8	71.2	66.6
134	599	71	7.26	6.89	40.37	1.60	4.71	331	1.41	17.87	2.68	1.51	2.02	336	678	0.502	638	0.301	20.0	71.8	64.4
136	584.5	69	7.26	6.87	42.38	1.54	4.57	299	1.39	18.58	2.42	1.47	1.89	332	739	0.337	666	0.289	20.0	66.6	62.6
138	570	67	7.26	7.49	37.85	1.70	4.54	275	1.38	18.85	2.30	1.49	1.88	345	623	0.206	705	0.288	19.6	62.0	64.2
139	562	66	7.26	7.88	36.80	1.74	4.69	285	1.39	19.51	2.40	1.52	1.96	371	690	0.217	779	0.300	20.2	64.9	67.0
141	546.5	64	7.26	7.50	38.11	1.69	4.63	287	1.40	18.89	2.54	1.52	1.94	365	630	0.390	758	0.294	19.1	65.4	65.3
143	530.5	62	7.26	8.35	33.50	1.73	5.10	268	1.45	17.11	2.59	1.67	2.21	416	603	0.181	735	0.326	19.2	66.6	73.0
145	516	60	7.26	8.04	34.69	1.64	4.93	255	1.42	18.36	2.56	1.61	2.17	409	637	0.247	736	0.319	19.6	64.6	70.6
147	498.5	58	7.89	7.56	40.45	1.51	4.43	307	1.28	19.87	2.35	1.45	1.97	345	686	0.348	820	0.283	18.1	63.9	64.5
149	485	56	7.89	7.38	43.32	1.64	4.01	335	1.29	20.24	2.62	1.32	1.83	321	707	0.524	793	0.261	17.2	76.3	57.7
151	471.5	54	7.89	7.53	41.65	1.59															
152	465.5	53	7.89	7.23	42.51	1.71															
153	456.5	52	7.89	7.20	43.52	1.47	3.93	259	1.15	20.45	2.13	1.28	1.76	307	632	0.483	812	0.251	16.0	56.0	58.3
154	449	51	7.89	6.72	44.65	1.59															
155	440.5	50	8.95	8.00	45.32	1.60	3.72	379	1.15	21.54	2.09	1.21	1.77	295	712	0.467	828	0.245	17.1	62.2	56.6
156	433	49	8.95	7.35	46.17	1.60															
157	425.5	49	8.95	7.23	45.91	1.57	4.15	429	1.23	18.71	2.42	1.34	1.90	305	751	0.659	692	0.271	18.5	74.9	60.0
158	418	48	8.95	7.97	45.32	1.47															
159	409	47	8.95	8.53	41.35	1.56	4.52	262	1.34	17.17	2.33	1.45	1.94	336	643	0.371	590	0.287	18.5	62.0	65.6
160	400	46	8.95	7.80	48.16	1.45															
161	393	45	8.95	7.33	46.82	1.46	4.28	349	1.26	19.83	2.40	1.38	2.00	319	720	0.597	697	0.283	19.2	65.3	63.3
162	385.5	44	8.95	8.53	42.91	1.55															
163	378.5	43	8.95	7.87	45.07	1.52	4.51	297	1.30	17.68	2.49	1.47	2.05	334	699	0.588	678	0.290	18.5	85.1	64.8
164	371	42	8.95	7.42	45.89	1.46															
165	364	42	8.95	8.54	43.39	1.51	4.35	269	1.28	17.92	2.26	1.42	1.94	331	628	0.396	696	0.277	17.1	61.1	62.8
167	346	40	8.95	8.34	42.49	1.53	4.29	279	1.26	17.94	2.25	1.39	1.89	325	608	0.359	664	0.273	17.3	62.2	61.8
169	329.5	38	8.95	8.95	41.59	1.58	4.75	281	1.32	18.86	2.49	1.55	2.20	370	678	0.326	738	0.306	19.0	67.3	68.5
171	313.5	36	8.95	8.53	40.67	1.63	4.64	271	1.34	17.38	2.52	1.50	2.07	356	654	0.401	659	0.294	18.4	64.3	66.1
173	299	34	8.95	9.08	40.83	1.54	4.55	259	1.33	17.09	2.42	1.47	2.10	347	598	0.273	633	0.289	17.8	62.6	66.0
175	286	33	8.95	8.51	41.49	1.58	4.40	245	1.35	17.70	2.42	1.42	2.04	337	617	0.302	657	0.283	18.1	62.3	70.4
177	273	31	8.95	8.92	40.26	1.56	4.62	270	1.40	16.28	2.46	1.50	2.15	358	626	0.282	651	0.295	18.9	63.9	68.8
179	262	30	8.95	9.03	40.08	1.70	4.35	231	1.32	16.96	2.34	1.42	2.08	348	591	0.302	670	0.278	17.5	59.7	61.9
181	247	29	8.95	7.90	44.08	1.64	3.98	228	1.23	18.48	2.30	1.31	1.92	309	590	0.474	689	0.257	16.5	56.3	57.0
183	231	27	8.95	7.59	47.58	1.49	4.04	246	1.23	18.75	2.28	1.33	1.89	306	588	0.463	698	0.259	16.7	57.7	57.5
185	215	25	8.95	8.45	43.02	1.54	4.18	236	1.29	17.98	2.23	1.36	1.88	320	566	0.291	718	0.266	16.7	57.8	59.9
187	199	23	9.70	9.14	41.61	1.62	4.01	222	1.23	18.46	2.24	1.32	1.92	317	591	0.358	745	0.259	16.2	55.8	56.3
189	183.5	22	9.70	8.58	44.93	1.45	4.06	243	1.20	20.18	2.25	1.32	1.99	311	585	0.385	820	0.255	15.9	55.0	53.8
191	166	20	9.70	8.32	45.21	1.34	3.76	237	1.17	19.64	2.15	1.25	1.88	303	535	0.385	745	0.243	15.1	54.5	51.9
192	159	19	9.70	8.42	44.75	1.42															
193	152	18	9.70	8.83	43.74	1.33	3.75	241	1.17	19.89	2.08	1.23	1.86	303	539	0.259	763	0.241	15.3	55.7	50.8
194	144	18	9.70	8.18	45.79	1.49															
195	136	17	9.70	8.31	45.83	1.34	3.92	249	1.21	18.89	2.17	1.30	1.95	316	543	0.247	763	0.248	15.8	55.7	54.4
196	128	16	9.70	8.34	45.77	1.52															
197	120.5	15	9.70	9.07	45.61	1.55	4.38	244	1.30	17.40	2.35	1.44	2.16	360	574	0.175	674	0.273	16.7	58.8	60.1
198	112.5	14	9.70	9.68	39.10	1.57															
199	106.5	14	9.70	10.02	37.62	1.59	4.60	225	1.33	17.79	2.42	1.50	2.33	396							

Sample	Factor 1	Factor 2	Factor 3	C-org (wt %)	$\delta^{13}\text{C}_{\text{org}}$ (‰PPB)	$\delta^{13}\text{C}$ (‰PPB)	$\delta^{18}\text{O}$ (‰PPB)	G.bulloides (%)	tot.plankton (No./g)	tot.benthos (No./g)	pteropod fragment index
1				0.37	-23.40	-0.07	0.47	5.5	1291	61	3
2	-0.08	-1.43	0.78			-0.13	0.31				
3	-0.51	-0.29	-0.77	0.86	-21.67	0.05	0.11	8.7	3545	77	2
4	-0.37	0.14	-0.64	1.21		0.04	-0.20				
5	0.01	-0.12	-0.47	0.93	-21.52	-0.07	-0.09	17.7	5418	206	0
6	-0.33	-0.04	0.05	1.10		-0.06	-0.20	19.5	5065	117	0.5
7	-0.13	0.60	-0.89	1.41	-20.73	-0.19	-0.13	21.7	5448	200	0
8	-0.86	0.55	-0.95	1.70		0.02	-0.18	18.8	6134	219	0
9	-0.75	0.89	-0.42	1.87	-20.91	-0.09	-0.15	23.0	9761	305	0
10	-1.15	0.92	-1.90	1.97		0.04	-0.07	25.6	11823	498	0
11	-0.32	0.84	-1.02	1.76	-20.87	0.02	-0.01	24.3	8356	279	0
12	0.89	1.78	-0.95	0.58		0.62	-0.54	18.2	2800	112	0
13	1.23	0.46	1.56	0.53	-22.96	0.34	-0.58	9.5	2767	91	0
15	1.28	-0.45	1.53	0.53	-22.25	0.20	-0.31	9.1	5273	188	0
17	1.51	1.11	0.02	0.85	-22.32	0.34	-0.67	28.6	1885	87	0
19	0.29	0.58	-0.38	1.21	-21.25	0.46	-0.22	22.0	5456	100	0
21	0.71	1.13	-0.09	1.53	-20.54	0.53	-0.16	14.7	9074	511	0
23	0.56	0.71	-0.95	1.50	-20.66	0.40	-0.01	14.1	4489	112	0
25	0.62	0.55	-0.91	1.13	-21.04	0.48	0.02	15.1	5087	112	0.5
27	0.21	-1.06	-0.50	0.53	-22.16	0.25	0.24	7.5	4500	185	2
28	1.13	-0.19	0.51								
30	1.46	-0.60	0.55	0.49	-22.58	0.45	0.00	5.3	3903	96	0.5
32	0.93	-1.13	0.67	0.42	-22.35	0.53	-0.18	12.8	4697	159	0
34	0.13	0.35	-0.60	0.78	-21.30	0.39	-0.40	12.9	6417	309	0
36	0.75	-0.63	-0.33	0.66	-21.32	0.51	-0.33	13.8	4158	203	0
37				1.61							
38	0.55	0.64	-0.58	1.33	-21.07	0.17	-0.39	22.8	9814	275	0
40	2.04	0.60	-1.04	1.42	-20.45	0.24	-0.17	20.5	5393	309	0.5
42	1.81	-0.40	-0.62	1.21	-20.62	0.61	0.32	12.4	3438	205	0.5
43	1.10	-1.19	0.12	0.69	-22.16	0.73	0.44	3.3	2716	45	2
44				0.67							
45	1.93	1.51	-4.11	2.71	-21.08	0.35	-0.16	35.0	2965	84	0
46				1.32		0.48	0.06				
47	1.30	-0.85	-0.68	0.92	-21.44			5.4	3273	35	1
48						0.53	0.38				
49	1.07	-0.32	-1.58	1.32	-21.33	0.30	-0.07	22.9	3455	102	0.5
51	0.99	-0.57	-1.86	1.11	-20.75	0.75	0.24	11.6	3471	229	0.5
53	1.30	-0.82	-0.07	0.69	-21.39	0.71	0.26	8.8	3083	129	1
55	1.47	-1.43	0.82	0.35	-23.05	0.75	0.68	5.6	2291	113	2
57	0.98	-1.38	-0.44	0.33	-22.49	0.58	0.56	3.9	2420	47	2
58	1.08	-1.22	0.09	0.35	-22.83	0.37	0.56	4.7	2070	90	2
60	-0.19	-0.92	-0.69	0.46	-22.26	0.42	0.17	13.9	3634	105	2
62	-0.17	-1.05	-0.42	0.45	-22.05	0.66	0.34	4.4	2396	52	2
64	-0.04	-0.95	-0.71	0.42	-21.45	0.81	0.28	7.1	3405	166	2
66	-0.67	-1.00	-0.44	0.66	-20.97	0.81	0.31	10.2	4074	180	1
67						0.72	0.33				
68	-0.90	-0.74	-0.72	1.15	-20.46			12.0	4331	234	1
69						0.44	0.23				
70	-1.76	-0.72	-0.84	1.36	-20.30			11.8	10830	455	0.5
72	-0.99	-0.17	-0.75	1.62	-20.18	0.43	0.23	8.6	7821	184	0.5
73				1.91							
74				2.71							
75	0.88	1.41	-1.82	3.58	-19.90			21.1	1242	113	0
76				3.78							
77	-0.59	0.26	-1.78	2.70	-20.26			1.8	5211	282	0.5
78	-0.34	-0.45	-1.04	2.06							
79	-0.31	0.62	-1.65	3.52		0.11	0.20	24.4	1733	1158	0.5
80				3.10				11.9	4277	1251	1
81	-0.44	0.34	-1.51	2.49	-20.06	0.26	-0.19	22.1	3708	298	1
82								17.9	3890	246	0.5
83	-0.73	0.14	-1.31	2.33	-19.99			20.4	2662	297	0
84						0.03	0.12				
85	-0.91	-0.02	-0.90	2.08	-20.16	0.48	0.15	14.4	5344	344	2
87	-1.09	-0.88	-0.86	1.29	-20.45	0.56	0.28	13.0	4009	226	3
88						0.37	0.15				
89	-1.11	-0.79	-1.29	1.37	-20.68			6.3	4076	398	3
91	-1.92	-0.72	-1.33	1.24	-21.07	0.33	0.00	7.1	5279	153	3
92						0.68	0.35				
93				0.73	-21.69	0.23	0.29	8.4	2768	122	3
95	-0.49	-0.30	-0.74	0.46	-22.33	0.13	0.23	5.1	768	33	3
97	-0.73	-0.15	1.19	0.34	-22.31	0.60	-0.85	13.4	9001	146	1
99	0.40	2.61	2.17	0.62	-21.54	0.18	-1.30	26.1	1881	211	0
101	0.08	1.45	1.12	1.03	-22.69	0.41	-1.09	26.1	963	181	0

Sample	Factor 1	Factor 2	Factor 3	C-org (wt %)	$\delta^{13}\text{C}_{\text{org}}$ (‰PPB)	$\delta^{13}\text{C}$ (‰PPB)	$\delta^{18}\text{O}$ (‰PPB)	G.bulloides (%)	tot.plankton (No./g)	tot.benthos (No./g)	pteropod fragment index
102	0.24	1.91	0.40	1.17	-21.69	0.32	-1.11	31.1	827	214	0
103								24.6	801	249	0
104	0.36	2.05	-0.06	1.36	-21.05			32.9	563	248	0
105								25.0	990	380	0
106	0.18	2.47	0.82	1.34	-20.90			23.4	1100	661	0
107						0.72	-0.89	18.5	2958	499	0
108	0.16	1.03	0.21	1.01	-21.59	0.74	-0.45	25.4	4563	420	0
109						0.59		19.0	4167	181	0
111	0.04	0.88	2.29	0.55	-22.03	0.53	-0.65	14.1	1956	92	0
113	-1.33	1.14	1.07	0.70	-21.34	0.85	-0.72	12.8	7924	247	0
115	-1.39	1.13	0.52	1.24	-20.97	0.76	-0.68	24.0	5577	159	0
117	-1.54	1.62	0.29	1.46	-20.62	0.82	-0.42	22.2	5878	360	0
119	-1.56	1.87	0.43	1.39	-20.80	0.89	-0.37	27.8	10570	725	0
121	-0.33	2.41	-0.02	1.22	-21.05	1.00	-0.48	17.6	5632	322	0
122						0.77					
123	1.29	-0.43	1.26	0.40	-21.99	1.10	-0.20	7.3	4320	140	0
125	-0.25	0.71	0.98	0.64	-21.26			13.4	5003	163	0
127	-0.30	1.92	1.28	1.06	-21.56	0.89	-0.84	14.1	5070	266	0
129	-0.41	1.46	1.30	1.16	-20.90	0.90	-0.56	22.9	4473	322	0
131	0.24	0.88	1.10	1.10	-21.44	0.67	-0.55	21.9	1201	130	0
132	0.98	0.27	1.03	1.05	-21.24	0.83	-0.09	19.3	3122	204	0
134	0.99	0.55	0.15	1.29	-20.85	0.66	-0.14	15.8	2136	256	0
136	0.55	0.39	0.82	1.28	-20.62	1.21	0.27	14.1	9356	866	0
138	0.42	-0.46	1.45	0.64	-21.25	1.20	0.34	14.7	8240	454	0.5
139	0.67	-0.13	1.73	0.67	-20.99	0.96	0.30	11.3	3564	230	0
141	0.65	-0.20	0.87	0.77	-20.83	0.93	0.24	8.5	2992	178	0.5
143	1.56	-1.03	1.46	0.37	-22.53	0.74	0.41	17.1	1627	81	2
145	1.27	-0.81	1.25	0.40	-22.28	0.24	0.20	12.8	1989	106	1
147	0.10	-0.09	0.99	0.77	-21.27	0.67	-0.21	18.6	4296	228	1
149	-0.23	0.98	-0.09	1.16	-20.43	0.34	-0.27	17.6	3905	177	0
151				1.00	-20.89	0.78	-0.14	17.0	4261	266	0
152						0.94	-0.33				
153	-0.98	-0.52	0.07	0.86	-21.07	0.55	-0.38	17.5	3916	114	1
154						1.53					
155	-1.12	0.62	0.54	1.28	-20.23	0.50	-0.41	19.1	4922	314	0
156						1.64					
157	0.01	1.42	-0.29	1.59	-20.35	0.48	-0.32	36.0	4263	205	0
158						1.52					
159	0.54	-0.57	0.20	1.02	-21.37	0.68	0.19	20.3	3119	123	0
160						1.98					
161	0.15	0.59	-0.02	1.61	-20.33	0.56	0.04	28.2	4129	190	0
162						1.31					
163	0.76	0.73	-0.30	1.35	-20.70	0.81	0.07	37.7	5875	288	0
164						1.44					
165	0.07	-0.65	0.15	1.09	-20.96	1.01	0.00	38.4	5474	102	0.5
167	0.00	-0.59	0.26	1.14	-20.75	1.08	0.13	21.0	5981	63	0
169	0.88	-0.37	0.81	0.85	-20.96	0.98	-0.13	19.3	4540	117	0.5
171	0.76	-0.48	0.12	0.82	-21.26	1.11	0.08	9.8	6688	281	0
173	0.63	-0.95	0.31	0.74	-21.01	1.23	0.04	12.0	5306	173	0.5
175	0.51	-0.80	0.39	0.75	-21.14	1.15	0.13	9.5	4985	144	0
177	0.91	-0.80	0.41	0.81	-20.59			12.2	3832	125	0.5
179	0.31	-1.15	0.04	0.80	-20.69	0.96	0.38	28.7	4358	170	3
181	-0.49	-0.86	-0.64	1.19	-20.17	0.96	0.29	17.4	6666	126	0
183	-0.45	-0.73	-0.37	1.31	-19.85	0.98	0.36	17.9	10801	276	0
185	-0.25	-1.07	0.32	0.87	-20.86	1.16	0.38	9.2	7565	132	1
187	-0.55	-1.05	-0.16	1.00	-20.82	1.01	0.48	8.0	6686	311	2
189	-0.79	-0.95	-0.05	1.05	-20.56			8.7	8501	141	0.5
191	-1.07	-1.17	-0.38	1.27	-19.95	1.20	0.60	12.5	6395	182	1
192						1.18	0.45				
193	-1.15	-1.15	0.14	1.26	-20.05	1.31	-0.30	15.1	4823	257	2
194						1.47	0.51				
195	-0.75	-1.23	0.22	1.18	-20.50			11.2	4534	127	1
196						1.36	0.57				
197	0.26	-1.42	0.29	0.92	-21.30			13.7	2431	94	3
198						0.75	0.83				
199	0.64	-0.98	0.77	0.47	-22.31			18.1	1459	94	3
201	-1.35	-1.16	0.63	0.65	-21.92	1.05	-0.25	10.5	4092	71	3
203	-2.63	-1.01	0.72	0.60	-21.46	1.15	-0.23	6.0	10916	235	2
204	-2.72	-0.71	0.70	0.58	-21.53	1.04	-0.36	13.3	9896	188	0.5
205	-0.53	-0.84	1.17	0.45	-21.98	0.82	-0.26	11.6	3808	108	1
207	-1.86	-0.03	1.30	0.38	-22.10	0.81	-0.85	17.3	9694	132	0
209	-2.90	0.17	1.47	0.61		1.05	-1.16	19.7	11515	151	0
210				0.71	-21.45	1.04	-1.35				

Enhanced preservation of organic matter in sediments underlying the oxygen minimum zone in the northeastern Arabian Sea

Cornelis H. van der Weijden, Gert Jan Reichart and Hendrik Jan Visser

Department of Geochemistry, Institute of Earth Sciences, Utrecht University, Budapestlaan 4, P.O.Box 80.021, Utrecht, The Netherlands

Abstract

The presence of a strongly developed oxygen minimum zone (OMZ) in the northeastern Arabian Sea affords the opportunity to investigate whether oxygen deficiency in bottom waters fosters the preservation of organic matter in the underlying sediments. We explored if the observed patterns of organic matter accumulation could be explained by differences in productivity, sedimentation rate, water depth, and mineral texture. The differences in the burial rates of organic matter in sediments underlying or below the OMZ could not be explained on the basis of these factors. All collected evidence points to a coupling of low oxygen concentrations and enhanced organic matter preservation. Under more oxygenated conditions bioturbation as well as the presence of labile manganese and iron oxides are probably important factors for a more efficient microbially mediated degradation of organic matter. Pore water profiles of dissolved Mn^{2+} and Fe^{2+} show that reduction of these metal oxides plays a minor role in sediments underlying and a large role in sediments below the OMZ.

Introduction

In the broader context of the discussion on the role of anoxia in the preservation of organic matter (OM) in marine sediments *Pedersen et al.* [1992, 1993], *Paropkari et al.* [1993a, b] and *Calvert et al.* [1995] discussed the preservation of OM in Arabian Sea sediments underlying the oxygen minimum zone (OMZ). The

general interest in the relation between oxygen deficiency and organic matter preservation is evident from many related papers published during the last couple of years. The various aspects of OM preservation have recently been fully discussed by *Henrichs* [1992], *Calvert and Pedersen* [1992], *Lee* [1992, 1994], *Canfield* [1994], *Wignall* [1995], so there is no need to repeat these discussions in

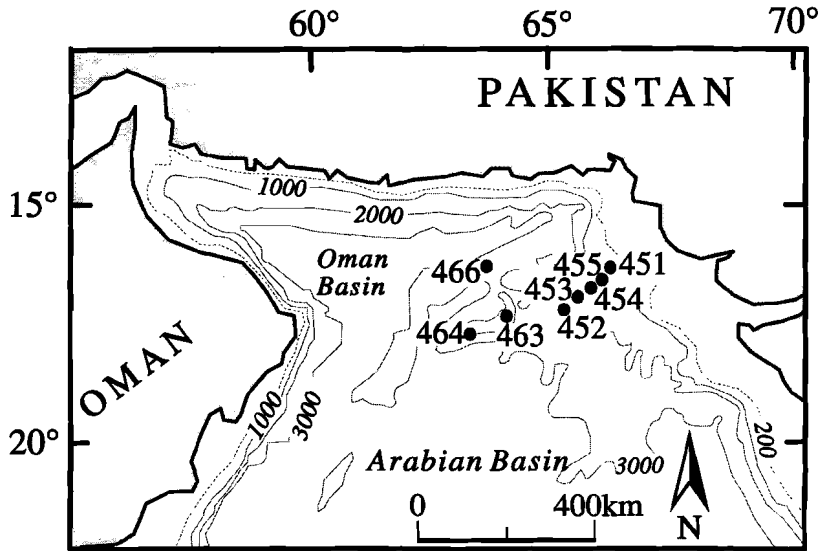


Fig. 1. Map showing locations of the NIOP stations discussed in this paper.

this paper. We will rather concentrate on presenting evidence for enhanced preservation of OM below the OMZ in the northeastern part of the Arabian Sea.

Sampling and Profiling

In October 1992, during the Netherlands Indian Ocean Programme (1992-1993), we measured CTD and dissolved-oxygen profiles in the water column, and collected box-cores in the northeastern Arabian Sea within the Exclusive Economic Zone of Pakistan. For the purpose of this paper we selected box-cores taken at stations 451, 452, 453, 454, and 455 on the Karachi continental margin, and 463, 464, and 466 in the Murray Ridge area. The locations of these stations are shown in Fig.1 and relevant details are given in Table 1.

All handling and sampling of the box cores started within one hour after recovery. From each box-core a few sub-cores were collected in PVC tubes lined with polyethylene foil. These sub-cores were kept vertical and stored at *in situ* bottom-water temperature until required. One sub-core was cut in two lengthwise, one half intended for sedimentological description, the other for measurements of pH and Eh and for sampling of wet sediment at selected intervals. The sediment samples, collected in small glass vials with snapcaps, were stored at 2 °C till used for analysis in the home laboratory. Another sub-core was introduced in a vertical position into a nitrogen-flushed glove box, installed in a laboratory container kept at *in situ* bottom-water temperature. This sub-core was cut into slices, after extrusion, at the same intervals

	boxcores	latitude (N)	longitude (E)	depth (m)
Karachi Margin	451	23° 41.40′	066° 02.90′	495
	452	22° 56.40′	065° 28.10′	2001
	453	23° 14.01′	065° 43.99′	1555
	454	23° 26.90′	065° 51.20′	1254
	455	23° 33.25′	065° 57.24′	998
Murray Ridge	463	22° 33.60′	064° 03.25′	970
	464	22° 15.00′	063° 34.70′	1511
Oman Basin	466	23° 36.20′	063° 48.50′	1960

Table 1: Details on positions and water depths of the stations where box cores were collected

as used for the sediment sampling, and pore-water from these slices was squeezed through a 0.2 μm membrane filter in a teflon Reeburgh-type press [cf. *De Lange*, 1992]. The pore water collected from each slice was split into 4 portions, one for nutrient analysis, one for alkalinity titration, one for trace element analysis after acidification with suprapur (Merck, 318.0250) HCl till pH \approx 1.5 in a PTFA vial, and a remaining portion. The former two portions were kept refrigerated in capped vials till shipboard analysis, the latter two portions were stored at 2 °C for further analysis in the home laboratory.

Analysis

Within 12 hours after their collection, pore-waters were analysed using routine autoanalyser techniques (Technicon TRAACS 800) for dissolved nutrients. In the home laboratory the dissolved major elements were measured by ICP-AES (ARL 34000) in the acidified pore-water samples after a tenfold dilution with 1 M suprapur HCl. For this paper we only use the sulphur concentrations, determined with a relative precision better than \pm 4%. Dissolved Mn and Fe were measured by ZGFAAS in the acidified sample after a

tenfold dilution with 1 M suprapur HNO₃ (Merck, 441.0250), using Mg(NO₃)₂ for Fe and Pd/Mg(NO₃)₂ for Mn as modifiers. All measurements were compared with standard samples prepared in a similar matrix and the absolute precision was \pm 5 $\mu\text{g/l}$ for Mn and \pm 10 $\mu\text{g/l}$ for Fe.

Porosity of wet sediment was calculated from the weight loss upon drying at 110 °C. The dried sediment sample was homogenized in an agate mortar. A 250 mg aliquot of the dried sample was dissolved in a mixture of HNO₃, HF and HClO₄ in a Teflon beaker. The beaker was sealed with a screw cap and was placed overnight in an oven at 95 °C. The next morning the solution was evaporated on a hot sandbath until just dry, the residue was taken up in 50 ml 1 M analytical grade HCl, and the solution was analysed by ICP-AES. International standards were used as a check for accuracy and precision of the methods. For this paper we only use the results for Al, Fe and Mn, measured with relative precisions of \pm 3%.

For the analysis of organic carbon (C_{org}), and the isotopic composition of organic carbon ($\delta^{13}\text{C}_{\text{org}}$), 1 gram of dry sediment was weighed in a centrifuge tube. Carbonate was dissolved in 1 M HCl under mechanical shaking during 12 hours, after

which the samples were rinsed in demineralized water in order to remove CaCl_2 and subsequently dried. Volumetrically the C_{org} content was determined, following dry oxidation with CuO at 900°C in a closed circulation system at 0.2 atm oxygen. The released CO_2 gas was cryogenically separated from the other gases. The $\delta^{13}\text{C}_{\text{org}}$ was measured with a VG SIRA 24 mass spectrometer with a precision better than 0.1 ‰. The isotope data reported are relative to the PDB standard.

Another aliquot of dry sediment was also used to determine C_{org} and N_{total} , using a Carlo Erba NA1500-CNS analyser with a relative precision of better than 10% for N and better than 3% for C_{org} . A good agreement was found between the C_{org} contents using this method and the volumetric method.

Hydrogen indices (HI), expressed in mg HC/g C, were obtained by Rock Eval pyrolysis with a relative precision better than $\pm 10\%$.

^{14}C -AMS datings [Van der Borg *et al.*, 1987] were performed on OM and on carbonate from planktonic foraminiferal tests.

The surface area of the mineral component of the sediment was analysed by the single-point BET method, which measures surface area by determining one point on a well-established adsorption isotherm. After the OM had been removed with sodium pyrophosphate/hydrogen peroxide, the adsorption of N_2 was measured with a Quantachrome Monosorb Analyser (precision on duplicates $\pm 1\%$).

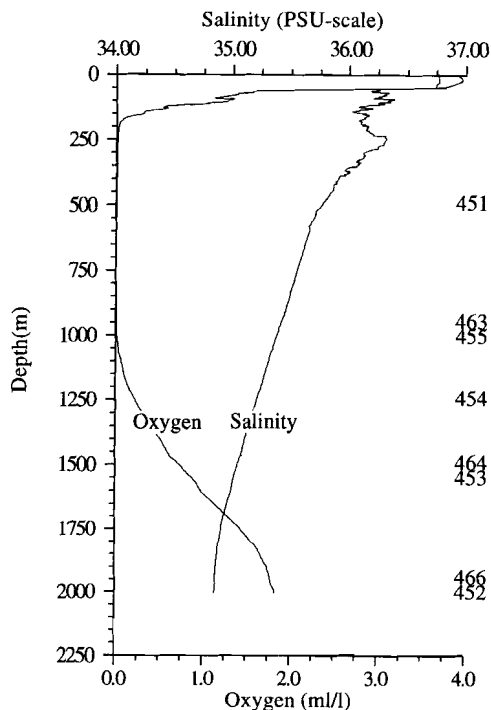


Fig. 2. Plot of the salinity and dissolved oxygen profiles. The station numbers are given on the right side according to the water depths.

Results and Discussion

The oxygen profiles in the water column and the water depths at the occupied stations are shown in Fig.2. Oxygen concentrations in the proximity of these stations show the presence of a very thick (between 150 and 1200 m) and very intense OMZ ($[\text{O}_2]$ at the very minimum dropping to $<2 \mu\text{M}$; Van Bennekom and Hiehle [1994]). Sediments at stations 451, 455 and 463 are underlying the OMZ with suboxic ($[\text{O}_2] < 10 \mu\text{M}$) conditions, the sediment at station 454 was deposited in

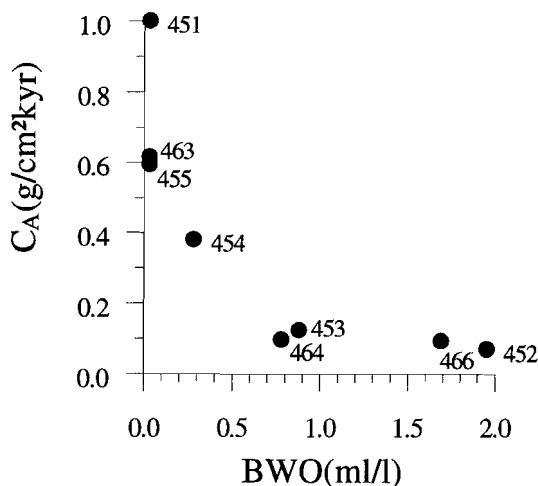


Fig. 3. Plot of the accumulation rates of organic carbon (C_A) against bottom water oxygen (BWO). Suboxic waters have < 0.2 ml O_2/l , dysoxic waters between 0.2 and 2 ml O_2/l [Wignall, 1994].

the transition zone from suboxic to dysoxic conditions ($[O_2] \approx 13 \mu M$) and turns out to have similar characteristics as sediments at the first three stations, the sediments at stations 452, 453, 464, and 466 are deposited under more oxygenated conditions ($36 < [O_2] < 90 \mu M$).

The relevant analytical results for solid material and for pore-waters to be used are presented in the Appendix.

^{14}C , $\delta^{13}C_{org}$, C_{org}/N_{total} , HI

The tops of the sediments underlying the OMZ have equal ^{14}C ages (Table 2) as the mean ocean reservoir age of 400 yr [Bard, 1988]. We believe that bioturbation caused deviation of these ages in the top of the sediments deposited below the OMZ. We have several reasons to rule out that the deviation is caused by transport of material from the shelf. Firstly, the sediments underlying the OMZ, not affected by bioturbation, have correct ages. Secondly

we did not observe the presence of a nepheloid layer in the overlying water column [Van der Weijden *et al.*, 1992]. Lastly, the sediments along the Karachi Margin transect (451-455) show a similar trend as those in the Murray Ridge area, while these areas would not receive such admixed material from the same source area. From the ^{14}C ages we calculated the sedimentation rates of the sediments at the various stations. These rates decrease, as expected, with increasing depth away from the continent at Karachi slope (Table 2). The high sedimentation rate at station 463 on Murray Ridge is caused by a relatively high porosity. Sedimentation rates and porosities are used to calculate mass accumulation rates (MAR's).

A comparison of the accumulation rate of C_{org} (C_A) in sediments underlying and below the OMZ shows a drastic decrease with increasing bottom-water-oxygen (BWO) concentrations (Fig.3). As we will discuss later, this trend cannot be fully attributed to differences in water depth.

	material	depth in core (cm)	age(bp) (yr)	error (yr)	mean age (yr)	S cm/kyr	biot. depth (cm)
boxcore 451	C-org	1.5	520	60	475		2.8
	foraminifera	1.5	430	70			0.8
	C-org	42.5	2229	36	2074.5	23.2	
	foraminifera	42.5	1920	50		28.0	
tripcore 452	C-org	1	2890	60	2064		11.6
	foraminifera	1	1238	41			4.4
	C-org	32	7241	58	6895.5	4.7	
	foraminifera	32	6550	70		5.2	
boxcore 453	C-org	1	1317	43	1565		7.1
	foraminifera	1	1813	49			12.1
	C-org	27	3901	47	3725.5	7.7	
	foraminifera	27	3550	70		8.6	
boxcore 454	C-org	1	960	42	520.5		6.3
	foraminifera	1	81	55			-2.8
	C-org	32.5	3271	46	3663	11.3	
	foraminifera	32.5	4055	90		8.9	
boxcore 455	C-org	1	638	47	447		3.8
	foraminifera	1	256	42			-2.3
	C-org	27.5	2134	42	2117	15.9	
	foraminifera	27.5	2100	60		16.2	
boxcore 463	C-org	0.5	500	80	470		1.7
	foraminifera	0.5	440	60			0.5
	C-org	16	1360	41	1480	16.7	
	foraminifera	16	1600	80		13.3	
	foram	29	2070	50		17.4	
boxcore 464	C-org	0.5	1210	60	1900		6.8
	foraminifera	0.5	2590	50			9.4
	C-org	20	2776	43	3913	8.4	
	foraminifera	20	5050	100		4.3	
boxcore 466	C-org	1	1664	58	1197		10.9
	foraminifera	1	730	40			2.5
	C-org	19	2598	49	2739	8.6	
	foraminifera	19	2880	60		7.7	

Table 2: Ages of organic carbon (C-org) and foraminiferal tests (*Globorotalia menardii*) as derived from ^{14}C -AMS ages determined on samples from the top of the sediments and from deeper in the various box cores. The mean ages are used to calculate linear sedimentation rates and to estimate bioturbation depths, taking into account a reservoir age of 400 kyr and assuming homogeneous mixing of the bioturbated zone.

The concomitant atomic C_{org}/N_{total} ratios decrease from values between 9-10.3 for sediments underlying the OMZ to values between 7-8 in sediments at 2 km depth. The values are comparable with values found in similar marine settings [Suess and Müller, 1980; Calvert and Pedersen, 1992; Calvert et al., 1995]. Since $N_{total} = N_{org(anic)} + N_{inorg(anic)}$, the C_{org}/N_{total} values are an underestimation of the C/N ratio in sedimentary OM. The average Redfield C_{org}/N_{org} ratio in fresh marine OM is equal to 6.6. Preferential mineralization of N_{org} during passage through the water column and during early diagenesis will increase this C/N ratio, which may be the reason of the high C_{org}/N_{total} ratios in sediments underlying the OMZ. Other causes, particularly admixing of terrigenous or reworked marine OM with higher C/N ratios have to be considered. Such admixing has been reported for slope

sediments in the western [Pedersen et al., 1992] and eastern [Calvert et al., 1995] Arabian Sea and in the Middle Atlantic Bight (SEEP study area; Anderson et al., [1994]). Taking a C_{org}/N_{org} ratio of 10 in the sediment and assuming that terrigenous OM has a C/N ratio of ~35, the contribution of terrigenous to total preserved OM would be approximately 12%. Assuming that only 10% of the primary productivity arrives at the seafloor, a value mentioned by Olson et al. [1993] for 1000 m depth, and that the burial efficiency is high, this means that admixing of terrigenous OM in the surface water needs only to be in the order of 1% or hardly noticeable on the basis of C/N ratios. Jochem et al. [1993] reported C/N ratios of 5-7 in OM in the surface layer in the central Arabian Sea and on the Karachi shelf, in some cases increasing to 7-8. These low values suggest indeed a minor

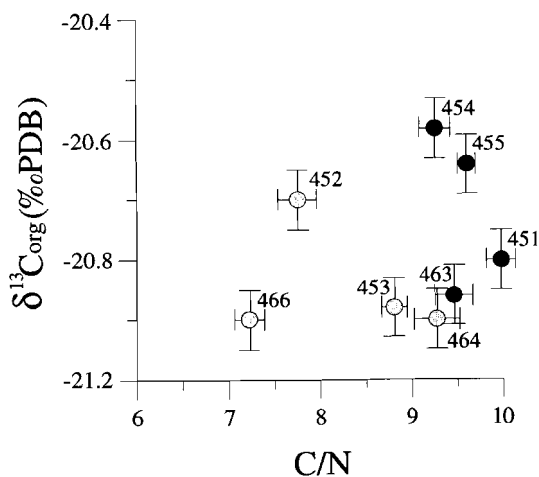


Fig. 4. Plot of the isotopic composition of organic carbon ($\delta^{13}C_{org}$ in ‰ relative to the PDB standard) versus the atomic organic-carbon over total-nitrogen (C/N) ratio. The dots represent average values for sediments deposited during the last 1000 year, the horizontal error bars represent the ranges observed in the C/N ratios, the vertical bars the standard deviations of the $\delta^{13}C$ values. Grey and black dots are used for sediments underlying and below the oxygen minimum zone respectively.

admixing of detrital OM in the surface layer, but even this may result in a relatively significant contribution of detrital OM buried at a greater depth. *Pollehne et al.* [1993] reported an increase in C/N ratios from ~ 5 in the photic zone to 7-9 in OM collected in sediment traps deployed below the photic zone in the central Arabian Sea and on the Pakistan shelf. They attribute this increase to preferential consumption of N_{org} compounds. Admixing of refractory OM with higher C/N ratios not necessarily occurs via the surface layer but can, in such settings, also occur at greater depths [*Anderson et al.*, 1994]. The striking similarity of the C_{org}/N_{total} ratios in sediments from equal depths on the Karachi slope and Murray Ridge is, however, a strong indication that such admixing is negligible in reality; these regions do not have the same source areas for terrigenous and/or reworked OM, and it would be too fortuitous when this still yields similar C/N ratios. The C_{org}/N_{total}

values found in the deeper stations can be considered to represent a high contribution of marine plankton [*Calvert et al.*, 1995], but may also be due to a relatively increasing N_{inorg} contribution to N_{total} or by preservation of N_{org} -rich compounds by sorption [*Müller*, 1977; *Cowie et al.*, 1995]. A relatively important input of terrigenous or reworked OM would most likely have resulted in higher C_{org}/N_{total} ratios at these stations as well, because the contribution of more refractory OM with high C/N ratios would relatively increase.

There are no significant differences in the $\delta^{13}C_{org}$ values between sediments on the Karachi slope and on Murray Ridge, nor between sediments underlying and below the OMZ. The observed $-20.7 \pm 0.3\text{‰}$ range of $\delta^{13}C_{org}$ values can be considered as typically marine with a range of $-20 \pm 2\text{‰}$ [*Hoefs*, 1980]. This range is narrower and lighter than reported for slope sediments of the eastern Arabian Sea [*Calvert et al.*, 1995]. Admixing of terrigenous OM (with mean $\delta^{13}C$ values of

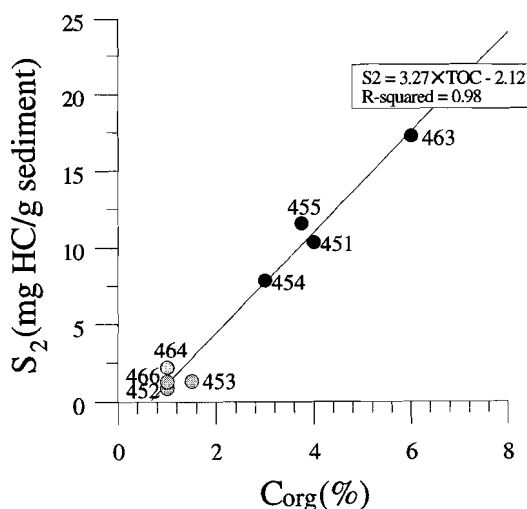


Fig. 5. Rock Eval S_2 vs. TOC graph of organic matter in the top layer of the sediments. Grey and black dots: see Fig.4.

~ -27 ‰ for C₃ plants and ~ -14 ‰ for C₄ plants), could have changed marine $\delta^{13}\text{C}$ values to higher mixed $\delta^{13}\text{C}$ values. If so, we would observe a trend in the $\delta^{13}\text{C}_{\text{org}}$ values in the Karachi slope sediments (stations 451-455) in a direction away from the continents [cf. *Calvert et al.*, 1995]. Also, we would observe a significant trend in the $\delta^{13}\text{C}_{\text{org}}$ values in the Murray Ridge area (stations 463, 464, 466) with similar input of wind-blown terrigenous OM, because a higher diagenetic decomposition of OM at the deeper stations in combination with a preferential preservation of terrigenous OM would enhance the terrestrial $\delta^{13}\text{C}$ signature of OM. Furthermore, if different mixtures of marine and terrigenous OM were responsible for the changes in the $\text{C}_{\text{org}}/\text{N}_{\text{total}}$ ratios and the $\delta^{13}\text{C}_{\text{org}}$ values, they should have an inverse relationship [Müller *et al.*, 1994]. This relation is not present in our $\delta^{13}\text{C}_{\text{org}}$ vs. $\text{C}_{\text{org}}/\text{N}_{\text{total}}$ plot (Fig.4).

Fig. 5 shows a linear correlation between the Rock-Eval S₂ peak and the C_{org} content of surface sediments, with an intercept at 0.65% C_{org} . As discussed by *Langford and Blanc-Valleron* [1990], the intercept typically represents an artifact caused by partial absorption of the pyrolysate by the sediment matrix. Samples with a low C_{org} content suffer relatively most from such absorption. The slope of this line represents the average HI value (=327) of the OM in the analyzed sediments. Obviously, there is no systematic change in the HI values, regardless of the position and depth of the sediments. For that reason, the uniform HI value does not support lateral admixing of terrestrial or reworked degraded OM, although the HI value is lower than in

well-preserved OM of marine algal origin [cf. *Pedersen et al.*, 1992]. On the other hand, this uniform HI value also does not corroborate a hypothesis of enhanced preservation of OM in the OMZ.

More support for the minor role of lateral transport can be based on a close inspection of the ¹⁴C-AMS ages (Table 2). The ages of OM and planktonic tests in the same sample of sediments collected at stations 451 and 455 at the upper slope off Karachi, nearest to the shelf, and in the same samples collected at the station 463 at Murray Ridge, are similar. These sediments have in common that they are underlying the OMZ with very limited bioturbation. Such observations are hard to reconcile with lateral input of reworked material from shelf or upper slope, because hydrodynamic sorting would have pulled apart the ages of OM and carbonate tests [cf. *Anderson et al.*, 1994]. At the deeper stations at the Karachi slope and Murray Ridge, below the OMZ, these ¹⁴C ages diverge, which can be caused bioturbation of layers with originally different quantities of organic matter or foraminiferal calcite [*Duplessy et al.*, 1986].

In sum, the data discussed in this section do not compel us to take into account sizeable contributions of either terrigenous or reworked marine OM.

Mineral-surface area (SA)

The SA's of the C_{org}-free sediment tops are given in Table 3. Since the samples did not contain appreciable amounts of smectites, no correction of the BET-determined SA for a contribution of the internal SA was necessary [cf. *Keil et al.*, 1994a]. The SA values are typical for

the box cores as a whole, because the mineralogical composition within the cores does not vary much with depth. The rather low SA's are caused by the relatively high contribution of carbonate particles; we noted that SA values increase with an increase of the lithogene fraction. The SA values measured in the top sediments can for these reasons be considered to be representative for an analysis of the relation between SA and OM preservation in sediments considered in this study. Strong evidence has been put out that OM is protected against mineralization by an intimate sorptive association with mineral surfaces [Keil *et al.*, 1994a,b; Mayer, 1994; Hedges and Keil, 1995]. In our samples we found no correlation between C_{org} and SA (Fig. 6). Lines indicating the range of monolayer-equivalent sorption to mineral surfaces [Suess, 1973; Mayer, 1994; Keil *et al.*, 1994a,b] lie below the observed values of C_{org} . The C_{org} -rich sediments underlying the OMZ show the largest deviation. On the basis of an observed significant

relationship between the preserved C_{org} content and SA, Hedges and Keil [1995] conclude that even super-monolayer coatings 2-5 times a monolayer equivalent appear are diagenetically stable in sediments underlying oxygen-deficient ($[O_2] < 20 \mu M$) bottom waters. In that case most of our observations could be explained by sorptive protection on mineral surfaces. Such stability ranges encompass, however, probably most marine sediments with high C_{org} contents, but enfeeble the basic monolayer concept, because there is no obvious reason why sorption of organic compounds should preferentially occur in a multi-layer fashion on mineral particles instead of on discrete organic debris. A relation between C_{org} and SA could be brought about as well by hydrodynamically similar behaviour of fine mineral particles and particulate OM. The super-monolayer hypothesis cannot explain why there is such a significant difference in the C_{org}/SA relation between the sediments underlying and sediments below the OMZ.

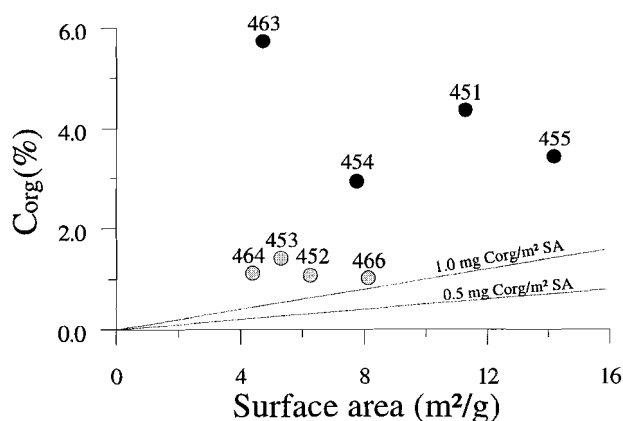


Fig. 6. Plot of the organic-carbon contents versus the surface areas of the organic-carbon-free fraction of sediments in the top layer of the box cores at the indicated stations. Grey and black dots: see Fig.4. The drawn lines represent the boundaries of the range of monolayer coverage of minerals by organic compounds.

boxcore	Water (%)	DBD (g/cm ³)	MAR (g/cm ² kyr)	C _A (g/cm ² kyr)	S ₂ mg HC/g sed.	Surface area (m ² /g)
451	63.2	0.96	24.5	1.00	10.36	11.3
452	48.7	1.33	6.6	0.07	0.85	6.3
453	52.4	1.24	10.1	0.12	1.32	5.3
454	56.9	1.12	11.3	0.38	7.82	7.7
455	66.6	0.87	13.9	0.60	11.54	14.2
463	72.1	0.73	10.9	0.62	17.21	4.7
464	53.3	1.21	7.7	0.10	2.19	4.4
466	50.5	1.29	10.5	0.09	1.27	8.1

Table 3: Summary of the measured or calculated porosities, dry-bulk densities (DBD), mass accumulation rates (MAR), accumulation rates of organic carbon (C_A), as well as hydrocarbon generated by pyrolysis, S₂, and surface areas of the organic-carbon-free fractions in the tops of the sediments.

Henrichs [1995] drew attention to the fact that time scales for which preservation is defined depend strongly on the combination of the adsorption coefficients and the rate constants of decomposition of dissolved OM. Using a simplified diagenetic equation, she demonstrated that sorptive preservation of very labile OM is much less likely than preservation of OM which is inherently somewhat refractory to biological mineralization. Her model predicts enhanced preservation by high sedimentation rates and by high inputs of labile OM, which are also key factors used in the transfer functions to be discussed in the next section.

As yet, we have no reason to accept that the preservation of OM in this region can be fully explained by protection of supermonolayer coatings from microbiological degradation.

Productivity, transit flux and sedimentation rate

Müller and Suess [1979] proposed the following relation between the C_{org} content (in w%) of sediments, the primary

productivity in the overlying surface layer, and the sedimentation rate:

$$C_{org} \propto P \times S^{0.3} \quad (1)$$

where P is the primary production (gC/m²yr) and S is the sedimentation rate (cm/kyr). This relation was derived for sediments deposited under more or less oxygenated conditions, at least seasonally. In this relation the C_{org} content is made a variable dependent on S, which is not the case for C_A. In Fig. 7 we plotted the C_{org} content against S. It is striking that the Karachi slope and Murray Ridge samples cluster together according to their position underlying or below the OMZ. It appears to be impossible to relate these clusters without invoking unrealistically large differences in P.

Only few estimates of P in the central to northern Arabian Sea have been published and they usually are based on measurements done over a short period of time in a certain season.

We found estimates for P of 180-360 [Ryther and Menzel, 1965], ~ 200 [Quasim, 1982; Codispoti, 1991], ~180 [Olson et al., 1993], 250 [Jochem et al.,

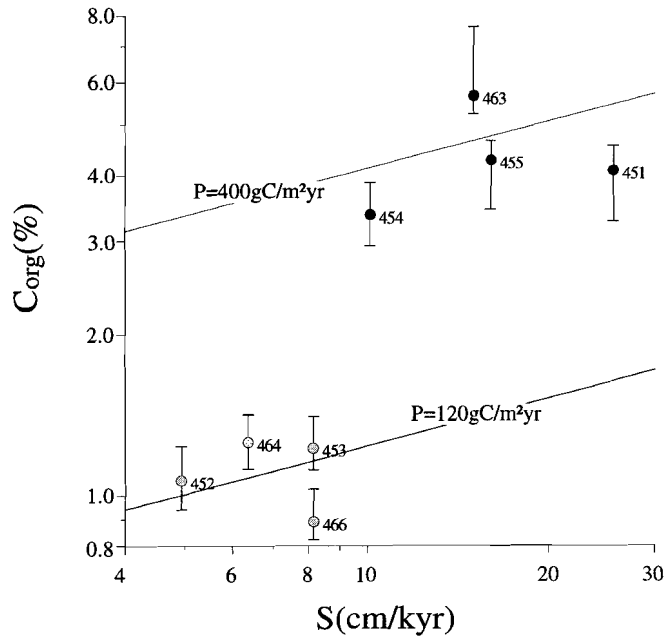


Fig. 7. Plot of organic-carbon contents against the sedimentation rates at the indicated stations. The dots represent the average values in sediments deposited during the last 1000 years; grey and black dots: see Fig.4. The vertical bars represent the observed ranges within this 1000 year period. The lines indicate the relation between C_{org} and S for $P=120$ and $400 \text{ gC/m}^2\text{yr}$ [Müller and Suess, 1979].

1993], 140-280 [Pollehne *et al.*,1993] $\text{gC/m}^2\text{.yr}$.

The simple relation represented by eq. 1 has been criticised because water depth was not explicitly considered. Sarnthein *et al.* [1992] incorporated the depth dependency of the transit flux of OM to the seafloor and derived the following equations relating the C_{org} burial flux, C_A , to P_{export} :

$$P_{export} = 9.354 \times C_A^{0.493} \times z^{0.3} / S_{ocf}^{0.105} \quad (2)$$

where S_{ocf} = organic-carbon-free sedimentation rate.

We calculated P_{export} from C_A , z and S_{ocf} and plotted the results in Fig. 10. Two clusters of P_{export} values are obtained, one

using sediments underlying the OMZ, the other on the basis of sediments below the OMZ. Since no data of long-term sediment-trap experiments are available for our research region, it is not possible to compare these results with independently obtained P_{export} values. The calculated values strongly suggest that there is no difference in P_{export} between the regions of Karachi margin and Murray Ridge. We consider the P_{export} value of $\sim 70 \text{ gC/m}^2\text{.yr}$ for the deep stations, relating to C_A 's in sediments below the OMZ, to be the best time-averaged value for the whole region. Somasundar and Naqvi [1988] on the basis of a denitrification model for the Arabian Sea estimated $P_{exp}=50 \text{ gC/m}^2\text{.yr}$. This value, however, comprises also the area of

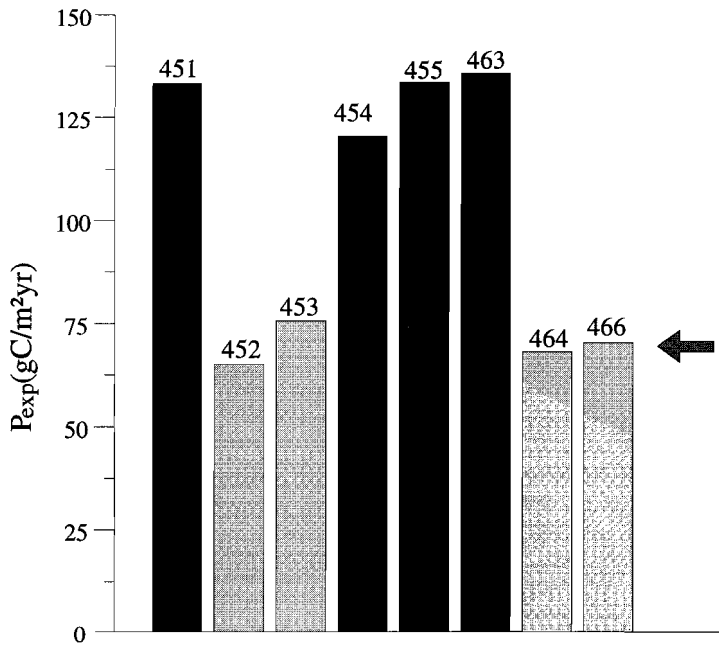


Fig. 8. Bar graph of export productivities of organic carbon calculated from accumulation rates of organic carbon using a transfer function (eq. 2) proposed by *Sarntheim et al.* [1993]. Grey and black: see Fig. 4. The arrow indicates the adopted value of the export productivity in the whole region; further explanation in text.

relatively low productivity in the eastern Arabian Sea. Primary production can be estimated using:

$$P = 61.390 \times C_a^{0.439} \times z^{0.3} / S_{ocf}^{0.049} \quad (3)$$

[*Sarntheim et al.*, 1992], which results in an estimate of $P \approx 170 \text{ gC/m}^2\text{yr}$ for the deep stations. These values come very close to the productivities directly measured in the area. If so, the only way to equalize the calculated P_{export} of the two groups is to accept a better preservation of OM in sediments underlying the OMZ.

On the basis of this discussion, we conclude that the differences in C_{org} content and in C_A in sediments underlying and below the OMZ cannot be solely explained on the basis of $P_{(\text{export})}$, z , and S .

We have already put forward strong arguments against lateral admixing of OM and textural causes of the observed differences. The only option left is that the condition of the low BWO concentrations within the OMZ in this region enhances preservation of OM.

Preservation and diagenetic degradation of OM

We will briefly discuss a number of differences in the biological and microbiological processes in sediments underlying and below the OMZ that may explain the dissimilarities in preservation of OM. In all cases these differences are directly or indirectly related to the differences in BWO concentrations.

We observed restricted benthic activity in the top of the sediments underlying the OMZ (Fig. 9). There were no signs of deep burrowing. Ingestion, enzymatic digestion and excretion by benthic organisms play a role in the transformation of OM, partly into low-molecular-weight organic compounds that are easier to mineralize by bacteria. The restricted benthic activity could explain why OM is not readily degraded at these low BWO concentrations [Henrichs, 1992; Lee, 1992; Aller, 1994; Canfield, 1994; Hedges and Keil, 1995].

From the point of view of early diagenetic processes, oxidants other than oxygen play a role in the degradation of OM as well. Nitrate, labile Mn and Fe oxides, and sulphate will be used in succession [cf. Froelich *et al.*, 1979] by specialized microbiological communities. Pore water profiles of NO_3^- , Mn^{2+} , Fe^{2+} (Fig.10) and SO_4^{2-} (Appendix) can tell us much about the actual diagenetic processes occurring in these sediments.

Bottom-water nitrate concentrations are $\sim 22 \mu\text{M}$ at 500 m and from ~ 35 to $\sim 42 \mu\text{M}$ from 1 to 2 km depth [Van Koutrik *et al.*, 1994]. Comparison of $[\text{N}_{\text{ox}}]$ ($= [\text{NO}_2^-] + [\text{NO}_3^-]$) (Fig. 10) with bottom-water $[\text{NO}_3^-]$ indicates that in sediments underlying the OMZ (451, 452, 454, 463) only denitrification of NO_3^- diffusing into the sediment from the bottom water plays a role in the degradation of OM. In the sediments below the OMZ a sub-surface $[\text{NO}_3^-]$ maximum reflects nitrification, which increases the contribution of denitrification but at the expense of the oxygen consumed by nitrification which would otherwise have been available for aerobic breakdown of OM [cf. Canfield *et al.*, 1993].

Aller [1994], Hedges and Keil [1995] and Mayer [1995] drew attention to the prominent part that metal oxides play in the degradation of OM. Absence of labile Mn and Fe oxides in sediments could lead to enhanced preservation of OM because these metal oxides are oxidants and catalysts for microbial degradation of OM. The measured Mn and Fe contents, normalized by Al to correct for dilutions with carbonates and OM, are shown in Fig. 10.

A baseline value of the Mn/Al ratio is 0.0055 ± 0.0001 for all sediments. The top layers of sediments underlying the OMZ (451, 455, 463) have these baseline values, implying that labile MnO_x has already been consumed as an oxidant, either in the water column or at the top of the sediment. This is in keeping with the relatively high dissolved Mn (and Fe) concentrations within the OMZ reported by Saager *et al.* [1989] and also found by us [unpublished data]. The sub-surface Mn/Al peak at station 454 is probably a non-steady-state phenomenon; the pore-water Mn profile suggests that this peak lies below the presently active redox front of the $\text{MnO}_x/\text{Mn}^{2+}$ couple. The tops of the sediments at deeper stations do contain MnO_x (Fig. 10) and probably have even been enriched in MnO_x due to re-oxidation of dissolved Mn^{2+} (and Fe^{2+}) at the base of the OMZ. In these sediments diagenetic reduction occurs below the zone of denitrification, followed by upward diffusional transport and re-oxidation of Mn^{2+} by oxygen. The degree to which the top layers are enriched in MnO_x increases with increasing water depth (Fig.10). The profiles of dissolved Mn^{2+} corroborate the role MnO_x reduction in the decomposition of OM. In sediments underlying the OMZ,

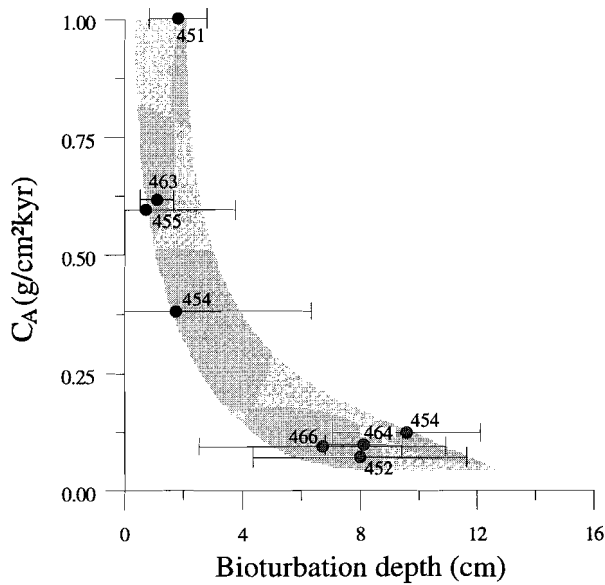


Fig. 9. Plot of the accumulation rates of organic carbon versus the bioturbation depth estimated on the basis of differences in AMS- ^{14}C ages between organic carbon and foraminiferal carbonates (see Table 3). The grey envelope suggests the best relation. Grey and black dots: see Fig.4.

$[\text{Mn}^{2+}]$ is and remains low downcore, indicating a negligible role of MnO_x reduction within these sediments. Sediments below the OMZ have Mn^{2+} profiles typical for MnO_x reduction, with $[\text{Mn}^{2+}]$ low in the top, increasing below the zone of denitrification, and approaching a constant value deeper downcore.

A baseline value of the Fe/Al ratio in the sediments is more difficult to give within narrow limits. For the stations underlying the OMZ the value is 0.55 ± 0.05 . This ratio is about constant downcore at station 451, which indicates the absence of diagenetic enrichment in the top. Oxidation of Fe^{2+} occurs at lower oxygen concentrations than oxidation of Mn^{2+} . This would mean that $[\text{O}_2]$ in the top of core 451 (500 m) is so low that even Fe^{2+} is not oxidized and can escape to the

bottom water, which agrees well with the relatively high dissolved Fe concentrations in the OMZ as referred to above. Less pronounced than in the case of Mn, the Fe/Al profiles in the other cores show diagenetic enrichment in Fe in the top of the sediments, even in sediments at 1 km depth but still underlying the OMZ (455, 463). The pore water profiles of dissolved Fe (Fig.10) also demonstrate the role of diagenetic reduction of labile Fe(III) in the degradation of OM. In essence these $[\text{Fe}^{2+}]$ profiles have, in most cases, the same shape as those of $[\text{Mn}^{2+}]$, but the maxima are approached at greater depths. Only in cores 463 and 466 the upper parts of these profiles show no consistent trends as expected, but this might be due to sampling artifacts.

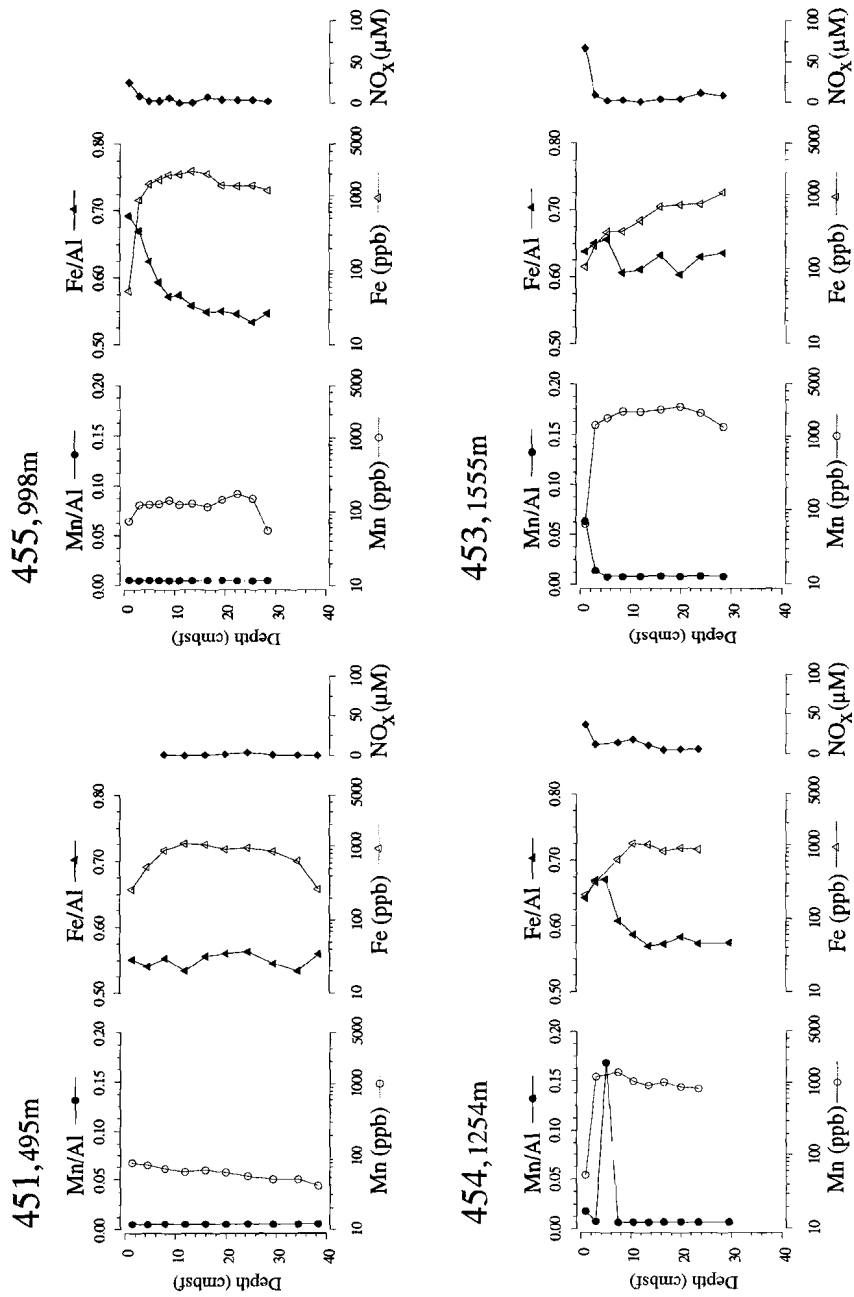


Fig. 10. Profiles of solid manganese and iron normalized by aluminium concentrations (Mn/AI and Fe/AI respectively) in dry sediments at the indicated stations. Normalization is used to eliminate dilution effects caused by carbonate phases and organic matter. In the same panels the pore-water concentrations of manganese, iron, and NO_x (nitrite + nitrate) are shown.

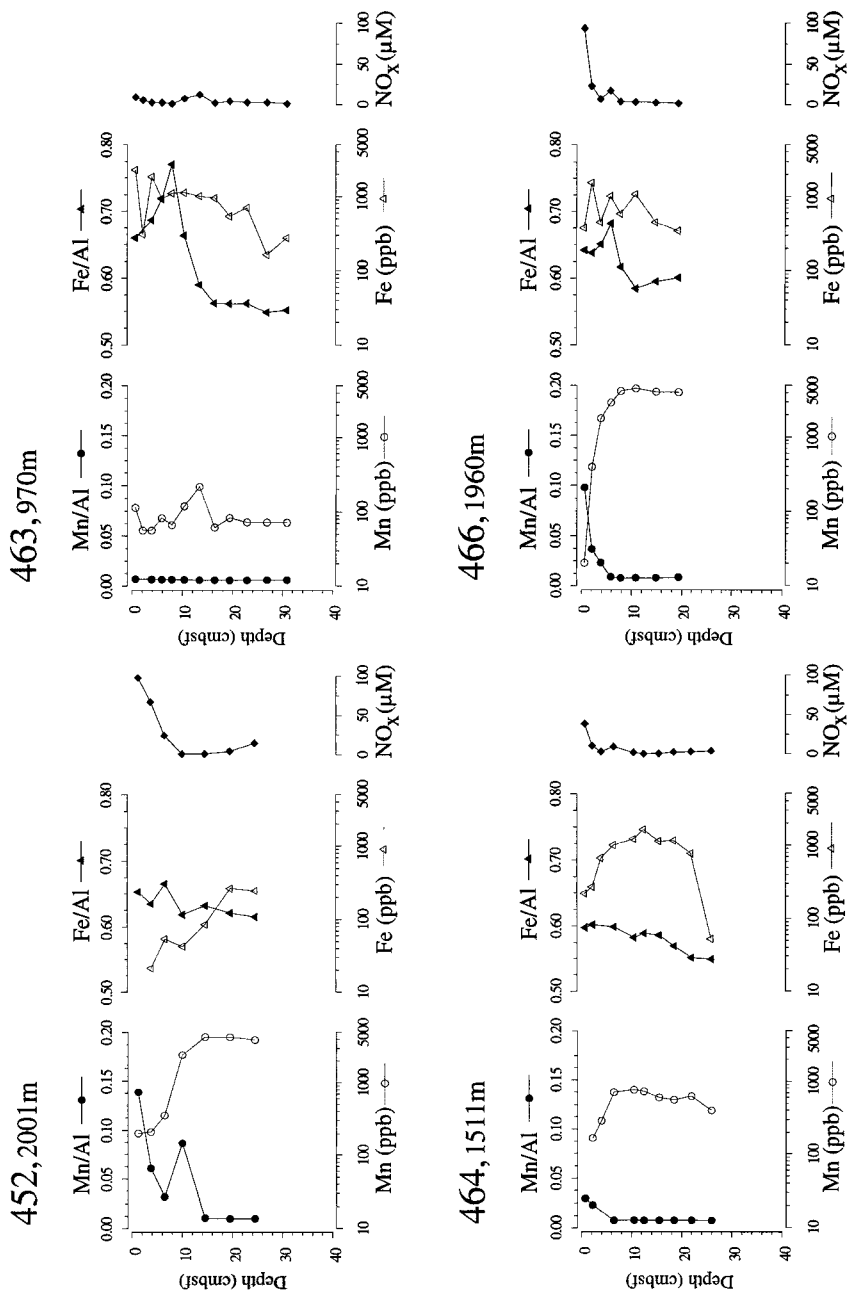


Fig. 10. Profiles of solid manganese and iron normalized by aluminium concentrations (Mn/Al and Fe/Al respectively) in dry sediments at the indicated stations. Normalization is used to eliminate dilution effects caused by carbonate phases and organic matter. In the same panels the pore-water concentrations of manganese, iron, and NO_x (nitrite + nitrate) are shown.

The profiles of solid and dissolved Mn and Fe demonstrate that the oxides of both metals are actively used in the decomposition of OM in sediments below the OMZ. This is most pronounced for MnO_x , probably because of a greater lability and rapid reduction kinetics. It seems that in sediments underlying the OMZ reduction of labile Fe oxide still plays a role at greater depths. This might be caused by a large range in crystallinities of sedimentary Fe oxides and concomitantly large ranges in lability and reduction kinetics.

Although the dissolved SO_4^{2-} concentrations (see Appendix) in some cases show a slight downcore decrease, this does not mean that sulphate reduction is active within these sediments. We did not smell any H_2S in these box-cores. The lowest Eh-value measured in these box-core sediments was -120 mV ($\text{pH } 7.5 \pm 0.3$), whereas a typical Eh-value measured in the sulphate reduction zone of piston cores collected in the area was -350 mV ($\text{pH } 7.4 \pm 0.1$). A slight trend of decreasing $[\text{SO}_4^{2-}]$ is the likely result of sulphate reduction at greater depth. The absence of sulphate reduction in the top 20-40 cm of these sediments is enigmatic, because the cores contain a relatively high OM content. It appears that sulphate reduction does not get started readily in these sediments, probably due to the presence of labile Fe(III) oxide but possibly also because of a shortage in simple organic components needed to sustain sulphate reduction [Van der Weijden, 1992; Canfield, 1994; Hedges and Keil, 1995]. In any case, we can rule out sulphate reduction as one of the diagenetic processes explaining differences in the degree of preservation of OM in these sediments.

Comparison with related studies in the Arabian Sea

The conclusion that bottom-water-oxygen deficiency in the northeastern region of the Arabian Sea enhances preservation of OM is opposed to the conclusions drawn for the western [Pedersen *et al.*, 1992] and eastern [Calvert *et al.*, 1995] regions. We have amply discussed the evidence on which our conclusion is based, for anyone to control and eventually to re-interpret.

Firstly, however, we note that there are discrepancies in the intensities of the oxygen minimum between the eastern (off India), western (off Oman) and northeastern (off Pakistan) regions. In the Indian region only the transects off Goa, Bombay and possibly Kathiawar [Calvert *et al.*, 1995] have oxygen minimum intensities similar to those observed in the Pakistan (Karachi continental Margin and Murray Ridge) region. Sediments along these three India transects have clearly higher OM contents within than below the OMZ, and the deduction that low bottom-water-oxygen (BWO) concentrations do not seem to foster OM preservation is mainly based on the Cochin transect along which BWO values within the OMZ are relatively high. In the Oman region most reported BWO values [Pedersen *et al.*, 1992] are higher than we measured in the OMZ of the Pakistan region. We observed a much more pronounced OMZ off Oman during a third leg of our Indian Ocean Programme [Van Bennekom and Hiehle, 1994]. A better relation between C_{org} and BWO appears when we plot Pedersen *et al.*'s [1992] C_{org} data versus our BWO values, though the OM contents of the sediments below the OMZ are indeed

relatively high. These remarks do not rule out other and possibly more important causes of the high OM contents on the studied continental slopes.

The main point made in *Pedersen et al.* [1992] and *Calvert et al.* [1995], but leading to negation of a role of low BWO concentrations on preservation of OM, is that a high C_{org} content is primarily due to a high OM flux, either related to a high P or to lateral admixing of OM from the upper slope.

We have considered the direct relation between C_A and P and we observe indeed a basin-wide (from Oman and Pakistan) correlation between these two variables in the sedimentary record (work still to be published). Since a higher P_{export} brings about an increase of the oxygen utilization in the water column, there will be a coupling between $P_{(export)}$ and the intensity and position of the OMZ. There need not be a causal relationship between C_A and BWO values, because these variables are both related to variations in $P_{(export)}$. This is the reason why we have paid due attention to P_{export} in the Pakistan region.

Lateral admixing of reworked OM is in this region a key argument for discrediting claims that BWO plays a role in OM preservation in this region. Winnowing of OM plays a very important role in the Oman region [*Pedersen et al.*, 1992], where strong bottom water currents not only prevent accumulation of small and light particulate matter, but also erode and winnow older sediment layers. Reworked marine OM has a 'quality' different from fresh marine OM. The intrinsic parameters used to characterize this quality are C_{org}/N_{total} ratios, $\delta^{13}C_{org}$ values, and HI indices. The problem with each of these parameters is that they are often not

unambiguous. In addition to their range in fresh marine OM, variations in the C_{org}/N_{total} ratios can be caused by admixing of allochthonous OM, by preferential microbial degradation of N_{org} -compounds, by contributions of $N_{inorg(anic)}$, or by preferential storage of N_{org} in the bacterial biomass. The $\delta^{13}C_{org}$ values may vary in fresh marine OM, also upon admixing with allochthonous OM, maybe even on preferential degradation of $^{12}C_{org}$ -compounds during early diagenesis. The HI values are at best semi-quantitative estimators of the degree of preservation of OM.

In combination these variables could have more cogency. For sediments in the Oman Margin, *Pedersen et al.* [1992] reported a good correspondence between C_{org}/N_{total} (range 7.3 to 12.3) and $\delta^{13}C_{org}$ (range -18.8 to -20.2 ‰), with high C/N ratios corresponding with less negative $\delta^{13}C$ values. Because in this region terrestrial inputs can relatively be ignored, they attributed this correlation to admixing of winnowed and reworked OM. For sediments in the India region, *Calvert et al.* [1995] found a rather good similar correspondence between C_{org}/N_{total} ratios (range 6 to 12) and $\delta^{13}C_{org}$ values (range -24 to -18 ‰). The authors ascribe this to lateral supply of terrigenous and/or reworked OM. For the Pakistan region, we did not find a similar correlation between C/N and $\delta^{13}C_{org}$ (cf. Fig.4), so this combination of variables does not corroborate the possibility of admixing of allochthonous OM.

The HI value of OM, as derived from an S_2 vs C_{org} plot in *Calvert et al.* [1995] for sediments in the Indian region is also uniform (=280). The authors use this observation as evidence of a lack of

enhanced preservation of OM in sediments underlying the OMZ off India. The HI value of OM, as calculated from a S_2 vs C_{org} plot based on the data given by *Pedersen et al.* [1992], for sediments in the Oman region, is again almost uniform (=323). The authors used, however, HI-values not corrected for the analytical artifact due to partial absorption of the pyrolysate to the sediment matrix, and in doing-so found a negative correlation between HI and C_{org}/N_{total} , supposedly supporting admixing of reworked degraded OM. Comparison of these uniform HI values with ours (=327, Fig. 5) for the Pakistan region, reveals that the HI values in surface sediments along the northwestern, northeastern and eastern slopes of the Arabian Sea are almost the same. For this reason, we believe that the HI value is of little or no use as an indicator of admixing of reworked OM, nor of differences in degree of preservation of OM in sediments underlying or below the OMZ in this part of the world ocean.

Based on our discussion of Fig. 4 and the AMS- ^{14}C ages of the OM, we concluded that admixing of allochthonous OM is negligible. An additional argument is that Murray Ridge is a topographically isolated feature and has not the same source areas for allochthonous sedimentary material as the Karachi slope. Winnowing from the high ridge occurs, but stations 463 and 464 in this region (Fig.1) lie so close together that systematic differences in import fluxes of such winnowed material between these two stations is highly unlikely. Since the clustering of the sediments in Figs. 4, 5 and 6 occurs according to their position relative to the lower boundary of the OMZ rather than to

their geographical position, we rejected the option of admixing as an explanation of the observed trend in apparent OM preservation. The good agreement of the ^{14}C ages of OM and of planktonic foraminiferal carbonate at the top of the sediments underlying the OMZ with the mean oceanic reservoir age gives strong credit to our conclusion.

Considering the differences in interpretation of the data for the Oman, India and Pakistan regions, it would be very valuable when in the latter region a study similar to the SEEP program [*Anderson et al.*, 1994] could be carried out.

Conclusions

The observed differences in the C_{org} contents of the sediments deposited within the OMZ and below the OMZ in the northeastern Arabian Sea cannot be fully explained by differences in production in the overlying water, in water depth, in sedimentation rate, and in mineralogical texture, nor by admixing of terrigenous or reworked OM. Enhanced preservation of OM in sediments underlying the OMZ is probably due to reduced bioturbation and to the absence of labile Mn and to a lesser extent of labile Fe oxide. This implies that the low oxygen concentration in the OMZ plays, directly or indirectly, a key role in the enhanced preservation of OM in this region.

Acknowledgements

This research was carried out as part of the Netherlands Indian Ocean Programme 1992-1993, undertaken in co-operation with Kenya, Pakistan and the Seychelles. The programme was organised and supported by the Netherlands Marine Research Foundation (SOZ) of the Netherlands Organization of Scientific Research (NWO). The chief scientist for our cruise was W.J.M. van der Linden. We thank the officers and crew of the R/V Tyro and the technical support given by the technicians of the Netherlands Institute of Sea Research (NIOZ). We also thank the following persons for the analytical and technical support: G. Steenbruggen, J.A. Meima, M. van Noort, A.P. Schmidt (pore water squeezing), G.H. Nobbe (shipboard nutrient analyses), P. Anten, S. Supit and H.P. de Wijs (ICP-AES), S. Huisinga (ZGFAAS, C_{org}), P. Elberse (BET), A.F.M. de Jong (¹⁴C-AMS) and R. Kreulen (Rock-Eval). The constructive remarks and suggestions on a previous draft of this paper by S. Calvert are highly appreciated. This does not imply that he shares the responsibility for the interpretation of our data. This research was funded partly by the Netherlands Organisation for Scientific Research (NWO), grant no.718-215 and Shell grant no. 11107072-EPR.

References

- Aller, R.C., Bioturbation and remineralization of sedimentary organic matter: effects of redox oscillation. *Chem. Geol.*, 114, 331-345, 1994.
- Anderson, R.F., G.T. Rowe, P.F. Kemp, S. Trumbore and P.E. Biscaye, Carbon budget for the mid-slope depocenter of the Middle Atlantic Bight. *Deep-Sea Res.*, 41, 69-703, 1994.
- Bard, E., M. Arnold, P. Maurice, J. Duprat, J. Moyes and J.C. Duplessy, Retreat velocity of the North Atlantic polar front during the last deglaciation determined by ¹⁴C accelerator mass spectrometry. *Nature*, 328, 791-794, 1987.
- Bard, E., Correction of accelerator mass spectrometry ¹⁴C ages measured in planktonic foraminifers: Paleooceanographic implications. *Paleoceanogr.*, 3, 635-645, 1988.
- Calvert, S.E. and T.F. Pedersen, Organic carbon accumulation and preservation in marine sediments: How important is anoxia? In *Organic matter* (Eds. J. Whelan & J.F. Farrington), 232-263 Columbia Univ. Press, New York, 1992.
- Calvert, S.E., T.F. Pedersen, P.D. Naidu, and U. Von Stackelberg, On the organic carbon maximum on the continental slope of the eastern Arabian Sea. *J. Mar. Res.*, 53, 279-296, 1995.
- Canfield, D.E., B.B. Jorgensen, H. Fossing, R. Glud, J. Gundersen, N.B. Ramsing, B. Thamdrup, J.W. Hansen, L.P. Nielsen and P.O.J. Hall, Pathways of organic carbon oxidation in three continental margin sediments. *Mar. Geol.*, 113, 27-40, 1993.
- Canfield, D.E., Factors influencing organic carbon preservation in marine sediments. *Chem. Geol.*, 114, 315-329, 1994.
- Codispoti, L.A., Primary productivity and carbon and nitrogen cycling in the Arabian Sea. In *U.S. JGOFS: Arabian Sea Process Study* (Eds. S.L. Smith, K. Banshe, J. K. Cochran, L.A. Codispoti, H.W. Ducklow, M.E. Luther, D.B. Olson, W.T. Peterson, W.L.

- Prell, N. Surgi, J.C. Swallow & K. Wishner), U.S. JGOFS Planning Report No. 13., 1991.
- Cowie, G.L., J.I. Hedges, F.G. Prahl and G.J. De Lange, Elemental and major biochemical changes across an oxidation front in a relict turbidite: An oxygen effect. *Geochim. Cosmochim. Acta*, 59, 33-46, 1995.
- De Lange, G.J., Shipboard routine and pressure-filtration system for pore-water extraction from suboxic sediments. *Mar. Geol.*, 109, 77-81, 1992.
- Duplessy, J-C., M. Arnold, P. Maurice, E. Bard, J. Duprat and J. Moyes, Direct dating of the oxygen-isotope record of the last deglaciation by ^{14}C accelerator mass spectrometry. *Nature*, 320, 350-352, 1986.
- Froelich, P.N., G.P. Klinkhammer, M.L. Bender, N.A. Luedtke, G.R. Heath, D. Cullen, P. Dauphin, D. Hammond, B. Hartman and V. Maynard, Early oxidation of organic matter in pelagic sediments of the eastern equatorial Atlantic: suboxic diagenesis. *Geochim. Cosmochim. Acta*, 43, 1075-1090, 1979.
- Hedges, J.J. and R.G. Keil, Sedimentary organic matter preservation: an assessment and speculative synthesis. *Mar. Chem.*, 49, 81-115, 1995.
- Henrichs, S.M., Early diagenesis of organic matter in marine sediments: progress and perplexity. *Mar. Chem.*, 39, 119-149, 1992.
- Henrichs, S.M., Sedimentary organic matter preservation: an assessment and speculative synthesis - a comment. *Mar. Chem.*, 49, 127-136, 1995.
- Hoefs, J., *Stable Isotope Geochemistry*. Springer-Verlag. Berlin etc.. 208 pp., 1980.
- Jochem, F.J., F. Pollehne and B. Zeitschel, Productivity regime and phytoplankton size structure in the Arabian Sea. *Deep-Sea Res.*, 40, 711-735, 1993.
- Keil, R.G., E. Tsamakis, C.B. Fuh, J.C. Giddings and J.I. Hedges, Mineralogical and textural controls on the organic composition of coastal marine sediments: Hydrodynamic separation using SPLITTT-fractionation. *Geochim. Cosmochim. Acta*, 58, 879-893, 1994a.
- Keil, R.G., D.B. Montluçon, F.G. Prahl and J.I. Hedges, Sorptive preservation of labile organic matter in marine sediments. *Nature*, 370, 549-552, 1994b.
- Langford, F.F. and M.M. Blanc-Valleron, Interpreting Rock-Eval pyrolysis data using graphs of pyrolyzable hydrocarbons vs. total organic carbon. *Bull. AAPG.*, 74, 799-804, 1990.
- Lee, C., Controls on organic carbon preservation: The use of stratified water bodies to compare intrinsic rates of decomposition in oxic and anoxic systems. *Geochim. Cosmochim. Acta*, 56, 3323-3335, 1992.
- Lee, C., Controls on carbon preservation - New perspectives. *Chem. Geol.*, 114, 285-288, 1994.
- Mayer, L. M., Surface area control of organic carbon accumulation in continental shelf sediments. *Geochim. Cosmochim. Acta*, 58, 1271-1284, 1994.
- Mayer, L.M., Sedimentary organic matter preservation: an assessment and speculative synthesis - a comment. *Mar. Chem.*, 49, 123-126, 1995.
- Müller, P.J., C/N ratios in Pacific deep-sea sediments: Effect of inorganic ammonium and organic nitrogen compounds sorbed by clays. *Geochim. Cosmochim. Acta*, 41, 765-776, 1977.

- Müller, P.J. and E. Suess, Productivity, sedimentation rate and organic matter in the oceans-I: Organic carbon preservation. *Deep-Sea Res.*, 26A, 1347-1362, 1979.
- Müller, P.J., R. Schneider and G. Ruhland, Late Quarternary $p\text{CO}_2$ variations in the Angola current: Evidence from organic carbon d^{13}C and alkenone temperatures. In: *Carbon Cycling in the Glacial Ocean: Constraints on the Ocean's Role in Global Change*. (ed. R.Zahn et al.); NATO ASI Series, 117, 343-366, 1994.
- Olson, D.B., G.L. Hitchcock, R.A. Fine and B.A. Warren, Maintenance of the low-oxygen layer in the central Arabian Sea. *Deep-Sea Res.*, 40, 673-685, 1993.
- Paropkari, A.L., A. Mascarenhas and C. Prakash Babu, Comment on "Lack of enhanced preservation of organic matter in sediments under the oxygen minimum on the Oman Margin" by T.F. Pedersen, G.B. Shimmiel and N.B. Price. *Geochim. Cosmochim. Acta* 57, 2399-2401, 1993a.
- Paropkari, A.L., C. Prakash Babu and A. Mascarenhas, New evidence for enhanced preservation of organic carbon in contact with the oxygen minimum zone on the western continental slope of India. *Mar. Geol.*, 111, 7-13, 1993b.
- Pedersen, T.F., G.B. Shimmiel and N.B. Price, Lack of enhanced preservation of organic matter in sediments under the oxygen minimum on the Oman Margin. *Geochim. Cosmochim. Acta*, 56, 545-551, 1992.
- Pedersen, T.F., G.B. Shimmiel and N.B. Price, Reply to the comment on "Lack of enhanced preservation of organic matter in sediments under the oxygen minimum in the Oman Margin. *Geochim. Cosmochim. Acta*, 57, 2403-2405, 1993.
- Pollehne, F., B. Zeitschel and R. Peinert, Short-term sedimentation patterns in the northern Indian Ocean. *Deep-Sea Res.*, 40, 821-831, 1993.
- Qasim, S.Z., Oceanography of the Northern Arabian Sea. *Deep-Sea Res.*, 29, 1041-1068, 1982.
- Ryther, J.H. and D.W. Menzel, On the production, composition, and distribution of organic matter in the western Arabian Sea. *Deep-Sea Res.*, 12, 199-209, 1965.
- Saager, P. M., H.J.W. De Baar and P.H. Burkill, Manganese and iron in Indian Ocean waters. *Geochim. Cosmochim. Acta*, 53, 2259-2267, 1989.
- Sarnthein, M., U. Pflaumann, R. Ross, R. Tiedemann and K. Winn, Transfer functions to reconstruct ocean palaeoproductivity: a comparison. In: C.P. Summerhayes, W.L. Prell & K.C. Emeis (eds.), *Upwelling Systems: Evolution since the Early Miocene*. Geol. Soc. Spec. Publ., 64, 411-427, 1992.
- Somasundar, K. and S.W.A. Naqvi, On the renewal of the denitrifying layer in the Arabian Sea. *Oceanol. Acta*, 11, 167-172, 1988.
- Suess, E., Interaction of organic compounds with calcium carbonate - II. Organo-carbonate association in Recent sediments. *Geochim. Cosmochim. Acta*, 37, 3233-3257, 1973.
- Suess, E. and P.J. Müller, Productivity, sedimentation rate and sedimentary organic matter in the oceans II. -elemental fractionation. *Colloques Internationaux du C.N.R.S.*, 293, 17-26, 1980.
- Van Bennekom, A.J. and M.A. Hiehle, CTD operations and calibrations during legs D1, D2 and D3 of the Netherlands Indian Ocean Programme. In: *Geological study of the*

Arabian Sea. Cruise report no.3 of the Netherlands Indian Ocean Programme (eds. W.J.M. van der Linden and C.H. van der Weijden), National Museum of Natural History, Leiden, 37-66, 1994.

Van Der Borg, K., C. Alderliesten, C.M. Houston, A.F.M. De Jong and N.A. Van Zwol, Acceleration Mass Spectrometry with ^{14}C and ^{10}Be in Utrecht. *Nuclear Instr. and Methods*, B29, 143, 1987.

Van Der Weijden, C.H., Early diagenesis and

marine pore water. In: *Diagenesis III* (Eds. K.H. Wolf and G.V. Chilingarian) *Developments in Sedimentology*, 47, Elsevier, Amsterdam, pp. 13-134, 1992.

Van der Weijden, C.H., W. J. Zachariasse, G. J. de Lange and G.W. Luther III, Shipboard report of NIOP cruise D3, Geological study of the Arabian Sea, 1992.

Wignall, P.B., *Black Shales*. Clarendon Press. Oxford. 127 pp, 1994.

	Porewater					Solid material					
	Depth in core (cm)	NOx (μM)	Fe (ppb)	Mn (ppb)	SO ₄ ²⁻ (mM)	Water (%)	Fe/Al (ppm/ppm)	Mn/Al (ppm/ppm)	C-org (%)	C/N atomic	delta 13-C (‰PDB)
Boxcore 455	1	25.30	52	73	29.50	65.3	0.6921	0.0062	3.43	9.4	-21.1
	3	8.36	872	123	30.01	68.3	0.6696	0.0057	4.47	9.6	-20.7
	5	2.83	1454	125	29.91	68.6	0.6245	0.0057	4.26	9.7	-20.5
	7	2.52	1666	126	29.98	69.3	0.5932	0.0056	4.31	9.6	-20.5
	9	5.88	1923	143	29.82	69.1	0.5718	0.0055	4.13	9.6	-20.4
	11	0.13	1964	123	29.92	64.4	0.5739	0.0053	4.44	9.6	-20.7
	13.5	0.69	2167	128	29.64	72.9	0.5581	0.0052	4.66	9.7	-20.6
	16.5	7.07	1987	116	29.49	68.5	0.5489	0.0054	4.53	9.6	-20.7
	19.5	4.19	1394	145	29.59	66.0	0.5495	0.0052	4.60	9.5	-20.5
	22.5	3.65	1369	174	29.16	61.1	0.5460	0.0050	5.88	9.7	-20.3
	25.5	3.52	1394	150	29.42	62.4	0.5334	0.0051	3.64	9.8	-20.6
	28.5	2.21	1198	54	29.21	63.5	0.5466	0.0050	5.28	10.0	-20.6
	Boxcore 463	0.75	9.16	2281	114	29.47	72.3	0.6604	0.0071	5.73	9.1
2.25		5.33	308	56	29.29	75.3			5.71	9.3	-21.1
4		2.29	1832	57	29.34	75.4	0.6867	0.0068	5.93	9.5	-21.1
6		2.14	922	83	29.38	74.3	0.7194	0.0067	5.23	9.5	-20.8
8		0.73	1109	67	29.29	73.5	0.7707	0.0066	5.73	9.5	-20.6
10.5		7.26	1126	119	29.24	72.4	0.6637	0.0064	7.12	9.8	-20.6
13.5		11.94	1009	216	29.38	72.7	0.5901	0.0061	7.63	9.5	-20.6
16.5		1.50	952	61	29.05	71.9	0.5622	0.0060	7.42	9.6	-20.7
19.5		3.59	539	83	28.97	71.1	0.5614	0.0059	7.14	9.9	-20.6
23		2.34	700	72	29.01	71.1	0.5616	0.0059	7.48	10.2	-20.7
27		2.15	164	72	28.82	67.6	0.5480	0.0060	6.91	9.9	-20.5
31		0.57	276	72	28.72	67.5	0.5516	0.0060	6.42	10.3	-20.5
Boxcore 464		0.75	38.83	222		29.22	57.5	0.5978	0.0298	1.12	9.5
	2.25	10.52	275	169	29.18	54.7	0.6021	0.0229	1.24	9.0	-21.0
	4	3.20	679	293	29.10	55.8			1.42	9.3	-20.9
	6.5	9.35	1006	713	29.01	55.0	0.5989	0.0078	1.24	9.0	-20.9
	10.5	2.17	1226	770	29.02	56.1	0.5826	0.0079	1.27	9.0	-20.8
	12.5	0.55	1660	732	28.92	53.3	0.5889	0.0077	1.13	9.1	-20.7
	15.5	0.98	1147	605	28.80	51.4	0.5863	0.0077	1.00	9.3	-20.8
	18.5	2.61	1165	562	28.73	51.7	0.5697	0.0076	1.09	9.2	-20.6
	22	3.12	777	630	28.75	48.2	0.5510	0.0077	1.24	9.6	-20.5
	26	4.33	53	403	28.81	48.9	0.5490	0.0075	1.14	9.6	-20.8
Boxcore 466	0.75	94.09	379	20	28.90	60.6	0.6424	0.0981	1.03	7.0	-20.9
	2.25	22.99	1543	396	29.04	54.5	0.6383	0.0366	0.91	7.1	-21.0
	4	6.53	451	1804	28.34	53.4	0.6511	0.0233	0.85	7.3	-20.9
	6	17.26	1024	2932	28.26	53.3	0.6818	0.0089	0.85	7.3	-20.8
	8	3.37	584	4229	28.18	47.5	0.6170	0.0078	0.82	7.4	-21.0
	11	3.03	1079	4554	28.13	45.9	0.5845	0.0080	0.89	7.3	-20.8
	15	2.30	451	4108	28.08	44.1	0.5952	0.0080	0.83	7.1	-21.0
	19.5	1.54	347	4061	28.11	44.5	0.6010	0.0087	0.77	7.3	-20.7

Appendix: Overview of selection of analytical results obtained by analyses of pore-waters and dry sediments. These values are used in the various figures shown in the paper. $N_{ox} = NO_2^- + NO_3^-$, C/N = atomic C_{org}/N_{total} ratio. To eliminate dilution effects by organic matter and carbonates, the Fe and Mn concentrations in the solid sediment samples have been normalized relative to the concomitant Al concentrations.

Porewater					Solid material						
	Depth in core (cm)	NOx (μM)	Fe (ppb)	Mn (ppb)	SO ₄ ²⁻ (mM)	Water (%)	Fe/Al (ppm/ppm)	Mn/Al (ppm/ppm)	C-org (%)	C/N atomic	delta 13-C (‰PDB)
Boxcore 451	1.5		265	80	29.69	69.3	0.5507	0.0055	4.37	9.7	-21.0
	4.5		528	74	29.45	60.8	0.5402	0.0052	4.57	9.9	-21.1
	8	1.09	879	66	29.08	63.6	0.5530	0.0057	4.50	10.0	-20.6
	12	0.12	1086	60	28.98	61.6	0.5333	0.0054	3.99	10.1	-20.5
	16	0.73	1053	63	28.88	63.7	0.5562	0.0057	3.27	10.1	-21.0
	20	1.58	903	58	28.41	58.1	0.5606	0.0054	3.98	10.2	-20.6
	24.5	3.76	948	53	28.19	61.3	0.5633	0.0057	4.07	10.0	-20.9
	29.5	0.80	844	47	27.96	64.5	0.5441	0.0053	3.95	10.2	-20.7
	34.5	0.46	634	48	28.11	63.2	0.5335	0.0055	3.70	10.2	-20.4
	38.5	0.06	266	39	28.24	66.0	0.5602	0.0059	4.07	10.2	-20.7
Boxcore 452	1.25	97.64		202	26.84	54.8	0.6533	0.1388	1.08	7.9	-20.6
	3.75	67.71	21	212	26.88	49.5	0.6349	0.0609	1.00	7.6	-20.8
	6.5	24.48	54	353	25.94	48.0	0.6657	0.0320	0.94	7.9	-20.7
	10	1.08	43	2407	26.34	54.6	0.6184	0.0865	1.24	7.4	-20.9
	14.5	1.14	86	4278	26.41	45.0	0.6319	0.0105			
	19.5	4.18	267	4267	26.13	44.9	0.6207	0.0100	0.81	8.0	-21.1
	24.5	14.44	245	3903	25.13	44.1	0.6149	0.0098	0.81	7.9	-20.7
Boxcore 453	1	67.65	108	65	29.25	62.3	0.6384	0.0634	1.41	8.6	-20.7
	3	9.40	211	1425	29.26	55.6	0.6511	0.0145	1.20	8.9	-21.0
	5.5	2.15	319	1752	28.96	51.8	0.6565	0.0076	1.12	8.8	-21.1
	8.5	3.05	326	2121	29.15	51.8	0.6058	0.0076	1.19	8.9	-20.7
	12	0.85	454	2101	29.02	47.2	0.6105	0.0078	1.14	8.9	-20.6
	16	4.25	695	2245	29.01	49.4	0.6321	0.0082	1.25	8.7	-20.5
	20	4.25	731	2453	29.07	52.3	0.6032	0.0078	1.25	8.7	-20.4
	24	12.35	754	2047	28.96	50.3	0.6298	0.0083	1.30	8.8	-20.6
	28.5	9.00	1072	1340	28.65	50.7	0.6357	0.0079	1.27	8.8	-20.5
	Boxcore 454	1	37.20	214	53	29.23	66.5	0.6430	0.0179	2.94	9.1
3		12.75	322	1213	28.87	61.0	0.6701	0.0071	3.87	9.1	-20.5
5		0.00				58.2	0.6713	0.1683	3.24	9.4	-20.6
7.5		14.50	641	1384	2.85	58.6	0.6078	0.0061	3.39	9.4	-20.5
10.5		18.55	1054	1049	28.80	55.9	0.5873	0.0062	3.37	9.3	-20.4
13.5		11.25	1013	912	28.69	48.6	0.5699	0.0062	3.26	9.6	-20.4
16.5		5.45	828	1015	28.54	54.3	0.5733	0.0065	3.00	9.6	-20.4
20		6.10	923	872	28.52	55.3	0.5839	0.0065	2.90	9.8	-20.3
23.5		6.70	876	825	28.35	55.7	0.5741	0.0065	2.83	9.9	-20.4
29.5		0.00				54.8	0.5749	0.0066	2.51	9.9	-20.4

Appendix: Overview of selection of analytical results obtained by analyses of pore-waters and dry sediments. These values are used in the various figures shown in the paper. $\text{N}_{\text{ox}} = \text{NO}_2^- + \text{NO}_3^-$, C/N = atomic $\text{C}_{\text{org}}/\text{N}_{\text{total}}$ ratio. To eliminate dilution effects by organic matter and carbonates, the Fe and Mn concentrations in the solid sediment samples have been normalized relative to the concomitant Al concentrations.

Orbital- and suborbital-controlled variability in the Oxygen Minimum Zone (OMZ) of the northern Arabian Sea during the last 225,000 yr

G.J. Reichert, L. J. Lourens and W.J. Zachariasse

Faculty of Earth Sciences, Utrecht University, Budapestlaan 4, P.O. Box 80.021, Utrecht, The Netherlands

Abstract

The Oxygen Minimum Zone (OMZ) in the northern Arabian Sea is one of the few regions in the open ocean where oxygen is severely depleted. Changes in the intensity of the OMZ over the past 225,000 yr were reconstructed using geochemical and paleontological proxies for surface water productivity, water column denitrification, deep convective turnover, and the depth of the Aragonite Compensation Depth (ACD). A prolonged summer monsoon caused by higher insolation at the end of the summer season resulted in maximum cumulative surface water productivity in the Arabian Sea and an intense OMZ. Periods with a weak OMZ are characterized by deep convective turnover, which introduced oxygen-rich waters at depths presently occupied by the OMZ. Deep convective turnover is inferred from peak occurrences of *G. truncatulinoides* and *G. crassaformis* and attributed to an intensified winter monsoon. Suborbital variations in convective turnover show a correlation with suborbital climatic events observed in the North Atlantic region. These suborbital ventilation-events in the Arabian Sea coincide with precession-controlled peak occurrences of *G. truncatulinoides* and *G. crassaformis*, indicating that at least part of these events are determined by the precession cycle.

Introduction

The northern Arabian Sea is one of the few regions in the open ocean where dissolved oxygen is severely depleted below the surface mixed layer. Studies on benthic foraminifers [Hermelin, 1991], carbonate dissolution [Ten Kate et

al., 1994], and nitrogen isotopes [Altabet et al., 1995] in the northern Arabian Sea have shown that there were significant variations in the intensity of the OMZ in the sub-recent and more distant past. It is suggested that these variations are controlled by changes in summer productivity and thermocline ventilation

[*Altabet et al.*, 1995]. Upwelling in the northern Arabian Sea stimulates primary productivity and organic particle flux, resulting in high rates of oxygen consumption in the water column, while ventilation of the thermocline is governed by the inflow of southern source water, with minor contributions of Persian Gulf and Red Sea water [*Olson et al.*, 1993]. To what extent these processes controlled past variations in the intensity of the OMZ is still unclear, however. The focus of this study is to portray the variability in time of the OMZ in the northern Arabian Sea, and to identify changes in climate responsible for these variations.

Present-day climate and hydrography

The climate in the Arabian Sea region is characterized by strong monsoonal winds, which invoke large seasonal changes in hydrography and of lithic and biogenic particle fluxes. Dry and cold northeastern winds prevail during the boreal winter when the Tibetan Plateau (~35°N) is an area of high pressure. In summer, when heating of the Tibetan Plateau is at its maximum, a strong pressure gradient between the Tibetan low pressure cell and high pressures over the southern ocean drives warm and humid southwestern winds, which are much stronger than the winter monsoonal winds. These summer winds cause coastal upwelling off Oman and open ocean upwelling northwest of the Findlater Jet and raise surface water productivity to values that are among the highest known for the open ocean

[*Wyrтки*, 1973; *Smith and Bottero*, 1977; *Swallow*, 1984; *Brock et al.*, 1992]. Annual productivity rates reach values between 200 and 400 g C/m²yr [*Kabanova*, 1968; *Qasim*, 1982; *Codispoti*, 1991]. Winter productivity is generally low, except in some areas off the Pakistan coast, where deepening of the mixed layer injects nutrients into the euphotic zone resulting in increased surface water productivity [*Wyrтки*, 1973; *Banse*, 1987; *Madhupratap et al.*, 1996].

The high summer productivity combined with moderate ventilation causes an intense Oxygen Minimum Zone (OMZ) between 150 and 1250 m [*Wyrтки*, 1971; 1973; *Deuser et al.*, 1978; *Olson et al.*, 1993]. Oxygen concentrations within the OMZ of the Arabian Sea reach values of < 0.05 ml/l [*Van Bennekom and Hiehle*, 1994] resulting in the reduction of nitrate in the water column [*Deuser et al.*, 1978]. Thermocline water in the Arabian Sea is ventilated from the south, since there is no subtropical convergence in the north [*Swallow*, 1984]. The mean renewal time for the Arabian Sea OMZ is ~11 years for the entire layer [*Olson et al.*, 1993] and ~4 years for the denitrifying layer [*Naqvi*, 1987]. The main source for thermocline ventilation is the oxygen poor (~1 ml/l [*Olson et al.*, 1993]) Indian Ocean Central Water (IOCW, ~6Sv), and there are only small contributions from oxygen rich Red Sea Water (RSW, ~3.5 mlO₂/l, [*Wyrтки*, 1971]) and Persian Gulf Water (PGW, ~2.6 mlO₂/l, [*You and Tomczak*, 1993]), 0.5 and 0.2 Sv respectively [*Olson et al.*, 1993]. Excess evaporation in the shallow Persian Gulf (average depth ~25 m) leads to the formation of warm saline water. This

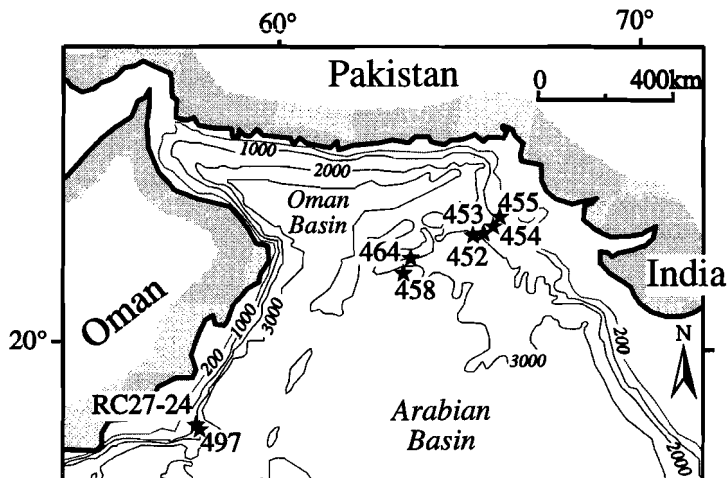


Fig. 1. Location of piston-cores in the northern Arabian Sea. NIOP497 is located on the Oman Margin, NIOP464 is located on a sub marine high, the Murray Ridge. The cores NIOP452, 453, 454, 455 and 458 are located on the Pakistan Margin. Sites 455 and 454 are overlain by the present oxygen minimum zone, the other sites are overlain by oxic water.

water flows through the Straits of Hormuz into the Gulf of Oman where it sinks to depths between 200 and 250 m [Shetye *et al.*, 1994]. The spreading of this water in the northern Arabian Sea is characterized by a salinity maximum at 200 to 400 m, which gradually deepens to the south [Wyrki, 1973]. Excess evaporation in the Red Sea also drives a distinct lagoonal circulation with surface water inflow from the Gulf of Aden and a subsurface return flow of dense water which sinks to ~800 m, and subsequently spreads out at that level [Wyrki, 1973]. The Persian Gulf and the Red Sea thus operate as salt sinks for Arabian Sea surface water.

Material and Methods

The piston cores described in this study were recovered during the Netherlands Indian Ocean programme (1992-1993)

and were taken from the Pakistan Margin (NIOP452, 453, 454, 455 and 458), the Murray Ridge (NIOP464) and the Oman Margin (NIOP497) (Figure 1). Their latitudes, longitudes and water depths are given in Table 1. Core stations NIOP454 and 455 are situated within the present OMZ, while all other cores are from below the OMZ. In general, the sediment consists of homogeneous, dark-greenish to light-greenish/grey hemipelagic muds. NIOP455 contains several laminated intervals. A greyish coloured turbidite sequence occurs in the basal part of NIOP452, 453, 454 and 455.

Water content of the sediment was determined by measuring the weight loss of fixed volume samples after freeze-drying, after which dry and wet bulk density values were calculated. Part of the sample was dried at 60°C for 4 days and thoroughly ground in an agate mortar prior to an HClO₄, HNO₃, HF acid digestion. The final residue was taken up

station	latitude (N)	longitude (E)	depth (m)
452	22°56'.9	065°28'.4	1992
453	23°15'.3	065°44'.5	1556
454	23°27'.6	065°52'.0	1221
455	23°33'.4	065°57'.0	1002
458	21°59'.4	063°48'.7	3001
464	22°15'.4	063°35'.1	1470
497	17°27'.0	057°57'.6	1885

Table 1. Core locations in the northern Arabian Sea. The NIOP cores were recovered during the fall of 1992 during the Netherlands Indian Ocean programme.

in 1 M HCl, after which the elements Ca and Sr were measured by ICP-AES (Perkin Elmer Optima 3000). The analytical precision and accuracy were checked by replicate analyses of samples and standards and were determined to be better than 3%.

Organic carbon was measured on a CNS analyser (Fisons NA 1500) after removal of carbonate. The carbonate was extracted by mechanical shaking with 6M HCl for 12 hours, after which the samples were rinsed with demineralized water in order to remove CaCl₂ and dried. The analytical precision and accuracy were better than 3%.

$\delta^{15}\text{N}$ values in NIOP455 and 464 were measured on bulk sediment and are expressed relative to atmospheric N₂, with a precision better than $\pm 0.2\%$. The particulate nitrogen was converted to N₂ in a CNS analyser, after which the N₂ was carried on a continuous He flow directly into the source of a mass spectrometer (VG PRISM).

$\delta^{18}\text{O}$ values in cores NIOP455, 464 and 497 were obtained by measuring

about 100 handpicked specimens of *Neogloboquadrina dutertrei* (NIOP455, 464 and 497) or *Globigerinoides sacculifer* (NIOP455). These foraminifers were roasted for 30 minutes at 470°C under a He flow to remove organic remains, and then transferred into glass reaction tubes that were evacuated for 14 hours, followed by 6 hours reaction with 100% phosphoric acid at 25.0°C. The released CO₂ was cryogenically separated from the other gases and the isotopic composition measured on a VG SIRA 24 mass spectrometer, with a precision of $\pm 0.1\%$.

Planktonic foraminiferal counts were made on splits (using an Otto microsplitter) from the 150-595 μm fraction. 200-400 specimens per sample were picked, mounted on Chapman slides, identified and counted. Because relative abundances of *G. truncatulinoides* and *G. crassaformis* are low ($\leq 3\%$), they were quantified separately by counting their numbers in 27 (of 45) fields of a rectangular picking tray, to a maximum of 30 specimens. Pteropod preservation is defined by an index which ranges from 0 to 3 (0 = no pteropods; 1 = some small fragments; 2 = many medium-sized fragments; 3 = abundant large sized fragments).

Age model

At present, most palaeoclimatologists adopt the SPECMAP timescale of *Imbrie et al.* [1984]. This timescale was based on the assumption that time lags for the obliquity and precession-related components in $\delta^{18}\text{O}$ are those of a single-exponential climate system with a

response time of 17 kyr. This last value is based on a simple ice sheet model of *Imbrie and Imbrie* [1980], who by visual comparison looked for the best fit between model output and the timing and relative magnitude of six radiometrically dated climatic ($\delta^{18}\text{O}$) events over the last 150 kyr. According to the SPECMAP timescale, the time lags between orbital forcing and the $\delta^{18}\text{O}$ record are 8 and 5 kyr for the obliquity and precession-related components, respectively. *Pisias et al.* [1990], however, took the *Imbrie and Imbrie* [1980] model and ran it with a variable response time for the climate system, which reduces obliquity and precession-related time lags to 7.2 and 3.5 kyr, respectively. This non-linear approach resulted in slightly older ages (up to 3.5 kyr at "termination II") for all isotopic events.

Edwards et al. [1987], *Bard et al.* [1990a, b] and *Gallup et al.* [1994], however, applied a new, and six to ten times more accurate radiometric technique, TIMS for measuring ^{230}Th and ^{234}U , on coral records from Barbados and the Bahamas, and concluded that the age of the Last Glacial Maximum (LGM), and those of isotopic stages 5.1, 5.3, 5.5 and 7.1, are systematically older than the ages given by SPECMAP. They stated that the obliquity and precession-related time lags used in the SPECMAP chronology are overestimated, and that the different isotopic stages are too young by a few thousands years. These observations agree well with the time lags derived from the Mediterranean piston core MD84641 [*Fontugne and Calvert*, 1992] when the sapropel timescale [*Hilgen*, 1990; *Hilgen et al.*, 1993; *Lourens et al.*, 1996] is used to

construct the $\delta^{18}\text{O}$ time series. This timescale is based on the correlation of sapropel patterns to the astronomical record, including a 3-kyr time lag between sapropel midpoints and their inferred 65°N summer insolation maximum [*Lourens et al.*, 1996]. This time lag, which has been kept constant for the entire timescale, was derived from a calendar age of 10.0-6.0 ka (i.e. 8.0 ka for midpoint) for the youngest Holocene sapropel S1 [*Fontugne et al.*, 1989; *Troelstra et al.*, 1991; *Rasmussen*, 1991; *Jorissen et al.*, 1993; *Perissoratis and Piper*, 1992; *Thomson et al.*, 1995] and the correlative insolation maximum at 11 ka [*Lourens et al.*, 1996]. Application of this timescale revealed time lags for the last 225 kyr of 2.9 (± 2.4) and 4.8 (± 14.9) for the precession and obliquity-related components, respectively. The duration of these time lags are on the average 2 kyr shorter than those obtained from the SPECMAP timescale, and are therefore in much better agreement with those expected from the new radiometric dates.

In order to determine the phase-relationships between orbital forcing and climatic variability in the Arabian Sea as accurately as possible, we correlated the $\delta^{18}\text{O}$ records in this study to the oxygen isotope time series of MD84641 by applying the sapropel chronology. We improved the resolution for the last 20 kyr by calibrating our Arabian Sea $\delta^{18}\text{O}$ time series with the AMS- ^{14}C calibrated $\delta^{18}\text{O}$ time series of core 74KL (northern Arabian Sea, $14^\circ 19.26'\text{N}$, $57^\circ 20.82'\text{E}$) [*Sirocko et al.*, 1993] and by including several AMS- ^{14}C dates. The latter were converted to calendar ages using a reservoir age of 400 kyr and

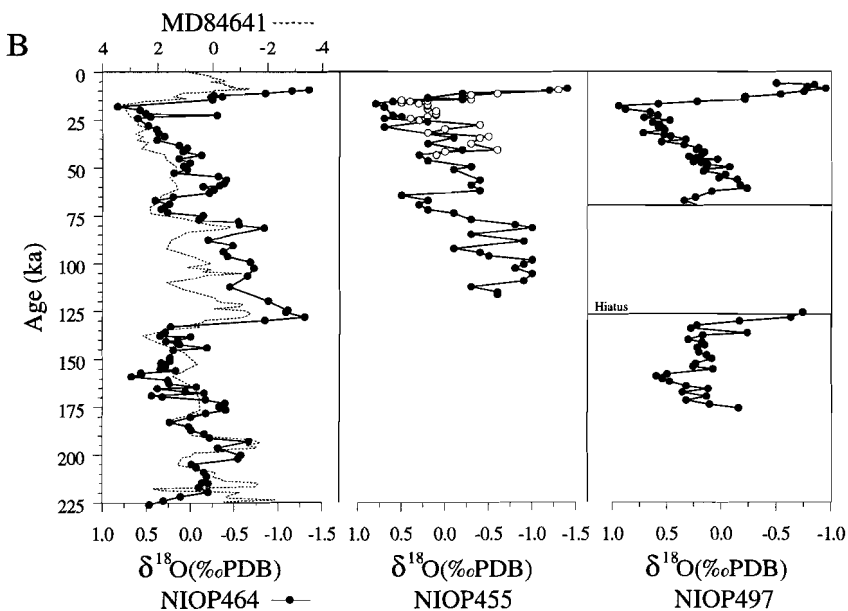
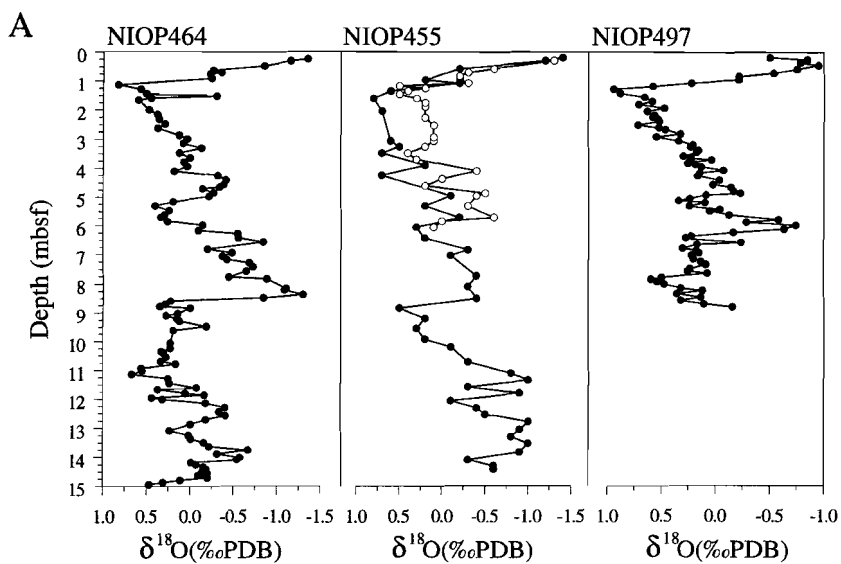


Fig. 2.A) The $\delta^{18}\text{O}$ of *N. dutertrei* (●) and *G. sacculifer* (○), in ‰ relative to the PDB standard, plotted versus depth for cores NIOP464, 455 and 497. Isotopic stage 5 in NIOP497 is largely missing due to a hiatus. B) $\delta^{18}\text{O}$ time series, using our revised (this paper) timescale. $\delta^{18}\text{O}$ of Mediterranean core MD84641 is plotted to show the consistency of our age model.

applying the correction given by the dendrochronology [Stuiver *et al.*, 1986] and U/Th ages [Bard *et al.*, 1990a].

The resulting depth to age conversion of the different cores is plotted in Figure 2. In this figure it can be clearly seen that the youngest 3-8 kyr of the sedimentary record is missing in most cores, due to coring disturbance. Finally, the last occurrence level of pink *Globigerinoides ruber*, which in the Indo-Pacific oceans occurs between isotopic events 5.5 and 5.3 [Thomson *et al.*, 1979] was used to check the chronology of NIOP464 and to constrain position and extent of hiatus in NIOP497. NIOP464 contains two full glacial cycles and covers the longest time interval (225 kyr) of all cores studied. NIOP455 and NIOP497 extend back to 120 and 175 ka, respectively.

Results

Organic Carbon, *Globigerina bulloides* and Summer Productivity

Figure 3a shows strongly covarying C_{org} patterns in three cores recovered from different locations and waterdepths (Figure 1 and Table 1). These covarying fluctuations reflect basin-wide changes in summer production or changes in organic matter preservation. Input of organic carbon derived from the shelf or adjacent continent is negligible [Chapter 2]. Changes in preservation could have been brought about by fluctuations in the intensity and thickness of the OMZ. There are, however, several arguments against a major role of preservation in the general shaping of the C_{org} patterns.

A first argument comes from the upwelling indicator species *G. bulloides*

[Prell *et al.*, 1980]. The relative abundance of this species co-varies with the C_{org} values (Figure 3a), suggesting, therefore, that changes in C_{org} reflect changes in surface water productivity.

A second argument is provided by the covarying C_{org} patterns in a series of cores from the Pakistan Margin in 1000 to 3000 m waterdepth (Figure 3b). Although the deep water cores have an overall lower C_{org} content, fluctuations can be correlated one by one with those in the shallow water cores. If these fluctuations would have been caused by changes in the lower depth limit of the OMZ, then the base of the OMZ should have extended periodically down to 3000 m. In view of the present-day deep water circulation this is highly unlikely.

A third argument comes from the Ba/Al ratio in NIOP464. This ratio, which is linked to surface water productivity through barite precipitation in decaying particulate organic matter while it settles through the water column [Dymond *et al.*, 1992], is positively correlated with the pattern of C_{org} and *G. bulloides* [Chapter 2].

We, therefore, conclude that fluctuations in C_{org} are primarily controlled by variations in surface water productivity that are driven by the summer monsoon.

Sediment $\delta^{15}N$ and Denitrification

The $\delta^{15}N$ records of NIOP464, NIOP455 and RC27-24 [Altabet *et al.*, 1995] also reveal strongly covarying patterns (Figure 4). Small offsets between peaks in RC27-24 and the NIOP cores are most likely caused by the slightly different age model used for RC27-24.

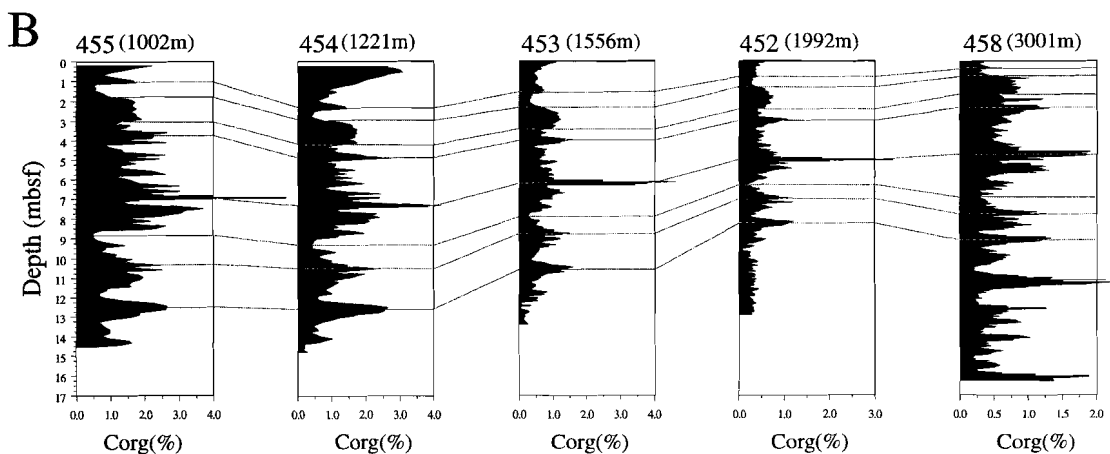
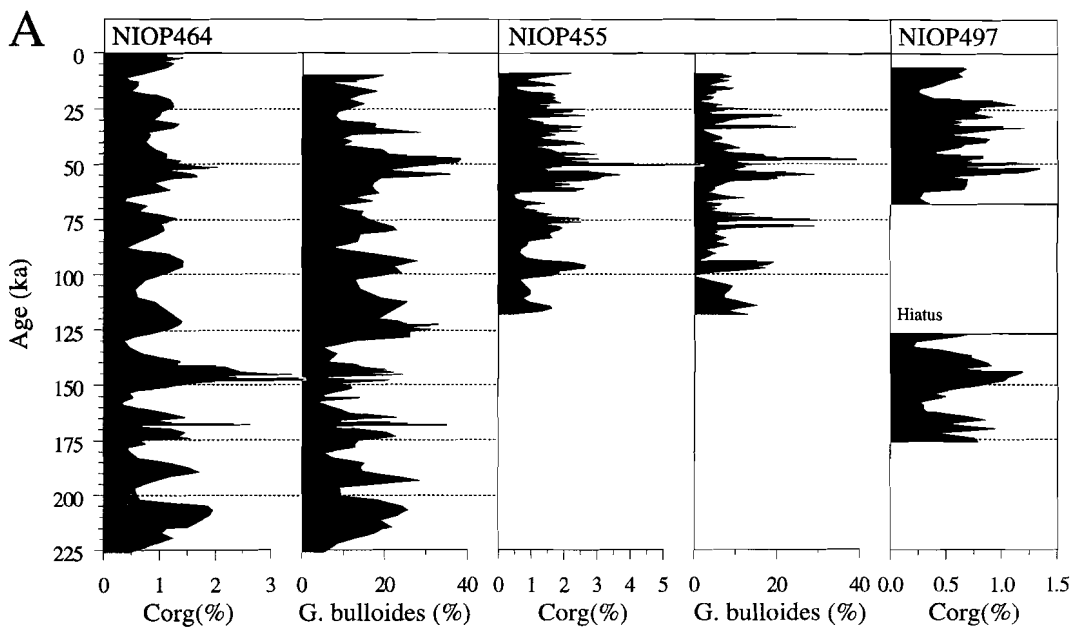


Fig. 3. A) The C_{org} records of NIOP464, 455 and 497 plotted versus age. Maximum C_{org} values correspond to maximum abundances of the upwelling foraminifer *G. bulloides*, demonstrating that basin wide changes in productivity are linked to upwelling. B) Correlation of organic carbon profiles from the Pakistan Margin, ranging in depth from 1000 to 3000m. Cores NIOP455 and 454 are taken from within the present OMZ (150-1250m), the other cores are from below the OMZ. C_{org} profiles can be correlated into great detail. Please note the variations in horizontal scales.

The $\delta^{15}\text{N}$ of particulate organic matter that settles from the surface is basically a function of the $\delta^{15}\text{N}$ of the nitrate source and of the fractionation that occurs during partial utilization of nitrate by phytoplankton [Altabet, 1988; Altabet and Francois, 1994; Montoya, 1994]. Denitrification enriches the ^{15}N content of the subsurface nitrate substantially [Cline and Kaplan, 1975; Liu and Kaplan, 1989], which, after welling up to the surface will influence the isotopic composition of sinking particulate nitrogen. Present-day denitrification rates in the northern Arabian Sea are sufficiently high to produce a significant subsurface enrichment in $\delta^{15}\text{N}$, which, through upwelling, will influence the $\delta^{15}\text{N}$ of the sinking particulate matter [Schäfer and Ittekkot, 1993; Altabet et al., 1995]. The $\delta^{15}\text{N}$ of the particulate and sedimentary organic matter, therefore, is strongly controlled by changes in water-column denitrification rates [Schäfer and Ittekkot, 1993; Altabet et al., 1995].

Downward transport of particulate nitrogen from the euphotic zone and early diagenesis in sediments do not seem to significantly alter the nitrogen isotopic ratios [Altabet and Francois, 1994]. Early diagenetic degradation of organic matter may increase the sedimentary $\delta^{15}\text{N}$ values, but such an increase is generally very small compared to the denitrification effect [Montoya, 1994]. This is confirmed by the great similarity in the $\delta^{15}\text{N}$ patterns of NIOP464 and 455, in spite of the fact that NIOP455 is located well within and NIOP464 below the present day OMZ. We conclude, therefore, that it is unlikely that past changes in early diagenetic degradation of organic matter have

significantly altered the sedimentary $\delta^{15}\text{N}$ signal.

When upwelled water containing elevated concentrations of NO_3^- is transported laterally, the isotopic fractionation that accompanies NO_3^- utilization by primary producers will cause an increase in $\delta^{15}\text{N}$ of the residual NO_3^- away from the upwelling area [Altabet and Francois, 1994]. Such an increase has been shown by Altabet et al. [1995] in surface sediment $\delta^{15}\text{N}$ values from the Oman margin to the Owen Ridge, but differences are small. Temporal (basin wide) $\delta^{15}\text{N}$ changes, on the other hand, must reflect changes in subsurface denitrification [Altabet et al., 1995]. Denitrification starts when oxygen concentrations decrease to values between 5 and 10 μMl^{-1} [Deuser et al., 1978], since nitrate reduction is, after the consumption of most of the free oxygen, the thermodynamically favoured next step in the oxidation of organic matter to CO_2 . The rate of denitrification as recorded in the $\delta^{15}\text{N}$ value of organic matter is, therefore, directly linked to the mid-water oxygen concentration and thus to the intensity of the OMZ.

Sr/Ca and the Aragonite Compensation Depth

Aragonite has a higher Sr content than calcite [Sutherland et al., 1984] and, therefore, variations in the Sr/Ca ratio reflect changes in the number of pteropods since predominantly their shells are made up of aragonite [see also Chapter 2]. Fig. 5 shows Sr/Ca ratio's in three cores from intermediate water-depths on the Pakistan Margin. Intervals without pteropods show Sr/Ca base level

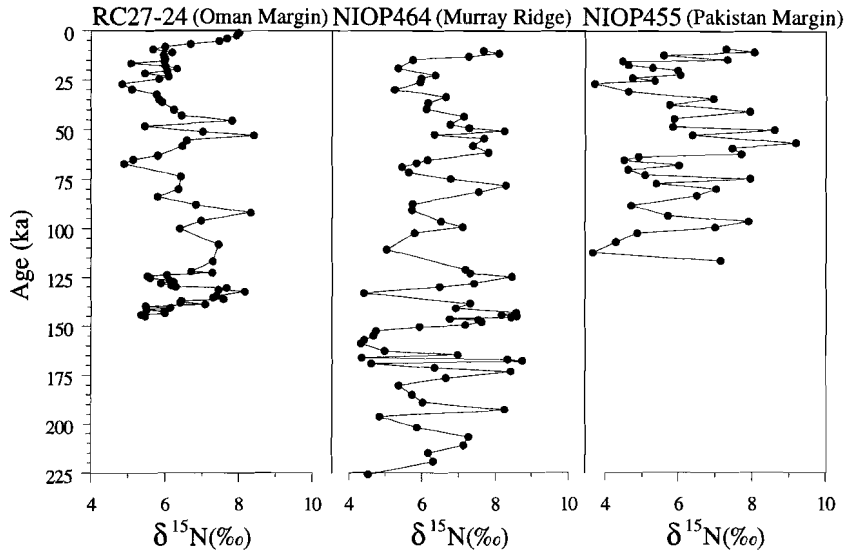


Fig. 4. Sedimentary $\delta^{15}\text{N}$ records from the Oman Margin, Murray Ridge and the Pakistan Margin. The $\delta^{15}\text{N}$ data of core RC27-24, Oman Margin, is from *Altabet et al.* [1995]. Variations in $\delta^{15}\text{N}$ are almost synchronous in all three cores. Because different age models have been used small offsets may occur between the records.

values of $\sim 40 \times 10^4$. Correlative Sr-enrichment events are recorded in all three cores (Fig. 5) and reflect periods during which the ACD must have deepened to at least 1556 m (being the present-day waterdepth of the deepest core, NIOP453). Intervals in NIOP455 depleted in Sr are associated with laminated sediments, whereas intervals enriched in Sr correspond with non-laminated (bioturbated) sediments. This relationship indicates that Sr-enrichment events represent periods characterized by more oxygenated bottom water conditions. The ACD in the modern northern Arabian Sea lies within the OMZ at about 500 m [Berger, 1977]. Water in the OMZ is undersaturated with respect to aragonite because oxygen consumption lowers the (solution) pH and carbonate saturation due to CO_2 addition and the oxidation of ammonia to

nitrate [Canfield and Raiswell, 1991]. Dissolution takes place at or close to the sediment/water interface, as the increase in alkalinity, brought about by sulphate reduction deeper in the organic-rich sediments, enhances pteropod preservation [Canfield and Raiswell, 1991]. We therefore suggest that enhanced pteropod preservation (reflected by high Sr/Ca values), reflects a substantial weakening of the OMZ. Low Sr/Ca values (and laminated sediments in NIOP455) on the other hand are indicative of an intense OMZ.

Comparison between the Sr/Ca, C_{org} and $\delta^{15}\text{N}$ profiles shows that the Sr/Ca maxima at 63, 30 and 15 ka correlate with minima in the C_{org} and $\delta^{15}\text{N}$ records (cf. Figures. 3A, 4 and 5). This indicates that a deep ACD (due to a higher oxygen availability and/or lower oxygen consumption) is associated with reduced

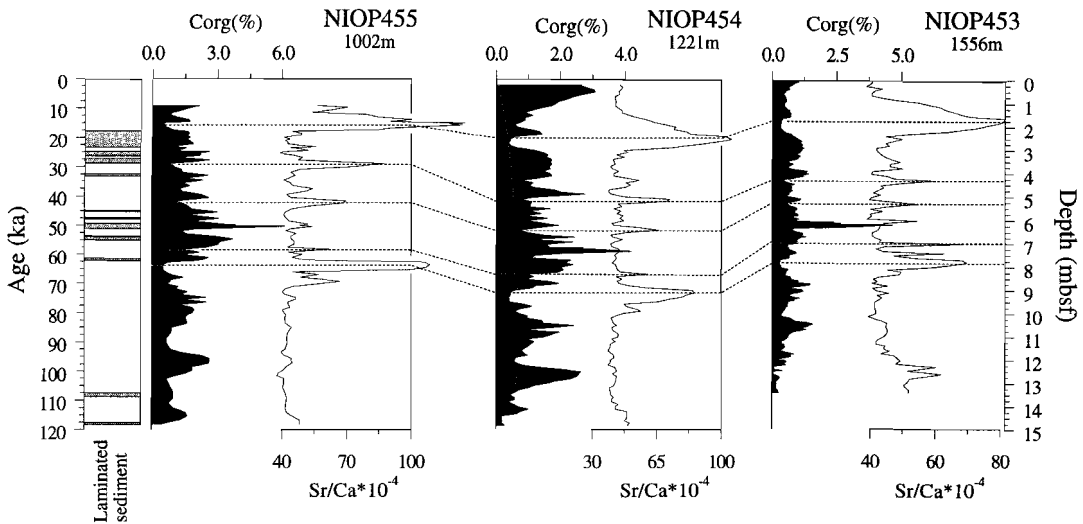


Fig. 5. C_{org} and Sr/Ca records from the Pakistan Margin, cores NIOP453, 454 and 455. The record of core NIOP455 is plotted against age, the records of NIOP453 and 454 are plotted against depth. The first column indicates laminated sediments in core NIOP 455. The major Sr/Ca peaks are connected with dashed lines, minor peaks can also clearly be correlated between cores.

surface water productivity conditions and decreased denitrification rates in the water column.

G. truncatulinoides, *G. crassaformis* and Vertical Mixing

The sedimentary record in the northern Arabian Sea contains 10 intervals with substantial numbers of *G. truncatulinoides* and/or *G. crassaformis* over the past 225 kyrs (Figure 6), which, as revealed in Figure 7, covary with variations in pteropod fragments and $\delta^{15}N$ values. These intervals represent periods during which environmental conditions must have been significantly different from today because reproducing populations of these two species are presently absent in the Arabian Sea [Zobel, 1971; Cullen and Prell, 1984;

Anderson, 1991; Curry *et al.*, 1992; Brock *et al.*, 1992].

Plankton tow and/or sediment trap studies in the western North Atlantic [Tolderlund and Be, 1971; Be *et al.*, 1971; Deuser *et al.*, 1981; Williams *et al.*, 1981; Hemleben *et al.*, 1985] suggest that *G. truncatulinoides* is a subtropical species, which reproduces in the mixed layer during winter just before the early spring bloom. This timing ensures the juveniles of an ample supply of food since this species feeds on phytoplankton, preferably diatoms [Hemleben *et al.*, 1985]. The juveniles sink to deeper water as they increase in size reaching water depths of 500-800 m during summer and fall [Be and Tolderlund, 1971; Durazzi, 1981; Hemleben *et al.*, 1985]. These deep living populations are supposed to return to the surface by deep

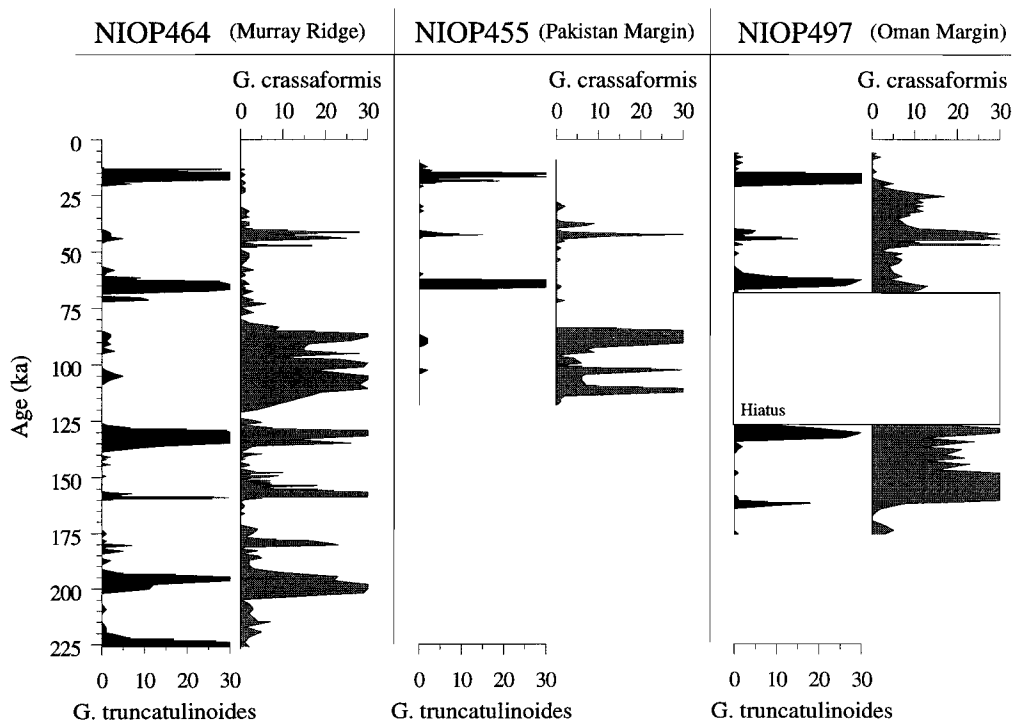


Fig. 6. Time series of *G. truncatulinoides* and *G. crassaformis* in cores NIOP464, 455 and 497 revealing several stratigraphic levels containing both species, which are presently absent from the northern Arabian Sea. Over the past 225 kyr the sedimentary record show 10 intervals with abundant *G. truncatulinoides* and/or *G. crassaformis*, which can be correlated across the Arabian Basin.

mixing in winter, whereafter the life cycle is completed by reproduction. Although the question of depth and timing of reproduction is not completely solved (Lohmann and Schweitzer [1990] suggest reproduction below 600 m before winter mixing), it is clear that reproducing populations require seasonal deep mixing to return either juveniles or adults to the surface: individuals sinking below the top of the main pycnocline will not complete their life cycle. Reproducing populations of *G. truncatulinoides*, therefore, occur in the cool subtropical gyres of the Atlantic [Be and

Tolderlund, 1971; Be et al., 1971], Pacific [Bradshaw, 1959], and Indian Ocean [Be and Hutson, 1977].

G. crassaformis is a deep living, warm-water species [Be and Tolderlund, 1971; Hemleben et al., 1989]. This species is generally rare in tow, trap, and core top samples, which is the main reason why we are ignorant of its life cycle. Hemleben et al. [1989] have speculated that the life cycle of *G. crassaformis* is similar to that of *G. truncatulinoides* and *G. hirsuta* (which is a fair guess because these three species are phylogenetically closely related). The

implication then would be that *G. crassaformis* matures at depth and reproduces at the surface. Substantial numbers of this species have been recorded from the (sub)thermocline water in the eastern equatorial Atlantic [Jones, 1967], with a relative abundance of 13% in one deep tow sample [Cifelli, 1967]. Also core top samples from this region contain *G. crassaformis* together with other species considered to be indicative of (seasonal) oceanic upwelling [Ravelo *et al.*, 1990]. Oceanic upwelling in this region resulting in shoaling, and surfacing of thermocline water in the northern summer [Herbland *et al.*, 1985]. Oberhansli *et al.* [1992] studied tow samples from the eastern South Atlantic and found high numbers of *G. crassaformis* in the upper 300 m at the edge of the Angola-Benguela Front, which is a region with a well-developed thermocline in the northern winter and vertical mixing in the summer [Merle, 1978]. *G. crassaformis* is also prolific in core top samples off the Zaire River [Van Leeuwen, 1989], which is a region of seasonal coastal upwelling [Van Bennekom *et al.*, 1978]. Finally, high percentages were found by Cifelli and Benier [1976] in deep tow samples south of Cape Blanc (NW Africa) in April, which is the time of the year of coastal upwelling [Wooster *et al.*, 1976]. *G. crassaformis* was absent in tow samples taken in the non-upwelling season. Most of these data suggest that the life cycle of *G. crassaformis* is tuned to seasonal upwelling. Seasonal upwelling may provide a mechanism to return adults to the surface (or juveniles in case reproduction takes place at depth). Upwelling water comes from depths not

greater than 200-300 m [e.g., Pond and Pickard, 1983]. This suggests that any process which enables *G. crassaformis* to complete its life cycle in the upper 200-300 m will result in locally reproducing populations. Usually, this process is seasonal upwelling but an alternative is seasonal vertical mixing. Seasonal mixing would explain the high numbers of *G. crassaformis* found by Oberhansli *et al.* [1992] at a station in the region of the Angola-Benguela Front.

Expatriates of *G. truncatulinoides* and *G. crassaformis* are probably continuously carried into the Arabian Sea via the Somali Current. Shallow (100-125m, Banse [1984]) winter mixing and extremely low oxygen values in the OMZ, however, prevent these expatriates from completing their life cycle. Obviously, these adverse conditions prevailed in the northern Arabian Sea over the past 225 kyr. Deeper (seasonal) mixing and resultant break-down of the OMZ must have occurred during 10 short periods in which large numbers of variably-sized shells of *G. truncatulinoides* and/or *G. crassaformis* accumulated on the seafloor (Figures 6 and 7).

Deepest mixing (to depths of 500-800 m) is suggested for sole peak occurrences of *G. truncatulinoides* at 225, 65 and 15 ka (provided that the juveniles produced in the Arabian Sea had similar growth and sinking rates as their modern representatives in the western North Atlantic). Such deep winter mixing may have had an adverse effect on the reproductive success of *G. crassaformis*. This species is generally rare and excessive deep mixing may have reduced the concentration of gametes below a

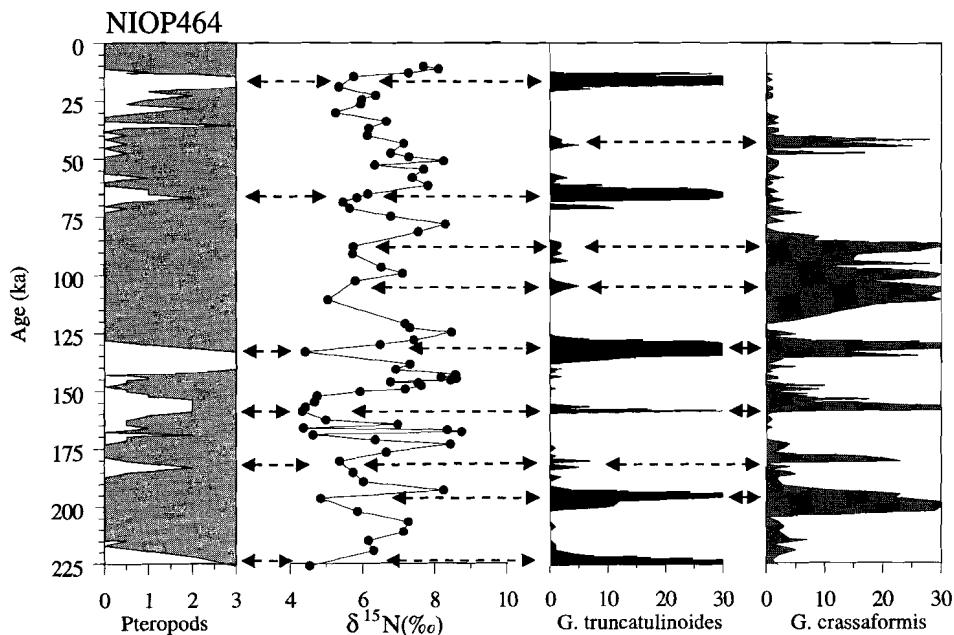


Fig. 7. Correlation between pteropod preservation index, $\delta^{15}\text{N}$ indicative for the intensity of the OMZ and records of *G. truncatulinoides* and *G. crassaformis*, indicative for the intensity of the convective overturn.

critical level and/or cooled sea water to beyond the reproductive temperature of *G. crassaformis*, which seems slightly higher than that of *G. truncatulinoides* [Pujol, 1980].

The presence of substantial numbers of *G. truncatulinoides* between 18 and 14 ka was found earlier by McKenna and Prell [1994] and by these authors also explained in terms of intensified convective overturn. Joint peak occurrences of *G. truncatulinoides* and *G. crassaformis* at ~132, ~158 and ~198 ka on the other hand point to shallower winter mixing, probably to depths of 300-500 m, whereas peak values of by *G. crassaformis* together with low numbers of *G. truncatulinoides* at ~42, ~87, ~107 and ~180 ka might represent periods with

vertical (winter) mixing to depths of 200-300 m.

Reproductive conditions for *G. crassaformis* appear on the average to have been better at site 497 than elsewhere in the Arabian Sea, in view of the higher overall abundance of this species in NIOP497 (Fig. 6). A plausible explanation for this is that summer coastal upwelling keeps annual mean oxygen levels in the upper 300 m sufficiently high [Wyrki, 1971; Van Bennekom et al., 1995] to maintain living populations at this site even during periods of shallow winter mixing and an intense OMZ. Optimum conditions at this site and elsewhere in the northern Arabian Sea prevailed during periods of intensified winter mixing.

Orbital Variations in OMZ Intensity

With core NIOP464 from the Murray Ridge we recovered the longest stratigraphic succession, i.e. 225,000 years. We therefore selected that core for cross-spectral analyses of its various climatic proxies.

The frequency distribution pattern of the $\delta^{18}\text{O}$ record of NIOP464 is in good agreement with that of MD84641 and in excellent agreement with that of SPECMAP (Figure 8), indicating that the $\delta^{18}\text{O}$ record of NIOP464 is strongly determined by variations in global ice volume. Cross-spectral analyses between the $\delta^{18}\text{O}$ records of NIOP464, MD84641 and SPECMAP revealed highly significant coherencies in all orbital frequency bands of the spectrum (Table 2). Time lags over the last 225 kyr between the precession and obliquity cycles and their derivative components in the $\delta^{18}\text{O}$ record of NIOP464 arrive at 2.3 (± 2.4) kyr and 3.6 (± 10.9) kyr, respectively. These time lags are considerably shorter than those obtained by SPECMAP, which arrive at 5.6 (± 3.7) kyr and 8.3 (± 5.7) kyr, respectively. This difference is due to our preference for the sapropel timescale over the SPECMAP chronology. We attribute the small differences in precession (± 0.6 kyr) and obliquity (± 1.2 kyr) lags between NIOP464 and MD84641 to uncertainties in our (visual) correlation procedure.

The spectra of the various climatic proxy records from the Murray Ridge (Figure 8) can be subdivided into two groups, which are 1) dominantly (120-kyr) glacial-controlled (Ba/Al, Ti/Al and pteropods) and 2) dominantly (23-kyr) precession-controlled (C_{org} , *G. bulloides*,

$\delta^{15}\text{N}$, and *G. truncatulinoides*+*G. crassaformis*). The influence of the 40 kyr-obliquity cycle is less clearly reflected in all spectra, but is present. Focusing on the 23-kyr precession period, the C_{org} , *G. bulloides*, $\delta^{15}\text{N}$ and Ba/Al records are nearly in phase (Table 2; Figure 9), indicating a strong link between variations in summer surface water productivity and OMZ intensity. These records show an anti-phase relationship with maximum abundances of *G. truncatulinoides* + *G. crassaformis* and pteropod fragments (Figure 9), indicating that maxima in summer surface water productivity and OMZ intensity coincide with minimum winter mixing and a shallow ACD, and visa versa. A comparison between the precessional time lags of the various proxy records and the last precession cycle reveals that on average summer surface water productivity and OMZ intensity were at a maximum between 7 and 4 ka. This implies that they lag the last precession minimum (at 11.5 ka) with 4.5 to 7.5 kyr and the $\delta^{18}\text{O}$ minimum (at 9 ka) with 2 to 5 kyr (Figure 9). Minima in OMZ intensity as indicated by maxima in pteropod fragments and high abundances of *G. truncatulinoides* - *G. crassaformis*, occur between 18 and 14 ka. The maximum in Ti/Al follows immediately after the paleoproductivity maximum at approximately 3 ka (Figure 9).

Suborbital Variations in OMZ Intensity

The Sr/Ca and C_{org} records from NIOP455 (Karachi Margin) show that suborbital changes in the intensity of the

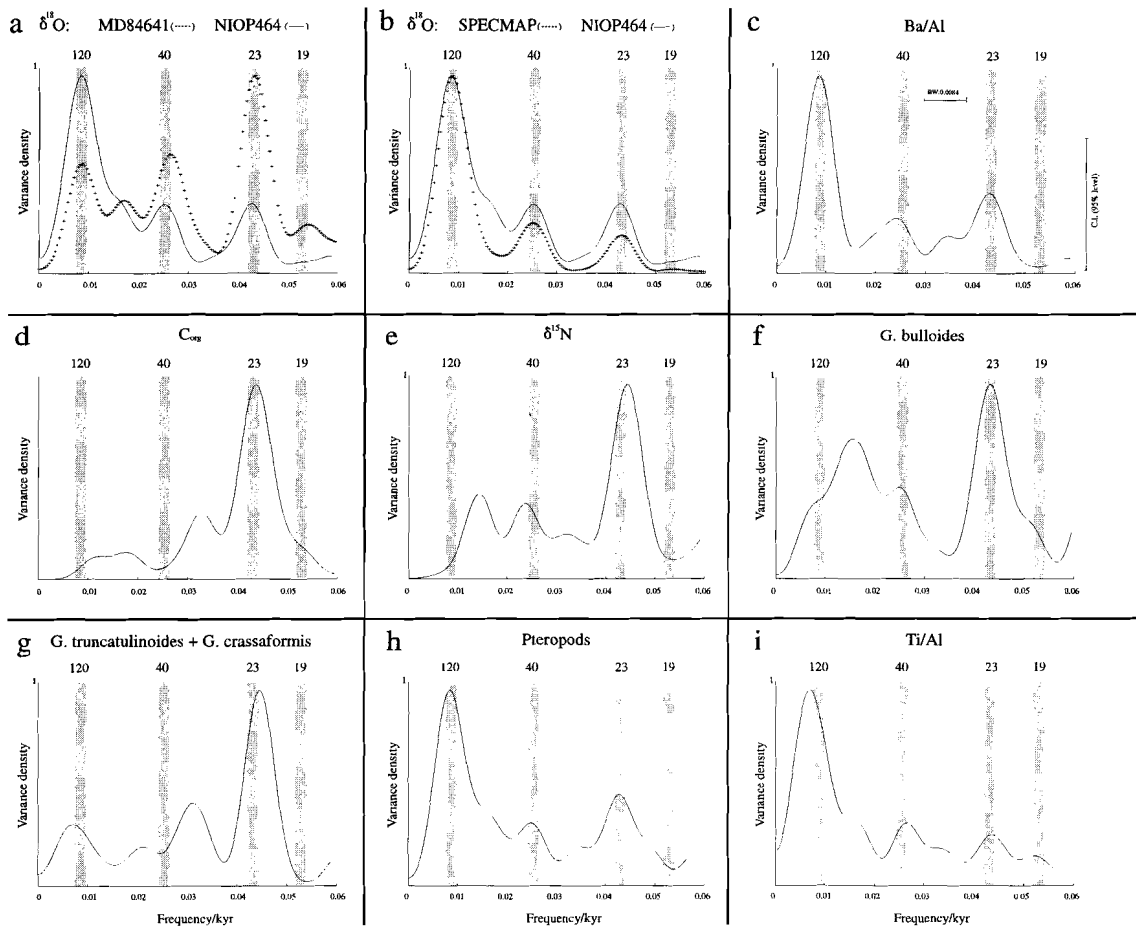


Fig. 8. Power spectra for a) $\delta^{18}\text{O}$ for cores NIOP464 and MD84641, b) $\delta^{18}\text{O}$ for core NIOP464 and SPECMAP, c) Ba/Al, d) C_{org} , e) $\delta^{15}\text{N}$, f) *G. bulloides*, g) *G. truncatulinoides* and *G. crassaformis*, h) Pteropod preservation index, and i) Ti/Al, for core NIOP464.

OMZ are superimposed on the orbital-scale changes (Figure 10). Sr/Ca maxima at 15 and 64 ka are closely associated with low C_{org} values and substantial numbers of *G. truncatulinoides*, while the Sr/Ca maximum at 42 ka is accompanied by abundant *G. crassaformis* and some *G. truncatulinoides* (cf. Figures 5 and 10). Intervening Sr/Ca maxima at 23, 29, 38 and 50 ka show correspondingly low C_{org} values, however, without significant numbers of *G. truncatulinoides* and/or *G. crassaformis* (Figure 10). All these Sr/Ca maxima and C_{org} minima represent periods of deep convective overturn in the northern Arabian Sea and correlate with brief and cold spells in North Atlantic climate which are generally associated with so-called Heinrich-layers [Bond *et al.*, 1992] and/or with the colder parts of the Dansgaard-Oeschger cycles [Dansgaard *et al.*, 1993] as recorded in the $\delta^{18}O$ of the GRIP summit ice core (Figure 10). Our correlation indicates that besides the orbitally-driven climatic variations, also climatic changes

associated with Heinrich-layers resulted in increased deep (winter) mixing, decreased summer surface water productivity, and decreased OMZ intensity.

Discussion

The most conspicuous feature of the OMZ in the northern Arabian Sea is that it fluctuates in intensity on both orbital as well as suborbital timescales. Maxima in OMZ intensity are accompanied by maxima in surface water productivity (Figures 3 and 4), while OMZ minima coincide with deep mixing, which resulted in a reduction of the denitrification rate and a deeper ACD (Figures 5 and 7). If the fluctuations in the OMZ are primarily driven by changes in surface water productivity then they are most likely related to changes in the intensity of coastal and open ocean upwelling during the summer months and, hence, to the strength of the summer monsoonal circulation. On the other

Proxy record	41-kyr		23-kyr	
	Coherency	Phase (degrees)	Coherency	Phase (degrees)
$\delta^{18}O$ (NIOP464)	0.88	215 ± 92	0.93	36 ± 68
$\delta^{18}O$ (MD84641)	0.81	225 ± 124	0.97**	45 ± 37
$\delta^{18}O$ (SPECMAP)	0.97**	252 ± 45	0.95*	88 ± 58
C_{org}	0.75	10 ± 434	0.99**	296 ± 29
$\delta^{15}N$	0.91	357 ± 86	0.96*	260 ± 49
Ti/Al	0.82	289 ± 120	0.98**	334 ± 33
Ba/Al	0.93	4 ± 68	0.89	250 ± 91
<i>G. bulloides</i>	0.94	27 ± 64	0.98**	283 ± 31
<i>G. trunc.-crass.</i>	0.33	261 ± 495	0.94	119 ± 64
Pteropods	0.94	264 ± 61	0.95*	71 ± 56

Cross-spectral parameters: analyses 6 to 228 ka. The hypothesis that the series are unrelated at frequencies 0.2458 (obliquity) and 0.4333 (precession), i.e. that both the true cross amplitude and coherency are zero, may be rejected at the 10% level (indicated by *) if the squared coherency > 0.90. This value is derived from the upper 10% point of the F-distribution on (2,d-2) degrees of freedom, with d is 4. This value is 0.95 (indicated by**) for the 10% level and 0.99 for the 1% level. Bandwidth, BW=0.008429; interpolated time interval is 2-kyr. Phase angle indicate phase leads with respect to orbital maxima.

Table 2. Coherency and phase lags between obliquity and precession and their related frequencies in the geological record.

hand, if these fluctuations are linked to deep mixing then they are most likely invoked by increased surface water cooling during winter and hence, related to the strength of the winter monsoonal circulation. The effect of winter mixing on OMZ intensity might have even been amplified by positive feedback mechanisms. Deep sinking of nutrient-depleted surface water in winter over a succession of years would have caused a progressive decrease in nutrient content of the subsurface waters even if the upwelling rate during summer remained constant. Moreover, higher subsurface oxygen levels would cause a reduction in the recycling of phosphates from the sediment. Today, there is additional input of phosphate at the suboxic water-sediment interface, since benthic regeneration of reactive phosphorus is more extensive when sediments are deposited under suboxic conditions [Van Cappellen and Ingall, 1994]. This extra input of regenerated phosphorus would be reduced after reoxygenation of the OMZ. Both mechanisms will therefore act as an internal feedback mechanism that amplifies the effect of deep winter mixing on the subsurface oxygen content and, hence, the variability of the Arabian Sea OMZ intensity. In the next sections we will discuss several processes, which may have triggered the variability of the Arabian Sea OMZ on different timescales and view them in the light of some conceptual hypotheses.

The 120-kyr Cycle

The occurrence of a strong 120-kyr cyclicity in the spectra of the $\delta^{18}\text{O}$, Ba/Al, Ti/Al and pteropod record and to

a lesser degree in that of the *G. truncatulinoides* - *G. crassaformis* record (Figure 8) indicates that at least part of the climatic variability observed in the Arabian Sea is determined by large-scale glacial cycles. In addition, a comparison between the individual *G. truncatulinoides* and *G. crassaformis* records further reveals that *G. crassaformis* is abundant during isotopic stage 5, whereas *G. truncatulinoides* is nearly absent (Figure 6), indicating that some specific glacial boundary conditions even controlled the intensity of deep (winter) mixing.

General circulation modelling (GCM) experiments suggests that variations in global ice volume can affect the intensity of the Indian summer monsoon [e.g., Kutzbach, 1981; Prell, 1984, 1993]. The modelled response, however, is very complex, because several glacial boundary conditions (including relatively high Indian Ocean sea surface temperatures (SST's), expanded northern hemisphere ice volume, lowered sea level and increased land albedo) alter the land-sea pressure gradient across the region from 0 to 30°N thereby influencing the strength of the summer monsoonal circulation [Kutzbach and Geutter, 1986]. Some sensitivity tests run by Manabe and Hahn [1977] indicated that changes in summer monsoon are more sensitive to changes in surface albedo than to changes in SST. Additional GCM experiments showed that the direct influence of the Laurentide ice sheet on the Asian surface temperatures was minor [Mitchell *et al.*, 1988], implying that glacial-controlled change in the Asian surface albedo is the most important factor controlling 120 kyr

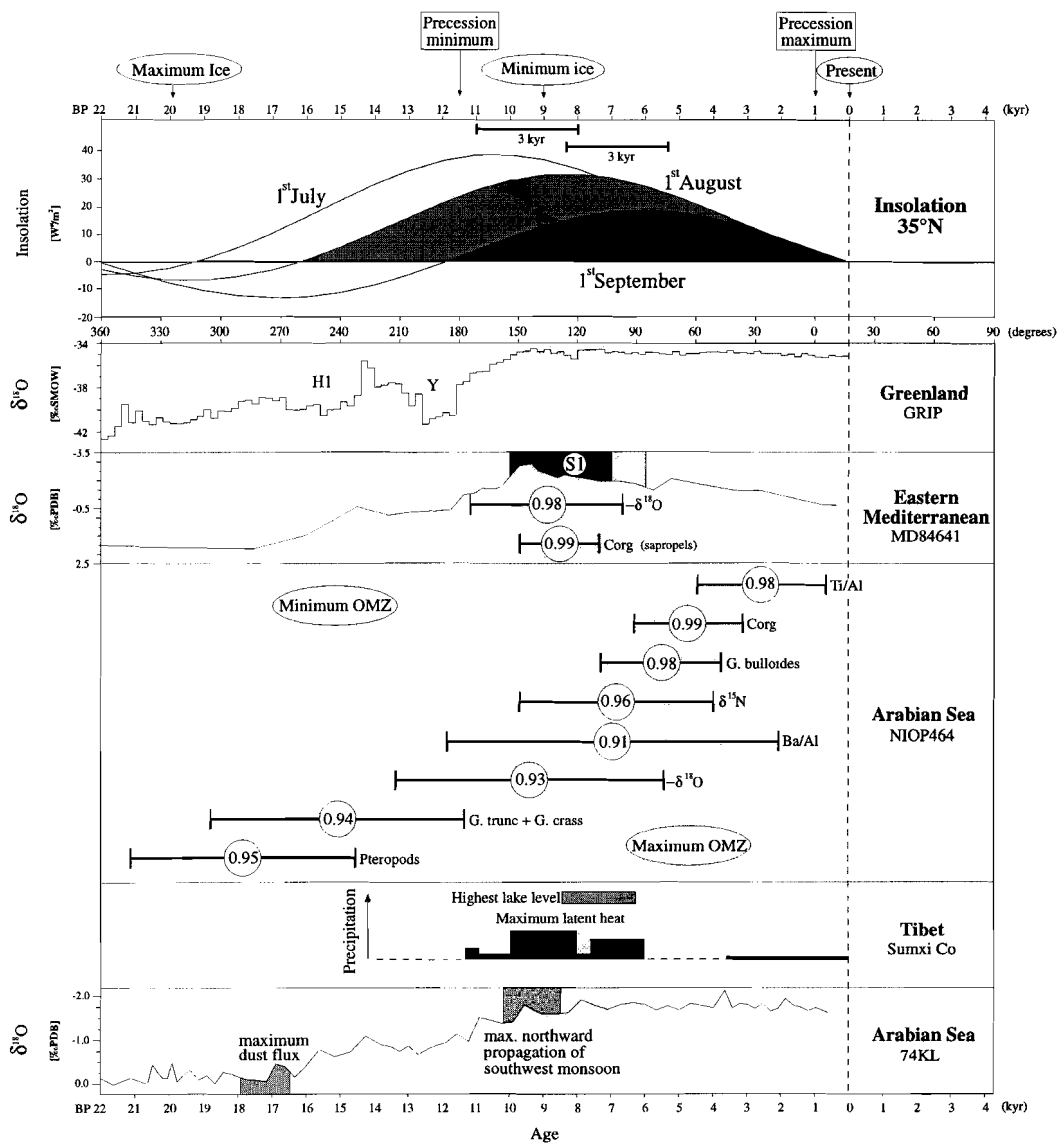


Fig. 9. Phase relationships between various proxy records from the Murray Ridge and Eastern Mediterranean and precession, based on cross-spectral analyses. Encircled numbers are coherencies; error bar marks 95% confidence interval. Insolation is plotted for 1st July, 1st August and 1st September, related to early, middle and late monsoonal stages. $\delta^{18}\text{O}$ records are from the Grip-Ice core [Dansgaard *et al.*, 1993] and from the eastern Mediterranean core MD84641 [Fontugne and Calvert, 1992]. S1 refers to the position of the most recent sapropel. The precipitation record of lake Sumxi Co (Tibet) for the last 13 kyr, is from Gasse *et al.* [1991]. The $\delta^{18}\text{O}$ record of 74KL (Oman Margin) and the maximum northward position of the ITCZ over the Arabian peninsula is from Sirocko *et al.* [1993].

variations in summer monsoon strength. Including the influence of seasonal variation in Asian snow cover [Barnett *et al.*, 1988], one would expect a weaker monsoon during glacials due to an increase in the areal extent of the (seasonal) snow cover over central Asia and to a decrease in continental albedo as a result of a reduction in vegetational cover. Minima in continental albedo and (seasonal) snow cover over central Asia prevailed during interglacial periods leading to more effective solar heating of the continental surface, a stronger Asiatic low pressure cell and, hence, to a stronger summer monsoon. However, some caution with respect to the outcome of most of these experiments is required, because they incorporate relatively high Indian Ocean SST's during the LGM as boundary condition, whereas there is growing evidence that also the tropical and subtropical (sea surface) glacial temperatures were significantly lower during glacial times [Guilderson *et al.*, 1994; Stute *et al.*, 1995; Thompson *et al.*, 1995; Miller *et al.*, 1997].

Variations in the glacial to interglacial boundary conditions may also have changed the intensity of deep (winter) mixing. At present, winter mixing in the northern Arabian Sea extends to depths of about 100 m [Banse, 1984; Madhupratap *et al.*, 1996], which is too shallow to ventilate the thermocline waters of the OMZ. During glacial periods, intensified winter monsoonal winds [Duplessy, 1982; Van Campo *et al.*, 1982; Sarkar *et al.*, 1990; COHMAP, 1988; Rostek *et al.*, 1993; Emeis *et al.*, 1995] could have increased the excess evaporation over fresh water input over much of the Arabian Sea, thereby

resulting in an increase in sea surface salinities (SSS's). The combined effect of decreased SST's and high SSS's will increase sea surface densities, thereby promoting deep winter mixing in the northernmost part of the Arabian Sea at glacial times. The outcome of some climate modelling experiments suggests an increase of approximately 50% in the winter monsoonal winds during glacial winter insolation minima [Bigg and Jiang, 1993].

Assuming that large-scale glacial cycles controlled the variability in summer and winter monsoonal wind strength, one would expect that variations in surface water productivity and OMZ intensity are closely related to the $\delta^{18}\text{O}$ record. If glacial-bound variations in the Ba/Al ratio and pteropod record [Chapter 2] would reflect changes in surface water productivity and OMZ intensity, then this may indeed have been the case. A similar relationship was suggested by Sirocko *et al.* [1996], who showed in a high-resolution study on a sediment core off Oman that changes in the Ba content associated with the last deglaciation occur in phase with changes in the $\delta^{18}\text{O}$ record (compare the papers of Sirocko *et al.* [1993, 1996]). However, the spectra of the C_{org} , *G. bulloides* and $\delta^{15}\text{N}$ record do not reflect a clear 120-kyr cyclicity (Figure 8), indicating that the relative strength and timing of the Arabian Sea summer productivity conditions and OMZ intensity are not primarily controlled by large-scale climatic changes associated with glacial-interglacial cycles, but rather by precessional forcing. This implies that the glacial-bound variations in the Ba/Al ratio and pteropod record do not

primarily reflect changes in the summer monsoonal circulation.

An alternative explanation may be that the large-scale variations in Ba/Al ratios associated with glacial cycles resulted from changes in intermediate water circulation [Shimmiel *et al.*, 1990; Hermelin and Shimmiel, 1995; Kallel *et al.*, 1988]. A reduction in intermediate water circulation flow during interglacial times may have increased the nutrient concentration in the northern Indian Ocean, thereby enhancing surface water productivity and the amount of barium scavenged into organic matter while settling through the water column [Dymond *et al.*, 1992; Hermelin and Shimmiel, 1995]. It is questionable whether an increased inflow of subsurface water from the south contributed to a weakening of the OMZ during glacial periods, because the inflowing subsurface water is relatively old and depleted in O₂ [You and Tomczak, 1993; Warren, 1994].

A lowering in sea level during peak glacial conditions on the other hand may have significantly reduced or even interrupted the water exchange between the Arabian Sea and the Persian Gulf and Red Sea [Rohling and Zachariasse, 1996], resulting in an increase in sea surface salinities and the elimination of the present-day salinity maximum at 200 to 400 m waterdepth in the Arabian Sea. The combined effect of a reduced subsurface density (salinity) gradient and increased sea surface water densities (due to lower SST's and higher SSS's) should have set the stage for deep mixing in the northernmost part of the Arabian Sea at glacial times.

The 120-kyr component in the Ti/Al

ratio most likely reflects glacial-interglacial differences in continental aridity [Shimmiel *et al.*, 1990; Chapter 2]. During glacial periods, dry continental climatic conditions may have resulted in high Ti/Al values and mass accumulation rates, whereas the more humid interglacial periods are reflected by lowest values in Ti/Al and mass accumulation rates [Chapter 2].

Precession-Controlled Variations in OMZ Intensity

Latent and sensible heat

The dominant influence of the precession cycle on the surface water productivity record from the Murray Ridge (NIOP464) and the inferred time lag of ~ 4 kyr with respect to the $\delta^{18}\text{O}$ record (Figures 8 and 9) are in good agreement with previous observations from the Owen Ridge [Clemens and Prell, 1990; Shimmiel *et al.*, 1990; Clemens *et al.*, 1991; Murray and Prell, 1992; Altabet *et al.*, 1995]. Clemens *et al.* [1991] proposed that the exceptional large time lag (~9 kyr between maxima in northern hemisphere June insolation and the average of a variety of monsoon tracers) is governed by cross-equatorial transport of latent heat rather than by maximum sensible heating of the Tibetan Plateau close to precession minima, as indicated by climatic modelling experiments [e.g., Kutzbach, 1981; Short and Mengel, 1986]. According to this theory, low SST's and increased wind speed over the southern Indian Ocean at times of minimum insolation at 20°S should have increased latent heat transport resulting in an intensified summer monsoon [Clemens *et al.*, 1996].

There are several arguments, however, which indicate that cross-equatorial latent heat transport associated with minimum southern hemisphere SST's could not be the cause for variations in summer monsoon intensity. In the first place, the explanation of the 9-kyr time lag by cross-equatorial latent heat transport, would require that the minimum southern hemisphere SST's should have occurred at 2.5 ka BP (or ~1.5 kyr before the precession maximum at 1 ka) (Figure 9). This is on average 4 to 5 kyr earlier than the estimate of *Imbrie et al.* [1992], who found a time lag of approximately 3-kyr between precession minima and maximum southern hemisphere SST's. Moreover, there is evidence that glacial cooling in the two hemispheres is synchronous [*Thompson et al.*, 1995; *Miller et al.*, 1997; *Bard et al.*, 1997]. If the amount of transported latent heat depends on the lowest southern hemisphere SST's then we would have to find the strongest summer monsoon and, hence, maximum OMZ intensity during the LGM. Figure 9 clearly shows that this is not the case. In contrast, OMZ intensity is close to a minimum during the LGM.

A second argument which contradicts this hypothesis is that the proposed maximum latent heat transport at 1 ka should coincide with a maximum in precipitation over northwest India and Tibet. Reconstructions of precipitation from lake records in Tibet and northwest India, however, consistently show that maximum rainfall occurred from 10 to 6 ka [*Bryson and Swain*, 1981; *Swain et al.*, 1983; *Gasse et al.*, 1991; *Gasse and Van Campo*, 1994], followed by arid conditions from ~4 ka to Recent (Figure

9). A minimum in dolomite dust input has been recorded off Oman from approximately 9 to 8 ka [*Sirocko et al.*, 1993], which is in phase with the most humid period recorded in the lake sediments (Figure 9). Because the dolomite dust input off Oman is constrained by continental aridity and the extent of the northwesterlies over the basin it can be concluded that the early-to mid-Holocene precipitation maximum is caused by a more inland position of the intertropical convergence zone (ITCZ) over Oman, which resulted in more rainfall over the Arabian peninsula and in a reduction of the influence of the northwesterly system. These more pluvial climatic conditions are also reflected in the eastern Mediterranean by the formation of the youngest sapropel, S1 (Figure 9), which is thought to be related to an intensified monsoonal circulation and increased river Nile discharge into the eastern Mediterranean [*Rosignol-Strick*, 1983]. Finally, this period is marked by the deposition of the S0 soil in the Chinese loess record, which again indicates intensified summer precipitation in central Asia during the early to mid-Holocene [e.g., *An et al.*, 1991]. In conclusion, we would expect that the maximum in summer surface water productivity and, hence, maximum OMZ intensity in the Arabian Sea was in phase with the more humid climatic conditions between 10 and 6 ka and not with the minimum in southern hemisphere winter SST's at 1 ka.

Part of the conflicting results can be explained by the use of the SPECMAP chronology in most paleoceanographic studies, whereas studies of the last ~20 kyr rely on AMS-¹⁴C dating. As

demonstrated earlier, application of that chronology may have led to an overestimation of the time lag between precession and the precession-related components in the monsoon tracers of more than 2 kyr. If we apply the sapropel timescale then this lag is reduced to 4.5 to 7-kyr (Figure 9). Another 2 to 3-kyr of this time lag can be explained by the results of climate modelling experiments [Short and Mengel, 1986]. These experiments have shown that variations in maximum temperatures oscillated in direct thermal response to variations in insolation with a time lag of ~3000 years, for latitudes lower than 20°. A similar time lag found between the last summer insolation maximum (at 11.5 ka) and the early- to mid Holocene humid phase (10 to 6 ka) indicates that the monsoonal circulation is strongly affected by variations in low-latitude insolation. Finally, the proxy used in many monsoon studies to determine variations in summer monsoon strength is the lithogenic grain size. If we adopt the Ti/Al ratio as a proxy for lithogenic grain size, we find that variations in the lithogenic grain size respond even later to changes in the precession index than surface water productivity and OMZ indicators (Figure 9). The time lag between the precession cycle and the precession component in the Ti/Al ratio arrives at ~8 kyr, which again (considering an adjustment factor of 2 kyr for the use of the different timescales) is in very good agreement with the lag found by Clemens *et al.* [1991] for the lithogenic grain size record from the Owen Ridge. If we interpret the Ti/Al and grain size records in terms of variations in summer monsoonal wind

strength, then these results suggest that wind strength was at a maximum around 3 to 1 ka. This maximum coincides with an increase in Arabian aridity, reflected by lowered lake levels, a decline in vegetational cover [Bryson and Swain, 1981; Swain *et al.*, 1983; Gasse *et al.*, 1991; Gasse and Van Campo, 1994], and the abandonment of neolithic settlements in the inner desert of Arabia that started between 5.6 and 5.2 ka [Uerpman, 1991]. This could imply that the maximum in grain size is not merely a reflection of maximum summer monsoonal strength, but can be related to an increase in source area aridity (controlling dust availability), intensified strength of the northwesterly winds (being the most important carrier of dust), a more offshore position of the ITCZ (controlling the extent of the northwesterlies over the basin) [Shimmiel *et al.*, 1990; Sirocko *et al.*, 1991; Hermelin and Shimmiel, 1995], and finally a decrease in the amount of the sediment supplied by the Indus river (which in turn depends on source area aridity [M. Prins, personal communications]).

Nevertheless, there remains a time lag of 2 to 3 kyr between the more humid climatic conditions in Tibet, northwest India, and Africa between ~10 and ~6 ka and the surface water productivity maximum observed in the Arabian Sea between ~7 and ~4 ka (Figure 9).

Internal phase-relationships

Data from three sediment traps in the central Arabian Sea show that the maximum rain of organic matter is in August and September [Haake *et al.*, 1992] or slightly earlier, during July and

August [Nair *et al.*, 1989], following maximum wind strength. Curry *et al.* [1992] studied foraminiferal fluxes from the same traps and measured maximum fluxes during the later stage of the upwelling season. Phytoplankton pigment distributions, based on Coastal Zone Color Scanner data, also suggest a summer monsoon-related pigment maximum in September [Banse, 1994], while recent trap studies off Somalia and Yemen showed that the highest biogenic fluxes continue even well into October [Van Iperen *et al.*, 1995].

Interannual differences in seasonal productivity indicate the importance of the length of the monsoon upwelling season. In the summer monsoon season of 1986, highest production of *G. bulloides* was about 137 000 specimens per m² during 62 days of high productivity. Over the same period in 1987, *G. bulloides* production was only 14% higher (156 000 specimens per m²), while the total production was nearly three times higher (372 000 specimens per m²) because productivity was elevated during 112 days instead of 62 days in 1986 [Curry *et al.*, 1992]. This indicates that the length of the summer monsoon upwelling season is more important for the total annual flux than maximum monsoonal wind strength.

If we transfer these observations to orbital timescales, then, this could imply that the time lag between precession and the surface water productivity indicators is linked to changes in late rather than early summer insolation variability (Figure 9). Maximum insolation at the end of the summer monsoon period (August, September), would extend the length of the upwelling season, resulting

in a higher annual biogenic particle flux. All this implies that the surface water productivity variations in the Arabian Sea either directly respond to changes in insolation (September), or with a relatively small (~3kyr) time lag (August), depending on the month considered. Analogous to the 3-kyr time lag found between maximum summer insolation and the early- to mid Holocene precipitation optimum, we assume that the August insolation is critical for Arabian Sea summer production (Figure 9).

Deep (winter) mixing

The anti-phase relationship between precession-driven fluctuations in summer production and deep (winter) mixing (Figure 9) may indicate that (due to internal feedback mechanisms as previously discussed) intensified mixing resulted in low summer productivity. Close inspection of figure 9 further reveals that periods of deep (winter) mixing (as indicated by maximum values in the pteropod and *G. truncatulinoides* - *G. crassaformis* record) occur slightly after maximum glacial conditions as inferred from the $\delta^{18}\text{O}$ record. Since the *G. truncatulinoides* - *G. crassaformis* record reveals a much stronger precession component in its spectrum (Figure 8) it can be considered to be more sensitive to the precessional forcing than the pteropod record. It, therefore, follows that periods of maximum deep (winter) mixing coincide with glacial terminations and not with maximum glacial conditions. This could imply that either these events are decoupled from maximum (precession-controlled) glacial boundary conditions or that $\delta^{18}\text{O}$ maxima

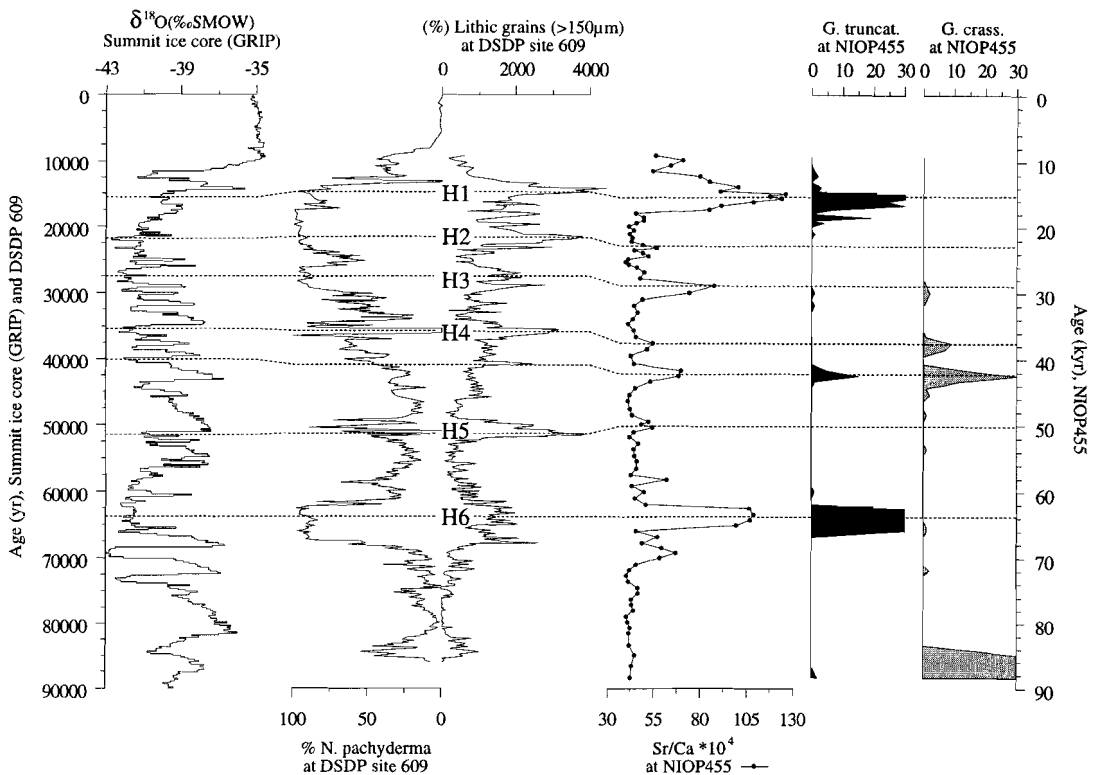


Fig. 10. Time series comparing the Sr/Ca, *G. truncatulinoides* and *G. crassaformis* record from the Pakistan Margin (NIOP455) with the $\delta^{18}\text{O}$ record from the GRIP ice core [Dansgaard *et al.*, 1993] and with the abundances of *N. pachyderma* and the ratio of lithic grains $>150\ \mu\text{m}$ from DSDP site 609 [Bond *et al.*, 1992; Bond and Lotti, 1995; Bond, 1996]. Ages of Heinrich layers H1-H6 are from Bond *et al.* [1993]. Heinrich events and some more pronounced stadials can be recognised in the Ca/Sr record of NIOP455. The Sr/Ca maxima at 15, 42 and 64 kyr are associated with abundant *G. truncatulinoides* and/or *G. crassaformis*. Small offsets between the records are caused by uncertainties in the age models.

do not coincide with the coldest winter temperatures over the Arabian Sea.

If the precession-controlled periods of deep (winter) mixing in the Arabian Sea are not related to optimum glacial boundary conditions then they are most likely related to variations in insolation at 35°N . Minima in winter insolation may have lowered temperatures over the Tibetan Plateau to such a degree that the winter high pressure cell is at a maximum. That would produce stronger and colder winter monsoonal winds over

the northern most part of the Arabian Sea and a subsequent deep mixing of the thermocline. However, due to the precession of the Earth's axis, minimum winter insolation (February) values at 35°N were reached near 11.5 ka. That minimum is considerably later than that of the last period of deep (winter) mixing (18-14 ka) (Figure 6), indicating that these (precession-controlled) ventilation events are not related to decreased winter insolation values at 35°N . Alternatively, minima in the early (June) to late

(August-September) summer insolation values (Figure 9) may have subdued SST's in the Arabian Sea to such a degree that it would facilitate deep convection during winter. To further unravel this enigma, we will first discuss the influence of the suborbital climatic variations on the intensity of the OMZ.

Suborbital Variations in the Monsoonal Circulation

Suborbital variations in $\delta^{18}\text{O}$ and various productivity and dust proxy records from the northern Arabian Sea have been recently shown by *Sirocko et al.* [1996] and *Schulz et al.* [1997]. *Sirocko et al.* [1996] proposed a teleconnection between reduced summer monsoon intensity and the youngest Heinrich-event in the North Atlantic. A reduction in summer monsoon productivity in phase with the Heinrich-layers is also indicated by the low C_{org} values during peaks in the Sr/Ca ratio (Figures 5 and 10). A possible link between low summer productivity in the Arabian Sea and Heinrich-layers in the North Atlantic could be through a reduction of North Atlantic Deep Water (NADW) formation [*Zonneveld, 1996*]. A reduction in NADW formation may have decreased transport of oceanic heat north across the equator, resulting in lower southern hemisphere SST's [*Gasse and Van Campo, 1994*]. If higher southern tropical Indian Ocean SST's would cause a reduction in cross-equatorial latent heat transport, as proposed by *Clemens et al.* [1990], then a reduction of NADW formation may have led to a weakened summer monsoon and, hence, to low productivity in the Arabian Sea.

On the other hand, *Porter and Zhisheng* [1995] have shown that the suborbitally-driven grain-size maxima in the Chinese loess sequences, with ages matching those of the last six Heinrich-layers, are related to variations in winter monsoonal wind strength, because a comparable high-frequency component was absent in the proxy (magnetic susceptibility) for summer monsoon strength. They linked these intensified winter monsoonal conditions to brief and cold spells in North Atlantic climate via the westerlies. Similar high-frequency components found in the Sr/Ca record of the Arabian Sea (Figure 10) suggest therefore that the sub-orbital variations in OMZ intensity are caused by variations in winter monsoon strength rather than by variations in summer surface water productivity. During the very cold intervals which are associated with the Heinrich-layers, polar air masses probably extended farther south over the Eurasian continent, facilitating frequent and intense cold air outbreaks over the northern Arabian Sea. Moreover, these severe glacial climatic conditions might have intensified cold mobile polar high pressure cells, following a Mediterranean /North African and Arabian path [*Leroux, 1993*], and/or decreased the temperatures over the Tibetan Plateau to such a degree that the winter high pressure cell would reach a maximum. That would bring unusually strong and cold winter monsoonal winds over the northern Arabian Sea and the subsequent intense deep mixing of the thermocline.

These suborbital ventilation-events in the Arabian Sea coincide with precession-controlled peak occurrences of *G. truncatulinoides* and *G.*

crassaformis (Figure 10), indicating that at least part of these events and of the associated Heinrich-layers are determined by the precession cycle. This would imply that either the precession-driven climatic processes causing periods of deep (winter) mixing in the Arabian Sea are triggered by the coldest glacial temperatures associated with some of the Heinrich-layers and Dansgaard-Oeschger cycles, or visa versa. According to the first option, one may conclude that maxima in the $\delta^{18}\text{O}$ record do not reflect the coldest (maximum) glacial conditions, because they lead these periods of deep (winter) mixing in the Arabian Sea systematically by ~ 5 kyr (Figure 9). Close inspection of several $\delta^{18}\text{O}$ records of the North Atlantic shows that at least some of the Heinrich-layers are deposited at the glacial terminations as indicated by the transition in the $\delta^{18}\text{O}$ record to lighter values (e.g., Figure 2, Bond *et al.*, [1992] and Figure 2, Fronval and Jansen, [1996]).

According to the second option, we speculate that the (dominant) precession-related climatic process which controls the variations in the Arabian Sea OMZ, via either summer production or deep (winter) mixing, interferes with global ice volume changes, resulting in the deposition of the Heinrich-layers found at glacial terminations. According to this hypothesis, the interference between minima in northern hemisphere summer insolation at high latitudes (65°N) and those at the end of the summer season at low latitudes ($\sim 35^\circ\text{N}$) may have been of prime importance in triggering suborbital climatic events and, hence, the deposition of Heinrich-layers.

Conclusions

Precession controlled surface water productivity in the Arabian Sea follows early summer insolation by ~ 6 kyr. Higher insolation in the later phase of the summer monsoon stretches the duration of the upwelling period, causing maximum seasonal sea water production, and an intensified OMZ.

Basin-wide occurrences of significant numbers of *G. truncatulinoides* and *G. crassaformis* combined with a reduction in denitrification and a lowering of the ACD in the northern Arabian Sea suggest that the local OMZ has been significantly reduced in intensity during several periods because of a more intense convective turnover.

Deepening of the thermocline during the winter season by the dry and cool winds of an intensified northeast monsoon is the most likely mechanism that causes this convective turnover and it introduces significant amounts of oxygen at mid-depth. Intensified winter mixing results in a weakening of the OMZ and a reduction of the nutrient concentration in the sub-surface waters. Lower nutrient concentrations in the up-welled waters subsequently reduces regional upwelling related productivity, at the same time reducing - oxygen consumption in the water column.

The sedimentary record from the northern Arabian Sea indicates that there is a connection between cooling events in the North Atlantic region and winter mixing in the Arabian Sea. The dominant precession component in the climatic processes, which control the intensity of the OMZ, shows that the interference between high and low latitude insolation has been of primary importance in the triggering of Heinrich events.

Acknowledgements

The chief scientists on our NIOP cruises, during the 1992-1993 Netherlands Indian Ocean Programme, were W.J.M. van der Linden and C.H. van der Weijden. We thank the director and our colleagues G.M. Memon, A.R. Tabrez and A.A. Khan of the National Institute of Oceanography, Karachi, for their cooperation. The collection of the material would not have been possible without the professional help of crew and technicians of the R.V. Tyro. M. den Dulk, B. West and D. van den Akker are acknowledged for their help in the foraminiferal analyses. Thanks are also due to H.J. Visser, G. Nobbe, A. van Dijk, H.de Waard, G.J. van het Veld, and G. Ittman for processing samples and analytical support. The $\delta^{15}\text{N}$ analyses were carried out at the University of British Columbia, Vancouver. This study was partly funded by the Netherlands Organization for Scientific Research (NWO grant no. 718-215).

References

- Altabet, M.A., Variations in nitrogen isotopic composition between sinking and suspended particles: implications for nitrogen cycling and particle transformation in the open ocean, *Deep-Sea Res.*, 35, 535-554, 1988
- Altabet, M.A., Francois, R., The use of nitrogen isotopic ratio for reconstruction of past changes in surface ocean nutrient utilization. In: *Carbon Cycling in the Glacial Ocean: Constraints on the Ocean's Role in Global Change* (eds. Zahn, R., Kaminski, M., Labeyrie, L. and T.F. Pederson), 281-306, Springer, Berlin, 1994.
- Altabet, M.A., Francois, R., Murray, D.W., and W.L. Prell, Climate-related variations in denitrification in the Arabian Sea from sediment $^{15}\text{N}/^{14}\text{N}$ ratios, *Nature*, 373, 506-509, 1995.
- An, Z.S., Kukla, G.J., Porter, S.C. and J.L. Xiao, Magnetic susceptibility evidence of monsoon variation on the Loess Plateau of central China during the last 130,000 years. *Quaternary Research*, 36, 29-36, 1991..
- Anderson, D.M., Foraminifer evidence of Monsoon upwelling off Oman during the late Quaternary. Thesis Dept. Geol. Sciences Brown University, May 1991.
- Banse, K., Overview of the hydrography and associated biological phenomena in the Arabian Sea, off Pakistan. In: B.U. Haq and J.D. Milliman (eds.), *Marine geology and oceanography of Arabian Sea and coastal Pakistan*, Van Nostrand Reinhold, New York: 271-303, 1984.
- Banse, K., Seasonality of phytoplankton chlorophyll in the central and northern Arabian Sea. *Deep-Sea Res.*, 34, 713-723, 1987.
- Banse, K., On the coupling of hydrography, phytoplankton, zooplankton, and settling organic particles offshore in the Arabian Sea. In: Biogeochemistry of the Arabian Sea. (Ed. D. LaL) *Proc. of the Indian Acad. of Sci.*, 103, 27-63, 1994.
- Bard, E., Hamelin, B., Fairbanks, R.G. and A. Zinder, Calibration of the ^{14}C timescale over the past 30,000 years using mass spectrometric U-Th ages from Barbados corals. *Nature*, 345,405-410, 1990a.
- Bard, E., Hamelin, B. and R.G. Fairbanks, U-Th ages obtained by mass spectrometry in

- corals from Barbados: Sea level during the last 130,000 years, *Nature*, 346, 456-458, 1990b.
- Bard, E., Rostek, F. and C. Sonzogni, Interhemispheric synchrony of the last deglaciation inferred from alkenone palaeothermometry. *Nature*, 385, 707-710, 1997.
- Barnett, T.P., Dumenil, L., Schlese, U. and E. Roeckner, The effect of Eurasian snow cover on global climate, *Science*, 239, 504-507, 1988.
- Be, A.W.H. and D.S. Tolderlund, Distribution and ecology of living planktonic foraminifera in surface waters of the Atlantic and Indian Oceans. In: B.M. Riedel and W.R. Funnell (Eds.), *Micropaleontology of the Oceans*. Cambridge University Press: 105-149, 1971.
- Be, A.W.H., G. Vilks, and L. Lott, Winter distribution of planktonic foraminifera between the Grand Banks and the Caribbean. *Micropal.*, 17, 31-42, 1971.
- Be, A.W.H. and W.H. Hutson, Ecology of planktonic foraminifera and biogeographic patterns of life and fossil assemblages in the Indian Ocean. *Micropal.*, 23, 369-414, 1977.
- Berger, W.H. Deep-sea carbonate: pteropod distribution and the aragonite compensation depth. *Deep-Sea Research*, 25, 447-452, 1978.
- Bigg, G.R. and D. Jiang, Modelling the late Quaternary Indian Ocean circulation. *Paleoceanogr.*, 8, 23-46, 1993.
- Bond, G., Heinrich, H., Broecker, W., Labeyrie, L., McManus, J., Andrews, J., Huon, S., Jantschik, R., Clasen, S., Simet, C., Tedesco, K., Klas, M., Bonani, G. and S. Ivy, Evidence for massive discharges of icebergs into the North Atlantic ocean during the last glacial period. *Nature*, 360, 245-249, 1992.
- Bond, G.C. and R. Lotti, Iceberg discharges into the North Atlantic on millennial time scales during the last glaciation. *Science*, 276, 1005-1010, 1995.
- Bond, G. Heinrich event data, DSDP 609. IGBP PAGES/World Data Center-A for Paleoclimatology Data Contribution Series # 96-019. NOAA/NGDC Paleoclimatology program, Boulder CO, USA, 1996.
- Bradshaw, J.S., Ecology of living planktonic foraminifera of the North and Equatorial Pacific Ocean. *Cushman Found. Foramin. Res.*, 10, 25-64, 1959.
- Brock, J.C., C.R. McClain, D.M. Anderson, W.L. Prell and W.W. Hay, Southwest monsoon circulation and environments of recent planktonic foraminifera in the northwest Arabian Sea. *Paleoceanogr.*, 7, 799-813, 1992.
- Bryson, R.A. and A.M. Swain, Holocene variations of monsoon rainfall in Rajasthan. *Quaternary Research*, 16, 135-145, 1981.
- Canfield, D.E. and R. Raiswell, Carbonate precipitation and dissolution. In: *Taphonomy: releasing the data locked in the fossil record* (eds. P.A. Allison & D.E.G. Briggs), Plenum Press, 411-453, 1991.
- Cifelli, R., Distributional analysis of North Atlantic foraminifera collected in 1961 during cruises 17 and 21 of the R/V Chain. *Cushman Found. Foramin. Res.*, 18, 118-127, 1967.
- Cifelli, R. and C.S. Benier, Planktonic foraminifera from near the West African coast and a consideration of faunal

- parcelling in the North Atlantic. *Jour. Foram. Res.*, 6, 258-273, 1976.
- Clemens, S.C. and W.L. Prell, Late Pleistocene variability of Arabian Sea summer monsoon winds and continental aridity: eolian records from the lithogenic components of deep-sea sediments. *Paleoceanogr.*, 5, 109-145, 1990.
- Clemens, S., Prell, W., Murray, D., Shimmield, G. and G. Weedon, Forcing mechanisms of the Indian Ocean monsoon. *Nature*, 353, 720-725, 1991.
- Clemens, S.C., Murray, D.W. and W.L. Prell, Nonstationary phase of the Plio-Pleistocene Asian Monsoon. *Science*, 274, 943-948, 1996.
- Cline, J.D. and I.R. Kaplan, Isotopic fractionation of dissolved nitrate during denitrification in the eastern tropical North Pacific Ocean. *Mar. Chem.*, 3, 271-299, 1975.
- Codispoti, L.A. Primary productivity and carbon and nitrogen cycling in the Arabian Sea. In *U.S. JGOFS: Arabian Sea Process Study* (Eds. S.L. Smith, K. Banse, J. K. Cochran, L.A. Codispoti, H.W. Ducklow, M.E. Luther, D.B. Olson, W.T. Peterson, W.L. Prell, N. Surgi, J.C. Swallow & K. Wishner), U.S. JGOFS Planning Report No. 13, 1991.
- COHMAP, Climatic changes of the last 18,000 years: Observations and model simulations. *Science*, 241: 1043-1052, 1988.
- Cullen, J.L. and W.L. Prell, Planktonic foraminifera of the northern Indian Ocean: distribution and preservation in surface sediments. *Mar. Micropal.*, 9, 1-52, 1984.
- Curry, W.B., D.R. Ostermann, M.V.S. Gupta, and V. Ittekkot, Foraminiferal production and monsoonal upwelling in the Arabian Sea: Evidence from sediment traps. In: C.P. Summerhays, W.L. Prell and K.C. Emeis (eds), *Upwelling Systems: Evolution since the early Miocene. Geol. Soc. Spec. Publ.* 64, 93-106, 1992.
- Dansgaard, W., Johnsen, S.J., Clausen, H.B., Dahl-Jensen, D., Gundestrup, N.S., Hammer, C.U., Hvidberg, C.S., Steffensen, J.P., Sveinbjörnsdóttir, A.E., Jouzel, J. and G. Bond. Evidence for general instability of past climate from a 250-kyr ice-core record. *Nature*, 218-220, 1993.
- Deuser, W.G., Ross, E.H. and Z.J. Mlodzinska, Evidence for and rate of denitrification in the Arabian Sea. *Deep-Sea Res.*, 25, 431-445, 1978.
- Deuser, W.G., E.H. Ross, Ch. Hemleben and M. Spindler, Seasonal changes in species composition, numbers, mass, size, and isotopic composition of planktonic foraminifera settling into the deep Sargasso Sea. *Palaeogr., Palaeoclim., Palaeoecol.*, 33:103-127, 1981.
- Duplessy, J.C., Glacial to interglacial contrasts in the northern Indian Ocean. *Nature*, 295, 494-498, 1982.
- Durazzi, J.T., Stable isotope studies of planktonic foraminifera in North Atlantic core tops. *Palaeogeogr., Palaeoclim., Palaeoecol.*, 33, 157-172, 1981.
- Dymond, J. Suess, E. and M. Lyle, Barium in deep-sea sediment: a geochemical proxy for paleoproductivity. *Paleoceanography*, 7, 163-181, 1992.
- Edwards, R.L., Chen, J.H., Ku, T.L. and G.J. Wasserburg, Precise timing of the last interglacial period from mass spectrometric determination of Thorium-230 in corals. *Science*, 236. 1547-1553, 1987.

- Emeis, K.C., Anderson, D.M., Dose, H., Kroon, D. and D. Schulz-Bull, Sea-surface temperatures and the history of monsoon upwelling in the northwest Arabian Sea during the last 500,000 years, *Quat. Res.*, 43, 355-361, 1995.
- Fontugne, M.R., Paterne, M., Calvert, S.E., Murat, A., Guichard, F. and M. Arnold, Adriatic deep water formation during the Holocene: implications for the reoxygenation of the deep eastern Mediterranean Sea, *Paleoceanogr.*, 4, 199-206, 1989.
- Fontugne, M.R. and S.E. Calvert, Late Pleistocene variability of the carbon isotope composition of organic matter in the eastern Mediterranean: Monitor of changes in carbon sources and atmospheric CO₂ concentrations, *Paleoceanography*, 7, 1-20, 1992.
- Fronval, T. and E. Jansen, Rapid changes in ocean circulation and heat flux in the Nordic seas during the last interglacial period. *Nature*, 383, 806-810, 1996.
- Gallup, C.D., Edwards, R.L. and R.G. Johnson, The timing of high sealevels over the past 200,000 years, *Science*, 263, 796-800, 1994.
- Gasse, F., Arnold, M., Fontes, J.C., Fort, M., Gibert, E., Huc, A., Bingyan, L., Yuanfang, L., Quing, L., Melieres, F., Van Campo, E., Fubao, W. and Z. Quigsong, A 13,000-year climate record from western Tibet. *Nature*, 353, 742-745, 1991.
- Gasse, F. and E. Van Campo, Abrupt post-glacial climate events in West Asia and North Africa monsoon domains., *Earth and Planet. Sci. Lett.*, 126, 435-456, 1994.
- Guilderson, T.P., Fairbanks, R.G. and J.L. Rubenstone, Tropical temperature variations since 20,000 years ago: Modulating interhemispheric climate change. *Science*, 263, 663-665, 1994.
- Haake, B., Ittekkot, V., Ramaswamy, V., Nair, R.R. and S. Honjo, Fluxes of amino acids and hexoamines to the deep Arabian Sea. *Mar. Chem.*, 40, 291-314, 1992.
- Hemleben, Ch., M. Spindler, I. Breitingner and W.G. Deuser., Field and laboratory studies on the ontogeny and ecology of some globorotaliid species from the Sargasso Sea off Bermuda. *J. Foram. Res.*, 15, 254-272, 1985.
- Hemleben, Ch., M. Spindler and O.R. Anderson, *Modern planktonic foraminifera*. Springer Verlag, New York, 1989.
- Herbland, A., A. le Bouteiller and P. Raimbault, Size structure of phytoplankton biomass in the equatorial Atlantic Ocean. *Deep Sea Res.*, 32, 819-836, 1985.
- Hermelin, J.O.R. The benthic foraminiferal faunas of sites 725, 726, and 728 (Oman Margin, northwestern Arabian Sea). In: Prell, W.L., Niitsuma, N., et al., *Proc. ODP Sci. Results, 117*: College Station, TX (Ocean drilling Program), 55-87, 1991.
- Hermelin, J.O.R. and G.B. Shimmield, Impact of productivity events on the benthic foraminiferal fauna in the Arabian Sea over the last 150,000 years. *Paleoceanography*, 10, 85-116, 1995.
- Hilgen, F.J., Closing the gap in the Plio-Pleistocene boundary stratotype sequence of Crotona, *Newsletters on Stratigraphy*, 22, 43-51, 1990.
- Hilgen, F.J., Lourens, L.J., Berger, A. and M.F. Loutre, Evaluation of the astronomically calibrated time scale for the late Pliocene and earliest Pleistocene, *Paleoceanogr.*, 8, 549-565, 1993.

- Imbrie, J. and J.Z. Imbrie, Modelling the climate response to orbital variations, *Science*, 207, 943-953, 1980.
- Imbrie, J. Hays, J.D., Martinson, D.G., McIntyre, A., Mix, A.C., Morley, J.J., Pisias, N.G., Prell, W.L. and N.J. Shackleton, The orbital theory of Pleistocene climate: support from a revised chronology of the marine $\delta^{18}\text{O}$ record. In: *Milankovitch and Climate, Part 1* (Eds. A.L. Berger, J. Imbrie, J. Hays, G. Kukla and B. Saltzman), Reidel Dordrecht, 269-305, 1984.
- Imbrie, J., Boyle, E.A., Clemens, S.C., Duffy, A., Howard, W.R., Kukla, G., Kutzbach, J., Martinson, McIntyre, A., Mix, A.C., Molino, B., Morley, J.J., Peterson, L.C., Pisias, N.G., Prell, W.L., Raymo, J.R., Shackleton, N.J. and J.R. Toggweiler, On the structure and origin of major glaciation cycles 1. Linear responses to milankovitch forcing. *Paleoceanogr.*, 7, 701-738, 1992.
- Jones, J.I., Significance of distribution of planktonic foraminifera in the Equatorial Atlantic Undercurrent. *Micropal.*, 13:489-501, 1967.
- Jorissen, F.J., Asioli, A., Borsetti, A.M., Capotondi, L., de Visser, J.P., Hilgen, F.J., Rohling, E.J., Van der Borg, K., Vergnaud-Grazzini, C. And J.W. Zachariasse, Late Quaternary central Mediterranean biochronology, *Mar. Micropaleontol.*, 21, 169-189, 1993.
- Kabanova, Y.G., Primary production in the northern part of the Indian Ocean. *Oceanology*, 8, 214-225, 1968.
- Kallel, N., Labeyrie, L.D. Juillet-Leclerc, A.J. and J.C. Duplessy, A deep hydrological front between intermediate and deep-water masses in the glacial Indian Ocean. *Nature*, 333, 651-655, 1988.
- Kutzbach, J.E., Monsoon climate of the Early Holocene: climate experiment with the earth's orbital parameters for 9000 years ago. *Science*, 214, 59-61, 1981.
- Kutzbach, J.E. and P.J. Guetter, The influence of changing orbital parameters and surface boundary conditions on climate simulations for the past 18,000 years, *J. Atmos. Sci.*, 39, 1726-1759, 1986.
- Laskar, J., Secular evolution of the solar system over 10 million years, *Astron. Astrophys.*, 198, 341-362, 1988.
- Leroux, M., The mobile polar high: a new concept explaining present mechanisms of meridional air-mass and energy exchanges and global propagation of palaeoclimatic changes, *Global Planet. Change*, 7, 69-93, 1993.
- Liu, K.K. and I.R. Kaplan, The eastern tropical Pacific as a source of ^{15}N -enriched nitrate in seawater off southern California. *Limnol. Oceanogr.*, 5, 820-830, 1989.
- Lohmann, G.P. and P.N. Schweitzer, Globorotalia truncatulinoides' growth and chemistry as probes of the past thermocline: 1 shell size. *Paleoceanogr.*, 5, 55-75, 1990.
- Lourens, L.J., Antonarakou, A., Hilgen, F.J., Van Hoof, A.A.M., Vergnaud-Grazzini, C. and W.J. Zachariasse, Evaluation of the Plio-Pleistocene astronomical timescale, *Paleoceanogr.*, 11, 391-413, 1996.
- Madhupratap, M., Kumar, S.P., Bhattathiri, P.M.A., Kumar, M.D., Raghukumar, S., Nair, K.K.C. and N. Ramaiah, Mechanism of the biological response to winter cooling in the northeastern Arabian Sea. *Nature*, 384, 549-552, 1996.
- Manabe, S. and D.G. Hahn, Simulation of tropical climate of an ice age. *Journal*

- Geophysical Research*, 82, 3889-3911, 1977.
- McKenna, V.S. and W.L. Prell., Glacial/interglacial contrast in G. truncatulinoides abundance patterns of the northern Indian Ocean. *Eos*, Trans. AGU 1994 Fall Meeting, Dec. 5-9, San Francisco, California, 351.
- Merle, J., Atlas hydrologique saisonnier de l'océan Atlantique intertropical. *Travaux et documents de l' O.R.S.T.O.M.*, 82, 1978.
- Miller, G.H., Magee, J.W. and A.J.T. Jull, Low-latitude glacial cooling in the southern hemisphere from amino-acid racemization in emu eggshells. *Nature*, 385, 241-244, 1997.
- Mitchell, J.F.B., Grahame, N.S. and K.J. Needham, Climate simulations for 9000 years before present: seasonal variations and the effect of the Laurentide ice sheet. *J. Geophys. Res.*, 93(D7), 8283-8303, 1988.
- Montoya, J.P. Nitrogen isotope fractionation in the modern ocean: implications for the sedimentary record. In: *Carbon Cycling in the Glacial Ocean: Constraints on the Ocean's Role in Global Change* (eds Zahn, R., Kaminski, M., Labeyrie, L. and T.F. Pederson), 259-279, Springer, Berlin, 1994.
- Murray, D.W. and W.L. Prell Late Pliocene and Pleistocene climatic oscillations and monsoon upwelling recorded in sediments from the Owen Ridge, northwestern Arabian Sea. In: *Upwelling Systems: Evolution Since the Early Miocene* (Eds. Summerhayes, C.P., Prell, W.L. and K.C. Emeis). Geological Society Special Publication No. 64, 301-321, 1992.
- Nair, R.R., Ittekkot, V., Manganini, S.J., Ramaswamy, V., Haake, B., Degens, E.T., Desai, B.N. and S. Honjo, Increased particle flux to the deep ocean related to monsoons. *Nature*, 338, 749-751, 1989.
- Naqvi, S.W.A. Some aspects of the oxygen-deficient conditions and denitrification in the Arabian Sea. *Journal of Marine Research*, 45, 1049-1072, 1987.
- Oberhänsli, H., C. Benier, G. Meinecke, H. Schmidt, R. Schneider and G. Wefer, Planktonic foraminifers as tracers of ocean currents in the eastern South Atlantic. *Paleoceanogr.*, 7, 607-632, 1992.
- Olson, D.B., Hitchcock, G.L., Fine, R.A. and B.A. Warren, Maintenance of the low-oxygen layer in the central Arabian Sea. *Deep-Sea Res. II.*, 40, 673-685, 1993.
- Perissoratis, C. and D.J.W. Piper, Age, regional variation and shallowest occurrence of S1 sapropel, *Geo-Marine Lett.*, 12, 49-53, 1992.
- Pisias, N.G. Mix, A.C. and R. Zahn, Nonlinear response in the global climate system: evidence from benthic oxygen isotope record in core RC13-110. *Paleoceanogr.*, 5, 147-160, 1990.
- Pond, S. and G.L. Pickard, *Introductory Dynamic Oceanography* (2e edition), Pergamon Press, 1983.
- Porter, S.C. and A. Zhisheng, Correlation between climate events in the North Atlantic and China during the last glaciation, *Nature*, 375, 305-308, 1995.
- Prell, W.L., Hutson, W.H., Williams, D.F., Be, A.W.H., Geitzenauer, K., Molino, B. Surface circulation of the Indian ocean during the Last Glacial Maximum, approximately 18,000 yr B.P., *Quat. Res.*, 14, 309-336, 1980.
- Prell, W.L., Monsoonal climate of the Arabian Sea during the Late Quaternary: a

- response to changing solar radiation. In: *Milankovitch and Climate, Part I* (Ed. A.L. Berger), 349-366, D.Reidel, Hingham, Mass., 1984b
- Prell, W.L. Variation of monsoonal upwelling: a response to changing solar radiation, *Climatic processes and climate sensitivity*, Vol. 29 (Eds. J.E. Hansen and T. Takahasi) American Geophysical Union. Geophys. Monogr. Ser., 48-57, Washington, D.C., 1993.
- Pujol, C., Les foraminifères planctoniques de l'Atlantique Nord au Quaternaire (eologie-stratigraphie-environment). *Mém. Inst. Geol. Bassin Aquitaine*, 10, 1-254, 1980.
- Qasim, S.Z., Oceanography of the northern Arabian Sea. *Deep-Sea Res.*, 29, 1041-1068, 1982
- Rasmussen, T.L., Benthonic and planktonic foraminifera in relation to the Early Holocene stagnation in the Ionian Basin, Central Mediterranean. *Boreas*, 20, 357-376, 1991.
- Ravelo, A.C., R.G. Fairbanks, and S.G.H. Philander, Reconstructing tropical Atlantic hydrography using planktonic foraminifera and an ocean model. *Paleoceanogr.*, 5, 409-431, 1990.
- Rohling, E.J. and W.J. Zachariasse, Red Sea outflow during the last glacial maximum. *Quat. Internat.*, 31, 77-83, 1996.
- Rosignol-Strick, M., African monsoons, an immediate climate response to orbital insolation. *Nature*, 304, 46-49, 1983.
- Rostek, F., Ruhland, G., Bassinot, F.C., Müller, P.J., Labeyrie, L.D., Lancelot, Y. and E. Bard, Reconstructing sea surface temperature and salinity using $\delta^{18}\text{O}$ and alkenone records. *Nature*, 364, 319-321, 1993.
- Sarkar, A., Ramesh, R., Bhattacharya, S.K. and G. Rajagopalan, Oxygen isotope evidence for a stronger winter monsoon current during the last glaciation. *Nature*, 343, 549-551, 1990.
- Schäfer, P. and V. Ittekkot, Seasonal variability of $\delta^{15}\text{N}$ in settling particles in the Arabian Sea and its palaeogeochemical significance. *Naturwissenschaften*, 80, 511-513, 1993.
- Schulz, H. Von Rad, U., Erlenkeuser, H. and P.M. Grootes, Correlations between planktic foraminiferal $\delta^{18}\text{O}$ -fluctuations in the Arabian Sea and Dansgaard-Oeschger events from Greenland Ice: implications for stage 3 stable isotope stratigraphy. Abstract Supplement No 1, Terra Nova Volume 9, 614, 1997.
- Shetye, S.R., Gouveia, A.D. and S.S.C. Shenoi, Circulation and water masses of the Arabian Sea. In: *Biogeochemistry of the Arabian Sea* (Ed. D. Lal), Indian Academy of Sciences, 9-25, 1994.
- Shimmield, G.B., Mowbray, S.R. and G.P. Weedon, A 350 ka history of the Indian Southwest Monsoon- Evidence from deep-sea cores, Northwest Arabian Sea. *Transactions of the Royal Society of Edinburgh: Earth Sciences*, 81, 289-299, 1990.
- Short, D.A. and J.G. Mengel, Tropical climate lags and Earth's precession cycle, *Nature*, 323, 48-50, 1986.
- Sirocko, F., Sarnthein, M., Lange, H. and H. Erlenkreuser, Atmospheric summer circulation and coastal upwelling in the Arabian Sea during the holocene and the last glaciation. *Quat. Res.*, 36, 72-93, 1991.

- Sirocko, F., Sarnthein, M., Erlenkeuser, H., Lange, H., Arnold, M. And J.C. Duplessy, Century-scale events in monsoonal climate over the past 24,000 years. *Nature*, 364, 322-324, 1993.
- Sirocko, F., Garbe-Schönberg, D., McIntyre, A. and B. Molfino, Teleconnections between the subtropical monsoons and high-latitude climates during the last deglaciation. *Science*, 272, 526-529, 1996.
- Smith, R. L. and J.S. Bottero, On upwelling in the Arabian Sea. In: *A voyage of discovery, George Deacon 70th Anniversary volume*. (Ed. M. Angel), Pergamon Press, 291-304, 1977.
- Stuiver, M., Pearson, G.W. and T. Braziunas, Radiocarbon age calibration of marine samples back to 9000 cal yr BP. *Radiocarbon*, 28, 980-1021, 1986.
- Stute, M., Forster, M., Frischkorn, H., Serejo, A., Clark, J.F., Schlosser, P., Broecker, W.S. and G. Bonani, Cooling of tropical Brazil (5°C) during the last glacial maximum. *Science*, 269, 379-383, 1995.
- Sutherland, H.E., Calvert, S.E., and R.J. Morris, Geochemical studies of the recent sapropel and associated sediment from the Hellenic outer ridge, eastern Mediterranean Sea. I: Mineralogy and chemical composition. *Mar. Geol.*, 56, 79-92, 1984
- Swain, A.M., Kutzbach, J.E. and S. Hastenrath, Estimates of Holocene Precipitation for Rajasthan, India, based on pollen and lake-level data. *Quaternary Research*, 19, 1-17, 1983.
- Swallow, J.C., Some aspects of the physical oceanography of the Indian Ocean. *Deep-Sea Res.*, 31, 639-650, 1984.
- Ten Kate, W.G.H.Z., Sprenger, A., Steens, T.N.F. and C.J. Beets, Late Quaternary monsoonal variations in the western Arabian Sea based on cross-spectral analyses of geochemical and micropalaeontological data. *Spec. Publ. Int. Ass. Sediment.*, 19, 127-143, 1994.
- Thomson, J., Higgs, N.C., Wilson, T.R.S., Croudace, I.W., De Lange, G.J. and P.J.M. Van Santvoort, Redistribution and geochemical behaviour of redox-sensitive elements around S1, the most recent eastern Mediterranean sapropel. *Geochim. Cosmochim. Acta*, 59, 3487-3501, 1995.
- Thompson, P.R. Be, A.W.H., Duplessy, J.C. and N.J. Shackleton, Disappearance of pink-pigmented Globigerinoides ruber at 120,000 yr BP in the Indian and Pacific Oceans., *Nature*, 280, 554-558, 1979.
- Thompson, L.G., Mosley-Thompson, E., Davis, M.E., Lin, P.N., Henderson, K.A., Cole-Dai, J., Bolzan, J.F. and K.B. Liu, Late glacial stage and Holocene tropical ice core records from Huascarán, Peru. *Science*, 269, 46-50, 1995.
- Tolderlund, D.S. and A.W.H. Be, Seasonal distribution of planktonic foraminifera in the western North Atlantic. *Micropal.*, 17, 297-329, 1971.
- Troelstra, S.R., Ganssen, G.M., Van der Borg, K. And A.M.F. De Jong, A late Quaternary stratigraphic framework for eastern Mediterranean sapropel S1 based on AMS ¹⁴C dates and stable oxygen isotopes, *Radiocarbon*, 33, 15-21, 1991.
- Uerpmann, H.P., PACT, 29-IV, 335-347, 1991.
- Van Bennekom, A.J., G.W. Berger, W. Helder and R.T.P. de Vries, Nutrient distribution in the Zaire estuary and river plume. *Neth. J. Sea Res.*, 12:296-323, 1978.

- Van Bennekom, A.J. and M.A. Hiehle, CTD operations and calibrations during legs D1, D2 and D3 of the Netherlands Indian Ocean Programme. In: *Geological study of the Arabian Sea*. (Eds. W.J.M. van der Linden & C.H. van der Weijden) Netherlands Geosciences Foundation, The Hague, 37-66, 1994.
- Van Bennekom, A.J., M.A. Hiehle, J. van Ooyen, E. van Weerle and M. van Koutrik, CTD and hydrography in: *Tracing a seasonal upwelling*. (Eds. J.E. van Hinte, Tj.C.E. van Weering & S.R. Troelstra) Netherlands Geosciences Foundation, The Hague, 37-66, 1995.
- Van Campo, E., Duplessy, J.C. and M. Rossignol-Strick, Climatic conditions deduced from a 150-kyr oxygen isotope-pollen record from the Arabian Sea, *Nature*, 296, 56-59, 1982.
- Van Cappellen, P. and E.D. Ingall, Benthic phosphorus regeneration, net primary production, and ocean anoxia: A model of the coupled marine biogeochemical cycles of carbon and phosphorus., *Paleoceanogr.*, 9: 677-692, 1994.
- Van Leeuwen, R.J.W., Sea-floor distribution and late Quaternary faunal patterns of planktonic and benthic foraminifers in the Angola Basin. *Utrecht Micropal. Bull.*, 38, 1989.
- Van Iperen, J.M., Brummer, G.J.A. and A.J. Van Bennekom, Diatoms in sediment traps off Somalia and in surface sediments off Somalia and southern Arabia. *Arabian Sea workshop, results of the Netherlands Indian Ocean programme 1992-1993, abstract book*, 35, 1995.
- Warren, B.A., Context of the suboxic layer in the Arabian Sea. In: *Biogeochemistry of the Arabian Sea* (Ed. D. Lal), Indian Academy of Sciences, 203-216, 1994.
- Williams, D.F., A.W.H. Be and R.G. Fairbanks, Seasonal stable isotopic variation in living planktonic foraminifera from Bermuda plankton tows. *Palaeogeogr., Palaeoclim., Palaeoecol.*, 38:71-102, 1981.
- Wooster, W.S., A. Bakun and D.R. McLain, The seasonal upwelling cycle along the eastern boundary of the North Atlantic. *J. Mar. Res.*, 34, 131-141, 1976.
- Wyrтки, K., *Oceanographic atlas of the international Indian Ocean expedition*, 531pp, 1971.
- Wyrтки, K., Physical Oceanography of the Indian Ocean. in: *The Biology of the Indian Ocean*. (ed. B. Zeitschel), 18-36, Springer, Berlin, 1973.
- You, Y. and M. Tomczak, Thermocline circulation and ventilation in the Indian Ocean derived from water mass analysis. *Deep-Sea Res. I*, 40, 13-56, 1993.
- Zobel, B., Foraminifera from plankton tows, Arabian Sea: areal distribution as influenced by ocean water masses. In: A. Farinacci (Ed.), *Proc. II Plankt. Conf., Roma 1970*:1323-1335, 1971.
- Zonneveld, K. Paleoclimatic and palaeo-ecologic changes in the eastern Mediterranean and Arabian Sea regions during the last deglaciation: a palynological approach to land-sea correlation. *LPP contributions series*, 3, 199pp., 1996

NIOP464

Depth (cmbfs)	Age (kyr BP)	$\delta^{18}\text{O}$ (‰PDB)	Corg (%)	$\delta^{15}\text{N}$ (‰)	G.Trunc. (No.)	G. Crass. (No.)	Depth (cmbfs)	Age (kyr BP)	$\delta^{18}\text{O}$ (‰PDB)	Corg (%)	$\delta^{15}\text{N}$ (‰)	G.Trunc. (No.)	G. Crass. (No.)	Depth (cmbfs)	Age (kyr BP)	$\delta^{18}\text{O}$ (‰PDB)	Corg (%)	$\delta^{15}\text{N}$ (‰)	G.Trunc. (No.)	G. Crass. (No.)
1494	226.0	0.47	0.37	4.53	30	2	1012	149.9				0	7	577	72.2				0	1
1487	224.1	0.31			30	1	1006	149.4	0.23	1.62	7.18	1	9	570	71.4	0.34	0.64	5.63	11	3
1479	221.8	0.11	0.86		6	2	1000	148.9		1.91		0	2	562	70.4	0.30	0.67		9	1
1470.5	219.5	-0.20	1.21	6.3	1	5	995	148.4		2.71		0	0	553.5	69.4				0	0
1462	217.1	-0.09	0.93		1	1	990	148.0		3.58	7.63	0	10	546.5	68.6	0.24	0.77	5.45	0	1
1454.5	215.0	-0.20	1.10	6.16	0	7	984.5	147.5		3.78		0	3	538.5	67.7				25	3
1453	214.6	-0.13	1.41		0	4	977.5	146.8		2.70	7.54	0	2	530.5	66.7	0.41	0.37	5.84	30	1
1440.5	211.2	-0.18	1.70	7.13	0	2	971	146.3		2.06	6.76	0	0	523	65.9				30	1
1433.5	209.2	-0.15	1.87		1	3	962	145.5	0.20	3.52	8.44	0	0	516	65.1	0.20	0.40	6.14	30	0
1425	206.9	-0.07	1.97	7.27	0	2	955.5	144.9		3.10	8.59	0	2	509.5	64.3				30	2
1418	204.9	-0.01	1.76		0	0	948.5	144.3	-0.19	2.49	8.17	2	2	498.5	63.0	-0.21	0.77		27	1
1408	202.2	-0.54	0.58	5.85	0	29	939	143.4				0	0	491.5	62.2				6	0
1401	200.2	-0.58	0.53		11	30	935.5	143.1		2.33	8.57	0	0	485	61.4	-0.27	1.16	7.81	9	0
1393.5	198.1		0.55		12	30	929.5	142.6	0.12			0	0	478.5	60.7				0	1
1387.5	196.5	0.31	0.53	4.84	30	22	923	142.0	0.15	2.08		1	1	471.5	59.9	-0.14	1.00		1	1
1381	194.7				30	23	917	141.4				0	0	465.5	59.2	-0.33			1	0
1375	193.0	-0.67	0.85	8.25	4	10	910	140.8	0.28	1.29	6.92	2	1	455.5	58.1	-0.38	0.86	7.38	3	3
1362.5	191.1	-0.22	1.21		0	3	903.5	140.2	0.15			0	2	440.5	56.3	-0.41	1.28		0	0
1349.5	189.2	-0.16	1.53	6.02	0	2	897	139.7		1.37		0	5	425.5	54.5	-0.32	1.59	7.69	0	1
1336.5	187.3	-0.01	1.50		2	2	890	139.0				0	0	409	52.6	0.19	1.02	6.33	0	2
1329.5	186.2				0	5	884.5	138.5	0.00	1.24	7.31	0	0	393	50.7	0.04	1.61	8.25	0	2
1323.5	185.3	0.02	1.13	5.73	0	4	878.5	138.0	0.35			3	1	378.5	49.0	0.07	1.35	7.28	0	0
1316.5	184.3				0	0	871	136.0	0.29	0.73		14	3	371	48.1		1.44		0	0
1308	183.0	0.24	0.53		5	4	866.5	134.9				30	26	364	47.3	0.00	1.09	6.77	0	17
1301	182.1				1	0	860	133.1	0.23	0.46	4.41	30	12	354.5	46.2				0	0
1294.5	181.3				0	1	854.5	131.7				30	30	346	45.2	0.13	1.14		1	2
1286.5	180.3	0.00	0.49	5.36	7	23	848	130.0	-0.85	0.34	6.48	30	30	335.5	44.0				5	25
1280	179.5				0	21	842.5	129.2				29	30	329.5	43.3	-0.13	0.85	7.14	2	19
1270.5	178.4	-0.18	0.42		1	16	836	128.2	-1.30	0.62	7.42	8	8	321.5	42.4				2	8
1264	177.6				0	5	826	126.6				1	0	315.5	41.4	0.08	0.82		2	28
1256.5	176.6	-0.40	0.78	6.65	0	1	820	125.7	-1.09	1.03		0	5	306.5	40.6				1	13
1243.5	175.0	-0.33	0.66		1	3	814	124.8	-1.11	1.17	8.46	0	3	299	39.7	0.04	0.74	6.12	0	2
1228.5	173.2	-0.39	1.33	8.43	0	4	808	123.8				0	0	291.5	38.9				0	0
1214	171.4	-0.17	1.42	6.34	0	0	802	122.9		1.36	7.31	0	0	286	38.2	0.13	0.75		0	2
1200.5	169.7	0.32	1.21		0	0	790	121.1		1.34	7.18	0	0	273	36.7		0.81	6.16	0	2
1195.5	169.1	0.44	0.69	4.62	0	0	783	120.0	-0.89			0	4	269.5	36.3				0	0
1190.5	168.5		0.67		0	0	777	112.5	-0.45	1.01		0	19	262	35.4	0.38	0.80		0	0
1185	167.8	-0.16	2.71	8.74	0	0	771	110.8		0.59	5.03	0	30	254.5	34.6				0	2
1179	167.1	0.06	1.32	8.34	0	0	764.5	108.9				0	28	247	33.7	0.29	1.19	6.65	0	1
1172	166.2		0.92	4.36	0	1	757	106.8	-0.65	0.55		2	30	231	31.8	0.36	1.31		0	2
1165.5	165.4	0.38			0	0	751	105.1				5	30	215	30.0	0.38	0.87	5.24	0	0
1159.5	164.7	-0.07	1.32	6.97	0	0	742	102.5	-0.72	0.70	5.79	1	17	199	28.1	0.48	1.00		0	0
1144	162.8	0.24	1.11	4.98	0	1	736	101.0				0	29	183.5	26.3		1.05	5.94	0	0
1128	160.8	0.26	0.69		0	0	729	99.3	-0.68	1.24	7.11	0	30	166	24.2	0.60	1.27	5.97	0	0
1121	159.9				0	1	723	97.8				0	24	159	23.4	0.45			0	1
1113.5	159.0	0.68	0.35	4.33	30	6	717.5	96.4	-0.42	1.46	6.51	0	8	152	22.6	-0.30	1.26	6.35	0	1
1107.5	158.5				16	30	712	95.1				0	28	144	21.7	0.51			0	1
1101.5	157.9	0.56	0.33		0	30	707	93.9	-0.37	1.39		3	15	136	20.7		1.18		0	0
1093	157.2	0.56	0.35	4.42	7	30	700.5	92.2				0	15	128	19.8	0.57			7	1
1085.5	156.5				2	30	694.5	90.8	-0.48	1.22	5.72	2	16	120.5	18.9		0.92	5.34	3	1
1078.5	155.9	0.17	0.46		0	21	689	89.4	0.77			1	26	112.5	18.0	0.83			30	0
1073	155.4				0	16	682	87.7	-0.20	0.40	5.74	2	30	106.5	17.1		0.47		30	0
1068.5	155.0	0.34	0.45	4.67	0	8	676.5	86.3				2	30	98.5	15.8				30	1
1061.5	154.4				0	5	671	85.0		0.64		0	8	90	14.5	-0.25	0.65	5.74	30	0
1054	153.7	0.28	0.42		0	18	664.5	83.4				0	9	82	13.9				7	0
1046	153.0				0	3	657	81.5	-0.84	1.06	7.54	0	2	75	13.4	-0.23	0.60		28	1
1040.5	152.5	0.31	0.66	4.74	0	7	643	79.9	-0.56	1.16		0	0	69.5	13.0	0.36	0.58	7.27	3	0
1035.5	152.0	0.33			0	1	628.5	78.2	-0.55	1.10	8.29	0	0	62	12.4	-0.26	0.45		0	0
1029.5	151.5		1.15		0	7	618	77.0	-0.09	1.05		0	3	46	11.2	-0.85	0.38	8.1	0	0
1024	151.0	0.23			0	0	599	74.7	-0.14	1.29	6.78	0	0	30	10.1	-1.16	0.61	7.68	0	0
1018	150.5		1.36	5.93	0	2	584.5	73.0	0.27	1.28		0	6	22.5	9.5	-1.35	0.71		0	0

Appendix 1.

Data for NIOP464 from the Murray Ridge, depth in centimetres below sea floor (cmbfs), age in kyr BP, $\delta^{18}\text{O}$ in ‰ (PDB) for *N. duterrei*, organic carbon content (%), $\delta^{15}\text{N}$ in ‰ relative to the atmosphere, *G. truncatulinoides* and *G. crassaformis* in number per 27 (of 45) fields of a rectangular picking tray, to a maximum of 30 specimens.

NIOP455

Depth (cmbsf)	Age (kyr BP)	$\delta^{18}\text{O}$ N.dute. (‰PDB)	$\delta^{15}\text{N}$ (‰)	Ca/Sr (*10 ⁻⁴)	Org (%)	<i>G.Trunc.</i> (No.)	<i>G. Crass.</i> (No.)	Depth (cmbsf)	Age (kyr BP)	$\delta^{18}\text{O}$ G.sacc. (‰PDB)	$\delta^{18}\text{O}$ N.dute. (‰PDB)	$\delta^{15}\text{N}$ (‰)	Ca/Sr (*10 ⁻⁴)	Org (%)	<i>G.Trunc.</i> (No.)	<i>G. Crass.</i> (No.)
1453	118.1			48.22	0.45	0	0	712	51.8				41.71	1.47	0	0
1442	116.7	-0.6	7.15	48.02	1.23	0	1	703	51.0		-0.1		43.98	1.93	0	0
1431	115.3	-0.6		44.68	1.63	0	1	694	50.3				54.03	6.33	0	0
1421	114.0			42.11	1.59	0	2	688	49.9			8.61	48.13	4.53	0	0
1409	112.5	-0.3	3.66	41.73	1.00	0	30	683	49.5		-0.3		52.04	3.36	0	0
1396	110.9			41.88	0.78	0	30	670	48.4			5.85	43.21	1.80	0	1
1383	109.2	-0.9		42.38	1.02	0	7	658	47.5				41.88	3.06	0	0
1366	107.1		4.29	41.29	1.01	0	6	643	46.3		0.2		40.65	1.52	0	0
1353	105.4	-1		40.41	0.90	0	6	632	45.4				41.51	3.01	0	2
1345	104.4			40.81	0.70	0	7	619	44.4			5.89	44.46	1.85	0	1
1330	102.5	-0.8	4.87	40.78	0.69	2	30	606	43.4	0.1	0.3		52.83	1.84	1	11
1317	101.5			37.77	1.11	0	14	595	42.5				68.21	1.68	15	30
1305	100.5	-0.9		38.58	1.71	0	0	585	41.7	0			69.50	1.14	5	15
1292	99.5		7	40.69	1.95	0	6	572	40.7	-0.6	-0.2	7.95	44.00	2.78	0	0
1278	98.4	-1		42.01	1.93	0	5	557	39.5				42.21	2.47	0	0
1262	97.1			44.77	2.68	0	4	544	38.5				51.06	1.50	0	7
1252	96.3	-0.5	7.91	44.23	2.77	0	1	532	37.5	-0.3	0.2	5.76	54.06	1.29	0	9
1244	95.7			44.56	2.59	0	1	520	36.6				44.99	1.73	0	1
1229	94.5	-0.4		40.91	2.33	0	9	507	35.5				43.82	1.36	0	0
1216	93.5		5.71	39.57	1.51	0	7	495	34.6	-0.4	-0.1	6.96	40.74	2.48	0	0
1204	92.5	-0.1		41.43	0.99	0	9	486	33.9	-0.5			43.27	1.49	0	0
1191	90.5			42.44	0.71	2	30	474	32.9				45.99	2.58	0	0
1178	88.5	-0.9	4.7	42.18	0.81	2	30	461	31.9	0.2			44.02	1.35	1	0
1166	86.6			42.73	0.74	0	30	449	30.9			4.63	48.60	1.34	0	1
1155	84.9	-0.3		44.38	1.13	0	30	437	30.0	0			73.92	1.02	1	2
1145	83.4		6.5	41.58	1.79	0	0	423	28.9		0.7		87.26	0.82	0	1
1133	81.5	-1		41.29	1.58	0	0	409	27.8	-0.4			47.36	2.64	0	0
1121	80.7			41.96	1.19	0	0	397	26.8			3.71	49.50	1.20	0	0
1108	79.8	-0.8	7.03	40.85	2.58	0	0	388	26.1		0.2		45.47	2.21	0	0
1095	78.9			40.09	1.88	0	0	378	25.7				41.02	2.28	0	0
1082	78.0			43.80	1.87	0	0	368	25.3	0.3		5.36	39.21	2.20	0	0
1069	77.1	-0.3	5.4	42.90	1.29	0	0	358	24.9				40.61	2.71	0	0
1057	76.2			42.74	2.50	0	0	346	24.4	0.4	0.7		51.94	1.15	0	0
1044	75.3			46.36	1.42	0	0	334	23.9			4.74	48.48	1.46	0	0
1032	74.5		7.95	46.27	2.47	0	0	324	23.5	0.2	0.5		43.85	1.59	0	0
1018	73.5	-0.1		41.24	1.15	0	0	316	23.1				56.30	1.09	0	0
1005	72.6		5.08	40.14	1.73	0	0	304	22.7	0.1	0.6		48.48	0.82	0	0
992	71.7	0.2		41.70	1.22	0	2	291	22.1	0.1	0.1	6.06	42.47	2.02	0	0
980	70.9			45.21	1.60	0	0	278	21.6				42.76	1.76	0	0
966	69.9		4.62	58.07	0.85	0	0	264	21.0				41.42	1.80	1	0
955	69.2	0.3		66.90	0.90	0	0	251	20.5	0.1			43.62	1.68	0	0
945	68.5			59.14	0.91	0	0	237	19.9			5.99	40.99	1.82	0	0
934	67.7		6.02	48.52	1.45	0	0	225	19.4	0.2			45.13	1.71	4	0
921	66.8	0.2		56.96	0.77	0	0	215	19.0				49.05	2.32	0	0
908	65.9			45.14	0.56	30	1	203	18.5		0.7	5.3	49.02	1.77	19	0
896	65.1		4.51	99.38	0.55	30	1	188	17.9	0.2			44.74	1.59	0	0
885	64.3	0.5		106.76	0.49	30	0	174	17.3	0.2		4.63	84.52	1.05	6	0
872	63.4		4.91	108.72	0.58	30	0	159	16.7	0.3	0.8		91.06	0.77	30	0
859	62.5			106.32	0.75	30	0	145	16.1	0.5			108.34	0.62	24	0
850	61.9	-0.4	7.71	50.45	2.31	0	0	133	15.6	0.4	0.6		123.57	0.89	30	0
836	60.9			44.62	2.74	0	0	124	15.3	0.2		4.47	117.44	0.57	30	0
822	60.0			49.42	1.46	1	0	115	14.9	0.5			125.51	0.64	30	0
809	59.1	-0.3	7.46	42.95	2.38	0	0	105	14.5	-0.3	-0.2	7.33	90.40	1.80	2	0
796	58.2			61.80	1.41	0	0	94	13.8	-0.2	0.2		100.12	1.68	3	0
785	57.4			42.44	2.61	0	0	81	13.0	-0.2			84.67	1.18	0	0
772	56.5	-0.4	9.19	45.36	3.08	0	0	68	12.2	-0.3		5.6	79.47	1.00	2	0
758	55.4			45.63	3.03	0	0	55	11.4	-0.6	-0.2		53.91	1.03	1	0
748	54.6			44.28	3.61	0	0	41	10.5			8.06	63.68	1.44	0	0
735	53.6			44.00	3.01	0	1	28	9.7	-1.3	-1.2		70.26	1.91	0	0
724	52.7		6.38	46.41	1.73	0	0	17	9.0	-1.4	-1.4	7.29	55.68	2.41	0	0

Appendix 2.

Data for NIOP455 from the Pakistan Margin, depth in centimetres below sea floor (cmbsf), age in kyr BP, $\delta^{18}\text{O}$ in ‰ (PDB) for *G. sacculifer* and *N. duertrei*, $\delta^{15}\text{N}$ in ‰ relative to the atmosphere, Ca/Sr ratio (*10⁻⁴), organic carbon content (%), *G. Truncatulinoides* and *G. Crassaformis* in number per 27 (of 45) fields of a rectangular picking tray, to a maximum of 30 specimens.

Appendix 3.

NIOP497

Depth (cmbsf)	Age (kyr BP)	$\delta^{18}\text{O}$ N.dut. (‰PDB)	Corg (%)	<i>G.Trunc.</i> (No.)	<i>G. Crass.</i> (No.)	Depth (cmbsf)	Age (kyr BP)	$\delta^{18}\text{O}$ N.dut. (‰PDB)	Corg (%)	<i>G.Trunc.</i> (No.)	<i>G. Crass.</i> (No.)
16	6.2	-0.5	0.64	1	1	465	56.5	-0.1	0.70	0	4
23	7.0	-0.8	0.68	0	0	478.5	59.5	-0.2	0.68	2	5
33	8.0	-0.8	0.63	2	2	485.5	61.0	-0.2	0.66	8	7
42	9.0	-0.9	0.60	0	0	492	62.5	0.1	0.29	30	4
56	10.5	-0.7	0.65	2	0	505	65.3	0.2	0.26	26	13
69.5	12.0	-0.5	0.51	0	0	512.5	67.0	0.3	0.32	1	11
81	13.2	-0.2	0.46	1	0	519	72.0	0.1	0.61	0	2
93	14.5	-0.2	0.39	0	1	533	82.7	0.3	0.55	0	5
104	15.7	0.2	0.27	30	0	543	90.3	0.0	0.82	0	5
116	16.9	0.6	0.25	30	0	549	94.9	0.1	0.43	1	9
126	18.0	0.9	0.27	30	1	562.5	105.3	-0.1	0.81	0	7
141	19.7	0.9	0.38	30	5	578	117.1	-0.6	0.34	1	30
154	21.2	0.7	0.91	0	2	587	124.0	-0.3	0.60	3	30
168.5	22.8	0.6	1.12	0	6	597.5	125.9	-0.7	0.79	0	9
179.5	24.1	0.7	0.80	0	11	611	128.2	-0.6	0.57	20	30
191.5	25.4	0.5	0.79	0	17	623	130.4	-0.2	0.23	30	30
202.5	26.7	0.6	0.73	0	10	636	132.7	0.2	0.21	26	12
216	28.2	0.6	0.91	0	12	644.5	134.2	0.3	0.46	0	24
222.5	29.0	0.6	0.82	0	9	658	136.6	-0.2	0.73	2	12
229	29.7	0.5	0.53	0	12	665	137.8	0.2	0.73	1	21
237	30.6	0.5	0.64	0	10	678	140.1	0.3	0.87	0	17
249.5	32.0	0.7	0.54	0	12	686	141.5	0.2	0.90	0	22
259	33.1	0.5	1.21	0	8	694	142.9	0.2	0.62	0	13
265	33.8	0.5	0.98	0	9	702	144.3	0.2	1.19	0	23
280	35.5	0.3	0.69	0	6	715	146.6	0.2	1.06	0	15
290	36.6	0.5	0.51	0	7	724	148.2	0.1	1.02	1	30
304	38.2	0.3	0.89	0	8	733.5	149.9	0.1	0.85	0	30
318	39.8	0.2	0.86	0	11	748	152.5	0.2	0.51	0	30
325.5	40.7	0.2	0.67	5	21	756.5	154.0	0.3	0.39	0	30
338	42.1	0.2	0.64	4	30	763.5	155.2	0.1	0.50	0	30
345	42.9	0.2	0.54	0	25	778.5	157.9	0.5	0.26	0	30
357	44.2	0.3	0.40	15	30	785	159.0	0.6	0.30	1	30
365	45.1	0.2	0.41	0	12	793	160.4	0.5	0.30	1	30
371	45.8	0.0	0.83	0	6	801	161.8	0.5	0.32	18	8
381.5	47.0	0.3	0.83	2	30	814.5	164.2	0.3	0.69	0	2
385.5	47.5	0.2	0.73	0	10	823	165.7	0.1	0.86	0	1
394.5	48.5	0.1	0.67	0	4	833.5	167.6	0.4	0.50	0	0
406	49.8	-0.1	1.25	0	2	845.5	169.7	0.1	0.95	0	0
415.5	50.9	0.1	0.50	1	7	857	171.7	0.3	0.42	0	3
425	52.0	0.2	1.34	0	5	869	173.8	0.1	0.75	0	5
440	53.7	0.0	1.17	0	7	879.5	175.7	-0.2	0.79	1	3
456	55.5	0.0	0.53	0	6						

Appendix 3.

Data for NIOP497 from the Oman Margin, depth in centimetres below sea floor (cmbsf), age in kyr BP, $\delta^{18}\text{O}$ in ‰ (PDB) for *N. dutertrei*, *G. truncatulinoidea* and *G. crassaformis* in number per 27 (of 45) fields of a rectangular picking tray, to a maximum of 30 specimens.

NIOP453

Depth (cmbsf)	Corg (%)	Ca/Sr (10 ⁻⁴)	Depth (cmbsf)	Corg (%)	Ca/Sr (10 ⁻⁴)
1339.5	0.26	51.91	649.5	0.93	40.67
1329.5	0.21	52.03	639.5	0.75	42.33
1308	0.13	50.36	630	1.76	42.81
1295.5	0.14	51.54	619.5	3.90	43.10
1280	0.28	52.24	609.5	2.73	42.13
1260	0.06	61.89	599.5	0.80	54.42
1244	0.40	51.53	589	0.84	39.09
1228.5	0.05	60.40	579.5	1.01	40.35
1214.5	0.42	48.11	569.5	0.86	40.06
1202.5	0.54	49.49	559.5	0.87	43.80
1189	0.62	48.27	549.5	0.95	40.11
1179	0.64	47.41	539.5	0.66	44.95
1169	0.65	43.45	529.5	0.57	54.28
1159	0.30	46.03	520	0.89	48.06
1149	0.43	44.18	509.5	1.13	39.76
1137	0.47	44.69	499.5	0.61	40.52
1129	0.38	41.86	489.5	0.64	43.13
1119	0.37	41.91	480	0.71	40.96
1109	0.56	42.52	469.5	0.71	42.56
1099.5	0.63	43.92	460	0.75	44.12
1089	0.67	45.04	450	0.72	43.35
1078.5	0.83	45.34	439.5	0.57	50.12
1068.5	1.33	45.46	429.5	0.41	59.55
1058.5	1.27	45.02	419.5	0.81	47.46
1048.5	1.45	44.98	409.5	1.22	45.38
1038	1.38	45.13	400	1.42	40.37
1028.5	0.84	43.77	390	1.37	40.74
1018.5	0.65	41.26	378	0.64	49.95
1009	0.36	39.51	368	0.65	46.25
998	0.39	41.74	358	0.80	46.11
988.5	0.45	41.87	348.5	0.63	49.25
978.5	0.52	41.56	338.5	0.94	46.65
968.5	0.58	41.48	328	1.01	44.93
959	0.60	41.50	318.5	0.97	43.61
948.5	0.61	41.52	309	1.07	42.80
939	0.78	42.71	298.5	1.14	42.09
929	0.82	43.80	289	1.23	41.98
918.5	0.71	42.31	278.5	1.16	45.90
909	1.07	45.92	268.5	1.09	44.81
898.5	1.19	41.96	259	1.15	47.38
888.5	0.73	40.89	249	0.98	49.83
878.5	1.42	45.62	238.5	0.83	44.89
868.5	1.01	40.73	228	0.70	52.13
859	1.03	42.35	218	0.44	64.28
848.5	0.72	41.12	203.5	0.31	72.37
839.5	0.58	43.20	183.5	0.34	79.42
829.5	0.52	49.19	174.5	0.33	81.20
819.5	0.55	49.52	163	0.36	81.28
809.5	0.60	45.43	153.5	0.71	70.90
799	0.32	59.21	144	0.73	67.53
789.5	0.28	65.06	133.5	0.67	65.61
779.5	0.30	69.77	124	0.56	62.96
769.5	0.33	68.43	114	0.46	61.55
759.5	0.67	53.62	104.5	0.47	58.50
749.5	0.65	47.26	93.5	0.51	54.79
740	0.96	62.72	83.5	0.54	48.22
729.5	0.77	44.00	73.5	0.51	43.66
719.5	0.66	41.84	63.5	0.44	40.48
709	0.62	44.52	53.5	0.47	40.54
699.5	0.97	68.12	43.5	0.51	41.42
690	0.98	42.83	33.5	0.64	43.71
679.5	1.02	43.31	24	0.69	38.87
669.5	1.32	41.47	13.5	0.83	40.11
659.5	1.19	40.64	4	1.07	40.71

NIOP454

Depth (cmbsf)	Corg (%)	Ca/Sr (10 ⁻⁴)	Depth (cmbsf)	Corg (%)	Ca/Sr (10 ⁻⁴)
1480.5	0.28	49.24	752.5	1.22	42.36
1470.5	0.17	50.32	743	2.08	43.01
1461	0.19	47.46	733	4.21	45.46
1451	0.18	48.91	722.5	2.76	43.81
1439.5	0.20	48.90	713	1.61	40.68
1430.5	0.65	49.00	703.5	1.61	39.99
1421	0.78	48.69	693	2.40	42.18
1410.5	1.02	42.73	682.5	1.07	46.28
1400.5	0.68	42.69	672	2.44	41.03
1390.5	0.56	44.02	662.5	1.46	40.12
1380.5	0.36	40.77	652.5	0.95	48.87
1371	0.60	40.38	642.5	0.76	66.30
1361	0.57	41.49	632.5	1.30	56.18
1350.5	0.43	40.06	622.5	1.95	41.65
1340.5	0.57	40.17	612.5	1.50	40.84
1330.5	0.72	39.54	602.5	0.95	47.09
1321	0.98	39.33	592.5	1.60	45.03
1310	1.18	41.80	582	0.91	46.61
1300	1.63	42.33	572.5	1.42	43.32
1290.5	1.79	42.84	562.5	1.03	45.41
1281	2.34	42.99	552.5	1.68	41.56
1271.5	2.51	43.32	543	1.05	45.97
1261	2.58	41.20	523	1.11	69.95
1251	2.63	43.14	512.5	0.77	71.97
1241	2.16	43.09	503	1.35	47.62
1231.5	1.34	42.21	490.5	2.77	40.42
1221	0.81	38.66	483	2.06	39.00
1211	0.59	40.00	472.5	1.80	39.08
1201	0.57	39.96	462.5	1.18	48.10
1191	0.61	41.82	452.5	1.04	50.75
1180.5	0.99	41.67	442.5	1.16	48.36
1171	0.88	40.45	432.5	0.80	55.49
1161.5	0.81	38.61	423	1.22	50.27
1151.5	0.88	39.44	412.5	1.74	41.69
1141.5	1.00	39.83	402.5	1.69	41.77
1131	1.09	40.07	392.5	1.48	44.28
1121.5	1.18	42.46	382.5	1.69	40.97
1111	0.99	40.75	372.5	1.66	39.92
1101	1.50	43.93	362.5	1.73	42.42
1091	1.73	44.30	353	1.70	42.00
1080	1.97	42.68	342.5	1.74	41.33
1070.5	0.88	41.03	332	1.58	47.49
1061	1.80	40.78	322.5	1.61	43.16
1051	2.43	43.24	312	1.47	49.19
1041	1.46	41.47	302.5	1.25	47.28
1030.5	1.44	40.91	292	0.66	72.92
1020.5	0.96	40.32	282.5	0.47	81.26
1010.5	0.98	42.79	272.5	0.38	92.68
1000.5	0.73	46.78	263	0.44	101.29
990.5	0.59	56.43	253.5	0.46	105.72
980.5	0.75	53.89	243	0.61	101.66
970	1.11	48.50	233	1.44	83.45
960	0.85	47.43	223.5	1.37	81.23
950.5	0.43	66.09	213.5	1.08	74.22
940	0.42	72.06	203.5	0.70	75.25
931	0.40	78.42	193.5	0.57	69.45
921.5	0.45	81.03	183.5	0.74	63.87
913	0.46	85.72	173.5	0.91	60.22
902.5	0.54	84.57	163	0.90	54.60
892.5	1.14	60.41	153	1.14	50.30
882.5	1.22	50.50	143	0.90	46.06
872.5	1.96	44.64	133	1.06	46.25
862.5	1.61	43.46	123	1.34	44.26
852.5	0.94	46.18	113	1.69	42.52
842.5	1.17	43.01	103.5	1.84	42.58
832.5	1.02	60.40	93	1.96	42.90
823	1.95	45.31	83	2.20	42.35
812.5	2.10	43.77	73	2.42	42.49
801.5	2.03	43.13	62.5	2.69	44.82
791.5	2.40	42.60	53	3.08	44.55
782.5	2.14	40.87	42	3.03	45.44
772.5	2.31	42.63	32.5	2.79	46.37
762.5	1.11	43.18	22.5	2.51	44.70

Appendix 4.

Data for NIOP453 and 454 from the Pakistan Margin, depth in centimetres below sea floor (cmbsf), Ca/Sr ratio (*10⁻⁴) and organic carbon content (%).

NIOP452

Depth (cmbsf)	Corg (%)	Depth (cmbsf)	Corg (%)	Depth (cmbsf)	Corg (%)
1292.5	0.29	790	0.26	390	0.44
1284.5	0.26	784.5	0.26	385	0.47
1278	0.33	779	0.37	380	0.53
1271	0.33	774	0.30	375	0.52
1264.5	0.30	769	0.35	370	0.46
1256.5	0.32	764	0.45	364.5	0.41
1248.5	0.28	759.5	0.46	360	0.51
1240	0.29	754.5	0.53	354.5	0.57
1232	0.37	750	0.59	350	0.38
1224.5	0.30	745.5	0.74	344.5	0.37
1215.5	0.31	741	0.63	340	0.36
1206	0.24	736	0.58	335	0.38
1198.5	0.22	733	0.44	330.5	0.54
1194	0.35	728	0.51	324.5	0.53
1186	0.35	723	0.71	320	0.58
1178.5	0.30	718	1.19	315.5	0.61
1171	0.29	712.5	0.68	310	0.79
1164.5	0.40	708	0.43	305	0.87
1157.5	0.44	703	0.83	300	0.90
1151	0.25	698	1.18	294.5	1.07
1145.5	0.26	693	0.84	289.5	1.02
1139	0.34	687.5	0.88	284.5	0.74
1129	0.32	683	0.60	280	0.43
1119.5	0.36	678	0.49	274.5	0.42
1113	0.31	673	0.57	269.5	0.39
1107	0.39	668	0.41	264.5	0.46
1102	0.12	663	0.35	260	0.48
1097.5	0.35	657.5	0.38	254.5	0.40
1092.5	0.31	653	0.45	250	0.39
1085.5	0.37	648	0.45	244.5	0.41
1078	0.31	643	0.30	240	0.39
1074.5	0.09	637	0.27	235	0.56
1066.5	0.37	631	0.22	230.5	0.56
1060.5	0.25	627	0.21	224.5	0.58
1054.5	0.31	621.5	0.24	219	0.59
1049	0.28	617	0.29	214.5	0.65
1042.5	0.27	612	0.33	209.5	0.69
1036.5	0.41	607	0.37	204.5	0.69
1028.5	0.19	601	0.43	199.5	0.65
1022.5	0.38	597	0.58	194.5	0.66
1017	0.42	592	0.63	190	0.65
1008.5	0.34	586.5	0.52	184.5	0.74
1002.5	0.19	582	0.48	180	0.69
998	0.20	577	0.39	174.5	0.75
992.5	0.26	572.5	0.37	170.5	0.64
986	0.23	567	0.61	166.5	0.65
980	0.23	562	0.61	161.5	0.60
975	0.24	557.5	0.69	156.5	0.66
970	0.25	552.5	0.84	152	0.63
964	0.07	546	1.16	146.5	0.55
954.5	0.08	540	0.98	142	0.58
948.5	0.22	535	0.88	137	0.55
941	0.34	530	0.62	132	0.44
934	0.09	525	0.57	127	0.36
925	0.34	521	1.08	122	0.31
919.5	0.41	515.5	0.49	117	0.25
913	0.51	510.5	1.39	112	0.28
904	0.59	505.5	2.05	107	0.26
898	0.33	501	3.39	102	0.27
893.5	0.30	495	1.67	97	0.29
887	0.38	489.5	1.01	92	0.30
881	0.39	484.5	0.72	87	0.26
876	0.34	479.5	0.73	82	0.37
871.5	0.29	475	0.81	77	0.41
866.5	0.36	470	0.61	72.5	0.34
861.5	0.46	465	0.85	68	0.38
856.5	0.49	459.5	0.71	62	0.38
851.5	0.46	454.5	0.60	56.5	0.38
847	0.52	449.5	0.69	51.5	0.34
842	0.65	445	0.52	47	0.35
836.5	0.95	440	0.42	42	0.38
832	1.00	435	0.40	36.5	0.37
826.5	1.07	430.5	0.67	32	0.35
821.5	1.12	424.5	0.70	26.5	0.36
816	1.20	420	0.56	22	0.47
811.5	0.78	415	0.47	16.5	0.41
806.5	0.71	410	0.35	12	0.36
802	0.48	405	0.40	7	0.49
797.5	0.35	400	0.48	2.5	0.58
794.5	0.30	394.5	0.38		

NIOP458

Depth (cmbsf)	Corg (%)	Depth (cmbsf)	Corg (%)	Depth (cmbsf)	Corg (%)	Depth (cmbsf)	Corg (%)
1628	1.38	1218.5	0.24	807	0.84	396.5	0.5
1624	1.35	1213	0.19	802	0.87	391.5	0.43
1620	1.37	1209	0.32	797.5	0.69	387	0.53
1614.5	1.32	1203	0.26	792	0.37	381.5	0.53
1611	1.87	1197.5	0.28	787	0.58	376.5	0.61
1606	1.89	1192.5	0.26	782	1.06	371.5	0.55
1601	1.10	1188	0.25	777	1.27	367.5	0.53
1595.5	1.11	1183	0.29	772.5	0.96	361.5	0.47
1591	0.66	1178	0.39	767	1.12	357	0.53
1584.5	0.50	1173	0.28	762	0.80	351.5	0.7
1580.5	0.26	1168	0.43	757	0.59	347	0.62
1576	0.26	1162.5	0.46	751.5	0.52	341.5	0.52
1571.5	0.21	1158	0.63	747	0.42	336.5	0.48
1565.5	0.40	1153	0.87	741.5	0.53	332	0.44
1561	0.51	1148	1.18	737	0.37	327	0.48
1556	0.52	1143	1.10	732	0.38	322	0.57
1551	0.59	1138	1.84	727	0.46	317	0.49
1546.5	0.55	1133.5	1.87	722	0.40	312.5	0.66
1541	0.52	1128.5	2.08	717	0.41	307	0.75
1535.5	0.32	1123	2.27	711.5	0.39	302	0.74
1528	0.44	1118	0.78	707	0.38	296.5	0.68
1523	0.17	1112.5	2.13	702	0.34	292	0.69
1518	0.23	1107.5	1.10	697	0.29	287	0.66
1513	0.18	1103	1.36	692	0.25	281.5	0.61
1508	0.21	1098	1.08	687	0.29	277	0.59
1503	0.19	1092.5	0.83	682	0.32	271.5	0.72
1498	0.34	1087.5	0.85	677	0.49	267	0.76
1493	0.44	1083	0.47	672.5	0.39	261.5	0.88
1488	0.46	1077.5	0.42	667	0.32	257	0.82
1482.5	0.52	1072.5	0.33	662	0.30	252	0.93
1478.5	0.64	1067.5	0.23	656.5	0.29	247	0.86
1473	0.51	1062	0.20	652	0.61	242	1.09
1468.5	0.39	1057	0.20	646.5	0.50	237	1.31
1463	0.27	1052	0.22	641.5	0.35	232	1.12
1458	0.33	1047	0.19	636.5	0.68	227	1.16
1453	0.46	1041.5	0.25	631.5	0.61	222	1.09
1447.5	0.38	1036.5	0.31	627	0.59	217	0.67
1442.5	0.36	1031.5	0.45	621.5	0.78	212	0.58
1438	0.42	1026.5	0.44	616.5	0.65	207	0.62
1433	0.33	1021.5	0.47	611.5	0.53	202.5	0.65
1428.5	0.41	1016.5	0.54	607	0.41	197	0.93
1423	0.78	1011.5	0.56	602	0.42	191.5	1.21
1418.5	0.77	1006.5	0.64	597	0.38	187	0.66
1413	0.82	1002	0.61	592	0.36	181.5	0.62
1408.5	1.03	997	0.68	587	0.45	177.5	0.62
1403.5	0.95	991.5	0.61	582	0.31	171.5	0.59
1398.5	0.85	986.5	0.74	577	0.64	167	0.57
1393	0.43	981.5	0.66	572.5	0.51	161.5	0.76
1388	0.28	976.5	0.46	567.5	1.11	157	0.84
1382.5	0.30	972.5	0.34	562	0.92	151.5	0.83
1378	0.34	967	0.54	557	1.33	147	0.79
1373.5	0.25	962	0.45	552	1.12	141.5	0.82
1368.5	0.33	957	0.38	547	1.22	137	0.87
1363	0.35	952	0.31	542.5	1.05	132	0.89
1358.5	0.36	947	0.30	537	1.26	127	0.73
1353.5	0.54	942	0.42	532	0.96	121.5	0.77
1348.5	0.43	937	0.48	527	1.04	117	0.82
1343.5	0.38	932	0.68	522	1.00	111.5	0.68
1338.5	0.71	927	0.62	517	0.62	107	0.78
1334	0.89	921.5	0.87	512	0.58	102	0.81
1328	0.84	917	1.12	507	0.52	97	0.73
1323	0.82	912	1.20	502	1.22	92	0.67
1318	0.62	907	1.23	497	0.90	87	1
1313	0.50	902	1.33	491.5	1.00	82	0.67
1308	0.44	897	1.23	486.5	1.46	77.5	0.62
1303	0.58	892	0.75	481.5	1.74	72	0.42
1298	0.43	887	0.66	476.5	1.94	67	0.36
1293	0.54	882	0.38	471.5	1.78	62	0.33
1288.5	0.63	877	0.31	467	1.73	57	0.25
1283	0.59	872.5	0.28	461.5	1.91	51.5	0.32
1278.5	0.72	867.5	0.25	456.5	1.18	46.5	0.3
1273	0.60	862	0.32	451.5	0.72	42	0.27
1268.5	0.76	857	0.65	447	0.86	37	0.47
1263	1.27	851.5	0.60	442	0.81	32	0.42
1258.5	1.01	847	0.81	437	0.90	26.5	0.35
1253	0.57	841.5	0.73	432	0.70	22	0.34
1248.5	0.69	837	0.83	427	0.67	17	0.26
1243.5	0.29	832	1.04	422	0.80	12	0.3
1238.5	0.26	827	0.77	417	0.65	7.5	0.33
1234	0.27	821.5	0.85	412	0.59	2	0.39
1228.5	0.25	817	0.64	407	0.56		
1223.5	0.23	812	0.53	402.5	0.49		

Appendix 5.

Data for NIOP452 and 458 from the Pakistan Margin, depth in centimetres below sea floor (cmbsf) and organic carbon content (%).

Organic carbon preservation and Oxygen Minimum Zone (OMZ) variability in the northern Arabian Sea

G. J. Reichart

Department of Geochemistry, Institute of Earth Sciences, Utrecht University,
Budapestlaan 4, PO Box 80.021, Utrecht, The Netherlands

Abstract

The sedimentary record of two cores from a sub-marine high in the northern Arabian Sea (the Murray Ridge) are compared. One core is taken from a site within the present day oxygen minimum zone (OMZ), the other one is taken from a depth below the OMZ. The history of surface water productivity, OMZ intensity, and sediment supply is reconstructed using various geochemical and micropaleontological proxies. Both cores experienced an essentially identical history of changes in sediment supply, however, under different bottom water oxygen conditions. We show that the intensity of the OMZ is controlled by variations in summer productivity and winter mixing and that synchronous variations in organic matter accumulation at both sites are linked to changes in surface water productivity. The large inter core difference in organic matter accumulation during periods of maximum OMZ intensity can not be explained by admixtures of terrigenous organic matter or difference in waterdepth, but is attributed to enhanced preservation of organic matter at the site within the OMZ. The burial efficiency of marine organic matter under low bottom water oxygen conditions is ~30%, which is 2.5 times higher than the ~12% burial efficiency calculated for oxic conditions.

Introduction

The distribution of organic carbon in marine sediments often displays a pronounced maximum at intermediate depths. Since these maxima are often associated with an oxygen minimum zone, it has been argued that preservation of organic matter is enhanced under low

oxygen conditions [e.g. *Slater and Kroopnick*, 1984]. This view is challenged by *Calvert* [1987], however, who suggested that the primary control on the mid slope organic matter maximum is not oxygen but a combination of factors related to the continental slope, such as reworking and sediment texture. The mid-depth organic carbon maximum in the

northern Arabian Sea [Von Stackelberg, 1972] has been the subject of several studies, which either link this maximum to the very strong oxygen minimum zone [Slater and Kroopnick, 1984; Paropkari et al., 1992, 1993; Chapter 3], or to sediment reworking and texture [Pedersen et al., 1992; Calvert et al., 1995].

A key argument in the decoupling of the organic carbon maximum from the OMZ is that the increasing waterdepth and decreasing surface water productivity away from the continent would suffice to cause a mid-depth organic carbon maximum. This implies that the ultimate control on organic matter accumulation is the supply of organic matter. The causality between productivity, organic carbon accumulation, and bottom water oxygenation is, furthermore, complicated by the fact that low bottom water oxygen concentrations are almost always caused by higher surface water productivity. It is, therefore, often not possible to infer whether a higher organic carbon content is due to an increased supply or better preservation.

To eliminate the effects mentioned above proxy records for paleoproductivity, intensity of the OMZ, and sediment supply are compared for two open ocean sediment cores from the northern Arabian Sea. These cores are retrieved from a submarine high (Murray Ridge), with the one (NIOP463) being located within the present day intense Oxygen Minimum Zone (OMZ), while the other (NIOP464) is from a site overlain by oxygenated bottom water (Fig. 1). Because of their location on a sub-marine high, sediments are unaffected by turbidites. Differences in surface water productivity between both sites are thought negligible. Suspended

material from the Indus plume, however, may have reached the Murray Ridge during periods of high Indus discharge [Chapter 2]

Climatic and oceanographic setting

The climate in the Arabian Sea region is characterized by strong monsoonal winds invoking large seasonal changes in hydrography and biological activity. During the northern winter, dry and cold northeast monsoonal winds are prevailing as the Tibetan Plateau is an area of high pressure. In summer, heating of the Tibetan Plateau causes a strong pressure gradient between the Tibetan low pressure cell and high pressures over the southern ocean, which drives warm and humid southwest monsoonal winds. These winds are much stronger than the winter monsoon winds. Discharge by the river Indus is linked to the summer monsoon, and peaks in August or September [Arian, 1985].

The summer monsoonal circulation results in coastal upwelling off Oman and open ocean upwelling northwest of the Findlater Jet [Wyrki, 1973; Smith and Bottero, 1977; Swallow, 1984; Brock et al., 1992], which raise productivity to values that are among the highest known for the open ocean. Annual productivity rates in the upwelling regions are between 200 and 400 g C/m²yr [Kabanova, 1968; Qasim, 1982; Codispoti, 1991]. In winter, productivity is generally low except in some areas off the Pakistan coast [Wyrki, 1973; Banse, 1987]. Surface water productivity during the winter results from mixed layer deepening and associated

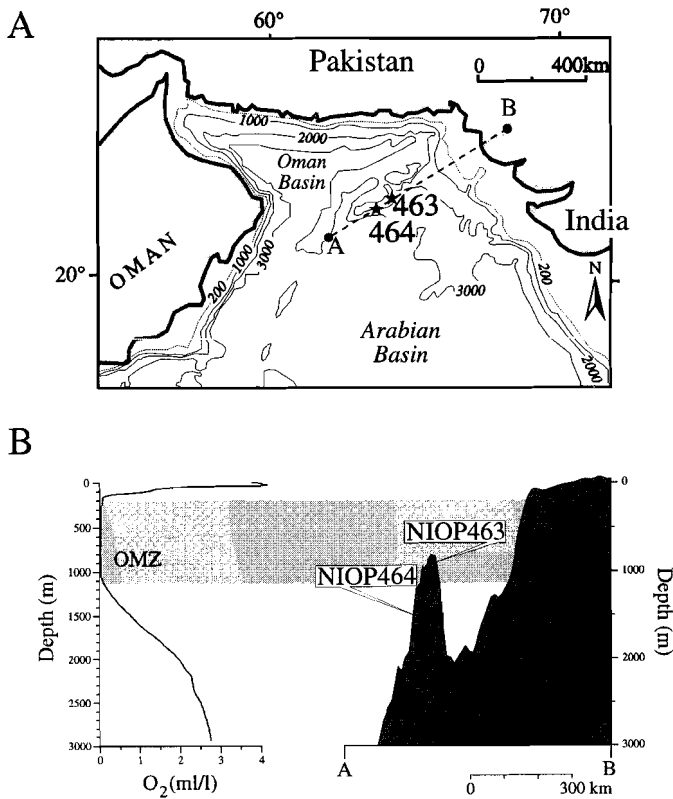


Fig. 1. A) Location map of NIOP464 (22°15'.4 N, 063°35'.1 E, 1470 mbss) and NIOP463 (22°32'.9 N, 064°02'.8 E, 920 mbss). B) Oxygen profile from CTD station NIOP458 (22°00'.3 N, 063°50'.4), seafloor topography along transect indicated by dashed line in 1A plus positions of sites NIOP463 and 464. Shading indicates the OMZ (site NIOP463 is overlain by sub-oxic water, NIOP464 is overlain by oxic water).

nutrient injection in the euphotic zone [Madhupratap *et al.*, 1996].

Today, high productivity combined with moderate ventilation causes an intense OMZ at water depths between 150 and 1250 metres [Wyrki, 1971; 1973; Deuser *et al.*, 1978; Olson *et al.*, 1993]. Within this OMZ oxygen values drop to $<2\mu\text{M}$ [Van Bennekom and Hiehle, 1994], which results in the reduction of nitrate in the water column [Deuser *et al.*, 1978]. Thermocline water in the Arabian Sea is ventilated from the south, since there is no subtropical convergence in the north [Swallow, 1984]. The main source for

thermocline ventilation is the oxygen poor ($\sim 1\text{ ml/l}$ [Olson *et al.*, 1993]) Indian Ocean Central Water (IOCW), with small contributions from Red Sea Water and Persian Gulf Water [You and Tomczak, 1993]. The sub-surface inflow from the Red Sea and Persian Gulf is relatively rich in oxygen, their contribution to the Arabian Sea, however, is small in volume [Olson *et al.*, 1993]). The mean renewal time for the Arabian Sea OMZ is ~ 11 years for the entire layer [Olson *et al.*, 1993] and ~ 4 years [Naqvi, 1987] for the denitrifying layer only.

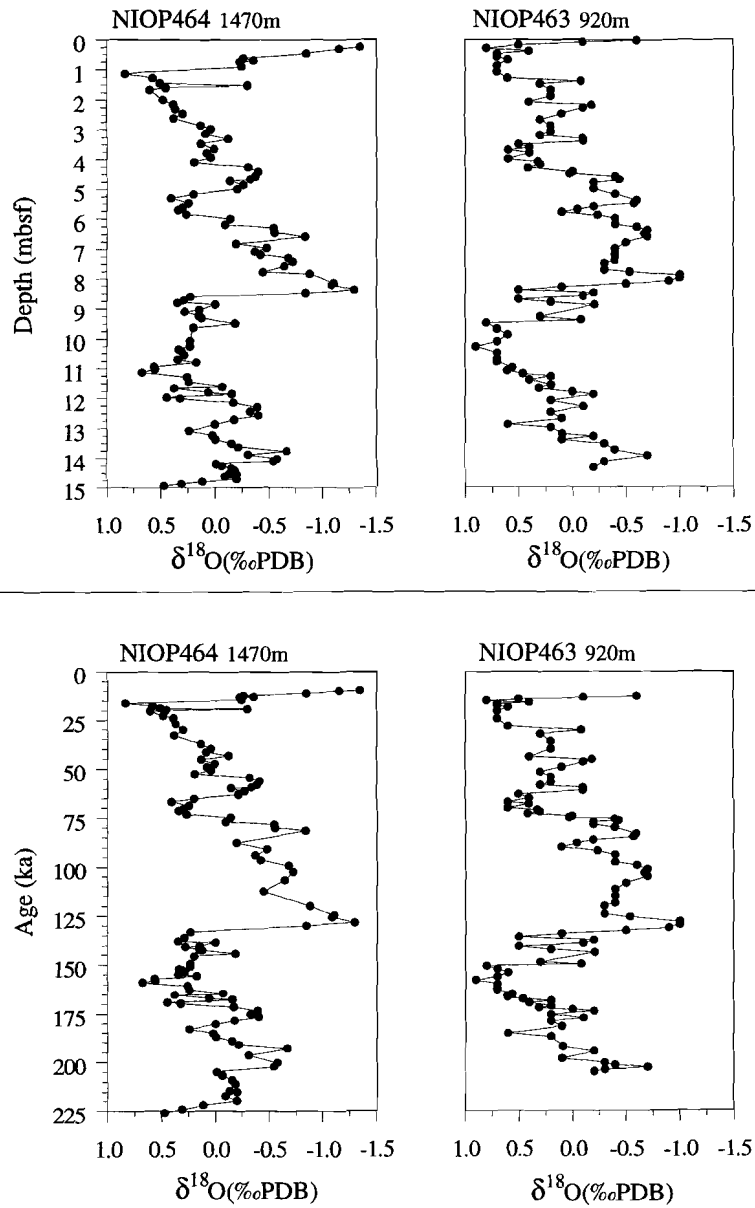


Fig. 2. A) The $\delta^{18}\text{O}$ pattern of *N. dutertrei*, in ‰ relative to the PDB standard plotted versus depth for cores NIOP463 and NIOP464, and B) versus age.

Material and methods

Pistoncores NIOP463 (22°32.9'N, 064°02.8'E) and NIOP464 (22°15.4'N, 063°35.1'E) were recovered during the Netherlands Indian Ocean Programme (1992-1993) from the Murray Ridge, from respectively 920 and 1470 meters water depth. The sediments generally consist of homogeneous, dark-greenish to light greenish/grey hemipelagic muds. Several laminated intervals occur only in NIOP463.

Water content of the sediment was determined by the weight loss of fixed volume samples after freeze-drying. Dry and wet bulk density values were calculated thereafter. Part of the sample was dried at 60°C for 4 days and thoroughly ground in an agate mortar prior to an HClO₄, HNO₃, HF acid digestion. The final residue was taken up in 1 M HCl, after which the elements Al, Ba, Mn, Ti and V were measured using ICP-AES (Perkin Elmer Optima 3000). After calibration, the analytical precision and accuracy were checked by replicate analyses of samples and standards. Both were found to be better than 3%. Because of the variable input of CaCO₃ and C_{org} elements are plotted as Al ratios.

Organic carbon was measured on a CNS analyser (Fisons NA 1500), after prior removal of carbonate, with a relative precision better than 3%.

δ¹⁵N values were measured on bulk sediment and are expressed relative to atmospheric N₂, with a precision better than 0.2‰. The particulate nitrogen was converted to N₂ in a CNS analyser (Fisons NA-1500), after which the N₂ was carried on a continuous He flow directly into the source of a mass spectrometer (VG

PRISM).

Planktonic foraminiferal δ¹⁸O values were obtained by measuring about 100 handpicked specimens of *Neogloboquadrina dutertrei*, which were roasted for 30 minutes at 470°C under a helium flow to remove organic remains. The foraminifers were then transferred into glass reaction tubes that were evacuated for 14 hours, followed by 6 hours reaction with 100% phosphoric acid at 25.0°C. The released CO₂ was cryogenically separated from the other gases and the isotopic composition measured on a mass spectrometer (VG SIRA 24), with a precision of 0.1‰.

Planktonic foraminiferal counts were made on splits (using an Otto microsplitter) from the 150-595 μm fraction. Per sample 200-400 specimens were picked, mounted on Chapman slides, identified and counted. Because percentages of *Globorotalia truncatulinoides* and *Globorotalia crassaformis* are low (≤3), they were quantified separately by counting their numbers in 27 (of 45) fields of a rectangular picking tray, to a maximum of 30 specimens. Pteropod preservation is defined by an index which ranges from 0 to 3 (0 = no pteropods; 1 = some small fragments; 2 = many medium-sized fragments; 3 = abundant large sized fragments).

Chronology

The chronology of both cores is based on the correlation of their δ¹⁸O patterns to the δ¹⁸O record of eastern Mediterranean core MD84641 [*Fontugne and Calvert, 1992*], which has been dated using the sapropel timescale [*Hilgen, 1990; Hilgen*

Sample	Depth (cm)	¹⁴ C ages (yr BP)	¹⁴ C _{cor.} ages (yr BP)	¹⁴ C _{cal.} ages (yr BP)
GrA-352	10.5	12,010±90	11,610	13,750
GrA-350	84.5	16,700±100	16,300	20,000

Table 1. AMS ¹⁴C ages of two levels from core NIOP463.

et al., 1993]. This time scale has been used because recent TIMS ²³⁰Th and ²³⁴U measurements showed that the obliquity and precession related time lags which are incorporated in the SPECMAP timescale have been overestimated [Edwards *et al.*, 1987; Bard *et al.*, 1990a,b; Gallup *et al.*, 1994]. The sapropel timescale assumes a constant time lag between sapropel midpoints and their inferred 65°N summer insolation of 3 kyr, which is based on the calendar age of 10.0-6.0 for the most recent sapropel S1 [Troelstra *et al.*, 1991; Rasmussen *et al.*, 1991; Jorissen *et al.*, 1993, Thomson *et al.*, 1995] and the correlative northern hemisphere insolation maximum at 11 ka [Lourens *et al.*, 1996].

Two AMS-¹⁴C datings from the top part of core NIOP463 were incorporated in the age model. The ¹⁴C ages were calibrated to the U/Th timescale [Bard *et al.*, 1990a] and corrected for a reservoir age of 400 year [Bard, 1988]. Because no ¹⁴C dates are available for NIOP464, the top part of this core was correlated to NIOP463. The characteristic C_{org} pattern has been used for further calibration between both cores. The last occurrence level of pink pigmented *Globigerinoides ruber* (between isotopic events 5.5 and 5.3 in the Indo-Pacific oceans, Thompson *et al.* [1979]) was used as an additional check on the chronology.

Figure 2 shows the depth to age conversion of the δ¹⁸O records for both cores (see also Fig. 7 for the spectra of the

δ¹⁸O records, and Fig. 8 for the phase relations of the precession component). The youngest sediments in both cores are clearly missing due to coring disturbances. Both cores contain two full glacial cycles. The base of NIOP463 has an age of 205 ka, while that of NIOP464 has been set at 225 ka.

Results

Paleoproductivity

The organic carbon content of both cores show a very good correlation on the precession scale of orbital forcing (Figs.3 and 8). The synchronous changes in organic carbon content have been caused by variations in organic carbon flux, or variations in preservation under the influence of a fluctuating OMZ, deeping periodically to 1470 mbss, being the present day depth of NIOP464. To distinguish between these two mechanisms other proxy records are needed to constrain the variability in paleoproductivity.

Barium is known to be enriched in sediments underlying areas with high surface water productivity, and is used as a proxy for paleoproductivity [Dehairs *et al.*, 1980; Bishop, 1988, Dymond *et al.*, 1992]. Sulphate reduction in sediments rich in organic matter, however, can obscure the productivity signal as barium

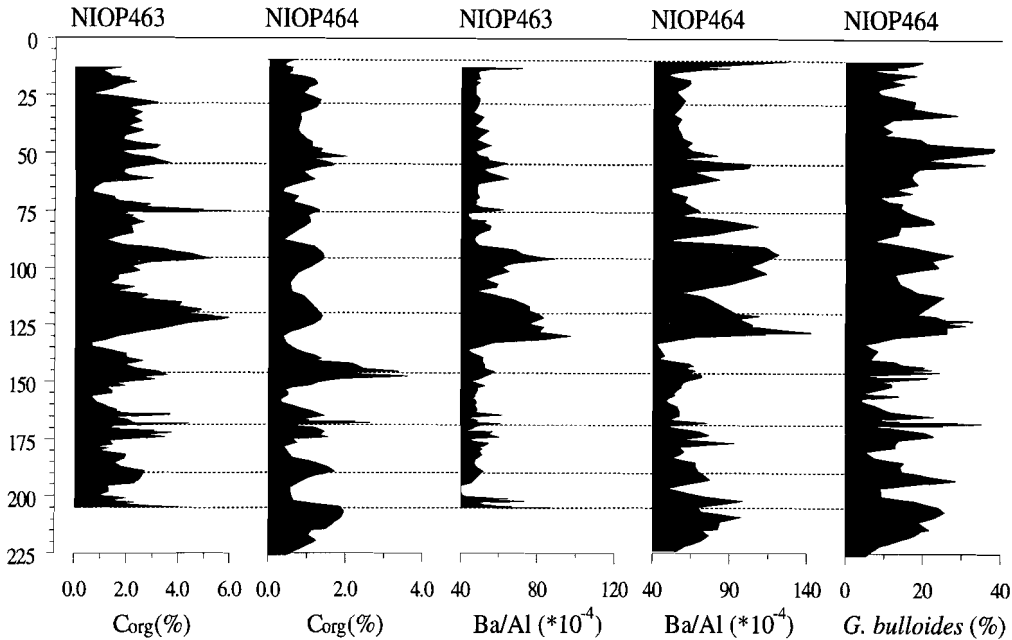


Fig. 3. Plot of organic carbon, and Ba/Al ratios for NIOP464 and NIOP463 and the percentages of *G. bulloides* for NIOP464.

gets mobilized when sulphate concentrations decrease [Van Os *et al.*, 1991; Von Breymann *et al.*, 1992]. This would, however, result in distinct barium fronts as the mobilised barium precipitates upon diffusion to less reducing sediments. No such peaks are observed implying that redistribution of barite did not occur in these two cores. Furthermore, porewater measurements on NIOP463 [unpublished data] show little sulphate reduction, even though organic carbon reaches concentrations up to 6%. Fig. 3 shows that the Ba/Al ratios show parallel changes in both cores. Ba/Al values are higher in NIOP464, which is likely due to the greater water depth of site NIOP464, since the flux of biogenic Ba has been shown to increase with depth [Dymond *et al.*, 1992]. The correlation between the Ba/Al record and the C_{org} record suggests that changes in

paleoproductivity have shaped the C_{org} profile.

The eutrophic planktonic foraminifer *Globigerina bulloides* is considered to be an upwelling indicator species [Prell *et al.*, 1980] and shows a good fit with the C_{org} and the Ba/Al records. The co-varying patterns of *G. bulloides* and C_{org} in NIOP464 (Figure 3) again suggest that changes in C_{org} primarily reflect changes in surface water productivity.

Furthermore, downcore variations in the C_{org} record from the northernmost Arabian Sea have been shown to correlate over a depth interval, down to 3000 mbss [Chapter 4]. This is another indication that the changes in C_{org} content must result from variations in surface water productivity, since it is highly unlikely that the OMZ periodically expanded to this great depth.

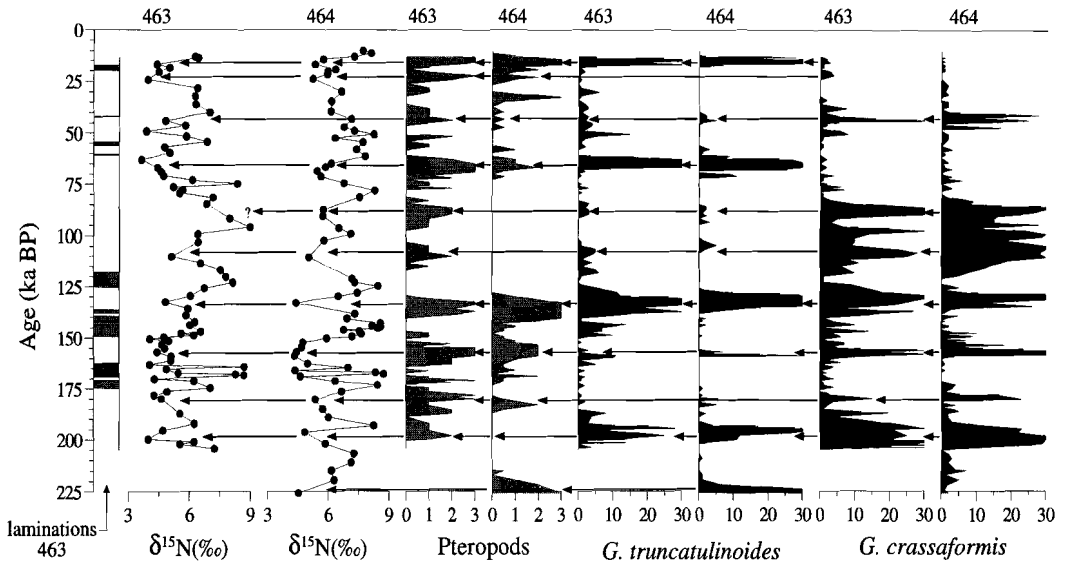


Fig. 4. Patterns of $\delta^{15}\text{N}$, *G. truncatulinoides*, *G. crassaformis*, the pteropod preservation index, and lamination in NIOP463 and NIOP464.

Variability in OMZ-intensity

The intensity of the OMZ has been shown to be closely related to sea surface productivity [Altabet *et al.*, 1995; Chapter 2 and 4]. Higher sea surface productivity results in higher oxygen consumption rates as the organic matter is degraded while settling through the watercolumn. Denitrification, caused by the present very low oxygen concentrations, causes a significant increase in $\delta^{15}\text{N}$ of the subsurface nitrate, which is after upwelling incorporated in the organic matter [Schäfer and Ittekkot, 1993; Altabet *et al.*, 1995]. Although fractionation during the partial consumption of nitrate during advection away from the upwelling areas influences the $\delta^{15}\text{N}$ signal, synchronous changes in $\delta^{15}\text{N}$ nearby and at a distance of the main upwelling areas are caused by denitrification [Altabet *et al.*, 1995]. The good correlation between the $\delta^{15}\text{N}$ record off Oman [Altabet *et al.*, 1995] and a

similar record of NIOP464 shows that the $\delta^{15}\text{N}$ record primarily reflects water column denitrification [Chapter 4]. The $\delta^{15}\text{N}$ record of NIOP463 and 463 shows an excellent correlation on a precession scale (Fig. 4). Fig. 4 also shows that laminated sediments in NIOP463 are restricted to intervals with higher $\delta^{15}\text{N}$ values. In spite of their different C_{org} content, the good correlation between the $\delta^{15}\text{N}$ records from NIOP463 and NIOP464 shows that early diagenesis has not significantly influenced the primary $\delta^{15}\text{N}$ signal. This signal can, therefore, be interpreted as a proxy for water column denitrification, and thus for OMZ intensity. Plotting $\delta^{15}\text{N}$ against C_{org} values reveals a good correlation for NIOP463, but shows an offset to lower C_{org} values for NIOP464 (Fig.5). This implies that the C_{org} content increases in NIOP463 during an intensified OMZ, whereas this relationship is less pronounced in NIOP464.

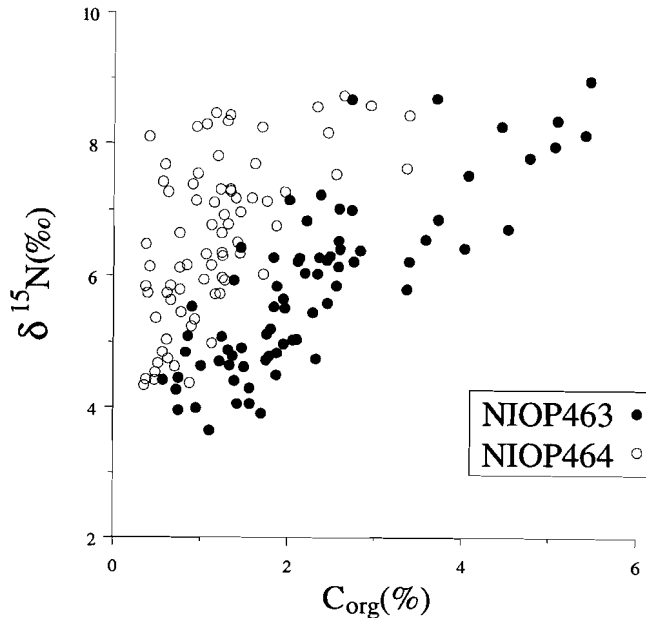


Fig. 5. Scatter plot between C_{org} (%) and $\delta^{15}N$.

The position of the aragonite compensation depth (ACD) is an other tracer which can be used in the northern Arabian Sea to reconstruct changes in the intensity of the OMZ [Chapter 4]. The present day ACD lies within the OMZ, at about 500 m [Berger, 1977], since -due to CO_2 addition and the oxidation of ammonia to nitrate- pH and carbonate saturation are lowered [Canfield and Raiswell, 1991]. The occasional occurrence of pteropods (made up of aragonite) at sites NIOP463 and 464 (Fig. 4), therefore, reflects a periodical lowering of the ACD to at least 1470 mbss, and a concomitant weakening of the OMZ. The shallower site NIOP463 (920 mbss), shows more intervals with pteropods preserved than the deeper site NIOP464 (1470 mbss). Pteropod occurrences in NIOP463 and

their absence in NIOP464 represent periods during which the ACD was positioned between 920 and 1470 m. The pteropod record show a good correlation with the $\delta^{15}N$ record, implying a deeper ACD when denitrification was less, and vice versa. Fig. 4 also shows that the deposition of the laminated sediments in NIOP463 is accompanied by a shallow ACD.

Deep convective overturn during glacial periods caused, by an intensified winter monsoon, is an important factor that influences the intensity of the OMZ in the northern Arabian Sea. Deep convective overturn is inferred from peak occurrences of the foraminiferal species *Globorotalia truncatulinoides* and *Globorotalia crassaformis* [Chapter 4]. The life cycle of these planktic foraminiferal species

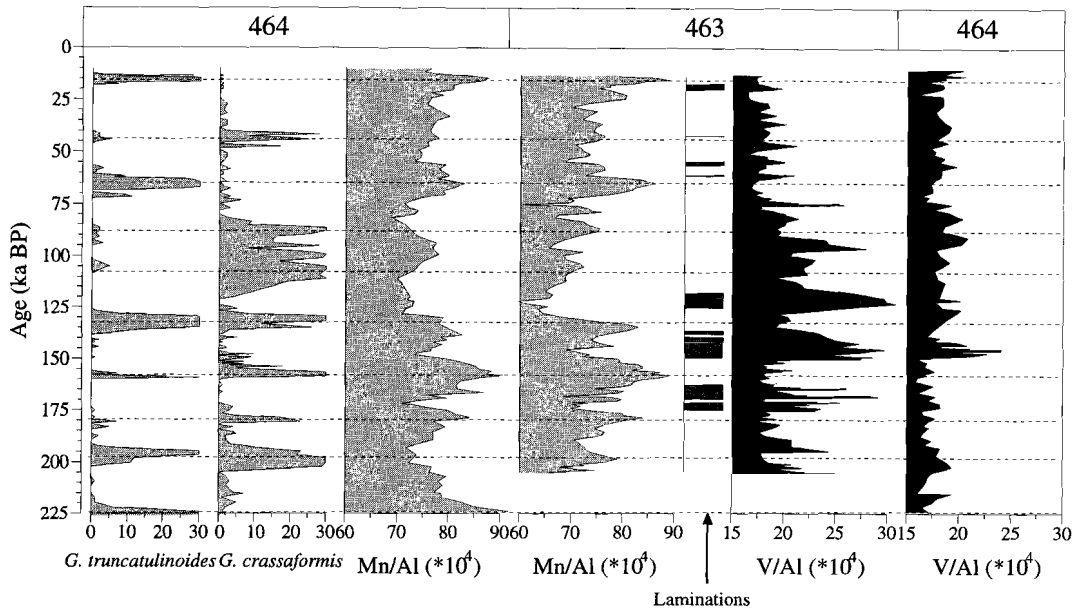


Fig. 6. Patterns of *G. truncatulinoides* and *G. crassaformis* in NIOP464; lamination in NIOP463, and V/Al and Mn/Al in both cores plotted versus age.

depend on the deepening of the mixed layer to 800 and 300 m respectively [Be and Tolderlund, 1971; Hemleben *et al.*, 1985; Lohmann and Schweitzer, 1990; Chapter 4]. An intensified and cooler winter monsoon, combined with a reduced halocline caused by suppressed outflow from the Persian Gulf and Red Sea during glacial sea level low stands, increased convective winter overturn, introducing oxygen rich waters to the deeper part of the water column [Chapter 4]. The effect of intensified winter mixing on the OMZ intensity might have been amplified by a positive feedback mechanism, since increased oxygen concentrations reduced the regeneration of the nutrient phosphorus [Van Cappellen and Ingall, 1994], thereby limiting surface water productivity.

Fig. 4 shows that during periods with intensified convective turnover in winter,

inferred from the peak occurrences of *G. truncatulinoides* and *G. crassaformis*, denitrification was reduced and the ACD deepened. The laminated intervals in NIOP463 are characterized by the absence of *G. truncatulinoides* and *G. crassaformis*. The lack of lamination in NIOP464 could indicate that bottom water oxygen levels at this site never reached the low values which influenced the sedimentation at site NIOP463. The peak occurrences of *G. crassaformis*, without *G. truncatulinoides*, during isotopic stage 5, when convective overturn must have been moderately intensified, are also accompanied by a modest deepening of the ACD, to depths somewhere between 920 (NIOP463) and 1470 mbss (NIOP464).

The redox-sensitive elements V and Mn are indicative of the paleoredox conditions

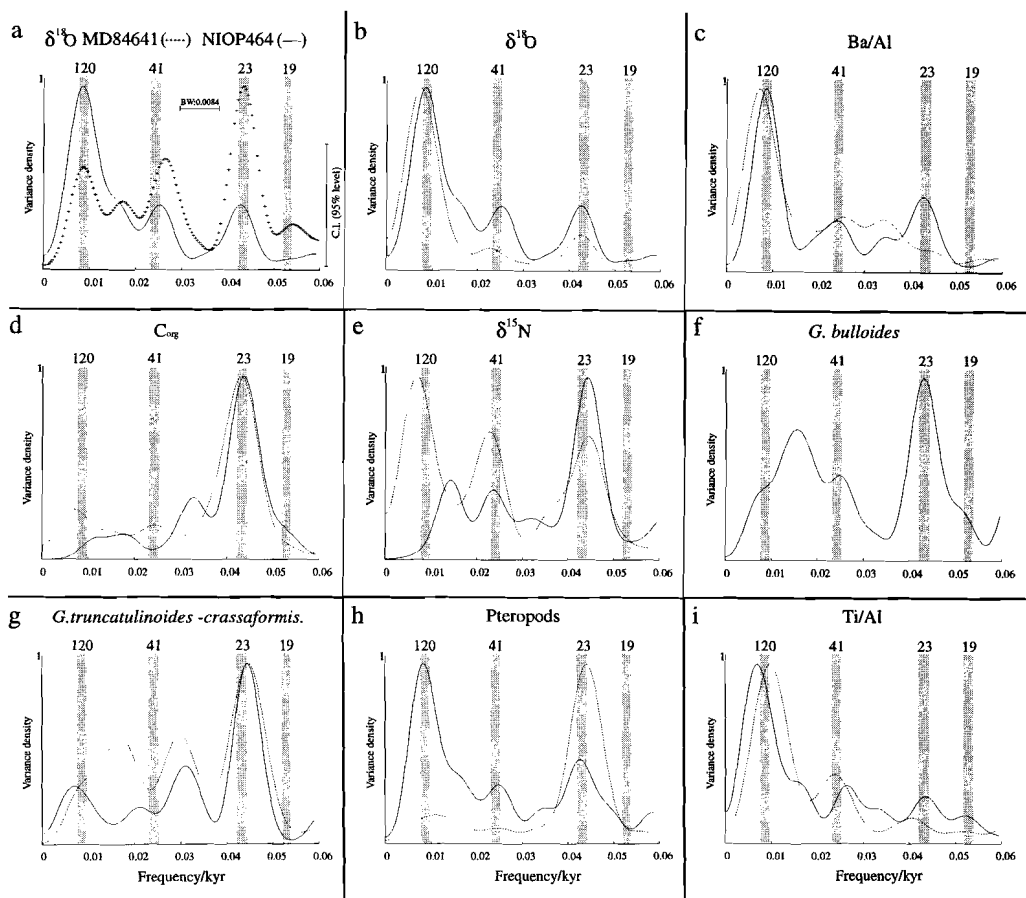


Fig. 7. Power spectra for NIOP463 (dashed lines), NIOP464 (solid lines) and MD84641 (crosses). a and b) $\delta^{18}\text{O}$, c) Ba/Al, d) C_{org} , e) $\delta^{15}\text{N}$, f) *G. bulloides*, g) *G. truncatulinoides* and *G. crassaformis*, h) Pteropod preservation index, and i) Ti/Al.

at the sediment water interface. During dysoxic conditions Mn (IV) is reduced to its soluble Mn (II) state, resulting in the loss of Mn. Surface sediments in the OMZ are depleted in Mn, because the low oxygen conditions prevent the recycling of Mn oxides and the soluble Mn escapes to the water column [Chapter 3]. Recycling of Mn is limited to sediments with an oxygenated surface, which is necessary for porewater Mn concentrations to get

sufficiently high to form Mn carbonate phases [Calvert *et al.*, 1996; Calvert and Petersen, 1996]. Higher Mn/Al ratios correspond to peak abundances of *G. truncatulinoides* and *G. crassaformis* (Fig.6), indicating that an intensified convective overturn resulted in higher oxygen concentrations at the sediment water interface. In contrast, the accumulation of V is favored by anoxic conditions as under oxygen depleted

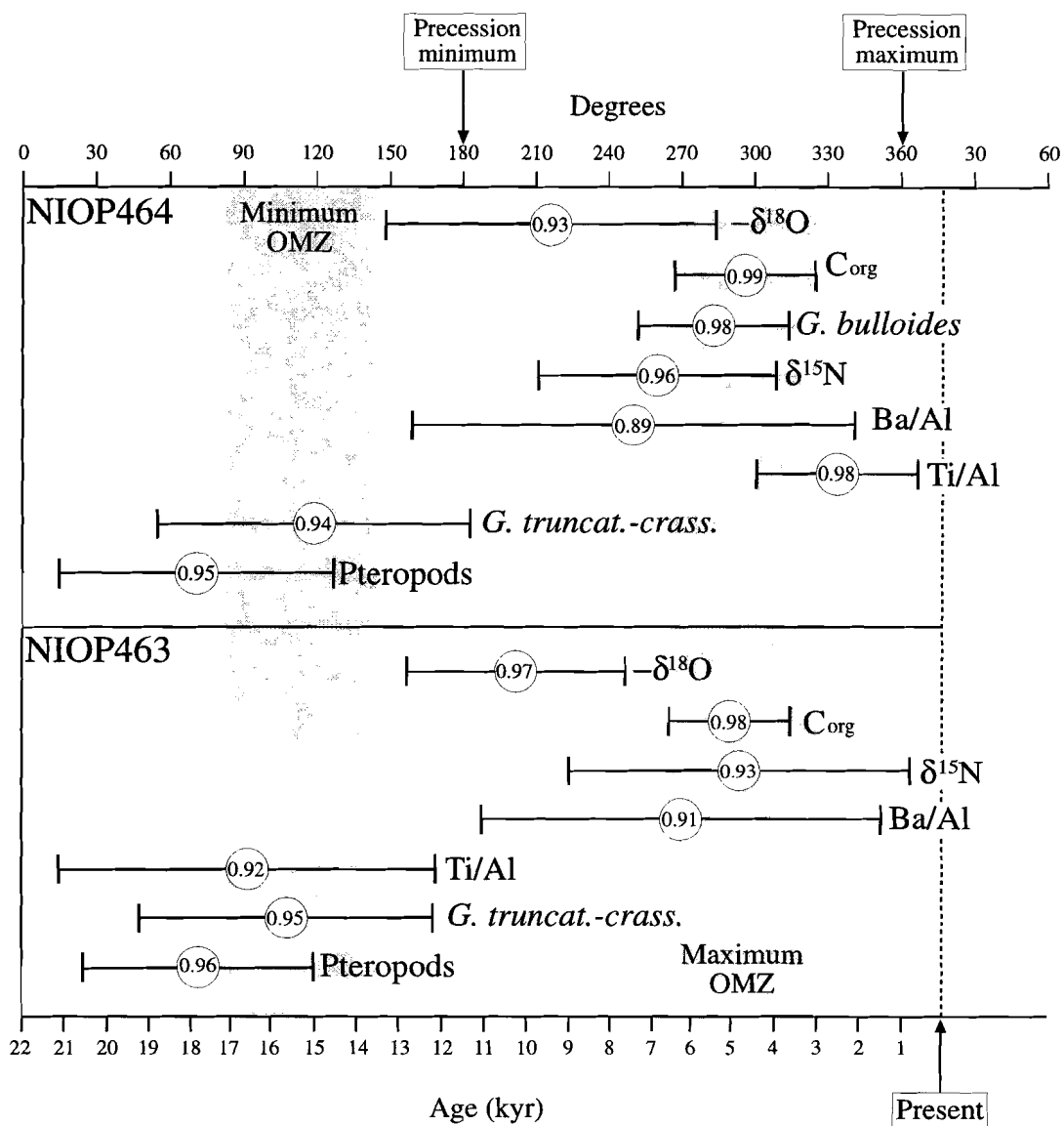


Fig. 8. Phase relationships between proxies for global ice volume ($\delta^{18}\text{O}$), summer monsoon intensity (*G. bulloides*, Ba/Al, C_{org} , Ti/Al), OMZ intensity ($\delta^{15}\text{N}$, *G. truncatulinoides* and *G. crassaformis* and pteropod preservation index) and precession. Encircled numbers are coherencies; error bars mark 95% confidence interval.

conditions dissolved vanadate V(V) is reduced to vanadyl V(IV), which is adsorbed to particles falling through the water column and added to the sediment [Ripley et al., 1990; Breit and Wanty, 1991]. Higher V/Al ratios are associated with laminated sediments, lower Mn/Al ratios, and a stable watercolumn indicated by the absence of both *G. truncatulinoides* and *G. crassaformis* (Fig.6). Comparing the Mn/Al and V/Al record of NIOP464 and 463 shows that during isotopic stage 5 Mn/Al is significantly lower in NIOP463 while V/Al is significantly higher. The synchronous, but unequal enrichments in V and Mn show that although sedimentation at both sites was influenced by changes in the intensity of the OMZ, oxygen depletion was more severe at site NIOP463.

Discussion

Spectral and cross-spectral analyses

The spectra of C_{org} and *G. bulloides* (Figs. 7d and f) clearly show a dominant 23 kyr precession signal, which is caused

by a dominant variability of summer monsoon related surface water productivity on the precession time scale of orbital forcing [Clemens and Prell, 1990; Shimmield et al., 1990, Chapter 2]. The precession component is reduced in the Ba/Al records, as a strong glacial-interglacial (120 kyr) signal dominates the spectra (Fig. 7c). Variability in the intensity of the OMZ reflected by the spectra of $\delta^{15}N$ and *G. truncatulinoides* / *crassaformis* (Figs. 7e and g) shows a dominant precession cycle, as does the spectrum of pteropod preservation in NIOP463 (Fig. 7h). This further confirms the relation between surface water productivity, deep convective overturn, and OMZ intensity. The spectrum of pteropod preservation in NIOP464 also shows significant variability at a lower frequency (120kyr) (Fig. 7h). This is probably the result of the greater water depth of site NIOP464, which prevented the registration of precession-scale ACD variability during interglacials, since the ACD resided at shallower depths during these periods.

The cross spectral analyses (Tab. 2 and Fig.8) shows very consistent results for the

Proxy record	NIOP463		NIOP464	
	Coherency	Phase (degrees)	Coherency	Phase (degrees)
$\delta^{18}O$	0.97	22 ± 45	0.93	36 ± 68
C_{org}	0.98	290 ± 25	0.99	296 ± 29
$\delta^{15}N$	0.93	294 ± 70	0.96	260 ± 49
Ti/Al	0.92	92 ± 77	0.98	334 ± 33
Ba/Al	0.91	270 ± 82	0.89	250 ± 91
<i>G. bulloides</i>			0.98	283 ± 31
<i>G. trunc.-crass.</i>	0.95	108 ± 60	0.94	119 ± 64
Pteropods	0.96	72 ± 47	0.95	71 ± 56

Cross-spectral parameters for precession frequency: for NIOP463 analyses from 13 to 205 ka, for NIOP464 analyses from 6 to 228 ka. Bandwidth, BW=0.008429; interpolated time interval is 2-kyr. Phase angle indicate phase leads with respect to orbital maxima.

Table 2. Coherency and phase lags between precession and the related signal in the records of NIOP463 and NIOP464.

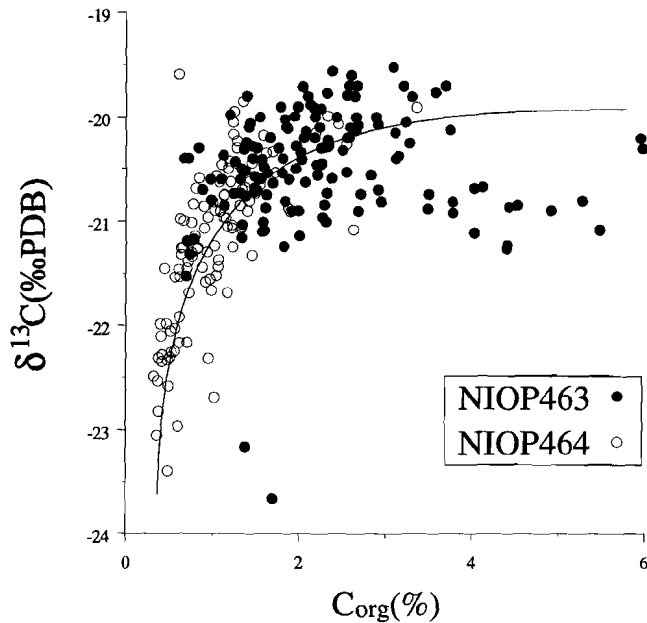


Fig. 9. Scatterplot of $\text{C}_{\text{org}}(\%)$ and $\delta^{13}\text{C}_{\text{org}}(\text{‰PDB})$, line indicates general trend.

different proxies used in this study. Maximum intensity of the OMZ is in phase with surface water productivity, and shows a 180° phase difference with tracers for convective overturn and depth of the ACD. The identical phase relationships in both cores indicates that the proxies at both sites responded in a similar way to various forcing mechanisms.

A proxy often used in studies on monsoon variability is the lithogenic grainsize [e.g. *Clemens and Prell, 1990*], which is reflected in the Ti/Al ratio, as Ti is enriched in the heavy mineral fraction [*Schmitz, 1987; Shimmiel et al., 1990*]. Because the terrigenous fraction is primarily of eolian origin, changes in grainsize are interpreted in terms of changes in dust carrying capacity of the monsoonal winds [*Clemens and Prell, 1990*]. The spectra of Ti/Al show primarily a 120 kyr variability (Fig. 7i), probably

reflecting glacial-interglacial changes in continental aridity and, thus dust availability. There is, however, also a precession signal present, which must be associated with changes in monsoon intensity. The Ti/Al record from both cores, however, shows a distinctly different phase relationship. The maximum Ti/Al in NIOP464 is associated with maximum southwest monsoon proxies, whereas it shows the reversed in NIOP463 (Fig. 8). This can be explained by differences in the position of the two cores with respect to the Arabian peninsula and the Indus river mouth (Fig. 1). The sedimentary record at site NIOP464, which is closer to the Arabian peninsula, show maximum grainsize associated with dust input during an intense summer monsoon. Site NIOP463, on the other hand, is farther away from the Arabian dust source areas but is closer to the mouth of the river Indus

and, therefore, possibly stronger influenced by fluvial input. A maximum of fine grained material in NIOP463 is associated with maximum summer monsoon intensity, as monsoonal rains increased the river Indus outflow diluting the eolian sediment component [M. Prins, personal communication].

Organic carbon preservation

The influence of the OMZ on the preservation of organic matter in the Arabian Sea is an issue of much debate [Pedersen *et al.*, 1992; Paropkari *et al.*, 1992; 1993; Calvert *et al.*, 1995; Chapter 3]. Studies on this issue primarily focussed on comparing the organic matter content in surface sediments deposited within and under the OMZ. Two major problems have complicated the discussion, firstly differences in sediment accumulation rates are not taken into account due to the lack of accurate time control and secondly, the surface sediments used in these studies are still undergoing diagenesis, and may contain more metabolizable organic matter than eventually will survive degradation. Although in Chapter 3 quite a few AMS-¹⁴C ages were incorporated in order to quantify sediment and organic carbon fluxes, it is still the question whether the organic matter represents the end result of different decomposition rates under oxic and anoxic conditions. This holds particularly for the organic matter in areas experiencing high, pulse like, organic carbon fluxes. In the Arabian Sea a large amount of fresh organic material accumulates each season at the sediment water interface after the high productivity (summer monsoon) period. The excellent age control in NIOP463 and NIOP464

allows an accurate calculation of sedimentation rates, and fluxes, whereas the organic carbon is buried deep enough to safely assume that early diagenetic degradation of the organic matter is largely completed.

From the Ti/Al ratio in NIOP463 and from the Zr/Al ratio in NIOP464 [Chapter 2] it is inferred that fine-grained, suspended sediments from the Indus river reached the Murray Ridge during at least several intervals. Organic matter associated with this suspended matter might be added to the marine organic carbon component, thereby, complicating the interpretation of the C_{org} accumulation record. The organic matter carried by the Indus is relatively degraded [Ittekkot and Arain, 1986], with a typical δ¹³C value of -26 ‰ [Fontugne and Duplessy, 1986, and references therein]. Sediments which have a high C_{org} content are characterised by less negative δ¹³C_{org} values, indicating a higher relative contribution of marine organic matter [Jasper and Gagosian, 1989; Müller *et al.*, 1994]. A plot of δ¹³C against the C_{org} content (Fig.9), shows that with an increasing C_{org} content the relative contribution of marine C_{org} (MC_{org}) increases, and that the MC_{org} has a typical value of -20‰. The relative contribution of terrigenous organic matter (TC_{org}) to the sediment can be calculated according to the formula:

$$TC_{org} = C_{org} \times \left[\frac{(\delta^{13}C_M - \delta^{13}C_i)}{(\delta^{13}C_M - \delta^{13}C_T)} \right] \quad (1)$$

where δ¹³C_i = δ¹³C_{org} of a given sample, δ¹³C_T = δ¹³C_{org} of a terrigenous end-member and δ¹³C_M of a marine end-member. The organic fraction of marine

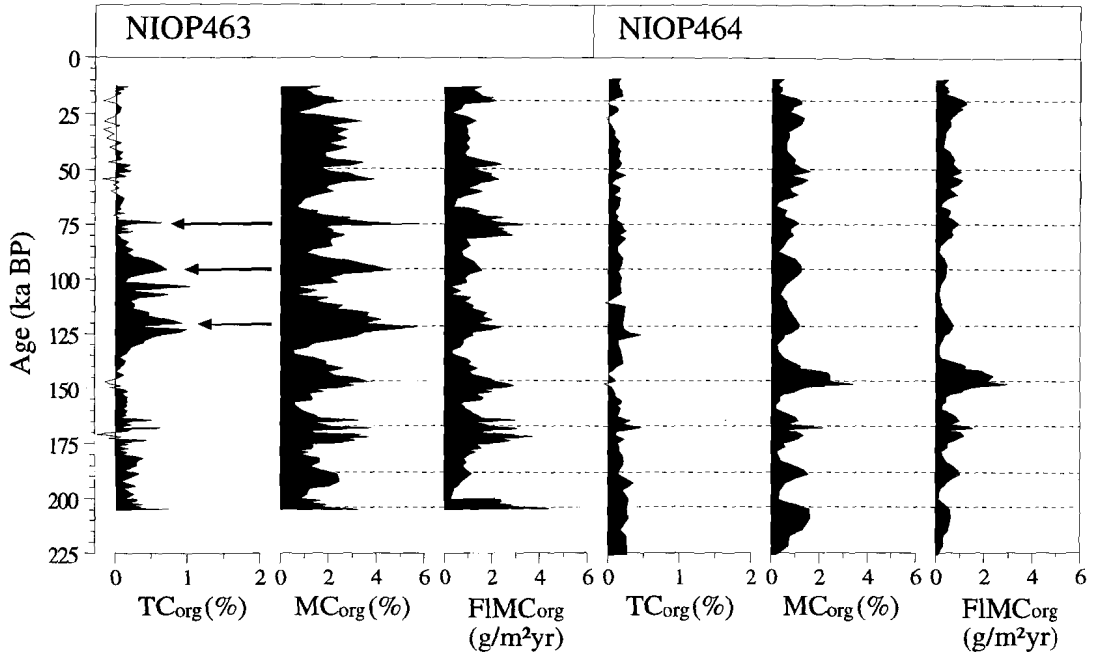


Fig. 10. Terrigenous organic carbon (TC_{org}), marine organic carbon (MC_{org}) and the accumulation rates of the marine organic carbon ($FIMC_{org}$) versus age. Arrows indicate increased TC_{org} during stage 5, associated with increased river Indus outflow. Note that the TC_{org} axes are exaggerated.

origin (MC_{org}) can be calculated according to formula 2:

$$MC_{org} = C_{org} \times \left[\frac{(\delta^{13}C_i - \delta^{13}C_T)}{(\delta^{13}C_M - \delta^{13}C_T)} \right] \quad (2)$$

This way the record of the marine and terrigenous organic carbon component can be plotted (fig.10). It is clear that the amount of terrigenous organic carbon may be negligible in NIOP464. The same holds true for NIOP463, except for stage 5 which is a period of higher terrigenous organic carbon input (Fig.10), although still minor compared to the marine fraction. High TC_{org} values in stage 5 are associated with high MC_{org} values as well. This indicates that an intensification of the summer monsoon resulted (through

increased upwelling) in higher MC_{org} , whereas (at the same time) increased rainfall caused a higher Indus river discharge, resulting in the lower Ti/Al ratios (Fig. 8) and higher TC_{org} values (Fig. 10).

Although the MC_{org} record in both cores shows parallel patterns, there are large differences in the MC_{org} content, and accumulation rates ($MC_{org-acc.}$). NIOP464 shows maximum MC_{org} and $MC_{org-acc.}$ values during stage 6, whereas NIOP463 shows maximum MC_{org} and $MC_{org-acc.}$ during stage 5. A comparison of the $MC_{org-acc.}$ for both requires a correction for the difference in water depth, since the flux of C_{org} to the sea floor is influenced by water depth. The effect of the different depths of deposition (z) can be corrected for by calculating the paleo export productivity

(P_{exp}) using the $MC_{org-acc.}$ curves, according to the formula given by *Sarnthein et al.* [1992]:

$$P_{exp} = 9.354 \times MC_{org-acc.}^{0.493} \times S_{B-C}^{-0.105} \times z^{0.300} \quad (3)$$

in which S_{B-C} is the (organic carbon free) sedimentation rate. Because this function was empirically fitted on C_{org} accumulation rates in sediments deposited in oxic environments, enhanced preservation of organic carbon due to lower bottom water oxygen levels should result in higher P_{exp} estimates for sediments deposited within the OMZ. Fig. 11 shows that at several levels calculated paleoproductivity values for NIOP463 are indeed higher compared to those calculated for NIOP464. The difference being higher during interglacial productivity maxima, and lower during periods with a weakened OMZ (Fig. 11). The glacial productivity maximum at ~145 ka, on the other hand, shows identical P_{exp} estimates for the two cores. This might have been caused by a deepening of the lower depth limit of the OMZ down to at least 1470m (being the depth of site NIOP464). In this case the effect of oxygen on the C_{org} preservation at both sites would be similar. A deepening of the lower depth limit of the OMZ could also explain the rather high P_{exp} calculated from the NIOP464 $MC_{org-acc.}$ at that time, because these high values are not associated with high values of *G. bulloides* and Ba/Al. The absence of laminated sediments at ~145 ka in NIOP464 can be explained by seasonally slightly higher oxygen levels at that depth. A slight rise of oxygen levels during part of the year may obliterate lamination, without substantially affecting the C_{org} content. For example the Galatheid crab *Pleuroncodes* survives

oxygen levels of only 0.25 ml/l and disturbs sedimentary structures down to 1 cm below the surface [Tyson, 1995]. With a sedimentation rate of 10 cm/kyr a short decrease in intensity, or a rise in the lower depth limit of the OMZ, every 100 years would be sufficient to completely destroy lamination. The same mechanism could also explain the absence of laminations in NIOP463 during periods in which other proxies suggest that laminations might have been present.

P_{exp} values calculated from $MC_{org-acc.}$ Values in NIOP464 suggest surface water productivity values of ~50 gC/m²yr during the productivity maxima in interglacial stage 5. This is in good agreement with P_{exp} estimates based on water column denitrification rates in the present day OMZ of the Arabian Sea [*Somasundar and Naqvi*, 1988]. Because P_{exp} is related to the primary productivity (PP) as follows:

$$P_{exp} = \frac{PP^2}{410} \quad (4)$$

[*Berger et al.*, 1989], it can be calculated that PP was ~150 gC/m²yr during these periods, which is lower than productivity estimates for the upwelling areas in the western Arabian Sea, but is in agreement with the position of the sites further away from the main upwelling areas.

Estimates for P_{exp} , during the same in surface water productivity maxima in NIOP463 are ~25 gC/m²yr higher. These P_{exp} estimates are based on an $MC_{org-acc.}$ of ~2 gC/m²yr, whereas it can be calculated (Eq. 3) that $MC_{org-acc.}$ should not have exceeded 0.66 gC/m²yr. This suggests a threefold higher $MC_{org-acc.}$, due to the enhanced preservation at site NIOP463 compared to site 464. From P_{exp} the flux of

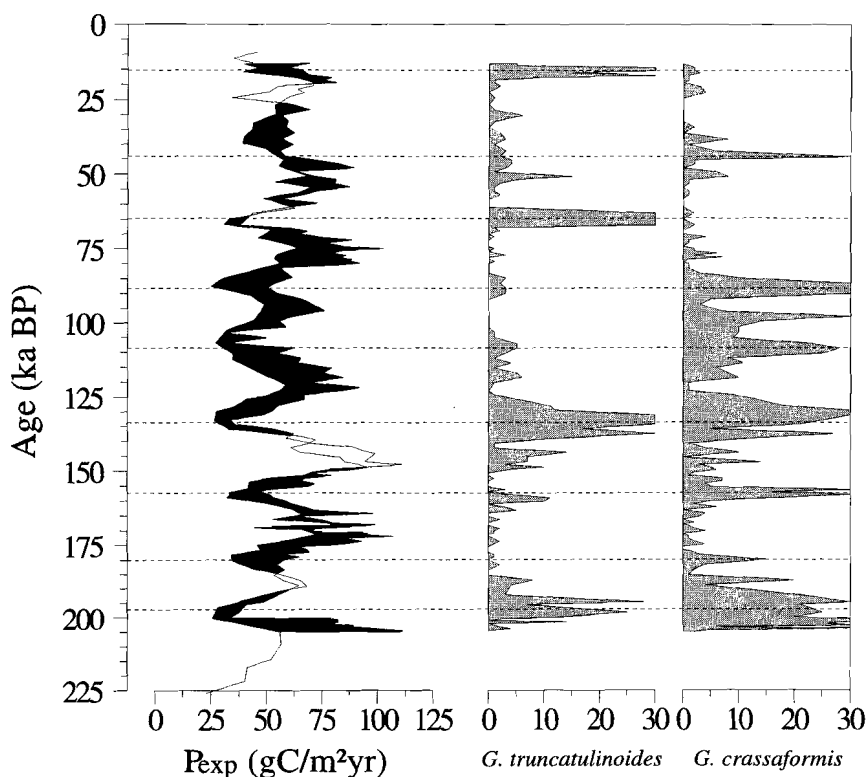


Fig. 11. Paleoproductivity patterns calculated for NIOP463 and 464 and plotted versus age. Black areas indicate intervals in which the calculated paleoproductivity at NIOP463 is higher compared to NIOP464. Peak occurrences of *G. truncatulinoides* and *G. crassaformis* indicate deep convective turnover.

organic matter (FIC_{org}) arriving at the sea floor at depth z can be calculated from:

$$FIC_{org} = 20.563 \times \frac{P_{exp}^{0.665}}{z^{0.554}} \quad (5)$$

[Sarnthein., 1992]. With a P_{exp} of ~50 this results in a FIC_{org} of ~6.3 gC/m²/yr at 920 mbss (=depth of site NIOP463). Subsequently the burial efficiency can be calculated according to:

$$Burial\ efficiency = \frac{MC_{org-acc.}}{FIC_{org}} \times 100\% \quad (6)$$

For sediments deposited at site NIOP463, during periods of an intense OMZ the burial efficiency is 31 % (= 2 / 6.3 × 100%), and at the same time at site NIOP464 the burial efficiency is only 12 % (= 0.6 / 4.9 × 100%).

Berger [1989] combined the FIC_{org} (P_{exp}, z) with the relation between P_{exp} and

the sedimentation rate (S) found by *Müller and Suess* [1979] and arrived at the following relation between burial efficiency and the sedimentation rate.

$$\frac{F_{burial}}{F_{sed}} (\%) = S \times (2.5 - 0.02 \times S) \quad (7)$$

Both cores have an average sedimentation rate of ~ 6 cm/kyr during stage 5, which implies that the burial efficiency should be $\sim 14\%$. This is in good agreement with the burial efficiency calculated for NIOP464, which is not surprising since the P_{exp} used was from this core. If we, however, previously had assumed the P_{exp} estimates from NIOP463 to be correct, it can be calculated (Eqs. 5 and 6) that burial efficiencies would have been, 9% for NIOP464 and 24 % for NIOP463. From equation 7 it is clear that in that case the burial efficiency would still be too high for NIOP463, and too low for NIOP464. In either case the ratio of the burial efficiencies from the oxic and the dysoxic locations remains the same, ~ 2.5 times higher under oxygen depleted conditions.

Critical for the calculation of the burial efficiencies is the assumption that an anoxic water column would not result in a decrease of degradation of organic matter during its transit to the sediment. If this is the case the flux equations used might underestimate FIC_{org} , resulting in too high burial efficiencies. This would, however, affect both sites and the organic carbon preservation factor ($= MC_{org}/P_{exp}$) would remain the same. Moreover the ratio of the burial efficiencies of the two sites would not change.

Higher organic carbon contents are

exclusively associated with higher surface water productivity, and down core variations in organic content can be correlated throughout the northern Arabian Sea, across a large range of water depths [down to 3000 mbss, *Chapter 4*]. The differences observed in the $MC_{org-acc}$ are primarily caused by changes in surface water productivity, the effect, however, of higher productivity is stronger when the sediments are deposited within the OMZ, under oxygen depleted conditions. Because the variations in the intensity of the OMZ are also closely related to changes in sea surface productivity, also the enhanced preservation of organic matter within the OMZ is, ultimately caused by increased sea surface productivity.

Conclusions

Sedimentary organic carbon accumulation in the northern Arabian Sea is primarily controlled by surface water productivity. Differences in surface water productivity and convective turnover caused significant changes in the intensity of the OMZ. This resulted in the complete breakdown of the OMZ during several periods, and during one interval in the last 200 kyr the lower depths limit of the OMZ might have extended down to ~ 1500 m. Enhanced preservation of organic matter under low oxygen conditions at the sediment water interface resulted in higher organic carbon accumulation rates. The burial efficiency of sediments deposited under oxygen depleted conditions is ~ 2.5 times lower compared to oxic conditions.

Acknowledgements

The chief scientists on the D-cruises, during the 1992-1993 Netherlands Indian Ocean Programme, were W.J.M. van der Linden and C.H. van der Weijden. The director and colleagues G.M. Memon, A.R. Tabrez and A.A. Khan of the National Institute of Oceanography, Karachi, are thanked for their cooperation. The collection of the material would not have been possible without the professional help of crew and technicians of the R.V. Tyro. J.W. Zachariasse and C.H. van der weijden are acknowledged for critical reading of the manuscript. Spectral and cross-spectral analyses were performed by L. Lourens. Thanks are also due to M. den Dulk, H.J. Visser, G. Nobbe, A. van Dijk, H.de Waard, G.J. van het Veld and G. Ittman for processing samples and analytical support. The $\delta^{15}\text{N}$ analyses were carried out at the University of British Columbia, Vancouver. This study was partly funded by the Netherlands Organization for Scientific Research (NWO grant no. 718-215).

References

- Altabet, M.A., Francois, R., Murray, D.W., and W.L. Prell, Climate-related variations in denitrification in the Arabian Sea from sediment $^{15}\text{N}/^{14}\text{N}$ ratios, *Nature*, 373, 506-509, 1995.
- Arian, R.J., Carbon and mineral transport of Indus river 1982-1983. *Mitt. Geol.-Paläont. Inst. Univ. Hamburg*, sonderband 58, 487-494, 1985.
- Bansc, K., Seasonality of phytoplankton chlorophyll in the central and northern Arabian Sea. *Deep-Sea Res.*, 34, 713-723, 1987.
- Bard, E., Correction of accelerator mass spectrometry ^{14}C ages measured in planktonic foraminifers: paleoceanographic implications. *Paleoceanography*, 3, 635-645, 1988.
- Bard, E., Hamelin, B., Fairbanks, R.G. and A. Zindler, Calibration of the ^{14}C timescale over the past 30,000 years using mass spectrometric U-Th ages from Barbados corals, *Nature*, 345, 405-410, 1990a.
- Bard, E., Hamelin, B. and R.G. Fairbanks, U-Th ages obtained by mass spectrometry in corals from Barbados: Sea level during the last 130,000 years, *Nature*, 346, 456-458, 1990b.
- Be, A.W.H. and D.S. Tolderlund, Distribution and ecology of living planktonic foraminifera in surface waters of the Atlantic and Indian Oceans. In: B.M. Riedel and W.R. Funnell (Eds.), *Micropaleontology of the Oceans*. Cambridge University Press: 105-149, 1971.
- Berger, W.H. Deep-sea carbonate: pteropod distribution and the aragonite compensation depth. *Deep-Sea Research*, 25, 447-452, 1978.
- Berger, W.H., Smetacek, V.S. and G. Wefer, Ocean productivity and paleoproductivity-an overview. In: Productivity of the Ocean: present and past (eds. W. H Berger, V.S. Smetacek and G. Wefer), Dahlem Workshop Report, 44, Wiley, New York, 1-34, 1989.
- Bishop, J.K.B., The barite-opal-organic carbon association in oceanic particulate matter. *Nature*, 332, 341-343, 1988.
- Breit, G.N. and R.B. Wanty, Vanadium accumulation in carbonaceous rocks: a review of geochemical controls during deposition and diagenesis. *Chem. Geol.*, 9, 83-97, 1991.
- Brock, J.C., C.R. McClain, D.M. Anderson, W.L. Prell and W.W. Hay, Southwest

- monsoon circulation and environments of recent planktonic foraminifera in the northwest Arabian Sea. *Paleoceanogr.*, 7, 799-813, 1992.
- Calvert, S.E., Oceanographic controls on the accumulation of organic matter in marine sediments. In: *Marine petroleum source rocks* (eds. J.P. Riley and R. Chester), *Geological Society Special Publication*, 26, 137-151, 1987.
- Calvert, S.E., Pedersen, T.F., Naidu, P.D. and U. von Stackelberg, On the organic carbon maximum on the continental slope of the eastern Arabian Sea. *J. Mar. Res.*, 53, 269-296, 1995.
- Canfield, D.E. and R. Raiswell, Carbonate precipitation and dissolution. In: *Taphonomy: releasing the data locked in the fossil record* (eds. P.A. Allison & D.E.G. Briggs), Plenum Press, 411-453, 1991.
- Clemens, S.C. and W.L. Prell, Late Pleistocene variability of Arabian Sea summer monsoon winds and continental aridity: eolian records from the lithogenic components of deep-sea sediments. *Paleoceanogr.*, 5, 109-145, 1990.
- Codispoti, L.A., Primary productivity and carbon and nitrogen cycling in the Arabian Sea. In *U.S. JGOFS: Arabian Sea Process Study* (Eds. S.L. Smith, K. Banse, J. K. Cochran, L.A. Codispoti, H.W. Ducklow, M.E. Luther, D.B. Olson, W.T. Peterson, W.L. Prell, N. Surgi, J.C. Swallow & K. Wishner), U.S. JGOFS Planning Report No. 13, 1991.
- Dehairs, F., Chesselet, R. and J. Jedwad, Discrete suspended particles of barite and the barium cycle in the open ocean. *Earth Planet. Sc. Lett.*, 49, 528-550, 1980.
- Deuser, W.G., Ross, E.H. and Z.J. Mlodzinska, Evidence for and rate of denitrification in the Arabian Sea. *Deep-Sea Res.*, 25, 431-445, 1978.
- Dymond, J. Suess, E. and M. Lyle, Barium in deep-sea sediment: a geochemical proxy for paleoproductivity. *Paleoceanography*, 7, 163-181, 1992.
- Edwards, R.L., Chen, J.H., Ku, T.L. and G.J. Wasserburg, Precise timing of the last interglacial period from mass spectrometric determination of Thorium-230 in corals, *Science*, 236, 1547-1553, 1987.
- Fontugne, M.R. and J.C. Duplessy, Variations of the monsoon regime during the upper Quaternary: evidence from carbon isotopic record of organic matter in north Indian Ocean sediment cores. *Palaeogeogr. Palaeoclim. Palaeoecol.*, 56, 69-88, 1986.
- Fontugne, M.R. and S.E. Calvert, Late Pleistocene variability of the carbon isotope composition of organic matter in the eastern Mediterranean: Monitor of changes in carbon sources and atmospheric CO₂ concentrations, *Paleoceanography*, 7, 1-20, 1992.
- Gallup, C.D., Edwards, R.L. and R.G. Johnson, The timing of high sea levels over the past 200,000 years, *Science*, 263, 796-800, 1994.
- Hemleben, Ch., M. Spindler, I. Breiteringer and W.G. Deuser., Field and laboratory studies on the ontogeny and ecology of some globorotaliid species from the Sargasso Sea off Bermuda. *J. Foram. Res.*, 15, 254-272, 1985.
- Hilgen, F.J., Closing the gap in the Plio-Pleistocene boundary stratotype sequence of Crotona, *Newsletters on Stratigraphy*, 22, 43-51, 1990.
- Hilgen, F.J., Lourens, L.J., Berger, A. and M.F. Loutre, Evaluation of the astronomically

- calibrated time scale for the late Pliocene and earliest Pleistocene, *Paleoceanogr.*, 8, 549-565, 1993.
- Ittekkot, V. and R. Arian, Nature of particulate organic matter in the river Indus, Pakistan. *Geochim. Cosmochim. Acta*, 50, 1643-1653, 1986.
- Jasper, J.P. and R.B. Gagosian, Glacial-interglacial climatically forced $\delta^{13}\text{C}$ variations in sedimentary organic matter, *Nature*, 342, 60-62, 1989.
- Jorissen, F.J., Asioli, A., Borsetti, A.M., Capotondi, L., de Visser, J.P., Hilgen, F.J., Rohling, E.J., Van der Borg, K., Vergnaud-Grazzini, C. and J.W. Zachariasse, Late Quaternary central Mediterranean biochronology, *Mar. Micropaleontol.*, 21, 169-189, 1993.
- Kabanova, Y.G., Primary production in the northern part of the Indian Ocean. *Oceanology*, 8, 214-225, 1968.
- Lohmann, G.P. and P.N. Schweitzer, Globorotalia truncatulinoides' growth and chemistry as probes of the past thermocline: 1 shell size. *Paleoceanogr.*, 5, 55-75, 1990.
- Lourens, L.J., Antonarakou, A., Hilgen, F.J., Van Hoof, A.A.M., Vergnaud-Grazzini, C. and W.J. Zachariasse, Evaluation of the Plio-Pleistocene astronomical timescale, *Paleoceanogr.*, 11, 391-413, 1996.
- Madhupratap, M., Kumar, S.P., Bhattathiri, P.M.A., Kumar, M.D., Raghukumar, S., Nair, K.K.C. and N. Ramaiah, Mechanism of the biological response to winter cooling in the northeastern Arabian Sea. *Nature*, 384, 549-552, 1996.
- Müller, P.J., R. Schneider and G. Ruhland, Late Quaternary $p\text{CO}_2$ variations in the Angola current: Evidence from organic carbon $\delta^{13}\text{C}$ and alkenone temperatures. In: *Carbon Cycling in the Glacial Ocean: Constraints on the Ocean's Role in Global Change*. (ed. R.Zahn et al.); NATO ASI Series, 117, 343-366, 1994.
- Naqvi, S.W.A. Some aspects of the oxygen-deficient conditions and denitrification in the Arabian Sea. *J. Mar. Res.*, 45, 1049-1072, 1987.
- Olson, D.B., Hitchcock, G.L., Fine, R.A. and B.A. Warren, Maintenance of the low-oxygen layer in the central Arabian Sea. *Deep-Sea Res. II*, 40, 673-685, 1993.
- Paropkari, A.L., Babu, C.P. and A. Mascarenhas, A critical evaluation of depositional parameters controlling the variability of organic carbon in Arabian Sea sediments. *Mar. Geol.*, 107, 213-226, 1992.
- Paropkari, A.L., Babu, C.P. and A. Mascarenhas, New evidence for enhanced preservation of organic carbon in contact with oxygen minimum zone on the western continental slope of India. *Mar. Geol.*, 111, 7-13, 1993.
- Pedersen, T.F., Shimmiel, G.B. and N.B. Price, Lack of enhanced preservation of organic matter in sediments under the oxygen minimum on the Oman Margin. *Geochim. Cosmochim. Acta*, 56, 545-551, 1992.
- Prell, W.L., Hutson, W.H., Williams, D.F., Be, A.W.H., Geitzenauer, K., and B. Molfino, Surface circulation of the Indian ocean during the Last Glacial Maximum, approximately 18,000 yr B.P., *Quat. Res.*, 14, 309-336, 1980.
- Qasim, S.Z., Oceanography of the northern Arabian Sea. *Deep-Sea Res.*, 29, 1041-1068, 1982.
- Rasmussen, T.L., Benthonic and planktonic foraminifera in relation to the Early Holocene

- stagnation in the Ionian Basin, Central Mediterranean. *Boreas*, 20, 357-376, 1991.
- Ripley, E.M., Shaffer, N.R. and M.S. Gilstrap, Distribution and geochemical characteristics of metal enrichment in the New Albany Shale (Devonian-Mississippian), Indiana. *Econ.Geol.*, 85, 1790-1807, 1990.
- Sarnthein, M. Pflaumann, U., Ross, R., Tiedemann, R. and K. Winn, Transfer functions to reconstruct ocean palaeoproductivity: a comparison. In: *Upwelling Systems: Evolution since the early Miocene* (Eds. C.P. Summerhays, W.L. Prell and K.C. Emeis). *Geol. Soc. Spec. Publ.* 64, 411-427, 1992.
- Schäfer, P. and V. Ittekkot, Seasonal variability of $\delta^{15}\text{N}$ in settling particles in the Arabian Sea and its palaeo-geochemical significance. *Naturwissenschaften*, 80, 511-513, 1993.
- Schmitz, B., The $\text{TiO}_2/\text{Al}_2\text{O}_3$ ratio in Cenozoic Bengal abyssal fan sediments and its use as a paleostream energy indicator. *Mar. Geol.*, 76, 195-206, 1987.
- Shimmield, G.B., Mowbray, S.R. and G.P. Weedon, A 350 ka history of the Indian Southwest Monsoon- Evidence from deep-sea cores, Northwest Arabian Sea. *Transactions of the Royal Society of Edinburgh: Earth Sciences*, 81, 289-299, 1990.
- Slater, R.D. and P. Kroonick, Controls on dissolved oxygen distribution and organic carbon distribution in the Arabian Sea. In: *Marine geology and oceanography of Arabian Sea and coastal Pakistan* (Eds. B.U. Haq and J.D. Milliman), 305-313, New York: Van Nostrand Reinhold, 1984.
- Smith, R. L. and J.S. Bottero, On upwelling in the Arabian Sea. In: *A voyage of discovery, George Deacon 70th Anniversary volume*. (Ed. M. Angel), Pergamon Press, 291-304, 1977.
- Somasundar, K. and S.W.A. Naqvi, On the renewal of the denitrifying layer in the Arabian Sea. *Oceanol. Acta*, 11, 167-172, 1988.
- Swallow, J.C., Some aspects of the physical oceanography of the Indian Ocean. *Deep-Sea Res.*, 31, 639-650, 1984.
- Thompson, P.R. Be, A.W.H., Duplessy, J.C. and N.J. Shackleton, Disappearance of pink-pigmented *Globigerinoides ruber* at 120,000 yr BP in the Indian and Pacific Oceans., *Nature*, 280, 554-558, 1979.
- Thomson, J., Higgs, N.C., Wilson, T.R.S., Croudace, I.W., De Lange, G.J. and P.J.M. Van Santvoort, Redistribution and geochemical behaviour of redox-sensitive elements around S1, the most recent eastern Mediterranean sapropel. *Geochim. Cosmochim. Acta*, 59, 3487-3501, 1995.
- Troelstra, S.R., Ganssen, G.M., Van der Borg, K. And A.M.F. De Jong, A late Quaternary stratigraphic framework for eastern Mediterranean sapropel S1 based on AMS ^{14}C dates and stable oxygen isotopes, *Radiocarbon*, 33, 15-21, 1991.
- Tyson, R.V., Sedimentary organic matter, organic facies and palynofacies. Chapman and Hall, London, 1995, pp.
- Van Bennekom, A.J. and M.A. Hiehle, CTD operations and calibrations during legs D1, D2 and D3 of the Netherlands Indian Ocean Programme. In: *Geological study of the Arabian Sea*. (Eds. W.J.M. van der Linden & C.H. van der Weijden) Netherlands Geosciences Foundation, The Hague, 37-66, 1994.
- Van Cappellen, P. and E.D. Ingall, Benthic phosphorus regeneration, net primary production, and ocean anoxia: A model of the coupled marine biogeochemical cycles of

- carbon and phosphorus., *Paleoceanogr.*, 9: 677-692, 1994.
- Van Os, B.J.H., Middelburg, J.J. and G.J. De Lange, Possible diagenetic mobilization of barium in sapropelic sediments from the eastern Mediterranean. *Mar. Geol.*, 100, 125-136, 1991.
- Von Breymann, M.T., Emeis, K.C. and E. Suess, Water depth and diagenetic constraints on the use of barium as a palaeoproductivity indicator. In: *Upwelling Systems: Evolution since the early Miocene* (Eds. C.P. Summerhays, W.L. Prell and K.C. Emeis). *Geol. Soc. Spec. Publ.* 64, 273-284, 1992.
- Von Stackelberg, U., Faziesverteilung in Sedimenten des Indisch-Pakistanischen Kontinentalrandes (Arabisches Meer). *Meteor Forschungs-Ergebnisse*, C.9, 1-73, 1972.
- Wyrтки, K., *Oceanographic atlas of the international Indian Ocean expedition*, 531pp, 1971.
- Wyrтки, K., Physical Oceanography of the Indian Ocean. in: *The Biology of the Indian Ocean*.(ed. B. Zeitschel), 18-36, Springer, Berlin, 1973.
- You, Y. and M. Tomczak, Thermocline circulation and ventilation in the Indian Ocean derived from water mass analysis. *Deep-Sea Res. I*, 40, 13-56, 1993.

NIOP463

Depth (cm)	Age (ka BP)	DBD (g/cm ³)	δ ¹⁸ O (‰pdb)	C _{org} (%)	δ ¹³ C _{org} (‰pdb)	δ ¹⁵ N (‰)	Al (%)	Ba (ppm)	Mn (ppm)	V (ppm)	Ti (ppm)	G. truncat. (No.)	G. crass. (No.)	Pter.
1432	205.0	0.76	-0.2	4.03	-21.11		3.97	344	260	99	2414	0	2	0
1422	204.4	0.97		2.92	-20.70	7.23	4.12	259	283	89	2538	0	5	0
1412	203.9	1.05	-0.3	2.27	-20.96		4.22	222	315	86	2640	4	30	0
1402	203.3	0.94		1.88	-20.60		3.99	202	281	75	2484	2	6	0
1392	202.7	0.83	-0.7	2.31	-21.00		3.60	173	253	78	2185	1	30	0
1382	202.2	0.89		1.55	-20.60	5.53	3.46	254	235	72	2109	0	26	0
1372	201.6	1.03	-0.4	1.58	-21.01		4.10	211	298	79	2521	14	30	0
1362	201.0	0.80		1.99	-20.90	6.22	3.87	250	277	80	2413	0	30	0
1352	200.5	1.02	-0.3	1.60	-21.09		4.37	191	322	86	2705	3	30	0
1344	200.0	0.96		0.98	-20.80	3.98	4.41	182	337	82	2746	13	20	1
1338	198.2	0.94	0.1	1.33	-21.16		4.22	169	333	76	2617	25	25	2
1329	195.5	0.99		1.33	-20.50	4.70	4.20	168	312	75	2599	7	21	1
1326	194.6	0.83	-0.2	2.32	-20.73		3.05	138	224	74	1924	28	30	1
1318	192.3	0.89	0.1	2.56	-20.20	6.24	4.47	214	324	93	2802	3	21	1
1307	189.0	0.86		2.71	-20.74		4.75	246	335	98	2949	4	4	0
1297	187.2	0.96	0.2	1.81	-20.40	5.53	4.52	219	343	82	2865	8	20	2
1287	185.4	1.09	0.6	1.57	-21.10		4.48	212	343	79	2835	0	1	2
1277	183.6	1.01		1.92	-20.90		4.34	207	325	82	2733	0	2	1
1267	181.8	0.90	0.1	2.00	-21.14		4.13	211	317	81	2663	2	4	1
1257	180.0	1.09		0.97	-20.60	4.63	4.53	226	363	79	2922	0	15	3
1246	179.0	1.02	0.2	1.31	-20.73		3.94	202	325	76	2546	1	8	2
1238	178.3	1.16		0.83	-20.30	4.26	4.43	221	372	78	2857	1	3	3
1228	177.4	1.05	-0.1	1.48	-20.72		3.92	209	314	72	2526	0	2	2
1217	176.4	0.94		1.41	-20.10	4.90	3.94	216	315	74	2558	0	0	1
1207	175.6	0.97	0.2	1.38	-20.76		4.35	202	333	78	2760	0	0	1
1197	174.7	0.85		2.57	-20.20	7.02	3.77	168	273	87	2343	1	4	1
1187	173.8	0.80	-0.2	3.51	-20.74		4.10	247	287	97	2546	2	2	0
1177	172.9	0.75	0.0	2.64	-19.80		4.53	250	326	91	2837	1	1	0
1167	172.0	0.89	0.3	3.75	-20.12		5.11	283	359	115	3249	0	1	2
1160	171.4	0.87		2.67	-19.70	6.22	4.79	272	351	102	3021	0	0	0
1156	171.0	0.79	0.2	3.09	-19.52		3.80	160	267	97	2438	1	1	3
1147	170.2	0.98		1.39	-19.80	4.29	4.55	211	359	80	2887	1	4	1
1138	169.4	1.11	0.4	1.51	-20.71		4.62	221	369	85	2930	2	2	1
1127	168.4	0.90	0.2	3.12	-20.40	8.68	4.35	224	340	107	2828	0	1	0
1122	168.0	0.85		4.43	-20.86	8.27	5.40	330	370	157	3455	0	0	0
1117	167.5	0.94	0.5	2.23	-20.10	5.45	4.96	240	364	105	3108	0	2	0
1107	166.4	0.99	0.6	2.07	-20.63		4.46	218	353	92	2855	2	0	1
1097	165.4	0.98	0.6	1.46	-20.40	4.87	4.60	199	369	86	2875	0	3	0
1087	164.3	0.96		3.78	-20.81	8.70	5.03	312	376	132	3231	0	4	0
1077	163.3	1.03	0.7	1.66	-20.20	4.05	4.75	229	380	89	3006	5	0	2
1067	162.2	1.00	0.7	1.63	-20.54		4.56	222	374	87	2944	3	6	2
1057	161.2	1.06		1.32	-20.60	5.08	4.51	218	371	81	2936	0	2	2
1047	160.1	1.15	0.7	1.13	-20.85		4.36	208	366	77	2802	10	5	2
1037	159.1	1.18		0.88	-20.70	5.09	4.44	215	388	83	2887	11	17	3
1027	158.0	1.21	0.9	0.78	-21.17		4.31	207	383	79	2824	4	30	3
1017	157.1	1.12		0.71	-21.20	4.41	4.52	210	387	81	2911	0	16	3
1009	156.4	1.25	0.7	0.73	-21.32		4.37	208	382	80	2841	3	30	3
997	155.3	1.01		1.48	-20.57	4.78	4.14	198	339	86	2251	0	5	3
986	154.2	1.14	0.6	1.48	-20.68		4.20	204	352	76	2731	0	4	0

Depth (cm)	Age (ka BP)	DBD (g/cm ³)	$\delta^{18}\text{O}$ (‰pdb)	C_{org} (%)	$\delta^{13}C_{org}$ (‰pdb)	$\delta^{15}N$ (‰)	Al (%)	Ba (ppm)	Mn (ppm)	V (ppm)	Ti (ppm)	G. truncat. (No.)	G. crass. (No.)	Pter.
977	153.4	1.01		1.37	-20.52	4.64	3.94	193	331	73	2559	0	7	2
967	152.5	1.11	0.7	1.26	-20.43		3.99	195	331	71	2585	1	7	1
957	151.6	1.02		1.96	-20.50	4.97	4.04	214	320	82	2581	0	1	0
947	150.7	0.98	0.8	1.57	-20.41	4.05	4.14	203	329	75	2632	0	2	0
937	149.8	0.95	-0.1	2.32	-19.77	4.74	3.72	170	294	94	2398	3	6	1
927	148.8	0.87	0.3	3.11	-20.15	6.22	4.23	208	306	121	2687	10	5	1
917	147.9	0.93		2.55	-19.79	5.59	4.14	217	305	100	2574	3	3	1
907	147.0	0.88		3.58	-19.76	6.56	0.00					7	14	0
897	145.4	0.97		3.24	-20.05		4.71	272	326	140	2955	7	0	0
887	143.8	0.86	-0.2	2.34	-20.28	6.03	3.93	206	308	99	2502	14	10	0
878	142.4	0.85	0.2	1.95	-19.99	6.27	4.02	210	304	110	2528	1	4	0
868	140.8	0.84	0.5	2.65	-20.13		4.19	214	310	105	2618	1	1	0
858	139.2	0.81	-0.1	2.02	-20.34	5.84	3.94	203	295	95	2450	13	13	2
848	137.6	0.92	-0.2	2.03	-20.41		3.71	174	289	87	2364	30	27	3
838	136.0	0.96	0.5	1.38	-20.25	5.93	3.85	168	313	85	2453	17	5	2
828	134.4	1.00	0.1	0.70	-21.19		3.47	175	288	67	2266	30	21	3
818	132.8	0.96	-0.5	0.69	-21.53	4.84	3.74	213	298	73	2404	30	26	3
808	131.2	0.94	-0.9	1.34	-21.03		3.62	301	265	75	2264	30	30	1
798	129.6	0.86	-1.0	1.82	-21.24	6.04	3.84	374	262	78	2314	12	30	0
788	128.0	0.76	-1.0	2.68	-20.90		3.89	315	252	76	2383	11	18	0
778	125.8	0.80	-0.5	3.78	-20.92	6.72	4.54	378	289	111	2737	5	13	0
771	124.3	0.74	-0.3	4.41	-21.23		4.11	311	269	113	2150	1	9	0
765	123.0	0.73		5.48	-21.08	8.14	5.12	408	312	158	3096	0	1	0
758	121.8	0.69		5.98	-20.30		5.19	432	311	155	3098			
748	120.2	0.64	-0.3	4.40	-21.26	7.79	4.40	355	289	130	2646	1	1	0
738	118.5	0.79	-0.4	4.91	-20.89		4.81	364	320	133	2875	6	10	0
728	116.9	0.74		4.03	-20.68	7.53	4.81	364	312	123	2883	5	8	0
718	115.2	0.79	-0.4	4.13	-20.67		4.35	313	286	96	2646	1	6	1
708	113.6	0.81		2.55	-20.53	6.54	4.08	273	274	89	2495	4	11	0
698	111.9	0.76	-0.4	2.83	-20.56		4.27	246	294	90	2589	1	8	1
688	110.3	0.95		1.62	-20.75	5.12	4.52	217	311	87	2724	3	25	2
678	108.6	0.91	-0.5	2.29	-20.84		4.13	241	285	92	2535	5	28	1
668	107.0	0.83		1.37	-23.16		3.39	201	238	74	2095	5	23	1
658	105.2	0.81	-0.7	1.69	-20.64		3.94	207	286	86	2480	1	9	1
648	103.3	0.73	-0.7	1.69	-23.66	6.43	3.64	210	260	82	2311	1	10	0
638	101.5	0.72	-0.7	2.50	-20.32		3.13	203	216	72	1983	0	10	0
627	99.5	0.76	-0.6	2.20	-20.46	6.41	3.14	194	215	65	1992	0	14	0
618	97.8	0.74	-0.4	2.95	-20.81		3.17	216	229	66	2087	0	30	0
608	96.0	0.68		5.28	-20.80	8.97	4.44	395	292	124	2768	0	7	1
598	94.0	0.76	-0.4	4.55			4.48	325	298	109	2800	0	3	1
588	92.0	0.79	-0.2	3.49	-20.88	7.97	4.36	299	299	105	2767	0	5	1
578	90.0	0.99	0.1	1.84	-20.81		4.33	213	310	84	2695	3	30	2
568	88.0	1.03	0.0	1.24	-20.74		4.23	199	317	83	2678	3	30	2
559	86.6	0.94	-0.2	1.61	-20.87		4.19	199	316	81	2672	2	30	2
548	84.8	0.79	-0.6	2.25	-20.30	6.84	3.93	194	287	79	2502	3	10	0
538	83.2	0.76	-0.6	2.23	-20.47		3.34	184	241	67	2098	0	3	1
528	81.6	0.66		2.17	-20.20	7.15	3.05	170	203	65	1910	0	1	0
518	80.0	0.77	-0.4	2.68	-20.08		3.31	171	223	67	2076	0	1	0
508	79.3	0.76		2.43	-20.00	5.51	3.26	174	237	65	2099	1	0	0

Depth (cm)	Age (ka BP)	DBD (g/cm ³)	δ ¹⁸ O (‰pdb)	C _{org} (%)	δ ¹³ C _{org} (‰pdb)	δ ¹⁵ N (‰)	Al (%)	Ba (ppm)	Mn (ppm)	V (ppm)	Ti (ppm)	G. truncat. (No.)	G. crass. (No.)	Pter.
498	78.6	0.87	-0.2	2.37	-20.59		3.83	172	290	74	2441	0	1	0
488	77.9	0.76		2.18	-20.00	5.65	4.00	180	296	76	2542	0	7	0
478	77.1	0.84	-0.2	2.26	-20.45		4.34	190	319	77	2754	3	2	2
468	76.4	0.84	-0.4	1.84	-20.10	5.20	4.37	191	316	78	2739	1	6	0
458	75.7	0.77	-0.4	2.29	-20.29		4.63	203	329	82	2896	0	2	1
448	75.0	0.58	0.0	5.95	-20.20	8.36	5.64	296	340	145	3597	1	2	1
441	74.3	0.58	0.0	4.53	-20.84		4.72	293	327	103	2974	0	0	1
428	73.0	0.69	0.4	2.66	-20.00	6.14	4.50	225	318	82	2891	0	1	0
418	72.0	0.84	0.3	2.91	-20.07		4.89	231	339	92	3090	0	1	2
408	71.0	0.91	0.3	1.78	-19.90	4.72	4.43	212	328	79	2813	1	4	1
398	70.0	0.89	0.6	1.59	-20.48		4.39	208	341	75	2789	0	0	2
388	69.0	0.94		1.54	-20.00	4.61	4.12	203	329	74	2677	2	0	3
378	68.0	1.07	0.4	1.12	-20.37		4.15	203	340	71	2638	1	1	3
368	67.0	1.12	0.6	0.72	-20.40	4.44	4.54	219	374	76	2907	30	2	3
358	65.0	0.99	0.4	0.76			4.44	215	383	76	2855	30	0	3
348	63.0	1.03	0.5	1.09	-20.60	3.64	4.35	213	362	76	2839	30	2	2
338	61.0	0.71	-0.1	3.03			3.67	237	267	77	2324	0	0	0
328	59.7	0.93	-0.1	2.09	-19.80	5.04	4.09	243	305	71	2677	0	0	0
318	58.4	0.65	0.3	1.87	-20.11		4.07	223	311	71	2632	0	0	0
307	57.0	0.83	0.2	1.98	-19.90	4.78	4.00	206	305	73	2565	2	1	1
297	55.7	0.79		2.59	-20.10		3.88	227	292	70	2542	1	1	1
287	54.4	0.75	0.2	3.70	-19.70	6.86	4.68	299	321	94	3001	1	0	0
277	53.1	0.79		3.28	-20.25		4.80	262	333	88	3047	2	1	1
267	51.8	0.87	0.3	2.89	-20.00	5.85	4.58	247	336	84	2932	5	1	2
259	50.7	0.99		2.21	-20.56		4.94	242	363	82	3161	15	8	0
247	49.2	0.89	0.1	1.76	-20.30	3.90	4.80	228	346	83	3015	1	6	0
237	47.9	1.03		3.15	-20.37		4.36	222	313	84	2767	3	0	0
227	46.6	0.77	-0.1	3.31	-19.80	5.80	4.71	262	332	100	2948	4	2	0
217	45.3	0.84	-0.2	2.32	-20.22		4.73	244	345	87	2971	4	2	1
207	44.0	0.97	0.4	1.86	-20.10	4.83	4.94	237	374	88	3141	2	30	2
198	42.2	0.87		1.97	-20.28		4.42	223	337	80	2793	3	6	1
187	40.1	0.73	0.2	2.64	-19.80	7.00	4.37	238	325	81	2789	1	1	1
177	38.1	0.85		2.05	-20.20		4.73	223	353	84	2975	3	8	1
167	36.2	0.75	0.2	2.58	-19.70	6.30	3.96	197	300	80	2513	2	0	0
157	34.2	0.79		2.24	-19.92		4.64	239	334	80	2914	0	2	0
147	32.2	0.67	0.3	2.60	-19.60	6.28	4.55	210	333	87	2863	1	0	0
137	30.3	0.83	-0.1	2.07	-20.14		4.58	221	343	80	2894	6	0	1
127	28.3	0.75	0.6	3.21	-19.70	6.39	4.95	244	348	92	3073	1	0	1
117	26.4	0.84		2.17	-19.91		4.84	241	356	89	3001	0	0	0
107	24.4	0.97	0.7	0.67	-20.40	3.95	4.57	217	367	76	2908	1	0	2
97	22.4	0.98		1.45	-20.28		4.77	227	385	79	3074	0	4	3
87	20.5	0.87	0.7	1.83	-20.02	4.49	4.62	219	359	76	2941	2	3	1
76	19.3	0.71		2.37	-19.56		4.54	226	342	90	2838	1	0	0
67	18.5	0.72	0.6	2.04	-19.71	5.03	4.52	210	351	85	2884	1	1	1
57	17.7	0.79	0.7	2.12	-19.88		4.43	221	343	81	2796	8	1	1
47	16.8	0.92	0.7	1.43	-20.06	4.40	4.29	210	354	75	2721	30	1	2
38	16.1	0.96	0.4	1.36	-20.31		4.41	217	373	77	2822	15	3	3
28	15.2	0.98	0.8	1.20	-19.98		4.19	202	373	72	2718	30	2	3
17	14.3	0.98	0.5	1.10	-20.60		4.01	199	345	69	2583	30	2	3
8	13.5	0.81	-0.1	1.51	-20.30	6.43	3.67	204	292	64	2324	5	1	3
2	13.0	0.80	-0.6	1.80	-20.54	6.28	3.24	233	256	58	2084	5	0	2

NIOp464

Depth (cm)	Age (ka BP)	DBD (g/cm ³)	$\delta^{18}\text{O}$ (‰pdb)	C_{org} (%)	$\delta^{13}\text{C}_{org}$ (‰pdb)	$\delta^{15}\text{N}$ (‰)	Al (%)	Ba (ppm)	Mn (ppm)	V (ppm)	Ti (ppm)	G. truncat. (No.)	G. crass. (No.)	Pter.	G. bulloides
1494	226.0	1.28	0.5	0.48	-23.40	4.53						30	2	3	5.5
1487	224.1	1.29	0.3				4.30	239	394	74	2796	30	1		
1479	221.8	1.18	0.1	0.98	-21.67		4.08	249	348	67	2630	6	2	2	8.7
1471	219.5	1.12	-0.2	1.24		6.3	4.07	291	337	71	2681	1	5		
1462	217.1	1.14	-0.1	1.03	-21.52		4.34	333	342	78	2811	1	1	0	17.7
1455	215.0	1.12	-0.2	1.12		6.16	4.16	300	327	80	2723	0	7	0.5	19.5
1453	214.6	1.07	-0.1	1.49	-20.73		4.16	343	321	67	2718	0	4	0	21.7
1441	211.2	1.00	-0.2	1.75		7.13	3.77	318	298	63	2509	0	2	0	18.8
1434	209.2	1.03	-0.2	1.90	-20.91		3.82	373	298	64	2532	1	3	0	23.0
1425	206.9	0.92	-0.1	1.96		7.27	3.53	253	281	60	2392	0	2	0	25.6
1418	204.9	1.02	0.0	1.87	-20.87		4.02	280	307	70	2634	0	0	0	24.3
1408	202.2	1.10	-0.5	0.65		5.85	4.64	458	356	90	2829	0	29	0	18.2
1401	200.2	1.11	-0.6	0.59	-22.96		5.00	364	362	95	3095	11	30	0	9.5
1394	198.1	1.20		0.56								12	30		
1388	196.5	1.14	-0.3	0.56	-22.25	4.84	5.00	248	368	89	3145	30	22	0	9.1
1381	194.7	1.04										30	23		
1375	193.0	1.12	-0.7	0.94	-22.32	8.25	4.90	378	352	89	3124	4	10	0	28.6
1363	191.1	0.97	-0.2	1.23	-21.25		4.39	325	326	73	2740	0	3	0	22.0
1350	189.2	0.95	-0.2	1.72	-20.54	6.02	4.53	317	349	79	2911	0	2	0	14.7
1337	187.3	1.00	0.0	1.54	-20.66		4.43	301	342	72	2871	2	2	0	14.1
1330	186.2	1.03										0	5		
1324	185.3	1.02	0.0	1.22	-21.04	5.73	4.47	304	344	74	2901	0	4	0.5	15.1
1317	184.3	1.03										0	0		
1308	183.0	1.31	0.2	0.61	-22.16		4.35	230	345	74	2778	5	4	2	7.5
1301	182.1	1.18					4.80	272	379	80	3101	1	0		
1295	181.3	1.28										0	1		
1287	180.3	1.18	0.0	0.48	-22.58	5.36	4.97	301	383	84	3111	7	23	0.5	5.3
1280	179.5	1.15										0	21		
1271	178.4	1.26	-0.2	0.41	-22.35		4.66	268	392	82	3052	1	16	0	12.8
1264	177.6	1.11										0	5		
1257	176.6	1.03	-0.4	0.75	-21.30	6.65	4.24	393	344	70	2699	0	1	0	12.9
1244	175.0	1.15	-0.3	0.63	-21.32		4.55	269	363	75	2925	1	3	0	13.8
1235	174.0	0.99		1.55											
1229	173.2	0.95	-0.4	1.33	-21.07	8.43	4.37	335	327	79	2833	0	4	0	22.8
1214	171.4	1.07	-0.2	1.45	-20.45	6.34	5.04	356	357	91	3264	0	0	0.5	20.5
1201	169.7	1.13	0.3	1.20	-20.62		4.99	265	383	85	3207	0	0	0.5	12.4
1196	169.1	1.19	0.4	0.70	-22.16	4.62	4.77	235	379		3049	0	0	2	3.3
1191	168.5	1.12		0.66								0	0		
1185	167.8	0.89	-0.2	2.63	-21.08	8.74	4.65	350	354	82	3067	0	0	0	35.0
1179	167.1	0.99	0.1	1.30		8.34						0	0		
1172	166.2	1.15		0.87	-21.44	4.36	4.76	244	413	76	2918	0	1	1	5.4
1166	165.4	1.13	0.4									0	0		
1160	164.7	1.07	-0.1	1.45	-21.33	6.97	4.48	259	367	75	2987	0	0	0.5	22.9
1144	162.8	1.04	0.2	1.13	-20.75	4.98	4.56	263	372	80	2865	0	1	0.5	11.6
1128	160.8	1.21	0.3	0.71	-21.39		4.77	268	394	76	3138	0	0	1	8.8
1121	159.9	1.17										0	1		
1114	159.0	1.25	0.7	0.35	-23.05	4.33	4.90	248	423	78	3198	30	6	2	5.6

Depth (cm)	Age (ka BP)	DBD (g/cm ³)	$\delta^{18}\text{O}$ (‰pdb)	C_{org} (%)	$\delta^{13}C_{org}$ (‰pdb)	$\delta^{15}N$ (‰)	Al (%)	Ba (ppm)	Mn (ppm)	V (ppm)	Tl (ppm)	G. truncat. (No.)	G. crass. (No.)	Pter.	G. bulloides
1108	158.5	1.22										16	30		
1102	157.9	1.26	0.6	0.32	-22.49		4.62	227	419	78	2977	0	30	2	3.9
1093	157.2	1.17	0.6	0.37	-22.83	4.42	4.75	237	414	79	2937	7	30	2	4.7
1086	156.5	1.17										2	30		
1079	155.9	1.13	0.2	0.52	-22.26		4.13	226	364	73	2654	0	21	2	13.9
1073	155.4	1.15										0	16		
1069	155.0	1.10	0.3	0.51	-22.05	4.67	4.19	225	360	73	2663	0	8	2	4.4
1062	154.4	1.03										0	5		
1054	153.7	1.12	0.3	0.44	-21.45		4.24	237	362	71	2702	0	18	2	7.1
1046	153.0	1.00										0	3		
1041	152.5	1.03	0.3	0.62	-20.97	4.74	3.95	230	331	66	2561	0	7	1	10.2
1036	152.0	0.96	0.3									0	1		
1030	151.5	0.94		1.10	-20.46		3.83	224	316	65	2495	0	7	1	12.0
1024	151.0	0.88	0.2									0	0		
1018	150.5	0.87		1.27	-20.30	5.93	3.50	210	281	58	2292	0	2	0.5	11.8
1012	149.9	0.87										0	7		
1006	149.4	0.87	0.2	1.58	-20.18	7.18	3.81	239	297	61	2502	1	9	0.5	8.6
1000	148.9	0.86		1.86								0	2		
995	148.4	0.78		2.53								0	0		
990	148.0	0.78		3.36	-19.90	7.63	4.51	325	330	96	2851	0	10	0	21.1
985	147.5	0.73		3.61								0	3		
978	146.8	0.79		2.55	-20.26	7.54	3.95	282	294	90	2519	0	2	0.5	1.8
971	146.3	0.94		1.86		6.76	4.15	258	317	76	2534	0	0		
962	145.5	0.78	0.2	3.39		8.44	4.07	272	312	97	2622	0	0	0.5	24.4
956	144.9	0.73		2.94		8.59	3.81	257	292	92	2432	0	2	1	11.9
949	144.3	0.87	-0.2	2.45	-20.06	8.17	4.02	250	312	74	2590	2	2	1	22.1
939	143.4	0.83					3.57	225	278	65	2264	0	0	0.5	17.9
936	143.1	0.80		2.32	-19.99	8.57	3.92	261	309	81	2501	0	0	0	20.4
930	142.6	0.85	0.1									0	0		
923	142.0	0.79	0.1	2.18	-20.16		3.86	248	297	77	2472	1	1	2	14.4
917	141.4	0.78										0	0		
910	140.8	0.87	0.3	1.26	-20.45	6.92	3.76	196	300	66	2430	2	1	3	13.0
904	140.2	0.90	0.1									0	2		
897	139.7	0.91		1.37	-20.68		3.81	167	298	69	2428	0	5	3	6.3
890	139.0	0.88										0	0		
885	138.5	0.91	0.0	1.22	-21.07	7.31	3.42	164	282	58	2195	0	0	3	7.1
879	138.0	1.00	0.3									3	1		
871	136.0	1.02	0.3	0.72	-21.69							14	3	3	8.4
867	134.9	1.12										30	26		
860	133.1	1.19	0.2	0.47	-22.33	4.41	4.18	178	326	76	2593	30	12	3	5.1
855	131.7	1.14										30	30		
848	130.0	1.06	-0.8	0.37	-22.31	6.48	4.10	280	324	78	2552	30	30	1	13.4
843	129.2	0.94										29	30		
836	128.2	0.98	-1.3	0.56	-21.54	7.42	4.50	644	319	88	2681	8	8	0	26.1
826	126.6	0.97										1	0		
820	125.7	0.98	-1.1	1.01	-22.69		4.35	454	312	88	2689	0	5	0	26.1
814	124.8	0.95	-1.1	1.16	-21.69	8.46	4.37	457	318	80	2729	0	3	0	31.1
808	123.8	0.93										0	0	0	24.6

Appendix 2. Continued

Depth (cm)	Age (ka BP)	DBD (g/cm ³)	$\delta^{18}\text{O}$ (‰pdb)	C_{org} (‰)	$\delta^{13}\text{C}_{\text{org}}$ (‰pdb)	$\delta^{15}\text{N}$ (‰)	Al (%)	Ba (ppm)	Mn (ppm)	V (ppm)	Ti (ppm)	G. truncat. (No.)	G. crass. (No.)	Pter.	G. bulloides
802	122.9	0.93		1.33	-21.05	7.31	4.49	440	328	81	2790	0	0	0	32.9
797	122.1	0.96					4.48	433	329	79	2788			0	25.0
790	121.1	0.94		1.40	-20.90	7.18	4.37	477	314	88	2742	0	0	0	23.4
783	120.0	0.92	-0.9				4.11	388	298	74	2543	0	4	0	18.5
777	112.5	0.94	-0.4	0.91	-21.59		4.49	330	317	84	2761	0	19	0	25.4
771	110.8	0.98		0.61	-19.59	5.03	5.01	292	351	90	3044	0	30	0	19.0
765	108.9	0.91										0	28		
757	106.8	1.02	-0.6	0.56	-22.03		4.41	408	323	78	2720	2	30	0	14.1
751	105.1	0.97										5	30		
742	102.5	0.80	-0.7	0.76	-21.34	5.79	3.75	426	281	72	2319	1	17	0	12.8
736	101.0	0.84										0	29		
729	99.3	0.94	-0.7	1.15	-20.97	7.11	3.66	379	286	67	2355	0	30	0	24.0
723	97.8	0.84										0	24		
718	96.4	0.82	-0.4	1.42	-20.62	6.51	3.53	405	271	63	2299	0	8	0	22.2
712	95.1	0.85										0	28		
707	93.9	0.91	-0.4	1.42	-20.80		3.56	432	276	72	2295	3	15	0	27.8
701	92.2	0.93										0	15		
695	90.8	0.89	-0.5	1.17	-21.05	5.72	4.06	455	300	84	2568	2	16	0	17.6
689	89.4	0.83		0.77								1	26		
682	87.7	1.09	-0.2	0.39	-21.99	5.74	5.00	242	363	92	3124	2	30	0	7.3
677	86.3	1.06										2	30		
671	85.0	0.85		0.64	-21.26		4.27	344	305	79	2639	0	8	0	13.4
665	83.4	0.81										0	9		
657	81.5	0.83	-0.8	0.96	-21.56	7.54	4.24	460	292	86	2594	0	2	0	14.1
643	79.9	0.89	-0.6	1.08	-20.90		4.20	395	308	82	2635	0	0	0	22.9
629	78.2	0.92	-0.5	1.06	-21.44	8.29	4.46	343	330	84	2865	0	0	0	21.9
618	77.0	0.96	-0.1	1.01	-21.24		4.84	282	349	85	3067	0	3	0	19.3
599	74.7	0.95	-0.1	1.31	-20.85	6.78	4.71	331	336	90	3011	0	0	0	15.8
585	73.0	0.89	0.3	1.07	-20.62		4.57	299	332	76	2889	0	6	0	14.1
577	72.2	1.11										0	1		
570	71.4	1.06	0.3	0.65	-21.25	5.63	4.54	275	345	77	2881	11	3	0.5	14.7
562	70.4	1.10	0.3	0.66	-20.99		4.69	285	371	77	3003	9	1	0	11.3
554	69.4	0.92										0	0		
547	68.6	1.05	0.2	0.77	-20.83	5.45	4.63	287	365	81	2945	0	1	0.5	8.5
539	67.7	1.19										25	3		
531	66.7	1.15	0.4	0.37	-22.53	5.84	5.10	268	416	89	3260	30	1	2	17.1
523	65.9	1.14										30	1		
516	65.1	1.07	0.2	0.41	-22.28	6.14	4.93	255	409	85	3189	30	0	1	12.8
510	64.3	1.03										30	2		
499	63.0	0.90	-0.2	0.81	-21.27		4.43	307	345	78	2834	27	1	1	18.6
492	62.2	0.90										6	0		
485	61.4	0.93	-0.3	1.19	-20.43	7.81	4.01	335	321	73	2609	9	0	0	17.6
479	60.7	0.83										0	1		
472	59.9	0.93	-0.1	1.02	-20.89							1	1	0	17.0
466	59.2	0.98	-0.3									1	0		
457	58.1	0.83	-0.4	0.90	-21.07	7.38	3.93	259	307	72	2513	3	3	1	17.5
449	57.2	0.88		1.08											
441	56.3	0.87	-0.4	1.28	-20.23		3.72	379	295	73	2445	0	0	0	19.1

Depth (cm)	Age (ka BP)	DBD (g/cm ³)	$\delta^{18}\text{O}$ (‰pdb)	C_{org} (‰)	$\delta^{13}\text{C}_{\text{org}}$ (‰pdb)	$\delta^{15}\text{N}$ (‰e)	Al (%)	Ba (ppm)	Mn (ppm)	V (ppm)	Ti (ppm)	G. truncat. (No.)	G. crass. (No.)	Pter.	G. bulloides
433	55.4	0.86		1.68											
426	54.5	0.85	-0.3	1.61	-20.35	7.69	4.15	429	305	75	2709	0	1	0	36.0
418	53.6	0.80		1.45											
409	52.6	0.91	0.2	1.06	-21.37	6.33	4.52	262	336	84	2873	0	2	0	20.3
400	51.5	0.75		2.04											
393	50.7	0.77	0.0	1.69	-20.33	8.25	4.28	349	319	75	2834	0	2	0	28.2
386	49.8	0.88		1.34											
379	49.0	0.84	0.1	1.34	-20.70	7.28	4.51	297	334	80	2903	0	0	0	37.7
371	48.1	0.79		1.38								0	0		
364	47.3	0.85	0.0	1.12	-20.96	6.77	4.35	269	331	75	2771	0	17	0.5	38.4
355	46.2	0.79										0	0		
346	45.2	0.88	0.1	1.12	-20.75		4.29	279	325	81	2729	1	2	0	21.0
336	44.0	1.17										5	25		
330	43.3	0.92	-0.1	0.94	-20.96	7.14	4.75	281	370	84	3057	2	19	0.5	19.3
322	42.4	0.85										2	8		
314	41.4	0.97	0.1	0.82	-21.26		4.64	271	356	85	2945	2	28	0	9.8
307	40.6	0.87										1	13		
299	39.7	0.91	0.0	0.75	-21.01	6.12	4.55	259	347	86	2890	0	2	0.5	12.0
292	38.3	0.92										0	0		
286	37.3	0.93	0.1	0.79	-21.14		4.40	245	337	84	2833	0	2	0	9.5
273	34.9	0.93		0.84	-20.59	6.16	4.62	270	358	85	2952	0	2	0.5	12.2
270	34.2	0.95										0	0		
262	32.8	1.02	0.4	0.80	-20.69		4.35	231	348	78	2785	0	0	3	28.7
255	31.4	0.85										0	2		
247	30.0	0.91	0.3	1.23	-20.17	6.65	3.98	228	309	71	2569	0	1	0	17.4
231	27.0	0.78	0.4	1.34	-19.85		4.04	246	306	74	2592	0	2	0	17.9
215	24.0	0.88	0.4	0.89	-20.86	5.24	4.18	236	320	77	2664	0	0	1	9.2
199	22.8	0.95	0.5	1.00	-20.82		4.01	222	317	74	2587	0	0	2	8.0
184	21.7	0.80		1.04	-20.56	5.94	4.06	243	311	65	2547	0	0	0.5	8.7
166	20.4	0.73	0.6	1.25	-19.95	5.97	3.76	237	303	65	2430	0	0	1	12.5
159	19.9	0.78	0.5									0	1		
152	19.3	0.75	-0.3	1.24	-20.05	6.35	3.75	241	303	68	2411	0	1	2	15.1
144	18.7	0.81	0.5									0	1		
136	18.1	0.72		1.17	-20.50		3.92	249	316	72	2484	0	0	1	11.2
128	17.6	0.82	0.6									7	1		
121	17.0	0.84		0.93	-21.30	5.34	4.38	244	360	80	2733	3	1	3	13.7
113	16.3	0.96	0.8									30	0		
107	15.9	0.99		0.50	-22.31		4.60	225	396	78	2914	30	0	3	18.1
99	15.2	1.06										30	1		
90	14.5	0.93	-0.2	0.61	-21.92	5.74	3.66	209	320	68	2338	30	0	3	10.5
82	13.9	0.75										7	0		
75	13.4	0.62	-0.2	0.61	-21.46		3.19	235	268	59	2006	28	1	2	6.0
70	13.0	0.79	-0.4	0.62	-21.53	7.27	3.13	281	248	64	1919	3	0	0.5	13.3
62	12.4	0.92	-0.3	0.46	-21.98		4.15	274	321	77	2549	0	0	1	11.6
46	11.2	0.85	-0.9	0.40	-22.10	8.1	3.52	342	265	67	2145	0	0	0	17.3
30	10.1	0.72	-1.2	0.58		7.68	2.98	380	228	60	1839	0	0	0	19.7
23	9.5	0.70	-1.4	0.70	-21.45							0	0		

Low latitude forcing of glacial cycles

L.J. Lourens and G.J. Reichert

Faculty of Earth Sciences, Utrecht University, Budapestlaan 4, P.O. Box 80.021, Utrecht, The Netherlands

Introduction

After Milankovitch's astronomical theory of climate [Milankovitch, 1941], many scientists assume that the intensity of solar radiation at high northern latitudes during summer is critical to the growth and decay of ice sheets during the Pleistocene. Especially, the July insolation curve at 65°N received much attention, because this curve fits perfectly with the patterns found in oxygen isotope records of planktonic foraminifers derived from several deep-sea cores and the outcome of a simple linear ice sheet model [Imbrie *et al.*, 1984]. In addition, this insolation curve displays a large obliquity component in its spectrum, which played an important role in the development of glacial cycles during the last 2.8 million years [Shackleton *et al.*, 1984; Raymo *et al.*, 1989; Ruddiman *et al.*, 1989].

We investigated the orbital phase relationships in two areas, which are influenced by monsoonal climate: the Mediterranean and Arabian Seas. We found that both the African and Asian-Indian monsoon are driven by the insolation gradient between the tropics of Cancer and Capricorn. Maxima in monsoonal intensity are related to maxima in the summer solstice insolation gradient.

The pattern reflected in this insolation gradient is remarkably similar to that displayed in the 65°N summer insolation curve, suggesting that changes in monsoonal circulation could have triggered glacial cycles. We propose that monsoonal-induced changes in atmospheric water vapor content played an important role in the growth and decay of ice sheets during the Pleistocene.

Present-day climate

Maximum heating of the Sun in the equatorial region of our globe results in the rise of warm humid air, which cools down with increasing height and causes heavy rainfalls in the tropics of Africa, America, Australia and Asia. This phenomenon is known as the intertropical convergence zone (ITCZ). At approximately 30°, when these air-masses start to descend they become warmer and drier, resulting in the large arid areas of Africa and Australia. Part of the air-masses returns to the equator as the trade-winds, whereas the resulting part moves further to the poles as westerlies. The poleward moving air masses absorb moisture during their transit, which is released at the continents between 50° and 70°, due to the collision

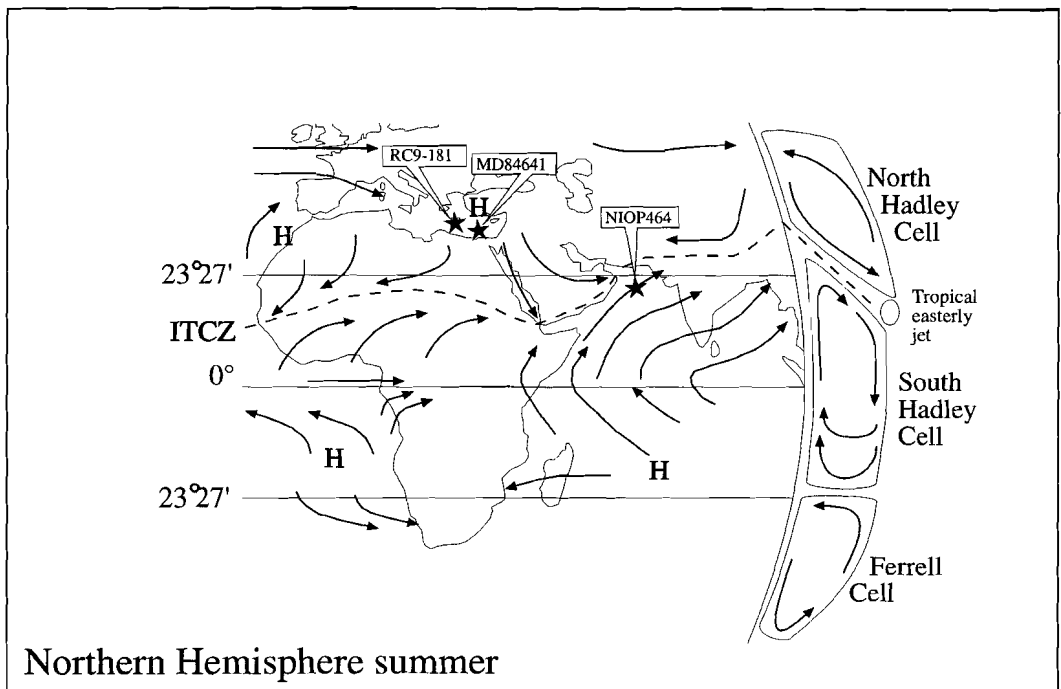


Fig. 1. Core location and general Northern Hemisphere summer atmospheric circulation pattern. The main trade (surface) winds are indicated as arrows pointing to the intertropical convergence zone (ITCZ, dashed line). The ITCZ is the place where the northern and southern Hadley cells meet, and where transport of water vapor to the higher atmosphere is at a maximum. Netherlands Indian Ocean Program (NIOP) core 464 (22°15'N, 63°35'E, 1470 m below sea surface (mbss)); RC9-181 (33°25'N, 25°01'E, 2286 m bss); MD84641 (33°02'N, 32°38'E, 1375 m bss).

with cold and dry air from the poles.

The nearly constant circulation between the Equator (E) and the 30th latitude in each hemispheres is known as the Hadley circulation. The ITCZ is the place where the northern and southern Hadley cells come together. Differential heating of the globe during the year moves the ITCZ between the two hemispheres, whereas the pole ward limb of the two Hadley cells remains relatively stable. Concomitant with the migration of the ITCZ, monsoonal winds invoke large seasonal changes in hydrography and biological activity in large areas of the equatorial Atlantic,

Pacific and Indian Oceans. For instance, during Boreal summer heavy rainfalls occur in large parts of Asia and northwest Africa, whereas the strong southwesterly monsoonal wind in the Arabian Sea (Fig. 1) causes coastal and open ocean upwelling, raising the biological productivity to values that are among the highest known for the open ocean.

The seasonal correlation between the intensity of the SW monsoonal winds and rainfall are related to the pressure gradient or temperature difference (sensible heat) between the two limbs of the southern Hadley cell (Fig. 1). The inter-hemispheric

pressure gradient is strengthened by moisture (latent heat) that is collected by the trade winds during their journey from the southern Indian ocean and its release to the Asian continent upon precipitation. This could indicate that, over orbital time scales, monsoon maxima are associated with maximum insolation differences (sensible heat) and, hence, a maximum pressure gradient between approximately the Tropics of Cancer (T_c) and Capricorn (T_{cc}). Maxima in this Summer Inter-Tropical Insolation Gradient (SITIG) and associated monsoon maxima occur slightly after minima in the precession index and are in accordance with climate modeling experiments [Kutzbach and Otto-Bliesner, 1982; COHMAP, 1988]. This is in contrast with the idea that monsoon maxima correspond with latent heat maxima which are associated with minima in southern hemisphere winter insolation [Clemens *et al.*, 1996], because over orbital time scales these conditions occur at times of precession maxima.

Mediterranean Sea

In 1983, *Rosignol-Strick* [1983] proposed a theory that the periodic occurrence of eastern Mediterranean sapropels is closely related to orbitally-driven variations in the African monsoon. To support her ideas she constructed a monsoon index (M), based on the gradient of insolation between T_c and E . According to her theory, maxima in M cause an intensified monsoonal circulation during Boreal summer, resulting in a larger amount of precipitation over eastern equatorial Africa by moving an intensified ITCZ further to the north, a larger Nile

River flood discharge into the eastern Mediterranean, and finally a change in the Mediterranean hydrography which resulted in bottom water anoxia and, hence, sapropel formation. We reconstructed M by applying a more recent and highly accurate astronomical solution [Laskar, 1990; Laskar *et al.*, 1993] than the one previously used by *Rosignol-Strick* [1983] (Fig. 2). Fig. 2 clearly shows that variations in M are dominantly precession-controlled. Although the sapropel patterns are primarily related to variations in the precession index, the obliquity cycle causes in some particular intervals for alternating thick/thin patterns. For instance, the small-scale sapropel clusters S3-S5 and S6-S9 are characterized by a thick-thin-thick and a thick-thin-thick-thin alternation of sapropels, respectively (Fig. 2). These alternating thick-thin patterns are not only restricted to the late Pleistocene time interval, but occur also in the sapropel and carbonate cycle patterns of Miocene to early Pleistocene age [Lourens *et al.*, 1996; Hilgen *et al.*, 1995]. The occurrence of these interference patterns cannot be explained by the monsoon index, because the influence of the obliquity cycle is not well reflected in this curve.

Application of the SITIG, however, reveals a clear obliquity signal, which mirrors all interference patterns (Fig. 2): thick sapropels correlate with high-amplitude maxima and thin sapropels with low-amplitude maxima. If we assume that the effect of obliquity on sapropel formation in the Mediterranean proceeds via variations in the intensity of the African monsoon, then a strong southern hemisphere component should be added to the monsoonal index. Surprisingly, the pattern reflected in the SITIG is equal to

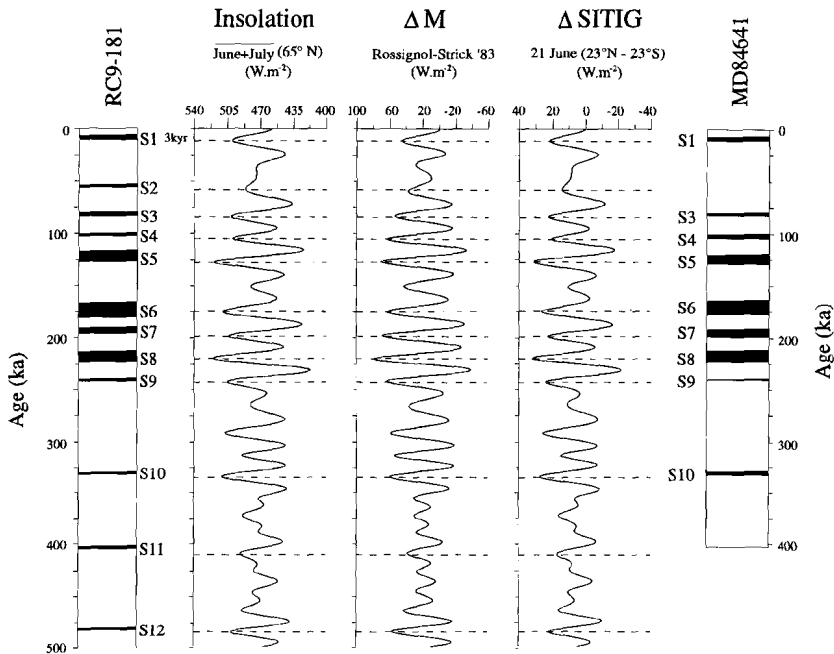


Fig. 2. Comparison between the eastern Mediterranean sapropel patterns of RC9-181 and MD84641 and the 65°N summer insolation curve, ΔM [Rossignol-Strick, 1983], and $\Delta SITIG_{21 \text{ June}}$.

that displayed in the 65° N summer insolation curve (Fig. 2), which was applied as orbital target to test the accuracy of different astronomical solutions over the last 5.3 million years [Lourens *et al.*, 1996] and to construct the astronomical timescale for the Miocene to early Pleistocene age [Lourens *et al.*, 1996; Hilgen *et al.*, 1995]. The climatic process, through which sapropel formation in the Mediterranean could be linked to the 65°N summer insolation, is the growth and decay of the northern hemisphere ice sheets. This mechanism, however, can not explain the interference patterns observed in sedimentary cycles of Miocene and

early Pliocene age, due to the lack of distinct obliquity-controlled glacial cycles in this time interval.

AMS ^{14}C dating of the youngest sapropel in the Mediterranean, S1, indicate that it was formed between 10 and 7 to 5.5 ka BP [Fontugne *et al.*, 1989; Troelstra *et al.*, 1991; Perissoratis and Piper, 1992; Jorissen *et al.*, 1993; Thomson *et al.*, 1995]. This time interval coincides with widespread moisture all over East Africa, Arabia, Pakistan, northern India and Tibet [Street and Grove, 1979; Van Campo *et al.*, 1982; Swain *et al.*, 1983; Gasse *et al.*, 1990; Street-Perrot *et al.*, 1990] and minimum dolomite dust input from the

Persian Gulf area into the Arabian Sea [Sirocko *et al.*, 1993], indicating that the track of the southwest monsoon and its associated pattern of precipitation was moved to its most northern position (Fig. 3). It is therefore feasible that during this time interval, the more pluvial climatic conditions at low latitudes led to an increase of the Nile River flood discharge into the eastern Mediterranean which resulted in sapropel formation, although there is some evidence that at times of sapropel formation precipitation in the northern borderlands of the Mediterranean increased as well [Shaw and Evans, 1984; Cramp *et al.*, 1988; Aksu *et al.*, 1995; Rossignol-Strick, 1987; Wijmstra *et al.*, 1990].

The interaction between intensified monsoonal circulation and sapropel formation in the eastern Mediterranean can also be deduced from some climate modeling experiments [Short and Mengel, 1986]. These experiments show that variations in maximum temperatures oscillated in direct thermal response to variations in insolation with a time lag of ~3 kyrs, for latitudes lower than 20°. The similar lag found between the SITIG and the sapropel midpoint suggests therefore that either the simulated low latitude lag is an intrinsic part of the climatic system for latitudes higher than 20° or that Mediterranean climate is strongly affected by variations in low latitude insolation and, thus, to variations in the intensity of the monsoonal circulation.

Arabian Sea

Time series analyses between monsoon tracers in the Arabian Sea and their

inferred orbital forcing showed that variations in the SW monsoon winds and associated coastal and open ocean upwelling processes behave non-stationary through time [Clemens *et al.*, 1996]. A time lag of approximately ~8 kyrs was observed between the average precessional components of four monsoon tracers and the June insolation curve over the late Pleistocene time interval [Clemens *et al.*, 1991]. This exceptional large time lag is on average ~5000 longer than that indicated by the more pluvial climatic conditions during the early Holocene. It was therefore proposed that maxima in the intensity of the SW monsoon are not related to direct sensible heating of the Asian plateau as indicated by climate modeling experiments [Kutzbach and Otto-Bliesner, 1982; COHMAP, 1988], but resulted from latent heat maxima associated with southern hemisphere winter insolation minima [Clemens *et al.*, 1996]. If we compare these phase relations and inferred orbital configuration with the climatic history over the last 22 kyr (Figure 3), the proposed latent heat maximum and, hence, maximum monsoonal circulation would have prevailed between 3 (average monsoon tracers) and 1 (orbital configuration) ka BP. This conclusion, however, needs some discussion. In the first place, the proposed latent heat maximum between 3 and 1 ka coincides with a time interval with relatively low monsoonal rainfall in large parts of Africa and Asia as can be deduced from for instance lake level studies [Street and Groove, 1979; Van Campo *et al.*, 1982; Swain *et al.*, 1983; Gasse *et al.*, 1990; Street-Perrot *et al.*, 1990; Gasse *et al.*, 1990; Street-Perrot *et al.*, 1990]. Secondly, the phase lead of the average

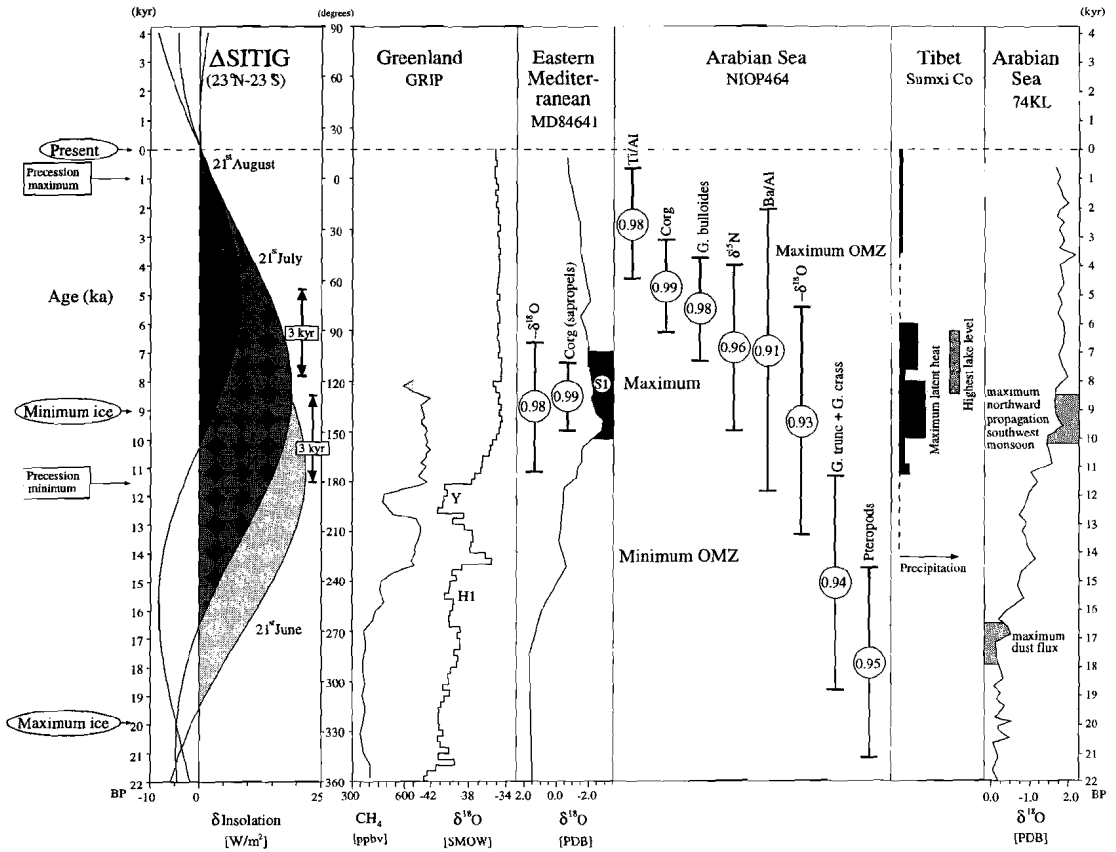


Fig. 3. Coherence and phase relations between various proxies from the Arabian and eastern Mediterranean Seas and precession over the last 225 kyr. Phase angles (time lags) are plotted in relation to the last full precession cycle and compared with the GRIP icecore $\delta^{18}\text{O}$ and CH_4 records [Dansgaard et al., 1993; Chappelaz et al., 1990], a lake level record from Tibet [Gasse et al. 1991], and the western Arabian Sea dolomite dust record [Sirocko et al. 1993]. The various proxy records are compared spectrally with the La90_(1,1) orbital solution [Laskar et al., 1993; Lillourens et al., 1996], using a bandwidth of 0.0084 kyr⁻¹. Coherence is indicated inside circles, error bars indicate 95% confidence limits. Mediterranean sapropel (black area) formation is associated with maximum summer solstice ΔSITIG (=SITIG-SITIG_{present}) (light shaded area) and coincides with maximum monsoonal rainfall and minimum dust flux (middle shaded band). Maximum Arabian Sea OMZ intensity (upper shaded band) is associated with late summer ΔSITIG (dark/black shaded area) and is in antiphase with Minimum OMZ intensities (lowest shaded band).

monsoon tracers with respect to their orbital configuration indicates that at least part of the monsoon maxima can be accounted for by sensible heating. This is further evidenced by the fact that the SPECMAP chronology applied in those studies overestimates the true lags for precession and obliquity by a few thousands of years. The SPECMAP timescale was based on the assumption that the time lags for the obliquity and precession-related components in $\delta^{18}\text{O}$ are those of a single-exponential climate system with a response of 17 kyr. This last value is based on a simple ice sheet model [Imbrie and Imbrie, 1980] and was determined by visual comparison of the model output and the timing and relative magnitude of six radiometrically dated climatic ($\delta^{18}\text{O}$) events over the last 150 kyr. An advanced, six to ten times more accurate, radiometric dating technique (TIMS for measuring ^{230}Th and ^{234}U) applied on corals from Barbados and the Bahamas revealed, however, that the age of the last glacial maximum and those of glacial stages 5.1-5.5 and 7.1 are systematically older than the ages given by SPECMAP [Edwards et al., 1987; Bard et al., 1990a; 1990b; Gallup et al., 1994]. These authors state therefore that the obliquity and precession-related time lags used in the SPECMAP chronology are overestimated, resulting in too young ages of the different isotopic stages with at least two thousands of years. These observations agree well with the timescale derived from the sapropel chronology [Lourens et al., 1996]. This timescale revealed time lags of 2.9 (± 2.4) kyr and 4.8 (± 14.9) kyr for the precession and obliquity components in the $\delta^{18}\text{O}$ time series of core MD84641, respectively.

These lags are considerably shorter than those derived from the SPECMAP chronology, which arrive at 5.6 (± 3.7) and 8.3 (± 5.7), respectively.

As a consequence, the precessional time lags derived from the monsoon tracers in the Arabian Sea may have been on average 2 to 3 kyr shorter, which results in an even larger phase lead of the monsoon tracers with respect to their inferred orbital configuration and associated latent heat maximum. This further implies that, over Holocene timescales, the proposed monsoon maximum coincides with a period of maximum aridity, characterized by low lake levels in North Africa and Asia [Street and Grove, 1979; Van Campo et al., 1982; Swain et al., 1983; Gasse et al., 1990; Street-Perrot et al., 1990], a decline of the vegetation cover [Swain et al., 1983; Gasse et al., 1990], and a general increase of the dust flux and the return of dolomite dust in the Arabian Sea [Sirocko et al., 1993]. This dry period also resulted in the formation of hierarchical societies in the then overpopulated Nile valley and Mesopotamia starting near 5.3 ka, whereas the neolithic settlements in the inner desert of Arabia were abandoned at that time [Uerpmann, 1991]. In our opinion it seems highly unlikely that the observed monsoon maximum coincided with maximum cross-equatorial latent heat transport, in view of the observed aridity in large parts of Africa and Asia.

To further unravel the complex nature of the monsoonal circulation in the Arabian Sea, we studied a piston core (NIOP 464) from the Murray Ridge taken just below the present-day Oxygen Minimum Zone (OMZ). This core exhibits a continuous succession of OMZ variability over the last 225 kyr, which can

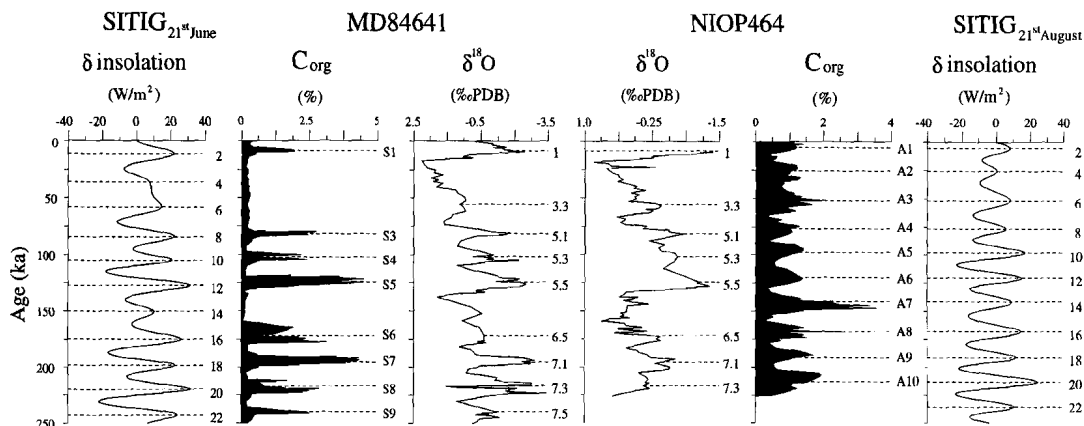


Fig. 4. Oxygen isotope ($\delta^{18}\text{O}$, relative to the Pee Dee belemnite standard) and organic carbon (C_{org}) records from NIOP464 and MD84641 [Fontugne and Calvert, 1992] plotted against time. The adopted timescale is based on the sapropel chronology [Lourens et al., 1996] and on tuning the $\delta^{18}\text{O}$ record of NIOP464 to that of MD84641. Increased C_{org} values in MD84641 are associated with sapropels (S1 to S9), while those in NIOP464 (A1 to A10) coincide with maximum oxygen minimum zone (OMZ) intensities.

be related to variations in coastal and open ocean upwelling processes associated with the intensity of the SW monsoon [Chapter 2]. The age model of this core is based on the sapropel chronology by tuning the oxygen isotope record of NIOP464 to that of MD84641 in the eastern Mediterranean. The precessional phase relations of the various geochemical and paleontological proxies are plotted in Figure 3. A ± 500 year lead of the $\delta^{18}\text{O}$ record of NIOP 464 with respect to that of MD84641 can be observed (Figure 3), which we attribute to small uncertainties in the correlation scheme and sample resolution. Nevertheless, the phase plot clearly indicates that the development of the OMZ, settled by the different proxies, proceeds in a succession of events, which followed immediately after the most northward propagation of the SW

monsoon (Figure 3). The first event is marked by an increase in the barium content of the sediment. This most probably indicates an intensification of the coastal and open upwelling processes, resulting in a larger flux of organic matter. This step is followed by denitrification of the water column, indicating that the available oxygen for the degradation of organic matter became depleted, and that an intense OMZ developed. Subsequently, seasonal upwelling of the resulting nutrient-rich waters should have induced the high relative abundances of the endemic upwelling foraminifer *G. bulloides* soon after the OMZ was formed. This process should have continued until the OMZ reached its maximum extent. This OMZ maximum is further indicated by the anti-phase relation with short influxes of *G. truncatulinoides* and *G.*

crassaformis. Both planktonic foraminiferal species depend for their life cycle on deep-mixing of the surface layer to approximately 300-600 m, which occurred most likely during winter when cold and dry air from the Asian continent cools the Arabian sea surface [Chapter 4]. Finally, maxima in Ti/Al coincides with the aridification phase which started around 5.3 ka BP. This increase can be explained by a larger grain size of the eolian transported material from the Arabian Peninsula by the Shamal winds in combination with drier climatic conditions.

This succession of events and their phase relations are in good agreement with those observed at the Owen Ridge [Clemens *et al.*, 1991; Murray and Prell, 1992] and Oman margin [Anderson and Prell, 1993; Emeis *et al.*, 1995], suggesting that a single mechanism can be held responsible for the OMZ variability in the Arabian sea. The phase relations further indicate that this mechanism started when the southwest monsoon track returned from its most northern position during the later phase of the summer monsoon. Intuitively one may speculate that these conditions are more favorable for at least the open ocean upwelling processes than in case the SW monsoon winds reached their maximum velocities near or over the Arabian Peninsula. In the first place, the area where open ocean upwelling processes can take place will be significantly enlarged if the jet axis associated with the SW winds migrates towards the southeast and secondly a less intense wind stress curl will produce stronger upwelling offshore [Anderson and Prell, 1993]. Indeed, modern sediment trap data indicate that the largest flux of opal and *G. bulloides* are in August and

September [Curry *et al.*, 1992; Schäfer and Ittekkot, 1993], whereas the largest windspeed values occur in June and July [Nair *et al.*, 1989]. This could imply that not the SITIG at the 21st of June or the maximal orbitally-driven intertropical pressure gradient results in maximum productivity in the Arabian Sea, but the less intense pressure gradient prevailing during August and September, which extends the upwelling season. To increase the annual cumulative flux, an extension of the upwelling season seems, therefore, more important than a maximum intensity of the summer monsoon [Chapter 4]. A comparison between the C_{org} timeseries with the SITIG obtained from the 21st of August (Figure 4) clearly demonstrates the dominance of the precession cycle on both records and the good visual correlation between them. For instance, the good correlation is corroborated by the characteristic precession-related peaks around 50 and 25 ka reflected in both curves, whereas these peaks are joined in the SITIG of the 21st of June. It seems therefore reasonable to assume that the upwelling intensity in the Arabian Sea is related to variations in the intertropical pressure gradient as well, with this respect that it starts to increase soon after maximum monsoonal circulation.

Implications for Global Climate

The similarity between the SITIG at the 21st of June and the 65°N summer insolation curve suggests that there could be a direct relation between monsoonal intensity and glacial cycles. This could imply that a long, cool summer and a short mild winter at high northern latitudes

which allow the positive value in the annual budget of snow and ice needed to increase the surface albedo [Murphy, 1876; Milankovitch, 1941], was not the primary mechanism initiating glacial periods. There are two important arguments which plead against the ice albedo scenario as has been addressed by Broecker and Denton [1989]. In the first place, the ice sheets cannot have changed fast enough to be responsible for the rapid transition from full glacial to full interglacial conditions. Secondly the interhemispheric synchrony excludes a primary forcing from the northern hemisphere ice fields [e.g. Denton and Hendy, 1994; Bard et al., 1997]. Broecker and Denton [1989] therefore postulated that reorganizations of the ocean-atmosphere system were responsible for the rapid climate changes. The ocean-atmosphere system was supposed to switch from one stable mode to another, involving changes in ocean circulation, the atmosphere's greenhouse capacity and reflectivity. These mode switches are directly linked to the Atlantic conveyor, which is turned on and off by changes in salinity in the northern Atlantic [Broecker and Denton, 1989].

The fast propagation of the Dansgaard-Oeschger events over the globe [e.g. Grimm et al., 1993; Lowell et al., 1995; McIntyre and Molino, 1996; Hughen et al., 1996], however, makes an oceanic mechanism less likely. The strong interhemispheric climate coupling inferred from glacier lobes in the Chilean Andes [Lowell et al., 1995] and in the New Zealand Alps [Denton and Hendy, 1994] implies a global atmospheric signal rather than regional changes caused by North Atlantic thermohaline switches or

Laurentide ice surges. Simultaneous submillennial-scale variations in the southwest monsoon intensity in southern Asia and the northeast Pacific winter climate have been linked through water vapor transport over the Indian and Pacific Oceans [Heusser and Sirocko, 1997]. These variations are too short to be caused by rearrangements of the thermohaline circulation.

Ice core $\delta^{18}\text{O}$ records from low latitudes showed both a significant reduction of low latitude temperatures and a significant reduction of atmospheric water vapor during the last glacial [Thompson et al., 1995]. Evidence for the role of (low latitude) moisture in climate also comes from the ice core methane record, which clearly shows higher methane concentration during the warm part of the Dansgaard-Oeschger events [Chappelaz et al., 1993]. Variations in CH_4 level are caused by moisture fluctuations, especially at low-latitudes, where the tropical wetlands are responsible for the increased production of methane during more humid periods [Chappelaz et al., 1993]. More evidence comes from the increased dust input to the atmosphere during glacial conditions [Taylor et al., 1993; Thompson et al., 1995] which suggests drier conditions, especially in the subtropics. These changes are synchronous in both hemispheres, as can be deduced from the most humid phase recorded in a lake 49°S, in Patagonia [Stine and Stine, 1990], which is in phase with the highest lake levels recorded at low latitudes in Africa and Asia [Bryson and Swain, 1981; Gasse and Van Campo, 1994].

Because water vapor is, by far, the atmosphere's most potent greenhouse gas, it is a potential forcing agent for glacial-

interglacial variability. The main route via which moisture is supplied to the atmosphere is via the ITCZ. It has been proposed that changes in the tropical sea surface temperature, induced by changes in the thermohaline circulation could be responsible for the inferred changes in atmospheric water vapor [Broecker, 1994; 1996]. Oscillations in NADW production may produce a large water vapor feedback, however, it is unlikely to be the trigger for the observed changes, as Curry and Oppo [1997] observed a decrease in NADW production well before the Heinrich events.

Although it is generally agreed upon that glacials are caused by changes in the Earth's orbital parameters, the nature of this link remains largely an unanswered question. Because of the good match between the insolation curve at 65°N and the oxygen isotope record the primary forcing of glacials has always been supposed to be primarily a high latitude (northern hemisphere) process. This implies that changes in the summer insolation at 65°N have to be translated from the northern high latitudes into a global climate signal. A forcing of glacials via atmospheric water vapor in that case has to be the result of indirect processes, e.g. changes in the thermohaline circulation. We propose a direct response to changes in insolation at low latitudes. Variations in the SITIG invoked changes in the intensity of the northern hemisphere summer monsoon, thereby changing the amount of moisture supplied to the atmosphere.

On an orbital timescale the methane record shows a strong precessional component, with precession related maxima in low latitude moisture in phase with the occurrence of sapropels in the

Mediterranean [Chappelaz *et al.*, 1990]. This indicates the major role of the monsoonal circulation for global methane concentrations, and the possible role of the monsoon in glacial-interglacial variations. Furthermore the changes observed in the CH₄ record appear to slightly lead the changes in oxygen isotopes [Chappelaz *et al.*, 1993]. Although this relation is not statistically very significant it may suggest that a wetter tropical climate preceded global warming and melting of the ice sheets. Because glacial atmospheric aerosol content caused global temperatures to be 2° to 3°C colder than they would have been in the absence of aerosols [Harvey, 1988], increased dust input from expanded desert areas could, therefore, as a natural feedback mechanism, contribute significantly to global cooling, induced by changes in water vapor.

The tropical response to insolation changes is very strong because differences in the thermal properties of continents and oceans amplify changes in monsoonal circulation, leading to climatic responses in the tropics of a magnitude greater than the response to glacial boundary conditions [Kutzbach and Guetter, 1986]. Changes in the monsoon intensity are, therefore, most likely not the result of glacial-interglacial feedback mechanisms but result directly from changes in low latitude insolation. Although variations in insolation at 65° probably did play a role in amplifying the climatic response (e.g. ice albedo), we believe that the primary mechanism causing glacial cycles is triggered at low latitudes. All evidence presented strongly suggests a forcing of glacial cycles through the varying input of water vapor to the atmosphere at the ITCZ, which are in turn controlled by changes in the SITIG.

References

- Aksu, A.E., Yaşar, D. and P.J. Mudie, Paleoclimatic and paleoceanographic conditions leading to the development of sapropel layer S1 in the Aegean Sea. *Palaeogeogr. Palaeoclimatol. Palaeoecol.*, 116, 71-101, 1995.
- Anderson, D.M. and W. L. Prell, A 300 kyr record of upwelling off Oman during the late Quaternary: evidence of the Asian southwest monsoon, *Paleoceanography*, 8, 193 (1993).
- Bard, E., Hamelin, B., Fairbanks, R.G. and A. Zindler, Calibration of the ^{14}C timescale over the past 30,000 years using mass spectrometric U-Th ages from Barbados corals, *Nature*, 345, 405 (1990a).
- Bard, E., Hamelin, B. and R. G. Fairbanks, U-Th ages obtained by mass spectrometry in corals from Barbados: sea level during the past 130,000 years. *Nature*, 346, 456 (1990b).
- Bard, E., Rostek, F. and C. Sonzogni, Interhemispheric synchrony of the last deglaciation inferred from alkenone palaeothermometry. *Nature*, 385, 707-710, 1997.
- Broecker, W.S. and G.H. Denton, The role of ocean-atmosphere reorganizations in glacial cycles, *Geochim. Cosmochim. Acta*, 53, 2465-2501, 1989.
- Broecker, W.S., Massive iceberg discharge as triggers for global climate change, *Nature*, 372, 421-424, 1994.
- Broecker, W.S., Paleoclimatology, *Geotimes*, 2, 40-41, 1996.
- Bryson, R.A. and A.M. Swain, Holocene variations of monsoon rainfall in Rajasthan. *Quat. Res.*, 16, 135-145, 1981.
- Chappellaz, J., Barnola, J.M., Raynaud, D., Korotkevich, Y.S. and C. Lorius, Ice-core record of atmospheric methane over the past 160,000 years, *Nature*, 345, 127-131, 1990.
- Chappellaz, J., Blunier, T., Raynaud, D., Barnola, J.M., Schwander, J. and B. Stauffer, Synchronous changes in atmospheric CH_4 and Greenland climate between 40 and 8 kyr BP, *Nature*, 366, 443-445, 1993.
- Clemens, S., Prell, W., Murray, D., Shimmield, G. and G. Weedon, Forcing mechanisms of the Indian Ocean monsoon. *Nature*, 353, 720-725, 1991.
- Clemens, S.C., Murray, D.W. and W.L. Prell, Nonstationary phase of the Plio-Pleistocene Asian Monsoon. *Science*, 274, 943-948, 1996.
- COHMAP members, Climatic changes of the last 18,000 years: Observations and model simulations. *Science*, 241: 1043-1052, 1988.
- Cramp, A., Collins, M. and R. West, Late Pleistocene-Holocene sedimentation in the NW Aegean Sea: a palaeoclimatic Paleocceanographic reconstruction. *Palaeogeogr. Palaeoclimatol. Palaeoecol.*, 68, 61-77, 1988.
- Curry, W.B., D.R. Ostermann, M.V.S. Gupta, and V. Ittekkot, Foraminiferal production and monsoonal upwelling in the Arabian Sea: Evidence from sediment traps. In: C.P. Summerhays, W.L. Prell and K.C. Emeis (eds), *Upwelling Systems: Evolution since the early Miocene. Geol. Soc. Spec. Publ.* 63:93-106, 1992.
- Curry, W.B. and D.W. Oppo, Synchronous, high-frequency oscillations in tropical sea surface temperatures and North Atlantic deep water production during the last glacial cycle. *Paleoceanography*, 12, 1-14, 1997.

- Dansgaard, W., Johnsen, S.J., Clausen, H.B., Dahl-Jensen, D., Gundestrup, N.S., Hammer, C.U., Hvidberg, C.S., Steffensen, J.P., Sveinbjornsdottir, A.E., Jouzel, J. and G. Bond, Evidence for general instability of past climate from a 250-kyr ice-core record, *Nature*, 364, 218-220, 1993.
- Denton, G.H. and C.H. Hendy, Younger Dryas age advance of Franz Josef glacier in the southern alps of New Zealand, *Science*, 1434-1437, 1994.
- Edwards, R.L., Chen, J.H., Ku, T.L. and G.J. Wasserburg, Precise timing of the last interglacial period from mass spectrometric determination of Thorium-230 in corals, *Science*, 236, 1547-1553, 1987.
- Emeis, K.C., Anderson, D.M., Dooze, H., Kroon, D. and D. Schulz-Bull, Sea-surface temperatures and the history of monsoon upwelling in the northwest Arabian Sea during the last 500,000 years, *Quat. Res.*, 43, 355-361, 1995.
- Fontugne, M.R., Paterne, M., Calvert, S.E., Murat, A., Guichard, F. and M. Arnold, Adriatic deep water formation during the Holocene: implications for the reoxygenation of the deep eastern Mediterranean Sea, *Paleoceanogr.*, 4, 199-206, 1989.
- Fontugne, M.R. and S.E. Calvert, Late Pleistocene variability of carbon isotope composition of organic matter in the eastern Mediterranean: Monitor of changes in carbon sources and atmospheric CO₂ concentrations, *Paleoceanography*, 7, 1-20, 1992.
- Gallup, C.D., Edwards, R.L. and R.G. Johnson, The timing of high sealevels over the past 200,000 years, *Science*, 263, 796-800, 1994.
- Gasse, F., T  het, R., Durand, A., Gibert, E. and J.C. Fontes, The arid-humid transition in the Sahara and the Sahel during the last deglaciation, *Nature*, 346, 141-146, 1990.
- Gasse, F., Arnold, M., Fontes, J.C., Fort, M., Gibert, E., Huc, A., Bingyan, L., Yuanfang, L., Quing, L., Melieres, F., Van Campo, E., Fubao, W. and Z. Quigsong, A 13,000-year climate record from western Tibet. *Nature*, 353, 742-745, 1991.
- Gasse, F. and E. Van Campo, Abrupt post-glacial climate events in West Asia and North Africa monsoon domains, *Earth and Planet. Sc. Lett.*, 126, 435-456, 1994.
- Grimm, E.C., Jacobsen, G.L., Watts, W.A., Hansen, B.C.S. and K.A. Maasch, A 50,000-year record of climate oscillations from Florida and its temporal correlation with the Heinrich events. *Science*, 261, 198-200, 1993.
- Harvey, L.D.D., Climatic impact of ice-age aerosols, *Nature*, 334, 333-335, 1988.
- Hilgen, F.J., Krijgsman, W., Langereis, C.G. Lourens, L.J., Santarelli, A. and W.J. Zachariasse, Extending the astronomical (polarity) time scale into the Miocene, *Earth Planet. Sci. Lett.*, 136, 495-510, 1995.
- Heusser, L.E. and F. Sirocko, Millennial pulsing of environmental change in southern California from the past 24 k.y.: a record of Indo-Pacific ENSO events? *Geology*, 25, 243-246, 1997.
- Hughen, K.A., Overpeck, J.T., Peterson, L.C. and S. Trumbore, Rapid climate changes in the tropical Atlantic region during the last deglaciation, *Nature*, 380, 51-54, 1996.
- Imbrie, J. and J.Z. Imbrie, Modelling the climate response to orbital variations, *Science*, 207, 943-953, 1980.
- Imbrie, J. Hays, J.D., Martinson, D.G., McIntyre, A., Mix, A.C., Morley, J.J., Pisias,

- N.G., Prell, W.L. and N.J. Shackleton, The orbital theory of Pleistocene climate: support from a revised chronology of the marine $\delta^{18}\text{O}$ record. In: *Milankovitch and Climate, Part 1* (Eds. A.L. Berger, J. Imbrie, J. Hays, G. Kukla and B. Saltzman), Reidel Dordrecht, 269-305, 1984.
- Jorissen, F.J., Asioli, A., Borsetti, A.M., Capotondi, L., de Visser, J.P., Hilgen, F.J., Rohling, E.J., Van der Borg, K., Vergnaud-Grazzini, C. and J.W. Zachariasse, Late Quaternary central Mediterranean biochronology, *Mar. Micropaleontol.*, 21, 169-189, 1993.
- Kutzbach, J.E. and P.J. Guetter, The influence of changing orbital parameters and surface boundary conditions on climate simulations for the past 18,000 years, *J. Atmos. Sci.*, 43, 1726-1759, 1986.
- Kutzbach, J.E. and B.L. Otto-Bliesner, The sensitivity of the African-Asian monsoonal climate to orbital parameter changes for 9000 years B.P. in a low-resolution general circulation model, *J. Atmos. Sci.*, 39, 1177-1188, 1982.
- Laskar, J., The chaotic motion of the solar system: a numerical estimate of the size of the chaotic zones. *Icarus*, 88, 266-291, 1990.
- Laskar, J., Joutel, F. and F. Boudin, Orbital, precessional, and insolation quantities for the Earth from -20 Myr to +10 Myr, *Astron. Astrophys.*, 270, 522-533, 1993.
- Lourens, L.J., Antonarakou, A., Hilgen, F.J., Van Hoof, A.A.M., Vergnaud-Grazzini, C. and W.J. Zachariasse, Evaluation of the Plio-Pleistocene astronomical timescale, *Paleoceanogr.*, 11, 391-413, 1996.
- Lowell, T.V., Heusser, C.J., Anderson, B.G., Moreno, P.I., Hauser, A., Heusser, L.E., Schlüchter, C., Marchant, D.R. and G.H. Denton, Interhemispheric correlation of late Pleistocene glacial events. *Science*, 269, 1541-1549, 1995.
- McIntyre, A. and B. Molfini, Forcing of Atlantic equatorial and subpolar millennial cycles by precession, *Science*, 274, 1867-1870, 1996.
- Milankovitch, M., Kanon der Erdbestrahlung und seine Anwendung auf das Eiszeiten problem, *R. Serb. Sci. Spec. Publ.* 133, 1941.
- Murphy, J.J., The glacial climate and the polar ice cap, *Quarterly J. Geological Society London*, 32, 400-406, 1876.
- Murray, D.W. and W. L. Prell, Late Pliocene and Pleistocene climatic oscillations and monsoon upwelling recorded in sediments from the Owen Ridge, northwestern Arabian Sea. in *Upwelling Systems: Evolution Since the Early Miocene* (Eds. C. P. Summerhayes, W. L. Prell, K. C. Emeis), Geol. Soc. Spec. Publ Vol. 64, 301-322, 1992.
- Nair, R.R., Ittekot, V., Manganini, S.J., Ramaswamy, V., Haake, B., Degens, E.T., Desai, B.N. and S. Honjo, Increased particle flux to the deep ocean related to monsoons. *Nature*, 338, 749-751, 1989.
- Perissoratis, C. and D.J.W. Piper, Age, regional variation and shallowest occurrence of S1 sapropel, *Geo-Marine Lett.*, 12, 49-53, 1992.
- Raymo, M.E., Ruddiman, W.F., Backman, J., Clement, B.M. and D.G. Martinson, Late Pliocene variation in northern hemisphere ice sheets and north Atlantic deep water circulation, *Paleoceanography*, 4, 413-446, 1989.
- Rosignol-Strick, M., African monsoons, an immediate climatic response to orbital insolation, *Nature*, 303, 46-49, 1983.

- Rossignol-Strick, M., Rainy periods and bottom water stagnation initiating brine accumulation and metal concentrations, 1, the late Quaternary, *Paleoceanography*, 2, 333-360, 1987.
- Ruddiman, W.F., Raymo, M.E., Martinson, D.G., Clement, B.M. and J. Backman, Pleistocene evolution: northern hemisphere ice sheets and the North Atlantic Ocean, *Paleoceanography*, 4, 353-412, 1989.
- Schäfer, P. and V. Ittekkot, Seasonal variability of $\delta^{15}\text{N}$ in settling particles in the Arabian Sea and its palaeo-geochemical significance. *Naturwissenschaften*, 80, 511-513, 1993.
- Shackleton, N.J., Backman, J., Zimmerman, H., Kent, D.V., Hall, M.A., Roberts, D.G., Schnitker, D. and J. Baldauf, Oxygen isotope calibration of the onset of ice-rafting and history of glaciation in the North Atlantic region, *Nature*, 307, 620-623, 1984.
- Shaw, H.F. and G. Evans, The nature, distribution and origin of a sapropelic layer in sediments of the Cilicia Basin, northeastern Mediterranean. *Mar. Geol.*, 61, 1-12, 1984.
- Short, D.A. and J. G. Mengel, Tropical climatic phase lags and Earth's precession cycle, *Nature*, 323, 48-50, 1986.
- Sirocko, F., Sarnthein, M., Erlenkeuser, H., Lange, H., Arnold, M. and J.C. Duplessy, Century-scale events in monsoonal climate over the past 24,000 years. *Nature*, 364, 322-324, 1993.
- Stine, S. and M. Stine, A record from Lake Cardiel of climate change in southern South America, *Nature*, 345, 705-709, 1990.
- Street, F.A. and A.T. Grove, Global maps of lake-level fluctuations since 30,000 yr B.P., *Quat. Res.*, 12, 83-118, 1979.
- Street-Perrot, F.A., Mitchell, J.F.B., Marchand, D.S. and J.S. Brunner, Milankovitch and albedo forcing of the tropical monsoons: a comparison of geological evidence and numerical simulations for 9000 yBP. *Trans. R. Soc. Edinb.: Earth Sciences*, 81, 407-427, 1990.
- Swain, A.M., Kutzbach, J.E. and S. Hastenrath, Estimates of Holocene Precipitation for Rajasthan, India, based on pollen and lake-level data. *Quaternary Research*, 19, 1-17, 1983.
- Taylor, K.C., Lamorey, G.W., Doyle, G.A., Alley, R.B., Grootes, P.M., Mayewski, P.A., White, J.W.C. and L.K. Barlow, The "flickering switch" of late Pleistocene climate change, *Nature*, 361, 432-436, 1993.
- Thompson, L.G., Mosley-Thompson, E., Davis, M.E., Lin, P.N., Henderson, K.A., Cole-Dai, J., Bolzan, J.F. and K.B. Liu, Late glacial stage and Holocene tropical ice core records from Huascarán, Peru, *Nature*, 269, 46-50, 1995.
- Thomson, J., Higgs, N.C., Wilson, T.R.S., Croudace, I.W., De Lange, G.J. and P.J.M. Van Santvoort, Redistribution and geochemical behaviour of redox-sensitive elements around S1, the most recent eastern Mediterranean sapropel. *Geochim. Cosmochim. Acta*, 59, 3487-3501, 1995.
- Troelstra, S.R., Ganssen, G.M., Van der Borg, K. and A.M.F. De Jong, A late Quaternary stratigraphic framework for eastern Mediterranean sapropel S1 based on AMS ^{14}C dates and stable oxygen isotopes, *Radiocarbon*, 33, 15-21, 1991.
- Uerpmann, H.P., Radiocarbon dating of shell middens in the Sultanate of Oman, *PACT*, 29-IV.5, 335-347, 1991.

Van Campo, E., Duplessy, J.C. and M. Rossignol-Strick, Climatic conditions deduced from a 150-kyr oxygen isotope-pollen record from the Arabian Sea, *Nature*, 296, 56-59, 1982.

Vergnaud-Grazzini, C., Ryan, W.B.F. and M.B. Cita, Stable isotope fractionation, climatic change and episodic stagnation in the eastern Mediterranean during the late

Quaternary, *Mar. Micropaleontol.*, 2, 353-370, 1977.

Wijmstra, T.A., Young, R. and H.J.L. Witte, An evolution of the climatic conditions during the late Quaternary in northern Greece by means of multivariate analysis of palynological data and comparison with recent phytosociological and climatic data, *Geol. Mijnbouw*, 9, 243- 251, 1990.

Acknowledgments

In the first place I want to thank Cees van der Weijden for setting up this project and for giving me the opportunity to do this research. His input and comments on earlier drafts greatly improved the quality of this thesis.

Special thanks to Jan Willem Zachariasse, who was always there when I needed him. His enthusiasm and broad field of interest were very important to me during the last 4 years. Our good and close cooperation and discussions were invaluable.

Lucas Lourens, besides being a very good friend, has been of major importance for the realization of this thesis. His expertise in cyclostratigraphy proved indispensable.

I am grateful to Hendrik Jan Visser for the pleasant time we had during the 3 years we shared a room. His enthusiasm for laboratory work provided much of the data used in this thesis.

Willem van der Linden is thanked for linguistic improvements and stimulating discussions.

Much work of this thesis was carried out in close collaboration with colleagues from other disciplines in Utrecht. I highly appreciated the stimulating collaboration with and Maryke den Dulk from the Micropaleontology department and with Maarten Prins from the Sedimentology department. Fruitful and stimulating discussions on the most divergent topics with colleagues at the institute as Hendrik Jan Bosch, Gert de Lange, Hans Hage Marcel Hoefs, Frits Hilgen, Thomas Keijzer, Sieger van der Laan, Ivar Nijenhuis, Hilde Passier, Peter Pruyzers, Arrian Rutten, Sjoerd Schenau, Arrian Steenbruggen, Johan ten Veen, Gerard van den Berg, Peter van der Linden, Patrick van Santvoort and Berend Wilkens were indispensable as well.

I thank Gijs Nobbe, Mark van Alphen, Arnold van Dijk en Hellen de Waard for analytical support, and Geert Ittman and Gerrit van het Veld for sample preparation.

This research would not have been possible without the material collected with the professional help of crew and technicians of the RV Tyro during the 1992 Netherlands Indian Ocean Programme.

Thank are also due to Guido Ypenburg, Freek Slangen, Doorke van den Akker and Bas West who worked, as students, on cores from the Arabian Sea, providing additional data.

I thank my parents, family and all my friends for their continuous support during the past years.

This study was funded by the Netherlands Organization for Scientific Research (NWO).

Curriculum Vitae

Gert-Jan Reichart was born on October 30, 1966 in Amsterdam, The Netherlands. After attending secondary school from 1978 to 1984, he studied Earth Sciences at Utrecht University from 1985 to 1992. He holds a Masters (“doctoraal”) degree in stratigraphy and micropaleontology, with sedimentology as subsidiary subject. From 1992 to 1996 he was employed with the Netherlands Organization for Scientific Research as an OIO. The Ph.D. research was performed at the Geochemistry department of Utrecht University. From October 1996 to June 1997 he was employed as a research associate at Utrecht University and is currently continuing his research as a post-doc.